

SOME INVESTIGATIONS ON MULTI-PHASE INDUCTION GENERATOR FOR WIND ENERGY APPLICATION

DISSERTATION/THESIS

SUBMITTED IN PARTIAL FULFILLMENT OF THE REQUIREMENTS
FOR THE AWARD OF THE DEGREE
OF

DOCTORATE OF PHILOSOPHY

Submitted by:

RAMESH SINGH
(2K10/PhD/EE/16)

Under the supervision of

PROF. VISHAL VERMA
EED, DTU



DEPARTMENT OF ELECTRICAL ENGINEERING
DELHI TECHNOLOGICAL UNIVERSITY
(Formerly Delhi College of Engineering)
Bawana Road, Delhi-110042

DEDICATION

This Thesis is dedicated to my Mother, Late Smt. Kamala Singh and my Father, Late Dr. D. R. Singh.

DECLARATION

I, RAMESH SINGH (2K10/PhD/EE/16) hereby declare that the work, which is being presented in the thesis entitled, “**SOME INVESTIGATIONS ON MULTI-PHASE INDUCTION GENERATOR FOR WIND ENERGY APPLICATION**” submitted for partial fulfillment of the requirements for the award of the degree of Doctor of Philosophy is an authentic record of my own work carried out under the able guidance of Prof. VISHAL VERMA, EED, DTU. The matter embodied in the dissertation work has not been plagiarized from anywhere and the same has not been submitted for the award of any other degree or diploma in full or in part.

Submitted by:-

RAMESH SINGH

(2K10/PhD/EE/16)

Electrical Engineering Department

DEPARTMENT OF ELECTRICAL ENGINEERING
DELHI TECHNOLOGICAL UNIVERSITY
(Formerly Delhi College of Engineering)



CERTIFICATE

This is to certify that the thesis entitled, “**SOME INVESTIGATIONS ON MULTI-PHASE INDUCTION GENERATOR FOR WIND ENERGY APPLICATION**”, submitted by Mr. **RAMESH SINGH**, Roll No. 2K10/PhD/EE/16, research scholar Electrical Engineering Department, Delhi Technological University (Formerly Delhi College of Engineering), is a dissertation work carried out by him under my guidance during session 2010-2018 towards the partial fulfillment of the requirements for the award of degree of Doctor of Philosophy.

The uniqueness of the thesis pertains to asymmetrical multiphase induction generators for wind energy conversion systems, and its detailed analysis which has not been reported elsewhere.

I wish him all the best in his endeavors

Prof. Vishal Verma
Professor EED, DTU
Supervisor

ACKNOWLEDGMENT

It is my pleasure to be indebted to various people, who directly and indirectly contributed in the development of this work and who influenced my thinking, behavior, and during the course of study. Firstly and foremost, I would like to express my sincere thanks to my respected and learned supervisor, **Prof. Vishal Verma**, for his guidance, and supervision as well as for his support throughout the period of research. It is a life time experience to work under both of my supervisors which I am cherished always.

I owe thanks to **Prof. Uma Nangia**, Head of Department Electrical Engineering DTU Delhi and **Prof. Madhusudan Singh**, Chairman DRC, Department of Electrical Engineering DTU. I also thank all the faculty, staff members and research scholars of Electrical Engineering Department of DTU Delhi, for their help and support as and when required. I am greatly thankful to **Mr. Anil Butola** for his help, support and encouragement throughout my PhD period.

The unconditional love, support, patience and encouragement of my parents, **Late Kamala Singh** and **Late Dr. D. R. Singh**, remain memorable. I would like to thank my sisters **Sudha Singh** and **Suman Singh**, brother **Nagesh Singh** and rest all family members for their support throughout. Lastly I would like to thank my wife, **Ritika Gour** whose unconditional love, support and patience has made all this possible.

SOME INVESTIGATIONS ON MULTI-PHASE INDUCTION GENERATOR FOR WIND ENERGY APPLICATION

ABSTRACT

With the depletion of the reserves of coal and fossil fuels, renewable sources viz. solar, wind, tidal waves, geothermal etc. are finding great attention for energy generation. The share of Wind energy is rapidly increasing due to their robust structure and direct connectivity to the grid. Latest research and development in the generator and power converter topology has led to remediation of generation constraint. New topologies of generators including multiphase induction generators with dual stator winding sets are represented as leading prominent contenders recently. The variable reactive power demanded by induction generators often pose a major issue which magnifies multifold when operated in a wind farm. Various researches are reported that minimize the contribution of reactive power from the grid along with interaction of generators on account of reactive power. Research is due for understanding the behavior of multiphase induction generator during low voltage on the grid end. This demand for analysis of air-gap flux for transient operations and development of model to explore the potential of multiphase induction generators for application to three port energy device for distribution of generated energy along with capability of power transfer across the winding sets.

The work carried out in this thesis is focused on the transient and steady state analysis of Asymmetrical Dual Stator Induction Generator (ADSIG) and comparing it with Squirrel Cage Induction Generator (SCIG) and Symmetrical Dual Stator Induction Generator (SDSIG) for various operating conditions. For doing so, a new decoupled equivalent circuit model of ADSIG is developed in d-q frame by transferring the rotor side winding

leakage inductance to both the stators side circuit and the magnetization branch. The developed model of ADSIG is developed in MATLAB SIMULINK environment for observing the response in generation mode. A finite element model of the machine is also developed in INFOLYTICA MOTORSOLVE software to estimate its performance. Based on the model and design a hardware prototype of ADSIG is developed in laboratory to study the behavior of ADSIG. A detailed comparison of SDSIG and ADSIG is done with special emphasis on the air-gap flux when these generators are subjected to different types of loading conditions. A comparison is also been drawn for reactive power demanded by ADSIG, SDSIG and SCIG in respect of peak inrush currents. The analytical study is then validated both through simulations and experimentation in grid coupled mode.

Three applications of ADSIG are also explored dually supported with study, simulation and experimental results namely soft coupling of two distribution feeder, dispatchable power transfer to grid, rural electrification.

Application 1: The application of ADSIG as a three port network for routing power two different AC feeders under conditions of with and without wind energy inception is evaluated. ADSIG here in acts as a soft coupler routing of power between the feeders depending upon the loading on the respective feeder in absence of wind, and distributing the generated energy to the loaded feeder side automatically. The analysis is duly validated through simulation and experimentation results.

Application 2: The problem of intermittent power generation is often not acceptable to weak AC grids in presence of variable wind conditions. An energy storage system (ESS) for curbing the intermittency and providing dispatchable study to such generation is often a requisite. A study of connection of ESS at one end and connection of grid at the other

end of ADSIG is made through analysis where in duly substantiated through analytical and experimental study.

Application 3: Further a cost effective method for rural electrification is also proposed by using multiple ADSIGs to harvest the generated energy and provides power to the rural loads. The analysis and experimentation is done using both low wind speed (transformer action of ADSIG) and sufficient wind speed conditions (generator action of ADSIG) for reducing the effective loading on the rural feeder. All the analytical, simulated and hardware results are coherent and support for the candidacy of ADSIG to such applications.

TABLE OF CONTENTS

Declaration	<i>i</i>
Certificate	<i>ii</i>
Acknowledgement	<i>iii</i>
Abstract	<i>iv</i>
Table of Content	<i>vii</i>
List of Figures	<i>xii</i>
List of Tables	<i>xxiv</i>
Abbreviations	<i>xxv</i>
CHAPTER 1 INTRODUCTION	1
1.1 General	1
1.2 Power in Wind	2
1.3 Issues with Induction Generators	4
1.4 Multi-Phase Generators for WECS	7
1.4.1 Brushless Doubly Fed Induction Generator And Split-Phase Induction Generators	7
1.4.2 Multi-Phase Induction Generators and their Merits	8
1.4.3 Dual Stator Induction Generator	10
1.5 State of The Art: Configuration and Control Techniques of DSIG	10
1.6 Scope of the Work	14
1.7 Organization of thesis	14

CHAPTER 2	SURVEY OF LITERATURE	17
2.1	General	17
2.1	Issues of Generators Employed in WECS	17
2.1.1	Inrush Currents in Variable Speed Generators	18
2.1.2	Reactive Power Demanded by Variable Speed Generators	20
2.1.3	Low Voltage Ride Through and Fault Ride Through Capability for WECS	21
2.1.4	Requirement of Energy Storage During Intermittent Generation in RES	23
2.2	Conventional Wound and Special Wound Generators	23
2.2.1	Issues of Conventional Three Phase Generators Connected in WECS	24
2.2.2	Issues of Multi-Phase Generators Connected in WECS	26
2.2.3	Emergence of Dual Stator Generators for WECS	28
2.3	Scope of the Work	31
2.4	Conclusion	32
CHAPTER 3	MODELLING AND DESIGN OF DUAL STATOR INDUCTION GENERATOR	33
3.1	General	33
3.2	Mathematical Modelling of ADSIG in MATLAB	33
3.3	Reduced Equivalent Circuit of ADSIG	43
3.4	Designing of ADSIG in INFOLYTICA MOTOSOLVE SOFTWARE	50
3.4.1	Selection of Material	50
3.4.2	Dimensions and other Design Parameters for ADSIG	51
3.4.3	Winding Layout used in MotorSolve	54

3.4.4	The Summary of Design for ADSIG Prototype	54
3.4.5	Simulated Performance Characteristics	56
3.5	Design and Winding of Hardware Prototype of ADSIG	57
3.5.1	Selection of Materials	57
3.5.2	Prototype Testing of ADSIG	60
3.5.3	Equivalent Circuit Parameters of ADSIG	62
3.6	Conclusion	62
CHAPTER 4	TRANSIENT PERFORMANCE ANALYSIS OF ADSIG	65
4.1	General	65
4.2	System Configuration of DSIG and SCIG for Analysis of Inrush Current	66
4.3	Mathematical Analysis of Inrush Current of DSIG	67
4.3.1	Mathematical Analysis of Current of ADSIG	67
4.3.2	Mathematical Analysis of Current of SCIG	73
4.3.3	Comparison of Forced Response of SCIG and DSIG	75
4.3.4	Comparison of Natural Response of SCIG and DSIG	77
4.4	MATLAB Simulation and Hardware Comparison	78
4.5	Transient analysis of Air-Gap Flux	90
4.6	Conclusion	99
CHAPTER 5	THREE-PORT ENERGY INTEGRATION AND SOFT COUPLING OF TWO DISTRIBUTION FEEDERS USING DSIG	101
5.1	General	101

5.2	System Configuration and Salient features of Three Port Network	102
5.3	Mathematical Analysis of ADSIG for Power Routing Capability of ADSIG Incorporating Loading on Feeders	103
5.4	MATLAB simulation of DSIG as Three Port Network	116
5.5	Hardware Implementation of DSIG for Routing Power in Three Port Network	117
5.6	Results and Discussion	118
5.7	Conclusion	126
CHAPTER 6	ADSIG AS HYBRID MICROGRID WITH ESS	129
6.1	Introduction	129
6.2	System Configuration and Salient features of ADSIG with ESS for grid coupling	130
6.3	Analysis of Power Flow to Grid from ADSIG coupled with ESS	131
6.4	Control of ESS	138
6.5	Performance Evaluation of ADSIG in tandem with ESS for Power Flow Control	139
6.6	Conclusion	145
CHAPTER 7	PERFORMANCE ANALYSIS OF GRID COUPLED ADSIG FOR RURAL ELECTRIFICATION	147
7.1	General	147
7.2	System Considered for Utilization of ADSIG for Rural Electrification	148
7.3	Mathematical Analysis of Power Flow from/across ADSIG	150
7.4	Performance Evaluation based on MATLAB simulation	156

	and Hardware implementation of ADSIG for Rural Electrification	
7.5	Conclusion	166
CHAPTER 8	CONCLUSION AND FUTURE SCOPE	169
8.1	Main Conclusions	169
8.2	Future Scopes of Work	172
	References	173

LIST OF FIGURES

Fig. No.	Figure Topic	Page No.
Fig. 1.1	SCIG with AC-DC-AC (BTB) Converter	5
Fig. 1.2	SCIG with MATRIX Converter	5
Fig. 1.3	DFIG with AC-DC-AC (BTB) Converter	5
Fig. 1.4	DFIG with AC-DC-AC converter connected to GRID	6
Fig. 1.5	DSIG with Diode Rectifier Feeding DC Load	11
Fig. 1.6	DSIG with AC-DC Converter Feeding AC Grid	11
Fig. 1.7	DSIG feeding AC Load from Power Winding with Active Rectifier on Control Winding	12
Fig. 1.8	DSIG feeding AC Load from Power Winding with Active Rectifier on Control Winding	13
Fig. 1.9	DSIG Feeding AC Grid/ Load with Star-Star-Delta Three	13
Fig. 3.1	Three Phase to Two Phase Conversion of $a_1b_1c_1$ Phases	34
Fig. 3.2	Three Phase to Two Phase Conversion of $a_2b_2c_2$ Phases	34
Fig. 3.3	Two Phase to Three Phase Conversion of d_1q_1 Phases	35
Fig. 3.4	Two Phase to Three Phase Conversion of d_2q_2 Phases	36
Fig. 3.5	Equivalent Circuit of ADSIG in d-axis	41
Fig. 3.6	Equivalent Circuit of ADSIG in q-axis	41
Fig. 3.7	Reduced Equivalent Circuit of ADSIG	43
Fig. 3.8	Modified Reduced Equivalent circuit of ADSIG	44

Fig. 3.9	Simplified Modified Reduced Equivalent circuit of ADSIG	44
Fig. 3.10	Decoupled Equivalent Circuit of ADSIG as Current Source	50
Fig. 3.11(a)	Winding Diagram of ADSIG	52
Fig. 3.11(b)	Winding Diagram of ADSIG in INFOLYTICA MOTOORSOLVE	53
Fig. 3.12	Performance Characteristics of ADSIG in INFOLYTICA MOTORSOLVE	56
Fig. 3.13	Empty Stator Induction Motor	57
Fig. 3.14	Rewinding of Empty Stator Induction Motor	58
Fig. 3.15	Empty Stator Induction Motor Wounded as ADSIG	59
Fig. 3.16	ADSIG Coupled with Prime Mover	59
Fig. 3.17	Hardware Test Rig of ADSIG	60
Fig. 3.18	Current Waveform of Two Phases of each Winding set of ADSIG recorded in DSO	61
Fig. 3.19	Voltage and Current Waveform of both the Winding set of ADSIG recorded in PQ Analyser	61
Fig. 4.1	System Configuration of SCIG for Analysis of Inrush Current	66
Fig. 4.2	System Configuration of ADSIG for Analysis of Inrush Current	66
Fig. 4.3(a)	Modified per phase Equivalent Circuit of ADSIG as a Current Source.	68
Fig. 4.3(b)	Equivalent per phase circuit of ADSIG with rotor inductance referred to stator side	69

Fig. 4.3(c)	Reduced equivalent circuit of ADSIG	69
Fig. 4.4	Forced Current Response of SCIG and ADSIG	76
Fig. 4.5	Phasor representation of stator and rotor currents of ADSIG	77
Fig. 4.6	SIMULATION Model of SCIG	79
Fig. 4.7	SIMULATION Model of ADSIG	79
Fig. 4.8	Inrush Current of SCIG and ADSIG	80
Fig. 4.9	Inrush Current of SCIG (Hardware)	81
Fig. 4.10	Inrush Current of ADSIG (Hardware)	81
Fig. 4.11(a)	D-Q Axis Flux for SCIG (0-3 cycle)	82
Fig. 4.11(b)	D-Q Axis Flux for SCIG (3-7.5 cycle)	82
Fig. 4.12 (a)	D-Q Axis Flux for ADSIG (0-3 cycle)	82
Fig. 4.12 (b)	D-Q Axis Flux for ADSIG (3-7.5 cycle)	82
Fig.4.13	d-q Flux for SCIG and ADSIG (resultant of Leading and Lagging Stator Winding)	83
Fig. 4.14	Transient Current Response of generators due to low voltage condition	85
Fig. 4.15	Settling time of SCIG and ADSIG currents during Low voltage condition	85
Fig. 4.16	Phasor of Voltage and Currents for (a) Normal (b) Low Voltage (c) Single Phasing Conditions when Grid and Load are connected to SCIG	87
Fig. 4.17	Phasor of Voltage and Currents for (a) Normal (b) Low Voltage (c) Single Phasing Conditions when Grid and Load are connected to ADSIG	87

Fig. 4.18	Current Waveform of SCIG for 10 cycles FRT; (Phase 'A' open circuited)	88
Fig. 4.19	Current Waveform of ADSIG for 10 cycles FRT; (Phase 'A' open circuited)	88
Fig. 4.20(a)	Asymmetrical DSIG: Projection of Lagging to Leading Winding- Phasor of I_d and I_q for both leading (I1) and lagging (I2) winding currents	91
Fig. 4.20(b)	Asymmetrical DSIG: Projection of Lagging to Leading Winding- Projection of I_d and I_q of lagging (I2) winding current on leading winding current (I1)	91
Fig. 4.20(c)	Asymmetrical DSIG: Projection of Lagging to Leading Winding- Resultant I_d and I_q of leading (I1) winding current	91
Fig. 4.20 (d)	Asymmetrical DSIG: Projection of Leading to Lagging Winding- Phasor of I_d and I_q for both leading (I1) and lagging (I2) winding currents	91
Fig. 4.20 (e)	Asymmetrical DSIG: Projection of Leading to Lagging Winding- Projection of I_d and I_q of leading (I1) winding current on lagging winding current (I2)	91
Fig. 4.20 (f)	Asymmetrical DSIG: Projection of Leading to Lagging Winding- Resultant I_d and I_q of lagging (I2) winding current	91
Fig. 4.20 (g)	Symmetrical DSIG: Projection of Lagging to Leading Winding- Phasor of I_d and I_q for both leading (I1) and lagging (I2) winding currents	93
Fig. 4.20 (h)	Symmetrical DSIG: Projection of Lagging to Leading Winding- Projection of I_d and I_q of lagging (I2) winding current on leading winding current (I1)	93
Fig. 4.20 (i)	Symmetrical DSIG: Projection of Lagging to Leading Winding- Resultant I_d and I_q of leading (I1) winding current	93

Fig. 4.20 (j)	Symmetrical DSIG: Projection of Leading to Lagging Winding- Phasor of I_d and I_q for both leading (I1) and lagging (I2) winding currents	93
Fig. 4.20 (k)	Symmetrical DSIG: Projection of Leading to Lagging Winding- Projection of I_d and I_q of leading (I2) winding current on lagging winding current (I1)	93
Fig. 4.20 (l)	Symmetrical DSIG: Projection of Leading to Lagging Winding- Resultant I_d and I_q of leading (I1) winding current	93
Fig. 4.21	Terminal Voltages of Symmetrical and Asymmetrical DSIG	95
Fig. 4.22	Effect of Loading on Air Gap Flux	97
Fig. 4.23	Effect of LG Fault (10Cycles) on Air Gap Flux	97
Fig. 5.1	ADSIG as Soft-Coupler for AC Feeders	103
Fig. 5.2 (a)	Equivalent Circuit of Proposed System with ADSIG as Soft Coupler	104
Fig. 5.2 (b)	Power Flow Diagram from Leading Winding Side to Lagging Winding Side of DSIG for Transformer Action	107
Fig. 5.2 (c)	Phasor Diagram for Lagging Side Impedance for Leading it by 30°	108
Fig. 5.2 (d)	Phasor Diagram for rotor impedance for Leading it by 15°	110
Fig. 5.2 (e)	Equivalent circuit seen by Leading winding side grid for routing power to Lagging winding side	111
Fig. 5.2 (f)	Phasor Diagram for Leading Side Impedance for Lagging it by 30°	113
Fig. 5.2 (g)	Phasor Diagram for Rotor Impedance for Lagging it by 15°	114

Fig. 5.2 (h)	Equivalent circuit seen by Lagging winding side grid for routing power to Leading winding side	115
Fig. 5.3	Matlab Simulink Model of Three Port Network	117
Fig. 5.4	Photograph of the developed prototype and hardware test bed of the proposed system	118
Fig. 5.5	Performance with load perturbation at leading winding of DSIG	119
Fig. 5.6	Performance with load perturbation at lagging winding of DSIG	119
Fig. 5.7	Performance of hardware prototype with load perturbation at leading winding of DSIG.	121
Fig. 5.8	Performance of hardware prototype with load perturbation at lagging winding of DSIG. X	121
Fig. 5.9	Performance under low voltage and fault condition at leading side of DSIG (3 synchronized oscilloscopes).	123
Fig. 5.10	Performance under low voltage and fault condition at lagging side of DSIG (3 synchronized oscilloscopes).	123
Fig. 5.11	Phasors depicting (a) Normal (b) Under Low voltage at leading winding and (c) Single phasing condition at leading winding of DSIG. Depiction of both leading and lagging side currents for power routing enacting soft coupling. Circle represents radius of 10 units	124
Fig.5.12	Phasors depicting (a) Normal (b) Under Low voltage at lagging winding and (c) Single phasing condition at lagging winding of DSIG. Depiction of both leading and lagging side currents for power routing enacting soft coupling. Circle represents radius of 10 units.	124
Fig. 6.1	Block diagram for system configuration of ADSIG with ESS for grid-coupling	130

Fig. 6.2(a)	Equivalent Circuit of Grid Connected Hybrid Microgrid with ADSIG and ESS	131
Fig. 6.2(b)	Phasor Diagram for IESS as seen on the leading winding side (grid side) of ADSIG	132
Fig. 6.2(c)	Phasor Diagram for ADSIG current for Leading it by 15°	133
Fig. 6.2(d)	Equivalent circuit seen on the Leading winding side grid	134
Fig. 6.2(e)	Equivalent circuit seen on the Leading winding side grid as in Mode 1	135
Fig. 6.2(f)	Equivalent circuit seen on the Leading winding side grid as in Mode 2	136
Fig. 6.2(g)	Equivalent circuit seen on the Leading winding side grid as in Mode 3	137
Fig. 6.2(h)	Equivalent circuit seen on the Leading winding side grid as in Mode 4	138
Fig. 6.3	Block Diagram of Control of ESS	138
Fig. 6.4(a)	Active and Reactive Power of ESS (off-grid) side of ADSIG Mode 1	141
Fig. 6.4(b)	Phasor of three phase current and voltage of one phase of ESS (off-grid)side of ADSIG Mode 1	141
Fig. 6.4(c)	Current THD at ESS (off-grid) side of ADSIG Mode 1	141
Fig. 6.4(d)	Active and Reactive Power of Grid side of ADSIG Mode 1	141
Fig. 6.4(e)	Phasor of three phase current and voltage of one phase of Grid side of ADSIG Mode 1	141
Fig. 6.4(f)	Current THD at Grid side of ADSIG Mode 1	141
Fig. 6.5(a)	Active and Reactive Power of ESS (off-grid) side of	142

ADSIG Mode 2

Fig. 6.5(b)	Phasor of three phase current and voltage of one phase of ESS (off-grid)side of ADSIG Mode 2	142
Fig. 6.5(c)	Current THD at ESS (off-grid) side of ADSIG Mode 2	142
Fig. 6.5(d)	Active and Reactive Power of Grid side of ADSIG Mode 2	142
Fig. 6.5(e)	Phasor of three phase current and voltage of one phase of Grid side of ADSIG Mode 2	142
Fig. 6.5(f)	Current THD at Grid side of ADSIG Mode 2	142
Fig. 6.6(a)	Active and Reactive Power of ESS (off-grid) side of ADSIG Mode 3	143
Fig. 6.6(b)	Phasor of three phase current and voltage of one phase of ESS (off-grid)side of ADSIG Mode 3	143
Fig. 6.6(c)	Current THD at ESS (off-grid) side of ADSIG Mode 3	143
Fig. 6.6(d)	Active and Reactive Power of Grid side of ADSIG Mode 3	143
Fig. 6.6(e)	Phasor of three phase current and voltage of one phase of Grid side of ADSIG Mode 3	143
Fig. 6.6(f)	Current THD at Grid side of ADSIG Mode 3	143
Fig. 6.7(a)	Active and Reactive Power of ESS (off-grid) side of ADSIG Mode 4	144
Fig. 6.7(b)	Phasor of three phase current and voltage of one phase of ESS (off-grid)side of ADSIG Mode 4	144
Fig. 6.7(c)	Current THD at ESS (off-grid) side of ADSIG Mode 4	144
Fig. 6.7(d)	Active and Reactive Power of Grid side of ADSIG Mode 4	144

Fig. 6.7(e)	Phasor of three phase current and voltage of one phase of Grid side of ADSIG Mode 4	144
Fig. 6.7(f)	Current THD at Grid side of ADSIG Mode 4	144
Fig. 7.1	Configuration 1 - ADSIG connected to Substation and Feeding Rural loads via distribution feeder	148
Fig.7.2	Configuration 2 - ADSIG connected to Grid and Feeding Local Home Loads	149
Fig. 7.3	Equivalent circuit of ADSIG connected to Substation and feeding Rural Loads via distribution feeder	149
Fig. 7.4	Equivalent circuit of ADSIG connected to ADSIG connected to grid and feeding Local / Home Loads	149
Fig. 7.5	Generalized Equivalent Circuit (for both configuration) for Transformer Action	151
Fig. 7.6(a)	Transformer Action Reduced Equivalent Circuit (Both configuration) as seen on the Grid/substation side of ADSIG	152
Fig. 7.6(b)	Transformer Action Reduced Equivalent Circuit (Both configuration) as seen on the load/rural feeder side of ADSIG	152
Fig. 7.7	Matlab Simulink Model for Rural Electrification	156
Fig. 7.8	Voltage and current waveform of Leading (Grid Side) and Lagging (Load Side) Winding Side of ADSIG during Change in Wind Speed	157
Fig. 7.9	Real and Reactive power drawn/supplied of Leading (Grid Side) and Lagging (Load Side) Winding Side of ADSIG during change in Wind Speed	157
Fig. 7.10(a)	Current (Three Phase) and Voltage (Single Phase) waveforms of Grid side ADSIG for Rural Electrification without Prime-mover and ADSIG operating in motoring	159

mode and acting as Isolation Transformer

Fig. 7.10(b)	Active and reactive Power of Grid side ADSIG for Rural Electrification without Prime-mover and ADSIG operating in motoring mode and acting as Isolation Transformer	159
Fig. 7.10(c)	Phasor Diagram of 3-Ø Current of Grid side ADSIG for Rural Electrification without Prime-mover and ADSIG operating in motoring mode and acting as Isolation Transformer	159
Fig. 7.11(a)	Current (Three Phase) and Voltage (Single Phase) waveforms of Load (off-Grid) side ADSIG for Rural Electrification without Prime-mover and ADSIG operating in motoring mode and acting as Isolation Transformer	160
Fig. 7.11(b)	Active and reactive Power of Load (off-Grid) side ADSIG for Rural Electrification without Prime-mover and ADSIG operating in motoring mode and acting as Isolation Transformer	160
Fig. 7.11(c)	Phasor Diagram of 3-Ø Current of Load (off-Grid) side ADSIG for Rural Electrification without Prime-mover and ADSIG operating in motoring mode and acting as Isolation Transformer	160
Fig. 7.12(a)	Current (Three Phase) and Voltage (Single Phase) waveforms of Grid side ADSIG for Rural Electrification with Prime-mover and ADSIG acting as Generator	161
Fig. 7.12(b)	Active and reactive Power of Grid side ADSIG for Rural Electrification with Prime-mover and ADSIG acting as Generator	161
Fig. 7.12(c)	Phasor Diagram of 3-Ø Current of Grid side ADSIG for Rural Electrification with Prime-mover and ADSIG acting as Generator	161
Fig. 7.13(a)	Current (Three Phase) and Voltage (Single Phase)	162

	waveforms of Load (off-Grid) side ADSIG for Rural Electrification with Prime-mover and ADSIG acting as Generator	
Fig. 7.13(b)	Active and reactive Power of Load (off-Grid) side ADSIG for Rural Electrification with Prime-mover and ADSIG acting as Generator	162
Fig. 7.13(c)	Phasor Diagram of 3-Ø Current of Load (off-Grid) side ADSIG for Rural Electrification with Prime-mover and ADSIG acting as Generator	162
Fig. 7.14	Voltage and Current waveform of Leading (Grid Side) and Lagging (Load Side) Winding Side of ADSIG during Change in Load levels	163
Fig. 7.15	Real and Reactive power drawn/supplied of Leading (Grid Side) and Lagging (Load Side) Winding Side of ADSIG during change in Load Levels	163
Fig. 7.16(a)	Active and Reactive Power of Grid side ADSIG for Rural Electrification with ADSIG active as Generator (with 1.5 A Load Current)	164
Fig. 7.16(b)	Phasor Diagram of 3-Ø Current of Grid side ADSIG for Rural Electrification with ADSIG acting as Generator (with 1.5 A Load Current)	164
Fig. 7.17(a)	Active and Reactive Power of Load (off-Grid) side ADSIG for Rural Electrification with ADSIG active as Generator (with 1.5 A Load Current)	164
Fig. 7.17(b)	Phasor Diagram of 3-Ø Current of Load (off-grid) side ADSIG for Rural Electrification with ADSIG acting as Generator (with 1.5 A Load Current)	164
Fig. 7.18(a)	Active and Reactive Power of Grid side ADSIG for Rural Electrification with ADSIG active as Generator (with 2 A Load Current)	165
Fig. 7.18(b)	Phasor Diagram of 3-Ø Current of Grid side ADSIG for	165

Rural Electrification with ADSIG acting as Generator
(with 2 A Load Current)

Fig. 7.19(a)	Active and Reactive Power of Load (off-Grid) side ADSIG for Rural Electrification with ADSIG active as Generator (with 2 A Load Current)	165
Fig. 7.19(b)	Phasor Diagram of 3-Ø Current of Load (off-grid) side ADSIG for Rural Electrification with ADSIG acting as Generator (with 2 A Load Current)	165

LIST OF TABLES

Table No.	Title	Page No.
Table 3.1	Different values of ‘ k’ and ‘ ki’ for common conversions	38
Table 3.2	Winding Layout of ADSIG	53
Table 3.3	Equivalent Parameters of ADSIG	62
Table 4.1	Rating of Different Loads	94
Table 4.2	Performance of different generators under Different Loading and Fault Conditions	98

ABBREVIATIONS

3D	:	Three Dimension
A	:	Amperes
AC	:	Alternating Current
ADSIG	:	Asymmetrical Dual Stator Induction Generator
BDFIG	:	Brushless Doubly Fed Induction Generator
BTB	:	Back to Back
CR	:	Cold Rolled
d-axis	:	Direct Axis
DC	:	Direct Current
DFIG	:	Doubly Fed Induction Generator
DPC	:	Direct Power Control
dq-axis	:	Direct-Quadrature Axis
DSIG	:	Dual Stator Induction Generator
DSO	:	Digital Storage Oscilloscope
DTs	:	Distribution Transformers
ESS	:	Energy Storage System
FRT	:	Fault Ride Through
FST	:	Fixed Speed Turbine
HAWT	:	Horizontal Axis Wind Turbines
HP	:	Horse Power
HPO	:	High Phase Order
HVDC	:	High Voltage Direct Current
IACS	:	International Annealed Copper Standard

IG	:	Induction Generator
IM	:	Induction Motor
KCL	:	Kirchhoff's Current Law
KE	:	Kinetic Energy
kVA	:	Kilo Volt Amperes
kVAr	:	Kilo Volt Amperes Reactive
KW	:	Kilo Watts
LVRT	:	Low Voltage Ride Through
MATLAB	:	Matrix Laboratory
PCC	:	Point of Common Coupling
pf.	:	Power Factor
PI	:	Proportional Integral
PMSG	:	permanent Magnet Synchronous Generator
pu	:	per unit
PV		Photovoltaic
PWM	:	Pulse Width Modulation
q-axis	:	Quadrature Axis
RES	:	Renewable Energy Sources
RMS	:	Root Mean Square
s	:	seconds
SCIG	:	Squirrel Cage Induction Generator
SDSIG	:	Symmetrical Dual Stator Induction Generator
SEC	:	Static Excitation Controller
SG	:	Synchronous Generator

SPIG	:	Split Phase Induction Generator
STATCOM	:	Static Compensator
SVM	:	State Vector Modulation
SWG	:	Standard Wire Gauge
THD	:	Total Harmonic Distortion
UPF	:	Unity Power Factor
V	:	Voltage
VA	:	Voltage Ampere
VAr	:	Voltage Ampere reactive
VAWT	:	Vertical Axis Wind Turbines
VFAC	:	Variable Frequency Alternating Current
VSC	:	Voltage Source Converter
VST	:	Variable Speed Turbine
W	:	Watt
WECS	:	Wind Energy Conversion System
WRIG	:	Wound Rotor Induction Generator

Chapter 1

Introduction

1.1 General

From the dawn of industrialization, the demand for electrical power has increased manyfolds and is still increasing at a greater rate than earlier. To cater the electric demand conventional sources such as coal (thermal power plant), water (hydropower plant), nuclear (nuclear power plant), etc. have been used as the major sources of electrical energy. Thermal power plant still contributes the highest share of power generation among all other sources of power. Nevertheless, this method suffers from the demerits of environmental pollution like emission of greenhouse gasses in add-on to depleting coal reserves. The gestation period and response time of thermal power plants are also long, whereas, the response time of these power plants is in the order of minutes.

Generation of electricity through hydroelectric power plants is seen to be a better alternative to zero emission of greenhouse gasses. These sources are quite cheaper but these can be located only where rivers are located thus limiting their scope for site selection. Deposition of silt is another major concern for hydropower plants which limits the operating lifespan. For the construction of hydropowerplants, dams are constructed, which disturb the natural habitat of humans along with the natural flora and faunas, moreover, there is always a risk of dam failures.

Nuclear power generation is very costly and also can cause the highest possible danger to human life. The depleting sources of conventional energy resources and the possible

hazards associated with them have forced the utility engineers and researchers to search for new and better ways of power generation.

Power generation from Renewable Energy Sources (RES) is hence gradually picking pace resulting in a continuous increase in their share in total power generation in last few decades. Amongst the various RES, the major sources are wind, solar, geothermal, biomass and tidal energy. Among the various sources, wind and solar are the fastest growing source for power generation. The solar power is converted into electrical energy mainly via Photovoltaic (PV) modules. It is one of the cleanest forms of energy but the solar power, available only during the daytime, needs large storage to cater the demand throughout a day. The large requirement of storage system limits the use of solar in many applications.

The wind power, on the other hand, available almost throughout the day, requires lesser storage support as compared to solar. The storage for wind energy conversion systems is only required for a fraction of their total capacity, with a payback period of usually 5-8 months. In wind farms, power of wind is captured through turbine blades and with the help of variable speed generator, this mechanical energy is converted to electrical energy. Power generation from wind is cheap, versatile and the environment-friendly source of energy. Among different renewable power sources available, Wind Energy Conversion Systems (WECS) have better prospects due to cheaper power conversion cost, and availability of wind throughout day and night. The generators used in WECS are the main focus of the thesis.

1.2 Power in Wind

Wind energy is the kinetic energy associated with the movement of atmospheric air

and in WECS this energy is converted to electrical energy using wind turbines and the associated generators. The wind that exists over the earth's surface is a result of variations in the air pressure caused due to the variations in solar heating. Wind is merely the movement of air from one place to another as warm air rises and cooler air rushes in to take its place. The kinetic energy of wind of mass 'm' (in kg), moving with velocity 'v' in (m/s) is given as:

$$KE = \frac{1}{2} m v^2 \quad (1)$$

The power in the wind is kinetic energy per unit time. Assuming the wind speed as constant, the wind power 'P_w' is given by equation (2).

$$P_w = \frac{1}{2} \left(\frac{dm}{dt} \right) v^2 \quad (2)$$

Where $\frac{dm}{dt}$ is the mass flow rate and according to the basics of fluid mechanics can be expressed as equation (3).

$$\frac{dm}{dt} = \rho A v \quad (3)$$

- Where ρ is wind density and
- A is the swept area.

Putting the value of $\frac{dm}{dt}$ from equation (3) in equation (2), power in the wind can be written as:

$$P_w = \frac{1}{2} \rho A v^3 \quad (4)$$

The effective wind power is lesser than indicated by the above equation. The wind speed before the wind turbine is more than the wind speed after the wind turbine. The effective wind power is the difference between these two wind speeds. The Betz

coefficient 'C_p' characterizes the relative power drawing coefficient of the turbine. According to Betz limit, the maximum power that can be extracted from a wind is given by equation (5).

$$P_T = \frac{1}{2} \rho A v^3 C_p \quad (5)$$

And the maximum value of C_p is $\frac{16}{27}$, so the maximum efficiency of any wind turbine can be only 59%.

1.3 Issues with Induction Generators

The unpredictable nature of wind speed poses a major problem in the generation and distribution of electrical power in WECS. To generate electrical power at different wind speeds, a variable speed generator capable of generating at different wind speeds is requisite. Induction generators are best suited for such application. The reliability, cost and complexity of Fixed Speed Generation is far better than those of Variable Speed Generators but, the uncontrolled reactive power demand along with poor power quality and high torque pulsation make variable speed generation more suitable for wind farms [1-4].

Also to increase the operating range and thus increase the output power of wind generators wind farms are equipped with variable speed turbines (VSTs) [4-13]. In same operating conditions the output of VSTs is 5% more than FSTs [4] [14-20] but the output is of variable magnitude and variable frequency AC.

For converting the variable frequency and variable magnitude AC to fixed frequency and voltage magnitude AC, either Back-To-Back (BTB) converter (Fig. 1.1) or MATRIX converter (Fig. 1.2), is employed with SCIG in wind farms.

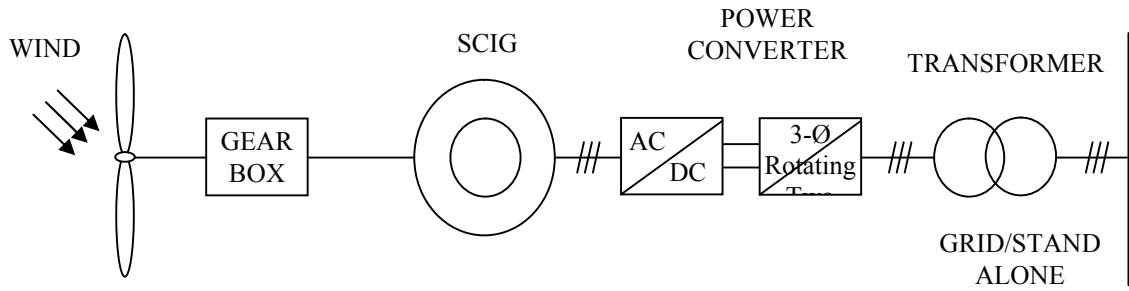


Fig. 1.1: SCIG with AC-DC-AC (BTB) Converter

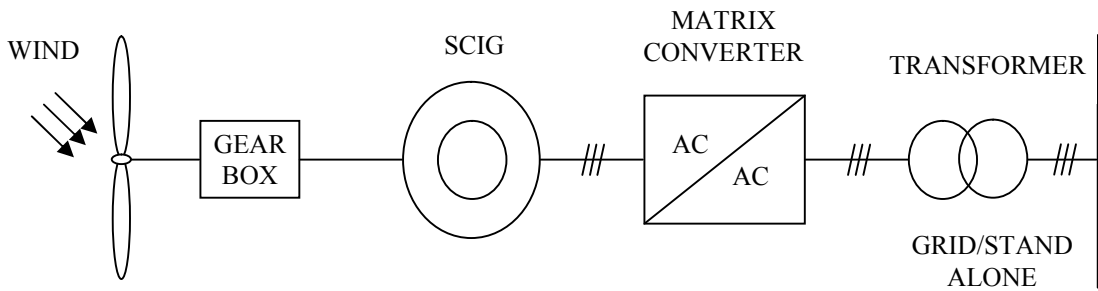


Fig. 1.2: SCIG with MATRIX Converter

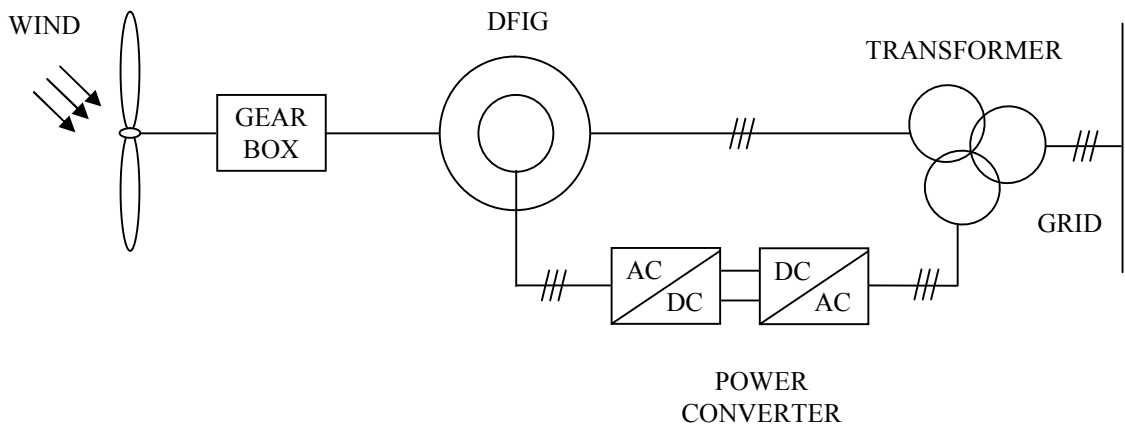


Fig. 1.3: DFIG with AC-DC-AC (BTB) Converter

With the increased involvement of power electronics the power generation in wind farms is becoming more and more smother but with add-on cost, complexity and lesser reliability [21-27]. The main advantage of SCIG topology lies in its simplicity and, cost effective operation. The disadvantages include its uncontrolled operation and

variable reactive power demand. DFIGs on the other hand are best suited for reactive power control and these works in a wide speed range as the BTB converters decouple the electrical and mechanical systems [28-36].

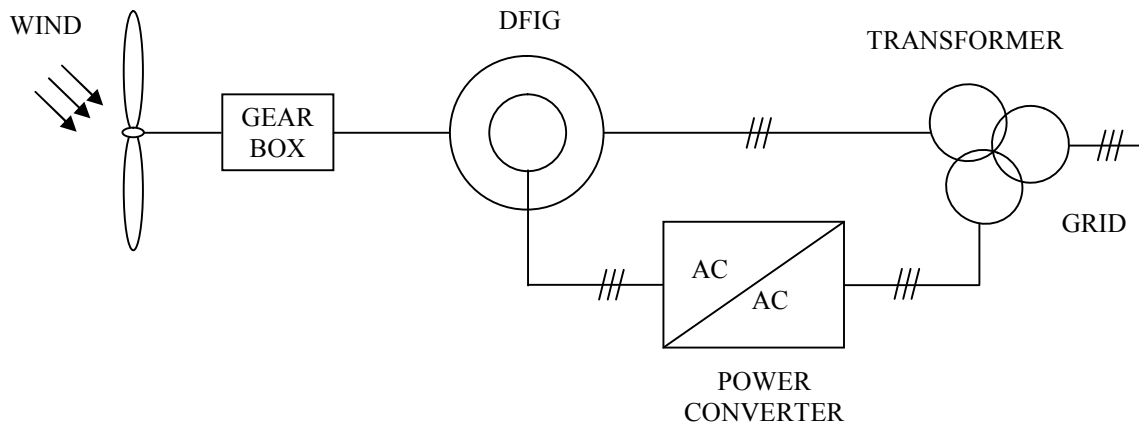


Fig. 1.4: DFIG with MATRIX Converter

Employing medium scale power electronic converters, like BTB converter (Fig. 1.3) or MATRIX converter (Fig. 1.4) the operating range speed can be increased up-to $\pm 30\%$ in both super-synchronous and sub-synchronous speeds [5-7] [25-27] [37-38]. Incorporation of full rated power electronic converters give extra flexibility of effective control over active and reactive power flow, but all these advantages come with extra cost which add to the system cost [25-27] [39-41]. The characteristics of different generators can be modified to achieve a better power generating solution by incorporation power electronic interfaces [42-45]. Synchronous generators on the other hand, are capable of controlling and regulating the power systems, moreover, the dependency of reactive power demand of IGs, on their loading conditions, makes these generating units incapable of providing any support for controlling or regulating the power system [46-49]. Since the DFIG employs wound rotor induction machine which increases the cost of the overall system as the rotor of the generator also wound and is externally brought out through slip-rings, which due to their regular wear and tear

have a limited lifespan and thus requires regular maintenance. Another problem with DFIG is their poor LVRT capabilities. The increased cost (initial and maintenance) and poor LVRT of capabilities of such machines can be offset by their advantages only when they are employed in big wind turbines. New, better and cost effective topologies for wind power generation are being researched to overcome these challenges and provide quality power.

1.4 Multi-Phase Generators for WECS

A number of research attempts have been done on different topologies of IGs having more than one stator winding. Recently multi-phase IGs with two or more windings on the stator has been reported for use in WECS [50]. The various topologies of multi-phase generator in WECS, for grid and off-grid operations, are also discussed in this section.

1.4.1 Brushless Doubly Fed Induction Generator And Split-Phase Induction Generators

To increase the suitability of DFIGs by making it maintenance free (by getting rid of slip rings) and better LVRT capabilities Brushless Doubly Fed Induction Generator (BDFIG) came into the picture, which have two stator windings with one nested loop rotor winding is reported in the literature [51]. BDFIGs have demonstrated better LVRT capability and have shown their suitability to work with variable speed operation. The power/flux coupling in BDFIGs between the two stator windings is through rotor circuit, whereas; direct power/flux coupling is not possible as both stators operate at different frequencies since they have different number of poles. BDFIGs akin DFIGs use converters with a quarter or lesser rating, and have

demonstrated good performance indices, but, with the increased cost of the specially wound rotor, they leave the scope for furthering in research with multi stator IGs for wind energy applications.

Other reported topology included split phase induction generators (SPIGs) [52-53] where there are two stator windings with squirrel cage rotor. The poles of both the stators are different akin to BDFIG and thus operate at different frequencies, hence do not provide direct coupling between two stators, and the sharing of power between stators is made via rotor, making transient response slower and incurring considerable losses. Control winding here also extracts/supply excess/deficit power required by the connected load through stator power winding via rotor circuit to maintain approximate rated values of voltage and frequency. power is transferred to load through power winding at power frequency whereas control winding works on a different frequency to maintain the air gap flux. BDFIG and SPIG generator topologies have their own drawbacks but, leaves window for the scope of work in configuration of generator with multiple stator windings.

1.4.2 Multi-Phase Induction Generators and their Merits

Recent advancement in generator topology is using IGs with a stator having higher number of phases, for example, five-phase, six-phase, nine-phase generator etc. The winding type and the angle between the phases make each machine suitable for different type of applications. There are various advantages of multi-phase generators which make them suitable for variable speed generations in WECS and are listed as:

- As the number of stator phases is more than three, the loss in one phase has

very less impact on generation as compared to conventional three-phase generators.

- Increased number of stator phase reduces the torque pulsations and also minimize the rotor harmonics.
- The total current in a poly phase machines/generators is now divided in more number of phases the RMS current per phase also reduces for the same rating three-phase generator. This property may be advantageous for the applications where high load currents are required.
- The reduced stator current also results in low cost of power electronic and magnetic circuits, as the cost of power electronic devices and magnetic circuits, increase many folds with a slight increase in the current rating.
- Reduction in stator current also results in reduced stator copper losses resulting in increased efficiency of the generator.
- Additional number of phases provides more degrees of freedom for various active, reactive and harmonic currents.
- The splitting of phase currents in the space at different angles also contributes to increased and more uniform power/ flux density in the air gap.

Aforementioned advantages of multi-phase IGs make them suitable for applications which require high reliability and high efficiency. But as the number of stator phases increase complexity of stator winding increases, and so the complexity of utilizing the generated power. Therefore the Dual Stator Induction Generators (DSIGs) are best suitable generators for WECS as they incorporate the advantages of multi-phase IGs along with their simpler stator construction as compared to other higher order multi-phase IGs.

1.4.3 Dual Stator Induction Generator

DSIGs have emerged as suitable alternative to both DFIG and BDFIG. In DSIGs two stator windings are used with squirrel cage rotor, and both the stators have the same number of poles and are excited with power frequency. Thus the transaction of power is through both windings to rotor and the flux coupling between both stators enhances the transient characteristics and efficiency of DSIG. The main limitation of narrow speed range of operation tends to include multi-gear systems for increasing wider range of operation. But this demerit is offset as the power density is high in such machines and rotor is cheaper with normal stator construction. The reliability of power generation is also increased in this case, as now two three-phase sets deliver power to the connected three phase loads. Normally the DSIG has been proposed with the symmetrical winding structure (60° phase difference between corresponding phases of the sets) for isolated application and with different kinds of load.

1.5 State of The Art: Configuration and Control Techniques of DSIG

Various topologies and configurations of DSIGs are used for WECS. Depending upon the winding structure DSIG may be categorized as

- **Symmetrical DSIG (SDSIG):** The relative angle between the two sets of three phase windings of the stator is 60° . The structure represents a symmetrical structure and hence the name SDSIG.
- **Asymmetrical DSIG (ADSIG):** The relative angle between the two sets of three phase windings is 30° . The stator winding looks asymmetrical and hence

the name ADSIG.

Some of the reported configurations and topologies using DSIG (Either SDSIG or ADSIG) are:

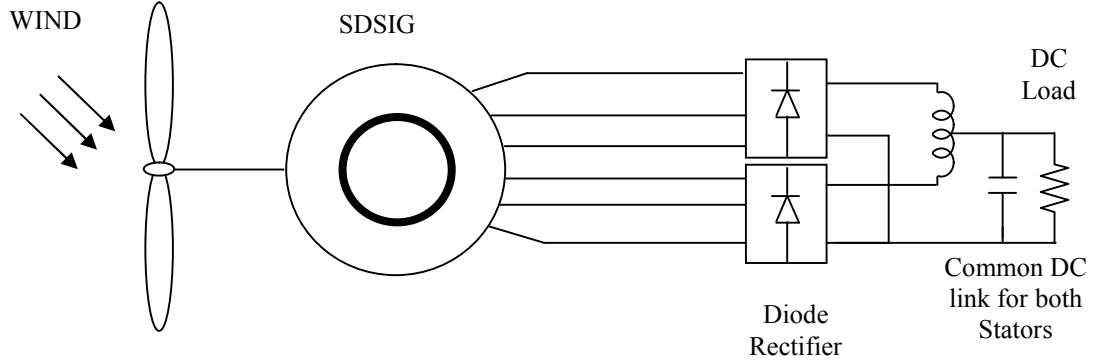


Fig. 1.5: DSIG with Diode Rectifier Feeding DC Load

- SDSIG in wind farms for DC load applications. Diode rectifiers are used to convert the AC power generated by SDSIG to DC power, and DC links of both the three phase winding sets are connected either in series or parallel to feed DC loads as shown in Fig.1.5 [54].

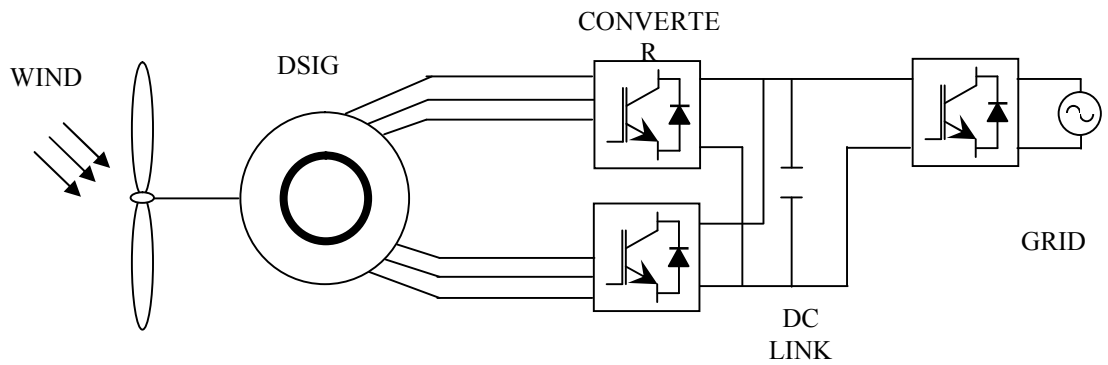


Fig. 1.6: DSIG with AC-DC Converter Feeding AC Grid

- In some applications diode rectifiers are replaced by controlled power electronic converters connected on both set of three phase winding sharing a

common DC bus and then another converter is used to convert this DC power back to AC. Now this can be either used directly by feeding the local AC load or may be connected to the grid. Block diagram for such topology is shown in Fig. 1.6 [55].

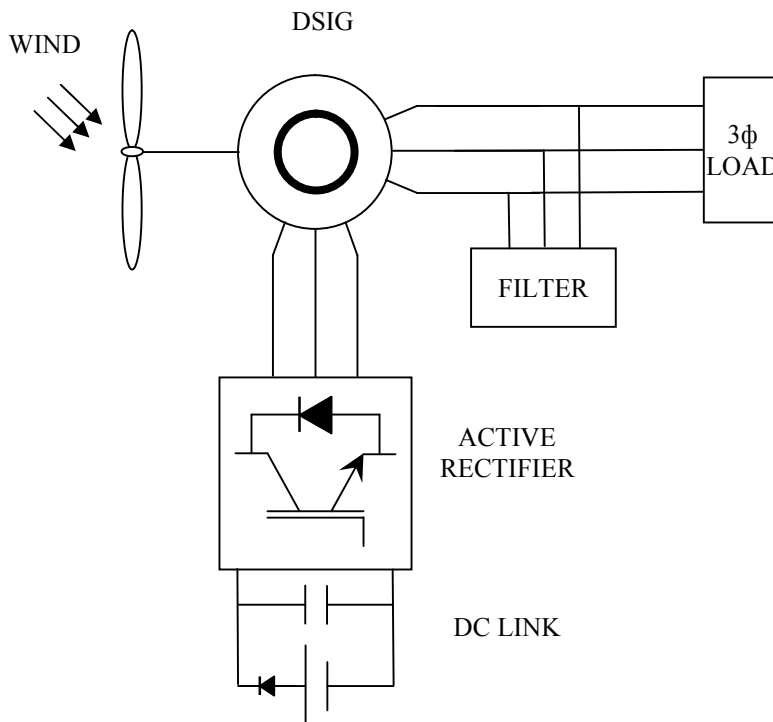


Fig. 1.7: DSIG feeding AC Load from Power Winding with Active Rectifier on Control Winding

- Other major applications of DSIG utilise one winding set of DSIG as power winding and the other winding set as control winding. Power winding is connected to either load or to the grid, whereas, control winding is used to control the reactive power demand required by the generator. Active rectifier is connected to the control winding for controlling the reactive power in smooth manner. Block diagram of this configuration is shown in Fig. 1.7 [56].
- Another configuration connects the DC side of above said converter to DC

loads/DC grid as observed in Fig. 1.8. This allow to feed both AC loads/grid and DC loads/grids from single WECS via DSIG [56].

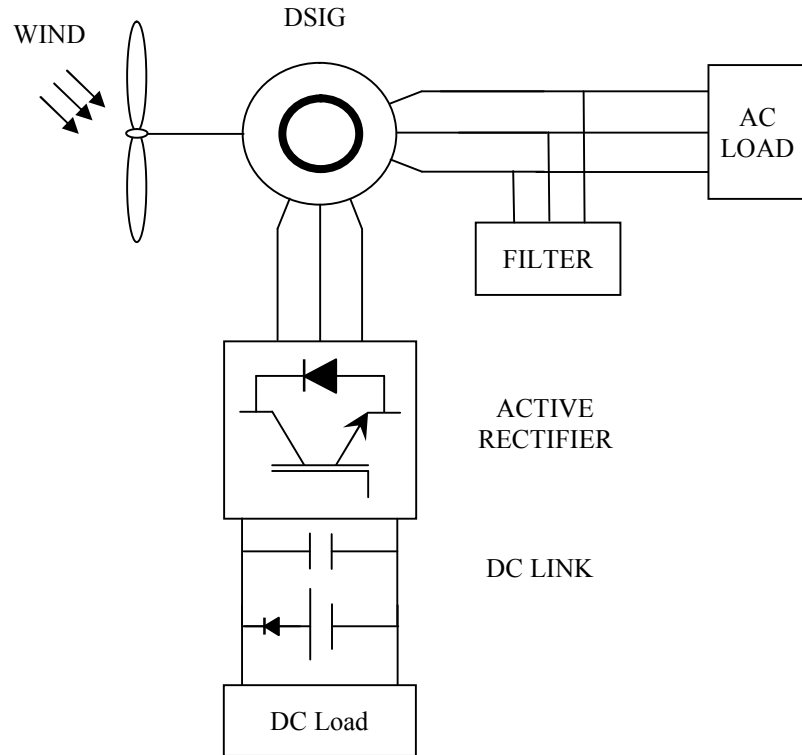


Fig. 1.8: DSIG feeding AC Load from Power Winding with Active Rectifier on Control Winding

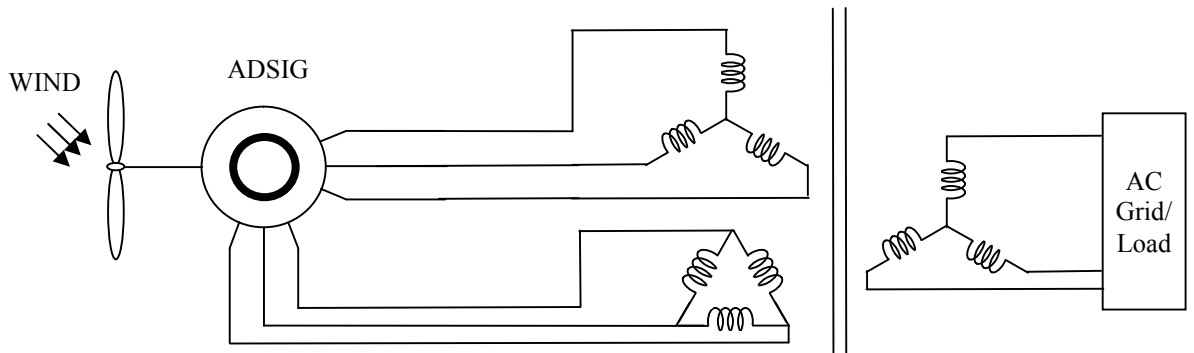


Fig. 1.9: DSIG Feeding AC Grid/ Load with Star-Star-Delta Three

- A typical application of DSIG using a star-star-delta transformer, for transfer of the power to feed AC loads via common AC feeder as shown in Fig. 1.9. This application is only pertains to asymmetrically ADSIG [57].

1.6 Scope of the Work

Among the various renewable energy sources wind is seen as one of the best alternative for power generation. And for extracting power from the wind, induction generators are the best alternative among different generator topologies for power generation in a WECS. From the various rotor and stator configurations for IGs, multi-phase stator induction generators, specialty DSIG, are picking pace for future generation topology for WECS. Therefore it is required:

- To study the dual stator induction generator for generation of power from wind source.
- To mathematically model, design and develop the dual stator induction generator.
- To analyse and compare the DSIG with the existing SCIG of similar ratings.
- To evaluate the performance of the DSIG for transient and steady state conditions.
- To study the applicability DSIG as three port network for interconnecting two different AC feeders, along with power harvesting from wind.
- To study the applicability of DSIG as reliable power source incorporating energy storage systems for curbing intermittency of power.
- To study the applicability of DSIG for powering rural loads utilizing the locally generated wind power.

1.7 Organization of thesis

To meet the objective of the thesis the thesis is organised as follow:

- **Chapter 2:** This chapter gives an overview of various literature available about existing generation topologies and the merits and demerits of these topologies reported in literature. The chapter also discuss about the research gap in the existing topology and the objective which need to be taken in the thesis.
- **Chapter 3:** A decoupled equivalent circuit is established and mathematical (d-q) modelling of ADSIG is made in the synchronous reference frame. A finite element model of ADSIG is also made in INFOLYTICA software for design of the machine by proper selection of stator, rotor and different material and thereon, different performance indices are recorded.
- **Chapter 4:** The mathematical models of ADSIG and SCIG, of similar ratings, are analysed and compared on the basis of the magnitude of inrush current, transient stability, their over-riding capabilities under low-voltage and fault condition. Further, the developed mathematical model of both the generators is compared through simulation on account of aforesaid parameters under MATLAB environment, and the same is also experimentally investigated on the developed prototype of same ratings. For investigation on fault ride through capabilities, one phase open condition is probed. The effect on current and flux of healthy phases and its capabilities to ride through such fault is also studied. A comparison is also drawn between ADSIG and SDSIG in simulation for generation of active power and requirements of reactive power driven at different speed ranges and their air-gap flux plots are investigated and compared for different conditions of loading.
- **Chapter 5:** Furthering in the investigation the ADSIG is used as a soft coupler for interconnecting two different AC feeders. The system is analysed as a three

port network with two electrical ports (two distribution feeders) and one port emanated from mechanical power input through a wind turbine. Active and reactive power flow transfer between these ports is studied both in simulation and in hardware during normal, low-voltage and single phasing conditions. Analysis of power routing is also studied for its connection with intermittent loads along with both simulation and hardware testing.

- **Chapter 6:** The efficacy of ADSIG is probed with a topology having energy storage system on one set of windings to emulate synchronous generator. A fixed active power commitment is probed for transfer to the grid over a wide range of wind speed variation. The performance of the system is evaluated for four different wind speed ranges. The investigation demonstrating the capability of ADSIG for interaction with four quadrants Energy Storage System (ESS) in curbing the intermittency for effective connectivity to the power grid is also carried out.
- **Chapter 7:** Application of ADSIG is further studied for providing electricity to remote areas fed from rural feeders on AC side along with harvesting of available wind energy by paralleling the WECS between the feeder and load bus. ADSIG for use as Gen-Former (acting as a generator when wind power is available and as a transformer when sufficient wind power is not available) is investigated through both simulations and experimentation on developed lab prototype. The investigation on overall loading reduction of the rural grid along with the study on the curbing of harmonic proliferation with asymmetrical stator structure is carried out to establish its reliability in terms of higher penetration of RES in the rural electricity distribution

Chapter 2

Survey of Literature

2.1 General

Difficulty in harnessing the wind power amidst wind speed variation called for the development of technologies involving both topologies of variable speed generator and power electronics converters. The prime concern for such development has been cost-effective, robust and reliable solution for energy generation. Induction generators are best suited as they can generate in a variable speeds cost-effective way having a robust and reliable part. The earliest use of induction generators dates back when power electronic converters were either not present or were in research labs. The first reported application of induction generator was in Danish generator concept, where a direct coupling of the generator with the grid was practised. Since then a number of generator- converter topologies have been practised to efficiently tap wind power and overcome the various challenges. The chapter based on a survey of Literature Bridge out key challenges while working with an induction generator for energy harvesting.

2.1 Issues of Generators Employed in WECS

The literature is surveyed based on the scope of work identified in the previous chapter, viz. inrush current in variable speed generators during inception, variable reactive power demand in variable speed generators, low voltage ride through and fault ride through capability in WECS and curbing of intermittent generation in WECS involving storage devices.

2.1.1 Inrush Currents in Variable Speed Generators

Fixed speed SCIGs may be connected to the grid directly or through any power electronic converter. When IGs are directly connected to the grid, large electrical transients are experienced in the grid (Point of Common Coupling, PCC) [58-60]. IGs when clutched with the grid draw huge reactive current to magnetize the core [1-3] [61-63]. These large reactive currents, the inrush currents, usually 4-6 times of the rated current, cause a dip in the voltage at the terminals (PCC) [64-75]. This poses a major power quality problem like voltage flicker and poses a threat to the healthy operation of the power system [58-63] [69-75]. The inrush also results in large fluctuations and spikes in the torque of the drive gear train [58-60] [64-68].

The problems of power quality and torque spikes can be eliminated by reducing the magnitude of the inrush current demand [73-75]. The inrush current demand is reduced by using soft-starters or by connecting resistances in series between grid and IG [1-3] [58-75]. The soft-starters are based on thyristor technology with two thyristors connected in anti-parallel in each phase [58-60] [64-75]. Initially, high resistance is connected in series and as the air gap starts getting magnetized the value of resistance is decreased and finally the resistance is cut-off as the air gap gets fully magnetized [61-63]. This method is used when the rotor speed is in between 75% - 102% of rated speed [61-63]. Soft starters are connected when the rotor speed reaches 70% - 90% of rated speed [64-68]. The firing angle of thyristors is gradually decreased from 90° to zero resulting in a gradual rise of each phase current from zero to the rated value [64-68]. The soft-starter module is in operation for a small period of time and when the rated current starts to flow in each phase then it is bypassed by a breaker. Each module of soft-starter is equipped with its turn-on, turn-off and protection circuit

[64-68].

The efficiency of IGs employing soft-starter module is lesser during the starting period due to some ohmic losses [64-68]. The reactive power drawn by the IG using resistance method is lesser as compared to that of the soft-starter method [61-63]. A detailed comparison between the two methods is reported [61-63]. The advantage of the soft-starter method is that the peak current demand is reduced to lesser than twice of rated current [69-72].

Another advantage of the soft-starter method is that the inrush current is totally controlled and thus the voltage build-up is gradual [73-75]. On the other hand, the disadvantage of soft-starters is in costly modules; an initial low power factor and poor efficiency along with a high content of current THD during the starting period. Resistance method is a cheaper solution and the current THD is relatively good but in this case, the efficiency of the system is very poor even poorer than that of soft-starter [73-75]. Authors in [73-75] have also simulated the damping of inrush current utilizing only one resistance instead of three resistances. The WECS topology equipped with full rating BTB power electronic converters, the control algorithm gets modified to quench the inrush current and its ill effects. It is observed from the literature survey that inrush current is a very harmful and deteriorating for IGs and if proper remediation is not employed it may have negative effects on the health of wind farms in terms of cascading effect, resulting in shutting down of others WECS, which adversely affect the power system at large.

The methods for controlling the inrush currents are also either very costly, or inefficient, or are very complex. Thus there is a need for devising a system which

demands lesser inrush currents and is capable of inherent additional control for quenching the inrush current. Various techniques are adopted by researchers to curb the sudden demand of current and such changes this usually comes with increased cost, complexity and unwanted harmonics in the system. A generator which can inherently control its inrush current demand due to its winding configurations would emerge as a better alternative.

2.1.2 Reactive Power Demanded by Variable Speed Generators

The reactive power demand of load is catered by grid; since SCIG itself looks upto the grid for its own requirements, thus, varies as per the loading on the generator terminals vary [76-80]. Moreover, requirements of constant flux linkage with variable speed operation also demand variable reactive power from the grid to stay with stiff voltage requirements at the PCC of the grid. Such reactive power requirements escalate to a high value which it is meant for a wind farm. The continuous variable demand of reactive power creates poor power quality issues in a wind farm [61-63]. The reactive power demand of SCIGs cannot be self compensated and it is neither controllable [46-49] [76-80]. The reactive power demand of SCIGs can be met partially or fully through external means by either using capacitor banks besides grid when operating in grid-connected mode to offload the burden from the grid [64-68] [76-80]. When capacitor banks are used for local support of reactive power then is ensured that the current THD should be less than 5% [1-3].

Unlike synchronous generators, SCIGs are unable to regulate the voltage at the PCC of the power system due to their demand of varying reactive power [46-49]. The reactive power demand of IGs operating with variable speed turbines has a better control over

their reactive power demand, reflecting in better control on the terminal voltage at PCC [8-12]. The control is further facilitated by modifying the control algorithm of the interfacing BTB power electronic converter interfaced between SCIG terminals and the grid [1-3] [14-19]. However, quenching of reactive power demand in a DFIG is reported by using a power electronic converter at the rotor terminals [69-72]. Moreover, simple structure, lower cost, robust structure and maintenance free approach goes to the advantages of SCIG and often overcome its shortfall according to continuous and variable reactive power demands [21-24].

DFIG comes with costly rotor structure and complex control circuitry. Whereas, the solution with BTB converter further mounts to costly hardware and there is a need for an exploration of SCIG based cheaper generating unit embedding provisions for reduction of reactive power demand under various operating conditions.

2.1.3 Low Voltage Ride Through and Fault Ride through Capability for WECS

The power system is usually subjected to various faults and overloads, often resulting in voltage dips leading to a number of deteriorating consequences. The power systems fed by IGs the situation becomes even grimmer since IGs need reactive power for magnetizing their air-gap. They suffer during the fault heavily and whenever any fault is cleared IGs draw huge reactive power from the grid to compensate its shortfall. This results in recurrence of further sudden dips in voltage at the generator terminals. Due to this transient in stator currents become visible proliferating power quality issue in the entire power system and often result in cascading failures in wind farm. The magnitudes of such transient currents are very dangerous for the rotor circuitry and

often damage it permanently [28-30].

Similarly other situations, including faults caused by sudden asymmetry of rotor/stator circuitry impacts in the form of huge transients resulting in oscillations and vibrations in a mechanical structure. If the quantum is high, it often results in stalling of operation due to ride through incapability.

DFIGs witnesses decoupling of electrical and mechanical systems, thus these transient currents pose even a greater threat to the generator and the associated power electronic converters [31-36]. Generators with a larger number of phases are reported to have a lesser magnitude of ill impacts during any phase loss (stator asymmetry) as compared to IGs with lesser number of phases [81-89]. Accordingly, the effects of phase loss or low voltage will have a lesser impact on the VSC based HVDC transmission employed for power evacuation from wind farm populated with IGs for offshore power transmission [58-60].

The power system is prone to unpredictable faults and low voltage conditions, and the participating grid coupled generating units are required to face these conditions with the capabilities of ride through such situations conforming to appropriate grid codes. Various schemes are adopted for overcoming such situations but the cost and complexity of the overall system becoming impeding factors. Hence there is a need for exploitation of cheaper IG units embedding capability to ride through such conditions in the machine structure which are cost-effective and should be able to keep generating even in such adverse conditions.

2.1.4 Requirement of Energy Storage During Intermittent Generation in RES

There are a number of advantages of wind energy resources over conventional energy sources, except their unpredictable and intermittent nature which results in intermittency of power posing reduced reliability [14-19]. Thus for a power system with deep penetrations of wind energy resources, there is a need for back up energy storage systems [14-19] [37-38]. With the help of energy storage systems, the electricity generation and demand become decoupled for better contingency planning [8-12]. It is observed that for eliminating the power intermittency problems of wind energy conversion systems the energy storage systems paves the way for their better penetration and maintains the reliability of power system.

2.2 Conventional Wound and Special Wound Generators

Environmental concerns and depleting stocks of fossil fuels have forced researchers to go for renewable sources of power generation [25-27] [90-93]. The basic disadvantage of renewable sources is their intermittency and unpredictable nature [39-41]. As the renewable sources are intermittent in nature to utilize their output in a better manner these sources are generally grid connected [39-41]. The focal points considered in any generator-converter topology for a wind energy conversion system are its transient behaviour, operation under low voltage and faulty conditions in the grid and the grid interconnectivity [13] [64-68] [90-93]. Among the various contenders available used for generation of electricity in a wind energy conversion systems SCIGs have an upper-hand due to their cheap and robust structure with inbuilt characteristics of short-circuit protection [21-24][28-30][42-45][76-80]. Still, the majority of power generation

in wind farms is carried out using SCIGs with least power electronic interfaces [25-27]. Hence to further elaborate the issues associated with different generators a survey of literature is carried out for conventional three-phase and multi-phase generators used in WECS.

2.2.1 Issues of Conventional Three Phase Generators Connected in WECS

IGs are connected with the grid either with fixed speed turbines or with variable speed turbines. Fixed speed turbines are connected to grid either directly or via soft-starter [64-68]. In Danish concept of generation single pole, SCIGs with fixed ratio gearbox is connected to the grid with a transformer [5-7] [14-19] [25-30] [42-45]. Generated power is controlled by stall and pitch control methods [28-30]. By controlling the rotation of turbine blades active power is controlled in active stall or pitches control methods, whereas power is controlled in the stall controlled turbines with a smooth overshoot and lesser output is produced at higher speeds [28-30].

The major drawback of SCIGs is their variable reactive power demand [64-68]. External capacitor banks (in both isolated mode and grid-connected mode) or grid (only in grid-connected mode) can be used for supplying this load dependent reactive power demand of SCIG [14-19] [46-49] [76-80]. Local capacitor banks connected for reactive power compensation of IGs often cause voltage instability issues in the power systems with deep penetration of wind farms [28-30]. The voltage profile of the power system fluctuates a lot whenever there is any fault or heavy loadings or sudden drawn of large reactive current. These voltage variations put a restraining factor for the wind farms to generate and transfer adequate power in a power system [58-60]. SCIGs with

partial of full rating power electronic converters have lesser requirement of reactive power externally and output active power is also controlled in a better way but with add-on of extra cost and increased complexity of control [14-19] [25-27] [37-38] [42-45]. Moreover, the efficiency of generators is about 85% and that of power electronic converters is near-about 96% [39-41].

Large variations in the wind speed not only reduce the net output but also put unwanted mechanical stress on the rotor shaft [42-45]. To capture more wind power variable speed turbines are incorporated and due to this the mechanical stress is also greatly reduced and the acoustical noise is also reduced considerably [14-19] [13]. The increased system stability and increased power quality add to the superiority of VST [14-19]. Researchers in [55] have also reported the use of the fuzzy logic technique for optimizing the generation process [55].

Thus it is observed that SCIG is the cheapest generator topology available till date but with add-on the requirement of variable reactive power. This demand for reactive power is load dependent is uncontrolled until any power electronic interface is utilized. PMSG is best suited for a small-scale generation due to their increased efficiency but there are add-on costs of the permanent magnet and full rating power converters. In Static Kramer drive generation is possible for wind speeds higher than the rated value also [21-24]. DFIG have a total control over the reactive power demand and can operate in a large range of wind speed but the loss of inertia makes this topology highly vulnerable for low voltage and fault conditions in a power system. Thus there is need of a generator which is cheap, robust in nature has inherent fault-tolerant capability and has control over its reactive power and can generate in both super-synchronous and sub-synchronous speeds at a cheaper cost.

2.2.2 Issues of Multi-Phase Generators Connected in WECS

Authors in [94-98] have suggested that as the number of phases increases there is an increase in the KVA rating of machines for example 29% increase for a six phase machine and 54% for a nine-phase machine as compared to a three-phase machine. By increasing the number of phases there is a reduction in insulation thickness and increase in conductor cross-sectional area resulting in a higher allowable current density [94-101]. Keeping the same power and current levels it is observed that there is a reduction of voltage levels also in multiphase machines; 75% and 60% in a six-phase machine and nine phase machine w.r.t. the voltage of a three-phase machine [94-98].

Investigations carried out in a show that the torque ripples are greatly reduced in High Phase Order (HPO) machines [81-89] [99-101]. A machine with a phase belt of 30° showed better performance characteristics as compared to machines with 0° and 60° phase belts [102-110]. When the operating frequency was intentionally increased to six times the rated frequency there was an increase of 25% in the torque ripple in a 0° and 60° phase belt machines [102-110]. Whereas for a 30° phase belt machine there was an increase of just 5% in the torque ripple even when the operating frequency was intentionally increased to twelve times the rated frequency [102-110]. The line current showed higher harmonic content for a 30° phase belt as compared to 0° and 60° phase belt machines. With the increase in the number of phases there is a decrease in phase belt which results in a higher harmonic winding factor, but in spite of this, the harmonic winding factor for the fundamental air-gap harmonic is considerably reduced with increasing number of phases [111-112].

In a semi twelve phase, six pole machine and semi eighteen phase for pole machine there is only one coil per pole per phase which gives larger winding factor resulting in a high power factor as compared to other machines [81-89]. These machines also have the highest torques due to their special stator structure as compared to other machines [81-89]. As the numbers of phases are increased the harmonics in the rotor circuit is also reduced giving lesser rotor I^2R losses [81-89]. The reliability of power delivery is greatly affected by the number of phases of the generator. [50][52][54] have done extensive research in this field and have concluded that as the number of phases of any generator are increasing the reliability of operation increases with loss of any of its phases. The torque pulsations and the ohmic losses in the rotor circuitry are greatly reduced with increasing number of generator phases [50]. Torque pulsations are greatly reduced in a six-phase machine having 30° phase belt [50]. [50] also suggested that the method of symmetrical components can be used for dynamic analysis of multiphase machines during unbalanced operations. Gearbox poses a major threat concerning the reliability in a VST and the reliability can be increased by replacing the gearbox system by utilizing multi-pole generators [4].

The renewable energy sources are available everywhere but their reliability throughout a period is very poor [37-38]. DFIGs operate in a large range of wind speed as compared to SCIGs due to the utilization of bidirectional power converters by decoupling the electrical and mechanical systems [48]. This results in a loss of generator inertia, which is harmful to a power system with deep penetration of renewable energy or in a weak grid [48].

With the increased number of phases, the reliability of power supply increases and the cost of power electronic converters and a magnetic circuit is also greatly reduced as

for a fixed voltage and power rating the current per phase is reduced.

2.2.3 Emergence of Dual Stator Generators for WECS

In Dual Stator Induction Generator (DSIG) there are two sets of stator windings. Depending upon the relative phase shift between the two stator windings the DSIG is classified as Symmetrical DSIG (SDSIG), when the relative phase shift is 60° and Asymmetrical DSIG (ADSIG), when the relative phase shift is 30° . One set of three-phase winding is used as a control winding and the other three-phase winding set is used as power winding in the isolated mode of operation [113].

A battery bank connected with a four switch inverter is used for providing excitation at the control winding side to control the terminal voltage at load end (power winding side) [113]. Power winding is used to feed the load and local capacitor banks are connected at the power winding set for providing fixed reactive power [113]. DSIG is used to feed DC loads using series-parallel connected AC-DC PWM rectifiers [114]. Both the three-phase winding sets are wound for a different number of poles [114]. DSIG is also used as a variable frequency AC (VFAC) generator with control winding connected to a static excitation controller (SEC) and power winding feeding both inductive and capacitive loads [115]. Space Vector Modulation technique is utilized in [116] for a decoupled control of DSIG [116]. DC loads are fed by power winding whereas SEC regulates the power winding voltage [116]. The voltage of control winding is kept higher than the power winding to reduce switching losses in SEC [116].

A novel direct power control (DPC) is shown to have better performance by

elimination of inner current loops and PWM modulation blocks for automotive power generation [117]. An AC-DC boost PWM rectifier connected in series with DSIG is proposed for different DC voltage levels [118]. The stators of DSIG are wound for a different number of poles [9f]. Optimal design of self-excitation capacitor is done and the analytical results are compared with experimental results in [119]. A PWM voltage source inverter connected with a DC source is connected at the control winding to feed AC load connected at the power winding side [120]. It is shown that harmonics induced at power/ control winding are not reflected in the control/ power winding of DSIG as both the windings are connected electromagnetically and isolated physically [120]. A new topology of DSIG for a large range of operating speed and reduced rating of SEC is investigated in [121] where both the stators are having a similar number of poles. Multi-phase generators used for feeding DC loads show that the DC voltage ripple ratio decreases with increasing number of generator phases [122].

The regulation of load voltage for delivering requisite active power to load is achieved by connecting one winding set of DSIG to a voltage source inverter and the other winding set connected to a three-phase load [113]. 3D finite element analysis shows that the dual stator arrangement in a hybrid excited dual stator synchronous generator results in an increased power density, control over air-gap flux and the output voltage [123]. Researchers in [119] have carried out the optimal design of excitation capacitance for voltage generation in DSIG and the required value of capacitor for self-excited is also calculated for achieving maximum efficiency. A novel stator voltage oriented control strategy for DSIG feeding DC loads and operating at high speeds is developed for conditions of variable load and wind speeds showing considerable improvement in the electromagnetic compatibility of the system [122].

Dual stator arrangement used in a doubly excited brushless reluctance machine employing field oriented control for generating electrical power results in an increased efficiency, enhanced reliability, reduced costs and improved controllability and flexibility over active and reactive power [124]. A detailed mathematical modelling and analysis of self-excited DSIG are presented in [125]. Various control schemes like sliding mode and fuzzy logic are also employed in simulation for the conditions of a step change in loading conditions and dynamics during self-excitation. A comprehensive comparison of the rating of the inverter connected with DSIG and SCIG both feeding DC loads is performed in [126]. The rating of the inverter is very less for DSIG feeding a DC load as compared to SCIG feeding the same DC load. Moreover, the reduction in rating is up to 43%, when the inverter is placed on the control winding whereas the reduction in rating of the inverter is smaller, up to 30% when the inverter is placed on the main winding.

In a conventional DSIG, there are two three-phase windings, power winding and a control winding. When such DSIG is used for feeding DC loads there are large harmonics in the load current associated with large noise and vibrations. To overcome these disadvantages a 6/3 phase DSIG is presented in [127] where there are two three-phase power windings shifted by 30° . This results in a great reduction of load current harmonics, noise and vibrations but the increased number of phases increases the winding and control complexities. Researchers in [128] have performed mathematical modelling of DSIG and have shown its superiority for power generation in wind farm and hydropower plants under variable speed conditions.

Since the introduction of DSIG in wind farms extensive research has been done for its grid connected and off-grid connected modes of operation. Majority of DSIG

topologies deliver power to AC or DC loads via one winding set (power winding) and the other winding set (control winding) is used for controlling the terminal voltage of power winding and maintaining high power quality. Both the windings of DSIG are having either same number of poles or a different number of poles and accordingly the control circuitry is modified.

2.3 Scope of the Work

Literature survey reveals that SCIGs are best suited for WECS due to their cheap and robust nature. The add-on advantage of SCIGs is their inherent fault-tolerant capability. The intermittent nature of wind makes the application of energy storage a must to maintain a reliable power flow. The variable reactive power demand makes the SCIG inferior as compared to PMSG and DFIG where the power factor can be easily controlled. PMSG and DFIG come with added cost and complexity of operation along with a demerit of poor LVRT and FRT capability. Overall there is still a need for such generating unit which is capable to inherently control its reactive power demand and has good LVRT and FRT capability, which should be cheap and the control should be easier. DSIG comes as a better contender which satisfies the above requirements and is being tested for various such situations. A number of DSIG topologies are reported in the literature for grid and off-grid modes feeding AC or DC loads with symmetrical and asymmetrical stator windings. The literature survey has also shown that asymmetrical DSIG (ADSIG) has better performance characteristics as compared to symmetrical DSIG (SDSIG). Due research is remaining to test ADSIG for the transient behaviour during the starting period and conditions of low voltage and faults at the grid side. Power routing from both the winding sets is also to be investigated

along with checking of self-compensation of reactive power demand.

2.4 Conclusion

A comprehensive literature review is done on the identified research gaps of the previous chapter. The various topics covered are broadly classified under the headings of inrush current of generators, the reactive power demand of variable speed generators, ride through capabilities of generators for WECS and the requirement of energy storage systems for RES. The literature review is further elaborated to include various issues of convention wound (Three Phase) and special wound (Multi-Phase) generators connected in a WECS. Finally, the literature review for dual stator generators is also done to access their merits and topologies adopted for generation in WECS. It is concluded that ADSIG has a promising future to be used for generation in WECS, but a detailed analysis of ADSIG is still left out to be carried. Hence the analysis of ADSIG during transient and steady state periods, in respect to inrush current (forced or transient response) and reactive power demand (natural or steady-state response), is carried out. The performance evaluation of ADSIG as a three port network for power routing between two different feeders under balanced grid conditions and abnormal grid conditions, like low voltage and one phase open faults is carried out. During intermittent wind conditions, the suitability of energy storage systems with ADSIG is also evaluated. Application of ADSIG for rural electrification and effect of loadings on the net reactive power demand is also done in forthcoming chapters.

Chapter 3

Modelling and Design of Dual Stator Induction Generator

3.1 General

The superiority of the multi-phase induction generator has been established in literature while making a comparison of different asynchronous generator topologies for wind power generation. This chapter studies the steady state and dynamic behaviour of multi-phase induction generators (Asymmetrical Dual Stator Induction Generator, ADSIG). A mathematical model of the same is modelled, developed and verified through the finite element base design software (INFOLYTICA MOTORSOLVE). Based upon this verified design, a hardware prototype of Asymmetrical DSIG (ADSIG) is tested for the similar performance characteristics. Machine parameters are also calculated to enable furthering of research on ADSIG system for generation of power through coupling with a wind turbine.

3.2 Mathematical Modeling of ADSIG in MATLAB

The modelling of ADSIG is similar to the modelling of conventional three-phase induction machines. Since the steady-state model and an equivalent circuit of ADSIG cannot be applied for analysing transients arising during load and speed changes, so dynamic modelling of ADSIG is done to study the effects of varying current/voltage and load perturbation. The differential equations of voltage/ current of induction machines are complicated (non-linear) due to the presence of time-varying

inductances. Moreover, the rotation of the machine at different speeds makes these equations even more complicated as the electrical circuit is in a rotating frame and the reluctance is also varying accordingly, which makes modelling even more complicated. So the dynamic modelling is done by transforming the two sets of three phase, which are phase apart by 30° , through two different sets of two-phase system, where the two sets of direct and quadrature axis are phase displaced by 30° with each other as shown in Fig. 3.1 and Fig. 3.2.

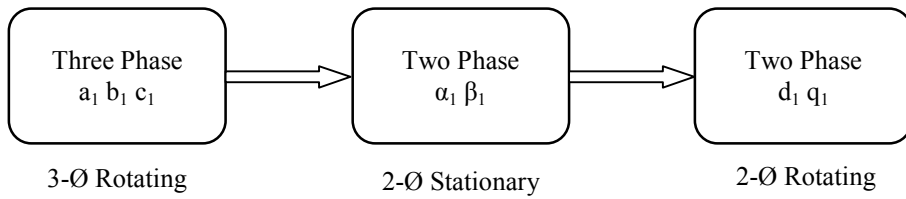


Fig. 3.1: Three Phase to Two Phase Conversion of a_1 b_1 c_1 Phases

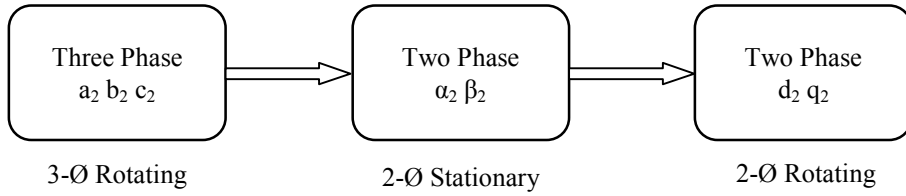


Fig. 3.2: Three Phase to Two Phase Conversion of a_2 b_2 c_2 Phases

For the conversion of three-phase quantities to two-phase Clarke and Park's transformations are used. The transformation equations for the first set of three-phase (a_1 , b_1 , c_1) are expressed in equation (3.1) to equation (3.3). Using Clarke transformation the three phase rotating signal is transformed to two-phase stationary signal, alpha (α) beta (β), as follows:

$$\begin{bmatrix} f_{\alpha_1} \\ f_{\beta_1} \end{bmatrix} = \frac{2}{3} \begin{bmatrix} \cos(0) & \cos(\gamma) & \cos(2\gamma) \\ \sin(0) & \sin(\gamma) & \sin(2\gamma) \end{bmatrix} \cdot \begin{bmatrix} f_{a_1} \\ f_{b_1} \\ f_{c_1} \end{bmatrix} \quad (3.1)$$

With the help of Park transformation this two-phase stationary signal is transformed to two-phase rotating signal, as follows:

$$\begin{bmatrix} f_{d_1} \\ f_{q_1} \end{bmatrix} = \begin{bmatrix} \cos \emptyset & \sin \emptyset \\ -\sin \emptyset & \cos \emptyset \end{bmatrix} \cdot \begin{bmatrix} f_{\alpha_1} \\ f_{\beta_1} \end{bmatrix} \quad (3.2)$$

Finally, two-phase rotating signal from a three-phase rotating signal is obtained as shown in equation (3.3).

$$\begin{bmatrix} f_{d_1} \\ f_{q_1} \end{bmatrix} = \frac{2}{3} \begin{bmatrix} \cos(\emptyset) & \cos(\emptyset - \gamma) & \cos(\emptyset + \gamma) \\ -\sin(\emptyset) & -\sin(\emptyset - \gamma) & -\sin(\emptyset + \gamma) \end{bmatrix} \cdot \begin{bmatrix} f_{a_1} \\ f_{b_1} \\ f_{c_1} \end{bmatrix} \quad (3.3)$$

The other set of three-phase (a_2 b_2 c_2) which is displaced by 30° from the first set (a_1 b_1 c_1), is also converted to two-phase as given in equations (3.4 – 3.6).

Clarke transformation for the second set of three phases is given as:

$$\begin{bmatrix} f_{\alpha_2} \\ f_{\beta_2} \end{bmatrix} = \frac{2}{3} \begin{bmatrix} \cos(30) & \cos(\gamma + 30) & \cos(2\gamma + 30) \\ \sin(30) & \sin(\gamma + 30) & \sin(2\gamma + 30) \end{bmatrix} \cdot \begin{bmatrix} f_{a_2} \\ f_{b_2} \\ f_{c_2} \end{bmatrix} \quad (3.4)$$

Applying Park transformation on equation (3.4):

$$\begin{bmatrix} f_{d_2} \\ f_{q_2} \end{bmatrix} = \begin{bmatrix} \cos \emptyset & \sin \emptyset \\ -\sin \emptyset & \cos \emptyset \end{bmatrix} \cdot \begin{bmatrix} f_{\alpha_2} \\ f_{\beta_2} \end{bmatrix} \quad (3.5)$$

Finally putting value of $\begin{bmatrix} f_{\alpha_2} \\ f_{\beta_2} \end{bmatrix}$ from equation (3.4) into equation (3.5):

$$\begin{bmatrix} f_{d_2} \\ f_{q_2} \end{bmatrix} = \frac{2}{3} \begin{bmatrix} \cos(\emptyset + 30) & \cos(\emptyset - (\gamma + 30)) & \cos(\emptyset + (\gamma + 30)) \\ -\sin(\emptyset + 30) & -\sin(\emptyset - (\gamma + 30)) & -\sin(\emptyset + (\gamma + 30)) \end{bmatrix} \cdot \begin{bmatrix} f_{a_2} \\ f_{b_2} \\ f_{c_2} \end{bmatrix} \quad (3.6)$$

Likewise, the reverse transformation from rotating two-phase to rotating three phases is given in Fig. 3.3 and Fig. 3.4.

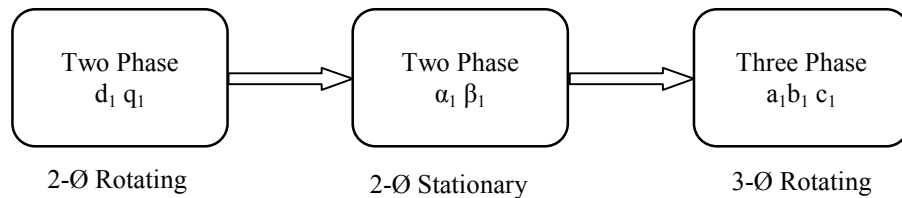


Fig. 3.3: Two phase to three phase conversion of d_1 q_1 phases

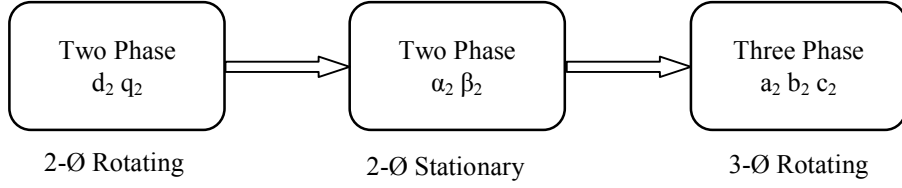


Fig. 3.4: Two phase to three phase conversion of d_2 q_2 phases

Using inverse Park transformation rotating two phases are transformed to stationary two-phase and given in equation (3.7).

$$\begin{bmatrix} f_{\alpha_1} \\ f_{\beta_1} \end{bmatrix} = \begin{bmatrix} \cos(\emptyset) & -\sin(\emptyset) \\ \sin(\emptyset) & \cos(\emptyset) \end{bmatrix} \cdot \begin{bmatrix} f_{d_1} \\ f_{q_1} \end{bmatrix} \quad (3.7)$$

Now, this stationary two-phase set is transformed to rotating three-phase set using inverse Clarke transformation and given in equation (3.8).

$$\begin{bmatrix} f_{a_1} \\ f_{b_1} \\ f_{c_1} \end{bmatrix} = \begin{bmatrix} \cos(0) & \sin(0) \\ \cos(\gamma) & \sin(\gamma) \\ \cos(2\gamma) & \sin(2\gamma) \end{bmatrix} \cdot \begin{bmatrix} f_{\alpha_1} \\ f_{\beta_1} \end{bmatrix} \quad (3.8)$$

Finally, set of three-phase signals as given by equation (3.9) are obtained.

$$\begin{bmatrix} f_{a_1} \\ f_{b_1} \\ f_{c_1} \end{bmatrix} = \begin{bmatrix} \cos(\emptyset) & -\sin(\emptyset) \\ \cos(\emptyset - \gamma) & -\sin(\emptyset - \gamma) \\ \cos(\emptyset + \gamma) & -\sin(\emptyset + \gamma) \end{bmatrix} \cdot \begin{bmatrix} f_{d_1} \\ f_{q_1} \end{bmatrix} \quad (3.9)$$

Similarly, the other set of three-phase a_2 b_2 c_2 is obtained by using reverse transformations:

The second-set of rotating two-phase is transformed to stationary two-phase set as in equation (3.10) using inverse Park transformation.

$$\begin{bmatrix} f_{\alpha_2} \\ f_{\beta_2} \end{bmatrix} = \begin{bmatrix} \cos(\emptyset) & -\sin(\emptyset) \\ \sin(\emptyset) & \cos(\emptyset) \end{bmatrix} \cdot \begin{bmatrix} f_{d_2} \\ f_{q_2} \end{bmatrix} \quad (3.10)$$

Similarly, the stationary two-phase set is transformed by rotating three phase as given

in equation (3.11) and finally is shown in equation (3.12).

$$\begin{bmatrix} f_{a_2} \\ f_{b_2} \\ f_{c_2} \end{bmatrix} = \begin{bmatrix} \cos(30) & \sin(30) \\ \cos(\gamma + 30) & \sin(\gamma + 30) \\ \cos(2\gamma + 30) & \sin(2\gamma + 30) \end{bmatrix} \cdot \begin{bmatrix} f_{\alpha_2} \\ f_{\beta_2} \end{bmatrix} \quad (3.11)$$

$$\begin{bmatrix} f_{a_2} \\ f_{b_2} \\ f_{c_2} \end{bmatrix} = \begin{bmatrix} \cos(\emptyset + 30) & -\sin(\emptyset + 30) \\ \cos(\emptyset - (\gamma + 30)) & -\sin(\emptyset - (\gamma + 30)) \\ \cos(\emptyset + (\gamma + 30)) & -\sin(\emptyset + (\gamma + 30)) \end{bmatrix} \cdot \begin{bmatrix} f_{d_2} \\ f_{q_2} \end{bmatrix} \quad (3.12)$$

Where, γ is the angle between any two phases (for a balanced system γ is 120°).

Generalizing the transformation equations can be written as:

$$f_{dq} = kTf_{abc} \quad (3.13)$$

And for Pseudo-inverse conversion, it is written as:

$$f_{abc} = k_i T^t f_{dq} \quad (3.14)$$

Where,

- T is a matrix such that $(2/3) T.T^t = U$ (Unity Matrix)
- k and k_i are constant having a relation $k_i = \frac{2}{3k}$ and the values of both depend upon the type of transformation done.

The different types of conversion are namely:

- (a) For equal magnitudes of three-phase and two-phase signals.
- (b) For equal power in three phases and two-phase.
- (c) For the magnitude of the three phase signal to be two-third ($2/3$) of the magnitude of two-phase signal.
- (d) For the rms of three-phase signal to be equal to the amplitude of two signal.

The different values of 'k' and ' k_i ' for these (a, b, c and d) transformations are

summarized in Table 3.1.

	a	b	c	d
k	2/3	$\sqrt{(2/3)}$	1	$\sqrt{2/3}$
k_i	1	$\sqrt{(2/3)}$	2/3	$\sqrt{2}$

Table 3.1: Different values of ‘k’ and ‘k_i’ for common conversions

For easy understanding and observation of the performance of machines different observer platforms, (reference frames), are used for understanding the complex operation of the machine which is governed by nonlinear equations. With the help of reference frame theory, the number of governing equations of voltages/ currents/ fluxes is reduced. Also, the time-varying nature of these equations changes to the time-invariant type and it becomes easy to analyze and apply different computation techniques. The three commonly used reference frame theories are stator reference frame theory, rotor reference frame theory and synchronous reference frame theory. Usually, ‘ τ ’ is the angular position of the reference frame and ‘ ξ ’ is the difference between the position of the reference frame and the electrical position of the rotor.

Under Synchronously Rotating Reference Frame, since the frame is rotating in synchronism with rotating magnetic field and both stator and rotor variables are transformed to a variable of the synchronous rotating frame, thus transforming all the sinusoids to dc signals. The method enables the decoupling of flux to express the modelling of the machine in quadrature components.

Here the angular position of reference frame is given as:

$$\tau = \omega_s t \quad (3.15)$$

As the differentiation of angular position gives the angular velocity:

$$\omega = \frac{d}{dt} \tau \quad (3.16)$$

Comparing equation (3.15) and equation (3.16):

$$\omega = \omega_s \quad (3.17)$$

Also the difference between the position of rotor and reference frame is given by:

$$\xi = \tau - \tau_r \quad (3.18)$$

Using equations (3.15) and equation (3.18) ξ' is written as:

$$\xi = \omega_s t - \tau_r \quad (3.19)$$

Differentiating equation (3.19) with respect to time, the difference of synchronous angular velocity and angular velocity of the rotor are obtained as shown in equation (3.20).

$$\frac{d}{dt} \xi = \omega_s - \omega_r \quad (3.20)$$

The equivalent circuit of ADSIG generator in the d-q reference frame is shown in Fig. 3.5 and Fig. 3.6 respectively. Two balanced three-phase windings displaced to each other by 30° (asymmetrical) and 60° (symmetrical) are considered for modelling of ADSIG with following assumptions:

- Air-gap is uniform and the windings are having sinusoidal distribution around the air-gap and the magnetic saturation and core-losses are neglected.
- The voltage equations are written in d-q axis for ADSIG in the synchronous reference frame. The terminal voltages are represented as the sum of drop

across the resistance, transformational voltage and rotational voltage.

The quadrature axis and direct axis voltage equation for both stators are given from equations (3.21 a) to (3.23 b) [129]

$$V_{qs1} = -R_1 i_{qs1} + \frac{d}{dt}(\psi_{qs1}) + \omega(\psi_{ds1}) \quad (3.21 a)$$

$$V_{ds1} = -R_1 i_{ds1} + \frac{d}{dt}(\psi_{ds1}) - \omega(\psi_{qs1}) \quad (3.21 b)$$

$$V_{qs2} = -R_2 i_{qs2} + \frac{d}{dt}(\psi_{qs2}) + \omega(\psi_{ds2}) \quad (3.22 a)$$

$$V_{ds2} = -R_2 i_{ds2} + \frac{d}{dt}(\psi_{ds2}) - \omega(\psi_{qs2}) \quad (3.22 b)$$

$$V_{qr} = R_r i_{qr} + \frac{d}{dt}(\psi_{qr}) + (\omega - \omega_r)(\psi_{dr}) \quad (3.23 a)$$

$$V_{dr} = R_r i_{dr} + \frac{d}{dt}(\psi_{dr}) - (\omega - \omega_r)(\psi_{qr}) \quad (3.23 b)$$

Equations of flux are also written in d-q frame incorporating the effect of mutual inductance due to currents in both winding sets and are written from equations (3.24a) to (3.26b).

$$\psi_{qs1} = -L_{ls1} i_{qs1} - L_{lm}(i_{qs1} + i_{qs2}) + L_{dq} i_{ds2} + L_m(i_{qs1} + i_{qs2} + i_{qr}) \quad (3.24a)$$

$$\psi_{ds1} = -L_{ls1} i_{ds1} - L_{lm}(i_{ds1} + i_{ds2}) - L_{dq} i_{qs2} + L_m(i_{ds1} + i_{ds2} + i_{dr}) \quad (3.24b)$$

$$\psi_{qs2} = -L_{ls2} i_{qs2} - L_{lm}(i_{qs1} + i_{qs2}) + L_{dq} i_{ds1} + L_m(i_{qs1} + i_{qs2} + i_{qr}) \quad (3.24c)$$

$$\psi_{ds2} = -L_{ls2} i_{ds2} - L_{lm}(i_{ds1} + i_{ds2}) - L_{dq} i_{qs1} + L_m(i_{ds1} + i_{ds2} + i_{dr}) \quad (3.24d)$$

Under conditions of linear magnetic conditions the term of $L_{dq}=0$; and thus can be neglected [129][130]. Hence equations (3.24a), (3.24b), (3.24c) and (3.24d) reduce to (3.25a), (3.25b), (3.25c) and (3.25d) respectively.

$$\psi_{qs1} = -L_{ls1} i_{qs1} - L_{lm}(i_{qs1} + i_{qs2}) + L_m(i_{qs1} + i_{qs2} + i_{qr}) \quad (3.25a)$$

$$\psi_{ds1} = -L_{ls1}i_{ds1} - L_{lm}(i_{ds1} + i_{ds2}) + L_m(i_{ds1} + i_{ds2} + i_{dr}) \quad (3.25b)$$

$$\psi_{qs2} = -L_{ls2}i_{qs2} - L_{lm}(i_{qs1} + i_{qs2}) + L_m(i_{qs1} + i_{qs2} + i_{qr}) \quad (3.25c)$$

$$\psi_{ds2} = -L_{ls2}i_{ds2} - L_{lm}(i_{ds1} + i_{ds2}) + L_m(i_{ds1} + i_{ds2} + i_{dr}) \quad (3.25d)$$

Similarly the rotor flux linkage is given as:

$$\psi_{qr} = -L_{lr}i_{qr} + L_m(-i_{qs1} - i_{qs2} + i_{qr}) \quad (3.26a)$$

$$\psi_{qr} = -L_{lr}i_{qr} + L_m(-i_{qs1} - i_{qs2} + i_{qr}) \quad (3.26b)$$

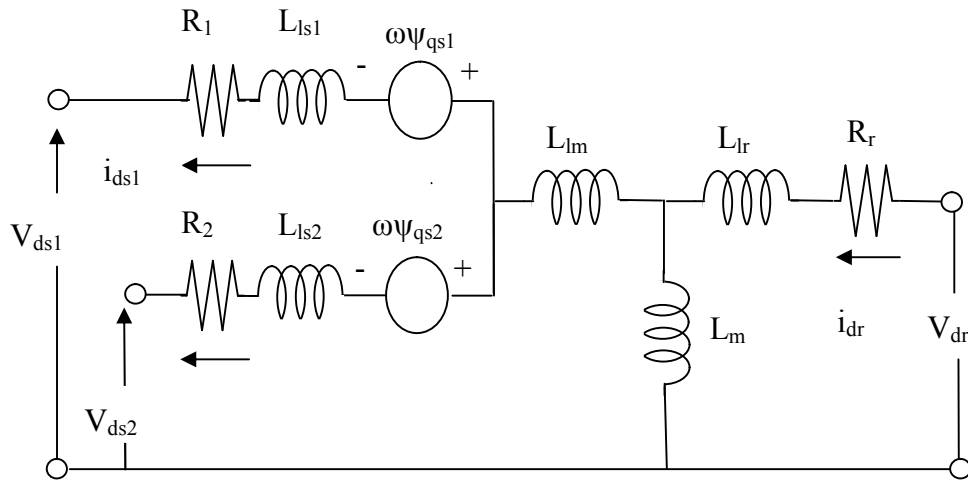


Fig. 3.5: Equivalent circuit of ADSIG in d-axis

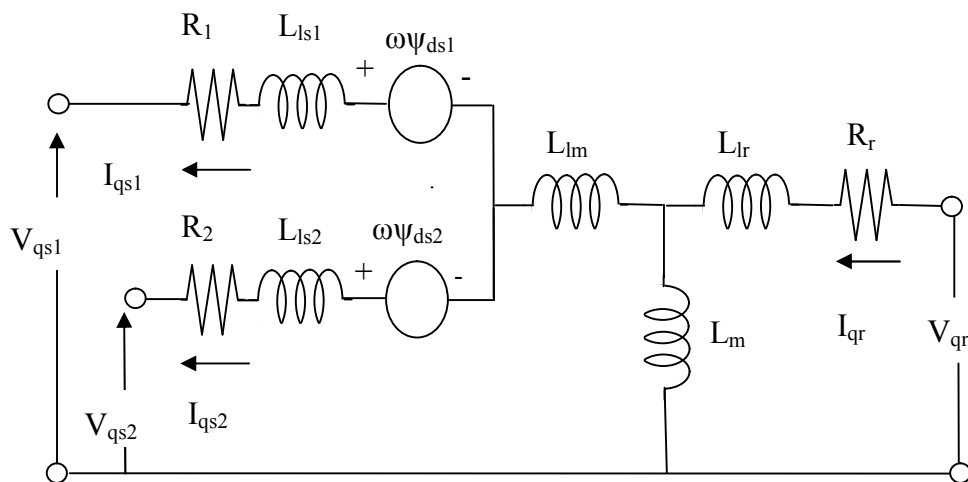


Fig. 3.6: Equivalent circuit of ADSIG in q-axis

Thus the real and reactive power flows of two stators can be represented as in equations (3.27a) to (3.27d) [131].

$$P_1 = V_{ds1}i_{ds1} + V_{qs1}i_{qs1} \quad (3.27a)$$

$$Q_1 = V_{qs1}i_{ds1} - V_{ds1}i_{qs1} \quad (3.27b)$$

$$P_2 = V_{ds2}i_{ds2} + V_{qs2}i_{qs2} \quad (3.27c)$$

$$Q_2 = V_{qs2}i_{ds2} - V_{ds2}i_{qs2} \quad (3.27d)$$

Where,

- ψ_{qs1}, ψ_{qs2} are stator q-axis flux linkage components,
- ψ_{ds1}, ψ_{ds2} are stator d-axis flux linkage components,
- ψ_{qr}, ψ_{dr} are rotor q-axis and d-axis flux linkage components,
- i_{qs1}, i_{qs2} are stator q-axis current components,
- i_{ds1}, i_{ds2} are stator d-axis current components,
- i_{qr}, i_{dr} are rotor q-axis and d-axis current components,
- L_{ls1}, L_{ls2} are stator leakage inductance,
- L_m is air gap inductance,
- L_{lm} is stator mutual leakage inductance,
- L_{lr} is rotor leakage inductance,
- L_{dq} is cross-saturation coupling of stator between d and q axis respectively,
- ω and ω_r are synchronous flux and rotor speed,
- R_1, R_2 and R_r are respective stator and rotor resistances,
- $V_{qs1}, V_{ds1}, V_{qs2}, V_{ds2}, V_{qr}$ and V_{dr} are the stator and rotor q-axis and d-axis voltages respectively.

3.3 Reduced Equivalent Circuit of ADSIG

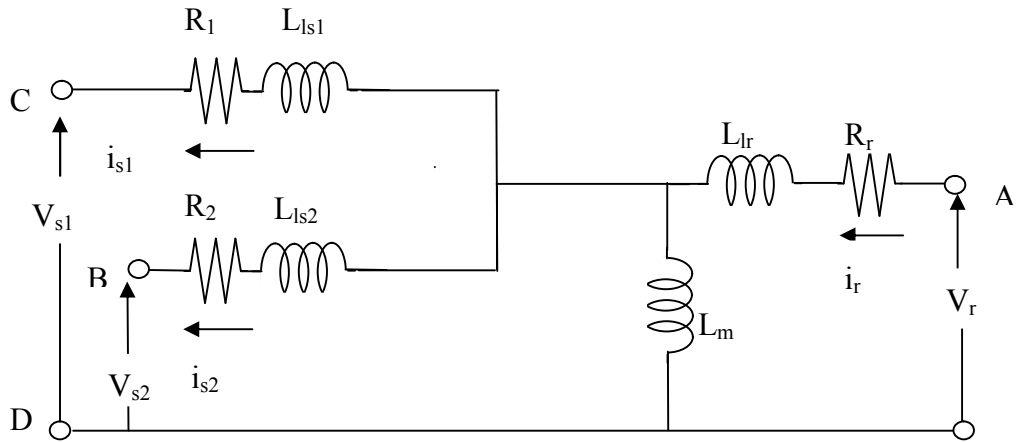


Fig. 3.7: Reduced Equivalent Circuit of ADSIG

The per-phase equivalent circuit of ADSIG is presented in Fig. 3.5 and Fig. 3.6, where two stator circuits are shown getting linked to common rotor circuit coupled through time and space displaced flux linkage. For ease of analysis, balanced and equal winding resistances and leakage inductances are considered. The mutual leakage inductance of stators is neglected assuming full coupling between both the stators. Besides these at the instant of clutching of IG with the turbine shaft, the dynamics of the rotor are considered negligible. The equivalent circuit gets reduced to as shown in Fig. 3.7.

The analysis of ADSIG under steady-state and dynamic conditions needs to be performed and hence for a better understanding of active and reactive power flow in ADSIG the real and reactive components of rotor current must be separated, i.e. the rotor circuit needs to be decoupled in real and imaginary components. Thus to make the equivalent circuit more lucid the coupling element of rotor side leakage reactance and resistance are decoupled and the rotor leakage inductance is transferred to magnetizing branch and both stator terminals as shown in Fig. 3.8. For easier analysis

both the stator resistances and inductances are assumed as same as given in equation (3.28) and equation (3.29).

$$R_1 = R_2 = R_s \quad (3.28)$$

$$L_{ls1} = L_{ls2} = L_s \quad (3.29)$$

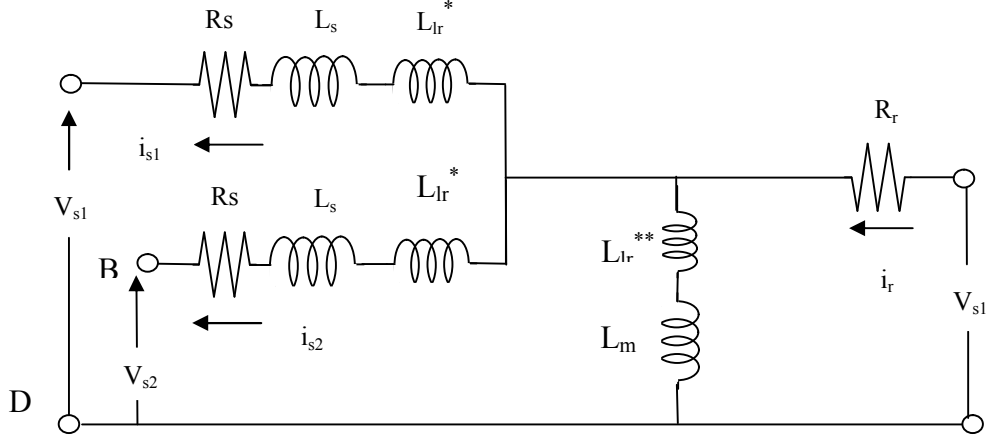


Fig. 3.8: Modified Reduced Equivalent circuit of ADSIG

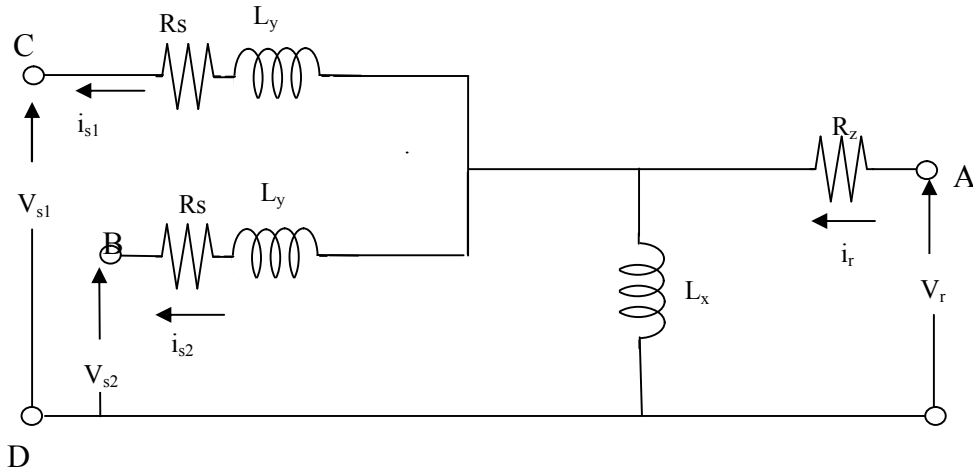


Fig. 3.9: Simplified Reduced Equivalent circuit of ADSIG

A simplified equivalent representation of Fig. 3.8 is shown in Fig. 3.9 and the values of new variables are given in equations (3.30) to equation (3.32). The parametric change in rotor circuitry results in a change in the values of net leakage reactance of stator, magnetizing reactance and equivalent rotor resistance but the overall performance of the ADSIG remains unaffected. To maintain the same performance

behaviour of ADSIG the net impedance seen from the stator terminals should remain unchanged for both the cases, before and after the decoupling of rotor circuitry.

Modified inductance of magnetizing branch becomes:

$$L_x = L_m + L_{lr}^{**} \quad (3.30a)$$

The equation (3.30a) can be re-written in reactance form as:

$$X_x = X_m + X_r^{**} \quad (3.30b)$$

Where,

$$X_x = j\omega L_x \quad (3.30c)$$

$$X_m = j\omega L_m \quad (3.30d)$$

$$X_r^{**} = j\omega L_{lr}^{**} \quad (3.30e)$$

Modified inductance of stator windings become:

$$L_y = L_{y1} = L_{y2} = L_s + L_{lr}^* \quad (3.31a)$$

Equation (3.31a) also can be written in reactance form as:

$$X_y = X_s + X_r^* \quad (3.31b)$$

Where,

$$X_y = j\omega L_y \quad (3.31c)$$

$$X_s = j\omega L_s \quad (3.31d)$$

$$X_r^* = j\omega L_{lr}^* \quad (3.31e)$$

Also the modified rotor resistance becomes:

$$R_z = R_r + r^* \quad (3.32)$$

Calculating the net impedance across terminals CD (Z_{CD}) for the equivalent circuit of

ADSIG, before decoupling of the rotor (as shown in Fig. 3.7) is given by:

$$Z_{CD} = R_S + jX_S + \frac{jX_m(R_r + jX_r)}{jX_m + R_r + jX_m} \quad (3.33)$$

$$Z_{CD} = R_S + jX_S + \frac{jX_m R_r - X_m X_r}{R_r + (jX_m + jX_r)} \quad (3.34)$$

Rationalizing the denominator:

$$Z_{CD} = R_S + jX_S + \frac{(jX_m R_r - X_m X_r)[R_r - (jX_m + jX_r)]}{R_r^2 + (X_m + X_r)^2} \quad (3.35)$$

Expanding the coefficients:

$$Z_{CD} = R_S + jX_S + \frac{jX_m R_r^2 - R_r X_m X_r + X_m^2 R_r + jX_m^2 X_r + R_r X_m X_r + X_r^2 X_m}{R_r^2 + (X_m + X_r)^2} \quad (3.36)$$

$$Z_{CD} = R_S + \frac{jX_S(R_r^2 + (X_m + X_r)^2) + j(X_m R_r^2 + X_m^2 X_r) + (X_m^2 R_r + X_r^2 X_m)}{R_r^2 + (X_m + X_r)^2} \quad (3.37)$$

Separating the real and imaginary terms in equation (3.37):

$$Z_{CD} = \left[R_S + \frac{(X_m^2 R_r + X_r^2 X_m)}{R_r^2 + (X_m + X_r)^2} \right] + j \left[\frac{X_S R_r^2 + X_S (X_m + X_r)^2 + X_m R_r^2 + X_m^2 X_r}{R_r^2 + (X_m + X_r)^2} \right] \quad (3.38)$$

Similarly calculating the impedance of the equivalent circuit across CD (Z_{CD}') in Fig.

3.9:

$$Z_{CD}' = R_S + jX_y + \frac{jX_x R_z}{jX_x + R_z} \quad (3.39)$$

Rationalizing the denominator:

$$Z_{CD}' = R_S + jX_y + \frac{jX_x R_z (R_z - jX_x)}{R_z^2 + X_x^2} \quad (3.40)$$

$$Z_{CD}' = R_S + jX_y + \frac{jX_x R_z^2 + X_x^2 R_z}{R_z^2 + X_x^2} \quad (3.41)$$

$$Z_{CD}' = R_S + jX_y(R_z^2 + X_x^2) + \frac{jX_x R_z^2 + X_x^2 R_z}{R_z^2 + X_x^2} \quad (3.42)$$

$$Z_{CD}' = R_S + \frac{jX_y R_z^2 + jX_y X_x^2 + jX_x R_z^2 + X_x^2 R_z}{R_z^2 + X_x^2} \quad (3.43)$$

Separating the real and imaginary components of equation (3.43):

$$Z_{CD}' = [R_S + \frac{X_x^2 R_z}{R_z^2 + X_x^2}] + j[\frac{X_y R_z^2 + X_y X_x^2 + X_x R_z^2}{R_z^2 + X_x^2}] \quad (3.44)$$

The performance of ADSIG for both the equivalent circuits remains the same and the impedance across CD also remains the same, i.e.

$$Z_{CD} = Z_{CD}' \quad (3.45)$$

$$\begin{aligned} [R_S + \frac{(X_m^2 R_r + X_r^2 X_m)}{R_r^2 + (X_m + X_r)^2}] + j[\frac{X_s R_r^2 + X_s (X_m + X_r)^2 + X_m R_r^2 + X_m^2 X_r}{R_r^2 + (X_m + X_r)^2}] \\ = [R_S + \frac{X_x^2 R_z}{R_z^2 + X_x^2}] + j[\frac{X_y R_z^2 + X_y X_x^2 + X_x R_z^2}{R_z^2 + X_x^2}] \end{aligned} \quad (3.46)$$

Equating the real and imaginary parts:

$$R_S + \frac{(X_m^2 R_r + X_r^2 X_m)}{R_r^2 + (X_m + X_r)^2} = R_S + \frac{X_x^2 R_z}{R_z^2 + X_x^2} \quad (3.47)$$

And

$$\frac{X_s R_r^2 + X_s (X_m + X_r)^2 + X_m R_r^2 + X_m^2 X_r}{R_r^2 + (X_m + X_r)^2} = \frac{X_y R_z^2 + X_y X_x^2 + X_x R_z^2}{R_z^2 + X_x^2} \quad (3.48)$$

The real and imaginary terms are expanded by putting the values of X_x , X_y and R_z in equation (3.47) and equation (3.48), using equation (3.30), equation (3.31) and equation (3.32). The real part, equation (3.47), reduces to:

$$\frac{(X_m^2 R_r + X_r^2 X_m)}{R_r^2 + (X_m + X_r)^2} = \frac{(X_m + X_r^{**})^2 (R_r + r^*)}{(R_r + r^*)^2 + (X_m + X_r^{**})^2} \quad (3.49)$$

or

$$\frac{(X_m^2 R_r + X_r^2 X_m)}{R_r^2 + (X_m + X_r)^2} = \frac{(X_m^2 R_r + 2X_m X_r^{**} + X_r^{**2})(R_r + r^*)}{(R_r + r^*)^2 + (X_m + X_r^{**})^2} \quad (3.50)$$

Further expanding the coefficients:

$$\begin{aligned} & \frac{(X_m^2 R_r + X_r^2 X_m)}{R_r^2 + (X_m + X_r)^2} \\ &= \frac{(X_m^2 R_r r^* + X_m^2 R_r^2 + 2X_m X_r^{**} r^* + 2X_m X_r^{**} R_r + X_r^{**2} r^* + X_r^{**2} R_r)}{(R_r + r^*)^2 + (X_m + X_r^{**})^2} \end{aligned} \quad (3.51)$$

Cross multiplying the numerator and denominator of LHS and RHS the equation reduces to:

$$\begin{aligned} & (X_m^2 R_r + X_r^2 X_m)[(R_r + r^*)^2 + (X_m + X_r^{**})^2] \\ &= (X_m^2 R_r r^* + X_m^2 R_r^2 + 2X_m X_r^{**} r^* + 2X_m X_r^{**} R_r + X_r^{**2} r^* \\ &+ X_r^{**2} R_r)[R_r^2 + (X_m + X_r)^2] \end{aligned} \quad (3.52)$$

Similarly, the imaginary components of equation (3.48) reduce to:

$$\begin{aligned} & \frac{X_s R_r^2 + X_s (X_m + X_r)^2 + X_m R_r^2 + X_m^2 X_r}{R_r^2 + (X_m + X_r)^2} \\ &= \frac{(X_s + X_r^*)(R_r + r^*)^2 + (X_s + X_r^*)(X_m + X_r^{**})^2 + (X_m + X_r^{**})(R_r + r^*)^2}{(R_r + r^*)^2 + (X_m + X_r^{**})^2} \end{aligned} \quad (3.53)$$

Cross multiplying the numerator and denominator of LHS and RHS the equation reduces to:

$$\begin{aligned}
& [X_s R_r^2 + X_s (X_m + X_r)^2 + X_m R_r^2 + X_m^2 X_r] [(R_r + r^*)^2 + (X_m + X_r^{**})^2] \\
& = [R_r^2 + (X_m + X_r)^2] [(X_s + X_r^*) (R_r + r^*)^2 + (X_s \\
& + X_r^*) \cdot (X_m + X_r^{**})^2 + (X_m + X_r^{**}) (R_r + r^*)^2] \quad (3.54)
\end{aligned}$$

Comparing and equating the LHS and RHS of real and imaginary components in equation (3.52) and equation (3.54) and using equations (3.30), equation (3.31) and equation (3.32) the values of variables of Fig. 3.9 as:

$$L_{lr}^* = \frac{2L_m L_{lr}'}{L_m + L_{lr}'} \quad (3.55 a)$$

$$L_{lr}^{**} = -0.5 L_{lr}^* \quad (3.55 b)$$

$$r^* = -L_{lr} (L_{lr} + 2L_m L_{lr}) \quad (3.55 c)$$

Calculating the values of variables of Fig. 3.9 using equations (3.30), equation (3.31), equation (3.32) and equation (3.55a), (3.55b), (3.55c):

$$L_x = L_m + L_{lr}^{**} \quad (3.56 a)$$

$$L_x = L_m - \frac{L_m L_{lr}'}{L_m + L_{lr}'} \quad (3.56 b)$$

$$L_x = \frac{L_m^2}{L_m + L_{lr}'} \quad (3.56 c)$$

Similarly, the modified rotor resistance reduces to:

$$R_z = R_r \left(\frac{L_m}{L_m + L_{lr}'} \right)^2 \quad (3.56 d)$$

The stator resistance remains unaffected as R_s , and the stator inductance reduces to:

$$\begin{aligned}
L_y &= L_{ls} + L_{lr}^* \\
L_y &= L_{ls1} + \frac{2L_{lr}' L_m}{L_m + L_{lr}'} \quad (3.56 e)
\end{aligned}$$

Lastly the induced voltage at rotor is transformed to current source and the final decoupled equivalent circuit of ADSIG as a current source is shown in Fig. 3.10 and the variables are given in equations 3.56(c), 3.56(d) and 3.56(e).

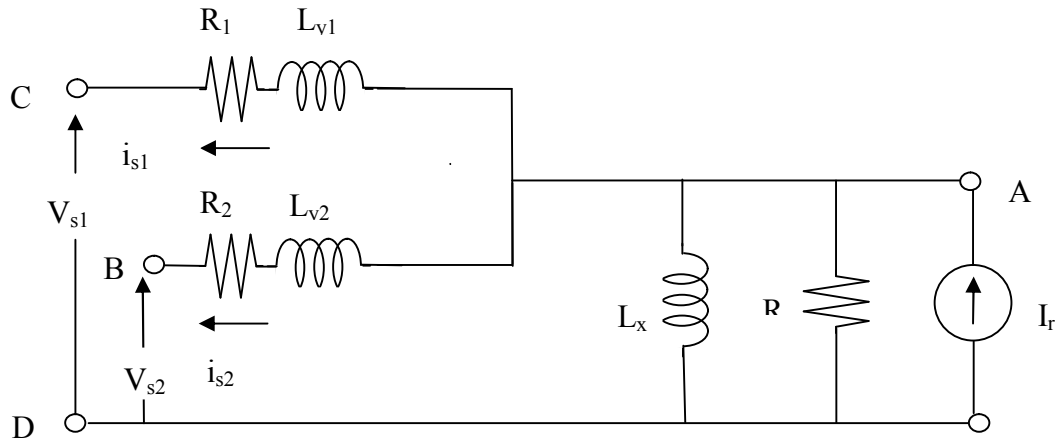


Fig. 3.10 Decoupled Equivalent Circuit of ADSIG as Current Source

3.4 Designing of ADSIG in INFOLYTICA MOTOSOLVE SOFTWARE

A prototype model of ADSIG is simulated in Infolytica Motorsolve design and analysis software. The performance of ADSIG is simulated using equivalent circuit calculations and finite element analysis tool.

3.4.1 Selection of Material

The material selected for rotor bar and end rings both are aluminium with conductivity of 50% according to International Annealed Copper Standard (IACS). The rotor tooth and rotor back iron material both are of M-19 29 Ga, the stator coil material is pure copper of 100% as per IACS and epoxy resin is used as stator slot liner material. The stator back iron material and stator tooth material are both M-19 29 Ga, material of

shaft is CR 10: cold rolled 1010 steel with non-magnetic hub.

Whereas shaft and hub both are not included in the magnetic analysis. The stacking factor for both stator and rotor are kept as 1. Stator and rotor iron loss adjustment factor both are chosen as 1. Epoxy resin is used as filler material both for stator core and rotor core. The stator coil filler material is also of epoxy resin. CR 10: cold roller 1010 steel is used in housing material, left end plate material, right end plate material, left bearing material, right bearing material, left flange material and right flange material. Air gap is filled with air and the machine is surrounded by air.

3.4.2 Dimensions and other Design Parameters for ADSIG

The outer diameter and stack length of ADSIG is taken as 379 mm with air-gap diameter of 208 mm. The number of stator slots is selected as 36 with parallel square shape. The rotor slots are 34 numbers of round back bars with parallel teeth. Machine aspect ratio is chosen to be 1 with air gap thickness of 0.5 mm. the number of poles are 6 and the number of phases is 6. The rotor-stator ratio is 0.55. The rotor-bar and rotor-end ring gap thickness is 0 mm. The rotor-hub gap thickness and stator-housing gap thickness both are selected as 0.156 mm.

The housing-left and right end plate gap thickness, left flange-left end plate gap thickness and right flange-right end plate gap thickness all are selected as 0 mm. The left bearing effective gap thickness and right bearing effective gap thickness both are 4.21 mm. The housing thickness is 16.8 mm with both left end region width and right end region width as 21.1 mm. The thickness of both left end plate and right end plate are 21.1 mm.

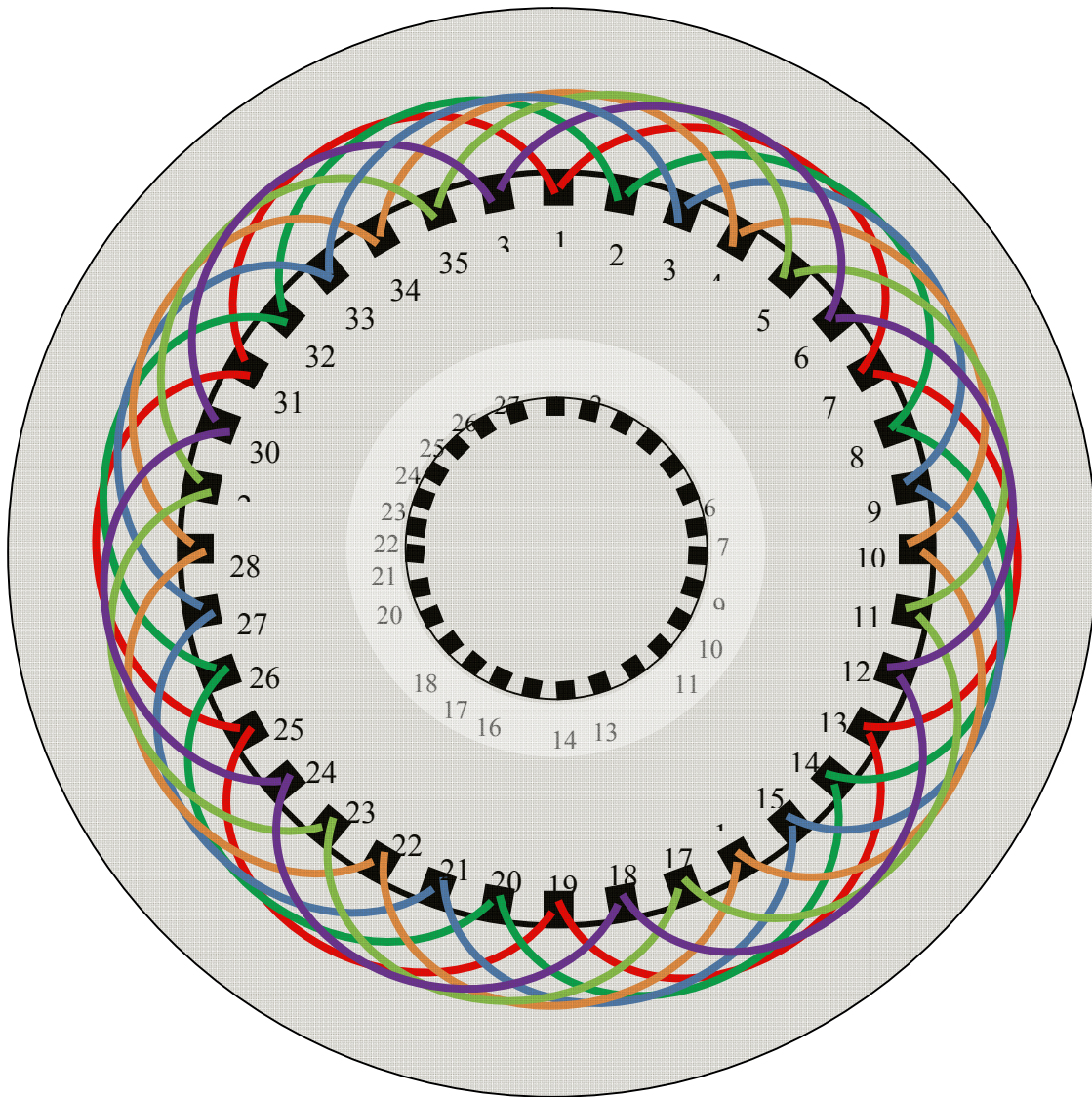


Fig. 3.11(a): Winding Diagram of ADSIG

The left flange thickness is 0 mm, left flange diameter is 505 mm, right flange thickness is 21.1 mm and right flange diameter is 505 mm. The shaft diameter is 33.7 mm, with left shaft extension of 0 mm, right shaft extension of 84.2 mm. The left bearing thickness, right bearing thickness, left bearing width and right bearing width all are of 33.7 mm. The machine orientation is horizontal and cooling method adopted is totally enclosed non-ventilated type.

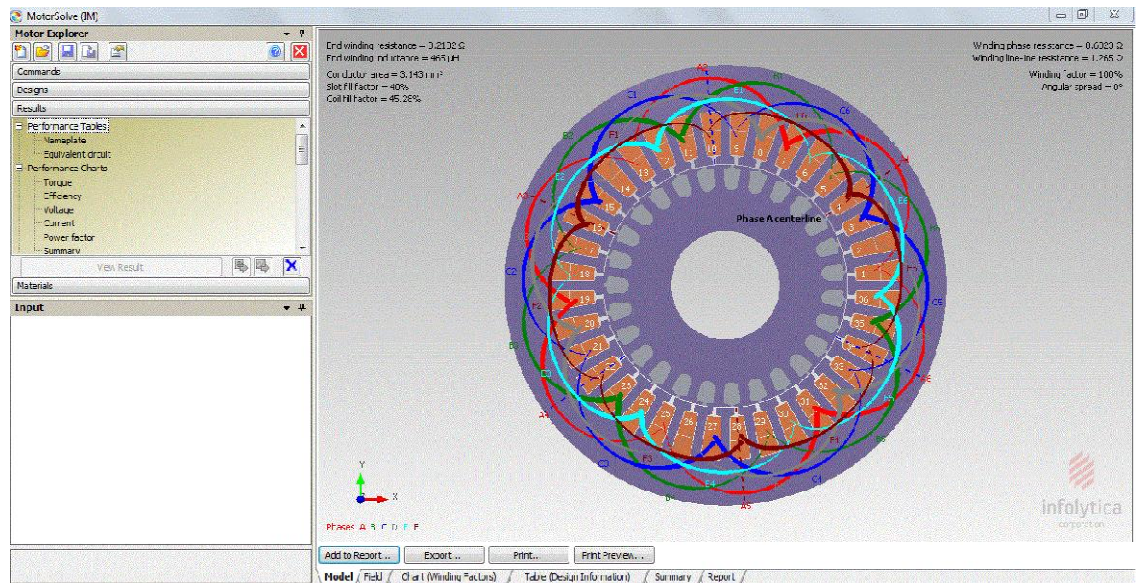


Fig. 3.11(b): Winding Diagram of ADSIG in INFOLYTICA MOTOR SOLVE

3.4.3 Winding Layout used in MotorSolve

The winding layout of six phases of ADSIG is presented in Table 3.2 and the winding diagram is shown in Fig. 3.11(a) and 3.11(b).

Table 3.2: Winding Layout of ADSIG

Phase	Coil Number	Go	Return	Number of Turns
Layout of Phase A	1	1	7	24
Layout of Phase A Layout of Phase B	2	13	7	24
	3	13	19	24
	4	25	19	24
	5	25	31	24
	6	1	31	24
	1	2	8	24
Layout of Phase B Layout of Phase C	2	14	8	24
	3	14	20	24
	4	26	20	24
	5	26	32	24
	6	2	32	24

	1	3	9	24
Layout of Phase C Layout of Phase D	2	15	9	24
	3	15	21	24
	4	27	21	24
	5	27	33	24
	6	3	33	24
	1	4	10	24
Layout of Phase D Layout of Phase E	2	16	10	24
	3	16	22	24
	4	28	22	24
	5	28	34	24
	6	4	34	24
	1	5	11	24
Layout of Phase E Layout of Phase F	2	17	11	24
	3	17	23	24
	4	29	23	24
	5	29	35	24
	6	5	35	24
	1	6	12	24
Layout of Phase F	2	18	12	24
	3	18	24	24
	4	30	24	24
	5	30	36	24
	6	6	36	24

3.4.4 The Summary of Design for ADSIG Prototype

The summary of design for ADSIG prototype is summarized below:

- Number of stator slots = 36
- Number of rotor slots = 27
- Number of poles = 6

- Synchronous speed = 1000 RPM
- Number of Phases = 6 (Two 3Ø windings)
- Angle between two sets of stator windings = 30°
- Slots/ Pole/ Phase = 1
- Type of winding = Concentrated winding
- Rated RMS Voltage/ Phase = 240 V
- Power rating of ADSIG (for 6 phase) = 5 HP (3.7Kw)
- Power rating of each three phase ≈ 1.8 Kw
- Rated RMS current per Phase = 2.5 A
- SWG of wire used for winding = 24 SWG
- Number of coils per phase = 6
- Slot pitch = 36°
- Pole pitch = 60°
- Phase spread = 30°
- Type of winding = Double layer winding
- Distribution factor = 1
- Pitch factor = 1
- Winding factor = 1

The design equations used for developing the hardware prototype are given below:

$$E_{ph} = 4.44 f \phi_m T_{ph} K_w \quad (3.57)$$

$$kVA = m E_{ph} I_{ph} 10^{-3} \quad (3.58)$$

or

$$kVA = 4.44 m f \phi_m T_{ph} K_w I_{ph} 10^{-3} \quad (3.59)$$

Specific Electric Loading is given by:

$$ac = m \frac{2 T_{ph} I_{ph}}{\pi D} \quad (3.60)$$

Average Magnetic Flux Density is given by:

$$B_{av} = \frac{P \phi_m}{\pi D L} \quad (3.61)$$

3.4.5 Simulated Performance Characteristics

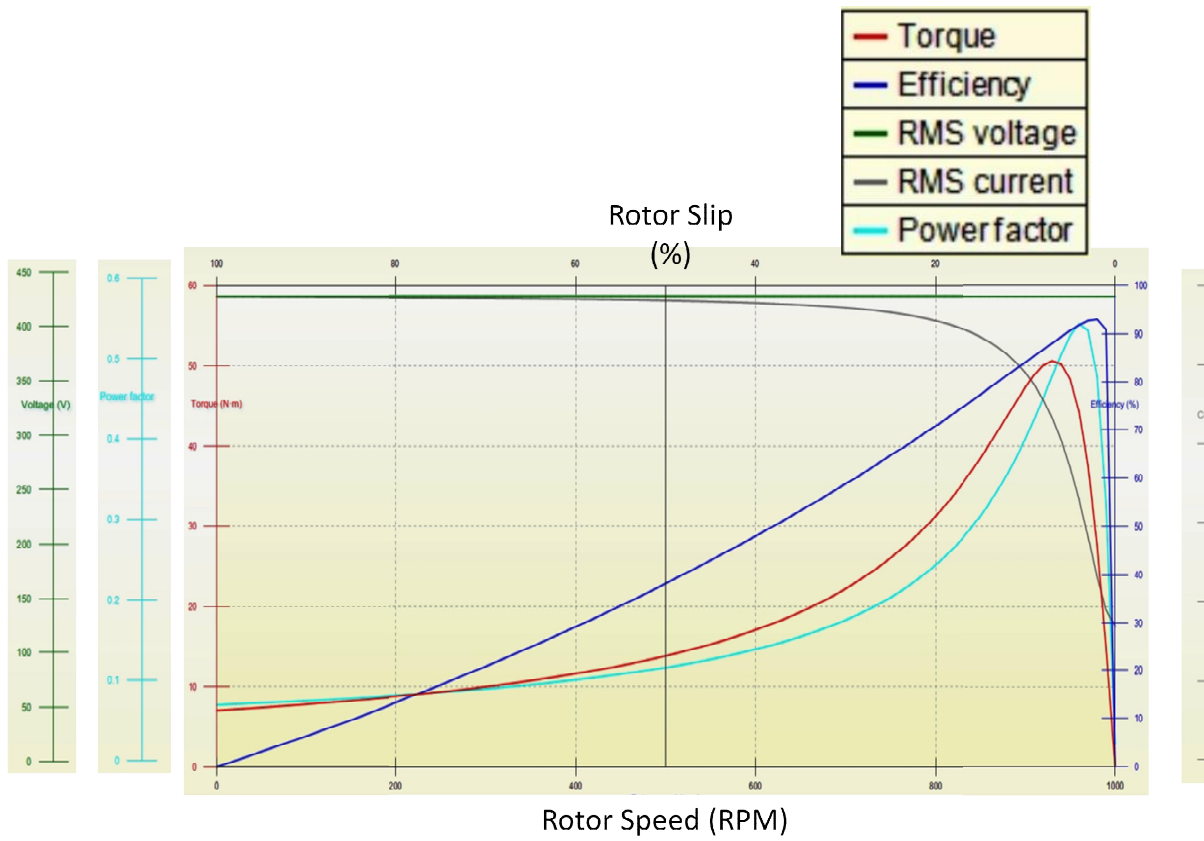


Fig. 3.12: Performance Characteristics of ADSIG in INFOLYTICA MOTORSOLVE

A comprehensive performance of the designed machine is simulated in the INFOLYTICA MOTORSOLVE to have first-hand assessment of the design. The torque, efficiency, voltage, current and power factor characteristics are depicted in Fig. 3.12. It is observed that the efficiency of machine is more than 90% and the no-load

current id near about 4A.

3.5 Design and Winding of Hardware Prototype of ADSIG

The hardware prototype of ADSIG is made keeping in mind the winding configuration of different phases and separate neutral for both stator windings.

3.5.1 Selection of Materials

An empty stator squirrel cage induction machine is bought from market and it is rewound for six phases. 24 SWG enamelled copper wire is chosen for making stator coils. Each coil group has 24 turns. The winding diagram of the machine is same as shown in Fig. 3.11.

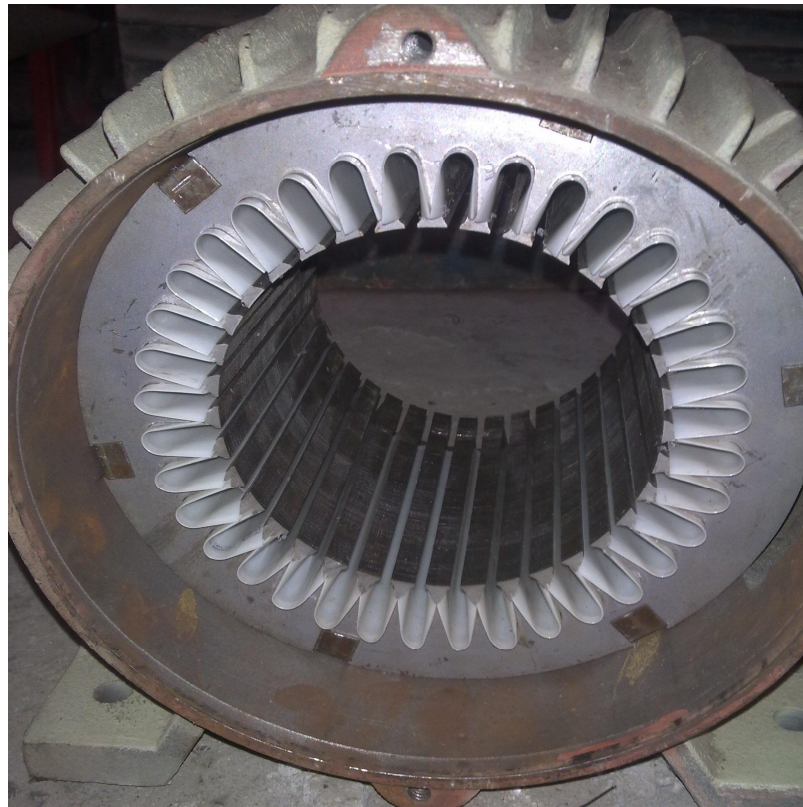


Fig. 3.13: Empty Stator Induction Motor

The developed hardware prototype, used as generator, is connected with 7.5HP squirrel cage induction motor, used as prime mover. The prime mover is connected to a delta drive of 7.5HP in open loop v/f control mode. The speed of prime mover is varied by the potentiometer knob of drive. The hardware picture of empty stator induction motor which is to be reconfigured as ADSIG is shown in Fig. 3.13. Fig. 3.14 shows the intermediate process of winding and Fig. 3.15 shows the final hardware prototype and Fig. 3.16 shows ADSIG coupled with Prime Mover.



Fig. 3.14: Rewinding of Empty Stator Induction Motor



Fig. 3.15 Empty Stator Induction Motor Wounded as ADSIG

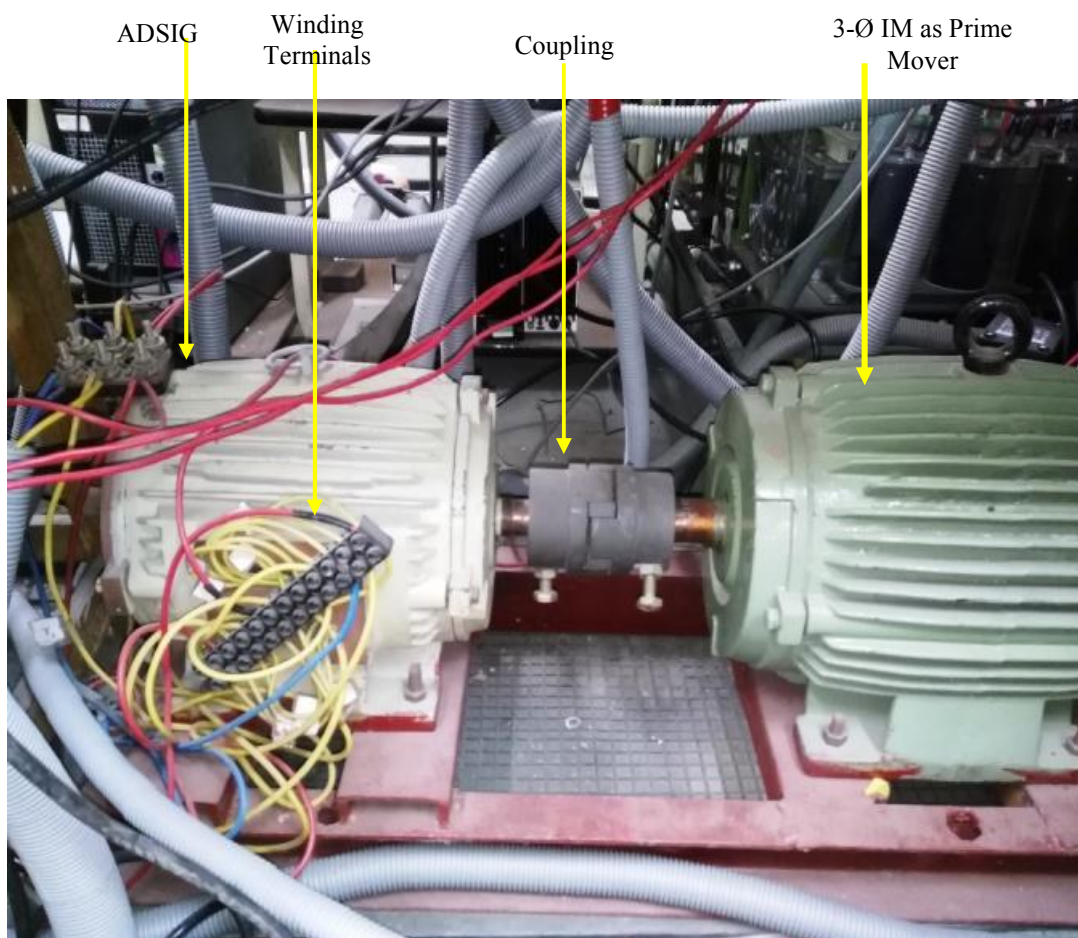


Fig. 3.16: ADSIG Coupled with Prime Mover

3.5.2 Prototype Testing of ADSIG

The performance indices of ADSIG are evaluated by performing standard tests on the machine. ADSIG is run as a motor with the help of star-star-delta transformer fed by three phase ac grid as shown in figure of test bench in Fig. 3.17. Three phase grid is connected to the input of three winding transformer with the leading winding of ADSIG is connected to the star output of secondary and the lagging winding is connected to the delta output of three phase transformer. The current and voltage waveforms of the machine are shown in Fig. 3.18 and 3.19. Standard tests, no-load, short-circuit and dc test, are performed on the machine to evaluate the machine parameters.

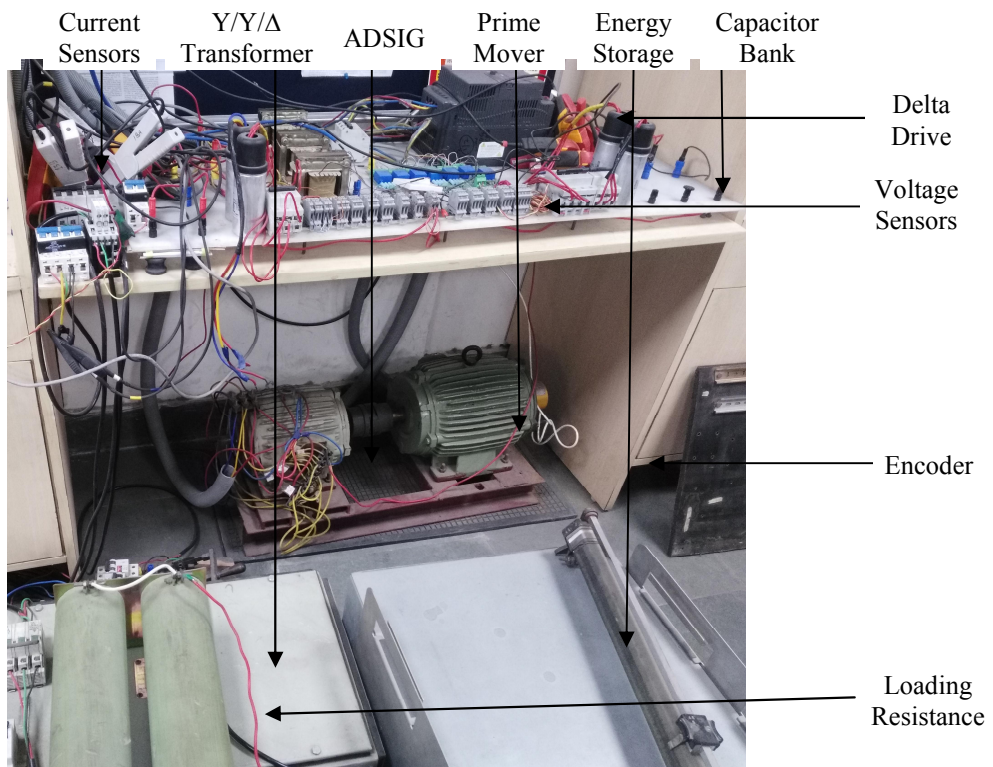


Fig. 3.17 Hardware Test Rig of ADSIG

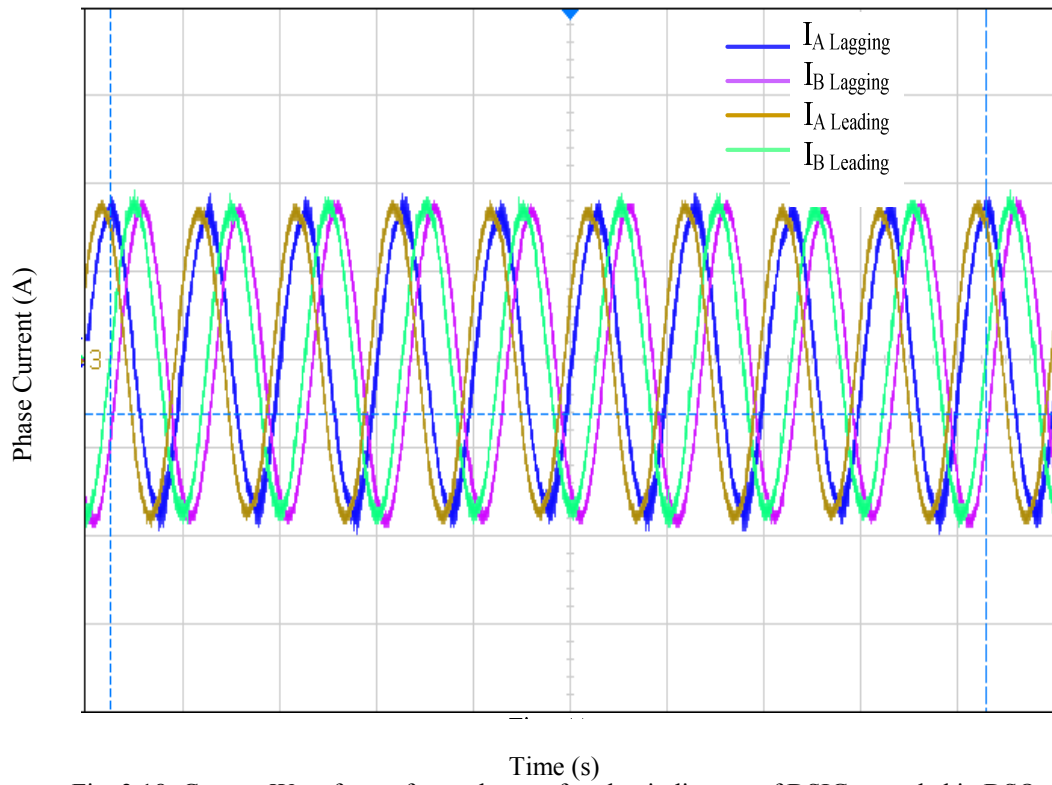


Fig. 3.18: Current Waveform of two phases of each winding set of DSIG recorded in DSO
Current Scale: 1Div. = 3A; Time Scale: 1 Div. = 20ms

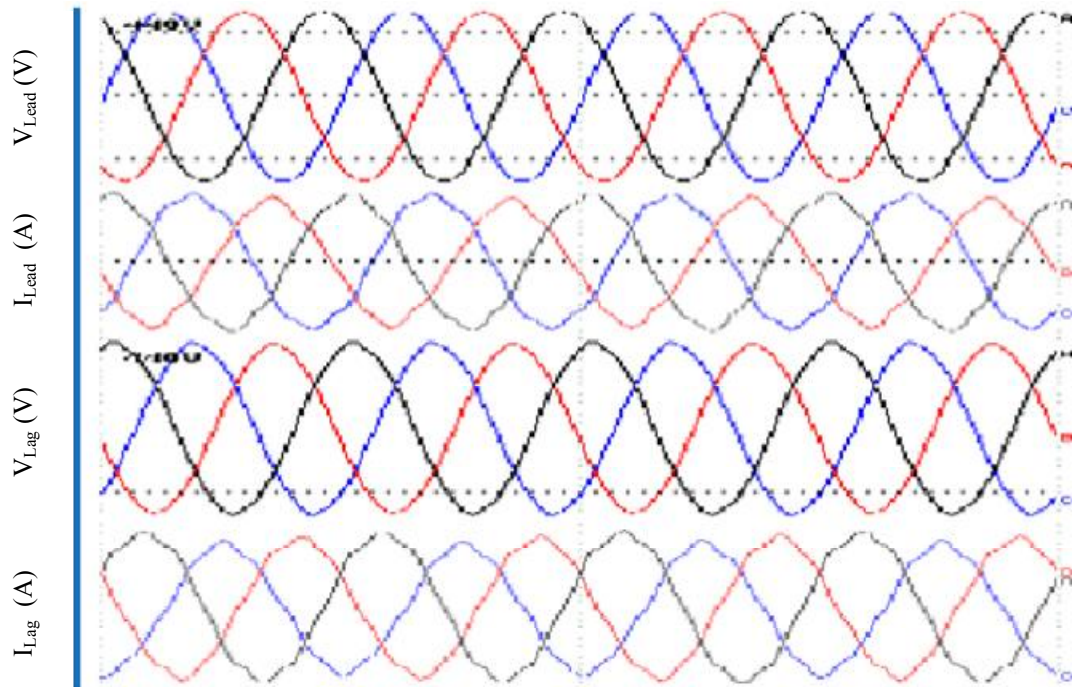


Fig. 3.19: Voltage and Current Waveform of both the winding set of DSIG recorded in PQ Analyzer
 $V_{Lead\ rms} = 240V$; $I_{Lead\ rms} = 3.2A$; $V_{Lag\ rms} = 240V$; $I_{Lag\ rms} = 3.2A$

3.5.3 Equivalent Circuit Parameters of ADSIG

The equivalent circuit parameters of ADSIG are shown in Table 3.3.

Table 3.3 Equivalent Parameters of ADSIG

S. No.	Parameters	Values
1	Stator 1 Resistance	4.375 Ω
2	Stator 2 Resistance	4.375 Ω
3	Rotor Resistance	13.625 Ω
4	Stator Inductance	61 mH
5	Stator 2 Inductance	61 mH
6	Rotor Inductance	61mH
7	Magnetizing Inductance	316 mH

3.6 Conclusion

A mathematical model of the ADSIG is developed using voltage and flux equations in d-q reference frame and its equivalent circuit is made in the d-q reference frame. To make the equivalent circuit more lucid and decoupled the coupling element of rotor side leakage reactance and resistance are decoupled and the rotor leakage inductance is transferred to magnetizing branch and to the both stator side circuits. The parametric change due to transfer of component from rotor circuitry resulted in a change in the values of net leakage reactance of stator, magnetizing reactance and equivalent rotor resistance but the overall performance of the ADSIG remains unaffected. This reduced simplified equivalent circuit with decoupled real and imaginary components of rotor circuitry, allows easy analysis for a better power flow study. For grid coupled

application the equivalent circuit so developed acts as current source and the final decoupled equivalent circuit of ADSIG as a current source is thus deduced. This deduced circuit eases the analysis of ADSIG in different conditions as discussed in the later chapters.

The developed mathematical model and equations are used for designing and developing ADSIG in INFOLYTICA MOTORSOLVE software. The various performance characteristics of ADSIG are noted and the machine parameters are calculated. This developed machine model is tested and verified for different operating conditions.

The winding configurations used in the INFOLYTICA MOTORSOLVE software are used for design and development of the hardware prototype of the ADSIG. The developed hardware prototype in the laboratory is tested based on the standard tests and the machine parameters are calculated. The machine parameters obtained by the prototype closely match with the parameters of simulated machine.

The decoupled model of ADSIG and the hardware prototype developed both are used for furthering the analysis of ADSIG during transient and steady state operations for three port power flow in next chapters.

Chapter 4

Transient Performance Analysis of ADSIG

4.1 General

Transient performance of induction machine is always a major concern and before using the machine it is always desirable to study and analyse it in detail. Whenever a SCIG is connected to grid there is a huge demand of magnetising inrush current for maintaining the air-gap flux. Due to the varying nature of wind speed, there is more often connection and disconnection of induction generator from the grid, resulting in a more often demand for inrush current from the grid. When many SCIG's are connected together, as in a wind farm, their collective demand of inrush current becomes very troublesome for the grid. The cumulative inrush current demand results in the drawl of heavy reactive currents from the grid, which causes a dip in the voltage of the grid making the other WECS vulnerable for grid connection.

In asymmetrical DSIG (ADSIG) this inrush current demand is distributed in two three-phase windings which are 30° phase apart from each other. To study the effect of this type of winding structure on the inrush current demand a transient analysis of ADSIG is done. Another problem usually encountered in the distribution networks is of low voltage, which may be either caused due to sudden application of any load or any fault in the network. To critically evaluate the behaviour of generators under conditions of one phase open and during low-voltage condition, the performance of symmetrical DSIG (SDSIG) and ADSIG are compared with conventional three-phase induction generators. The comparison is extended to observe the reactive power demand during steady-state conditions by plotting and critically examining their air-gap flux.

4.2 System Configuration of DSIG and SCIG for Analysis of Inrush Current

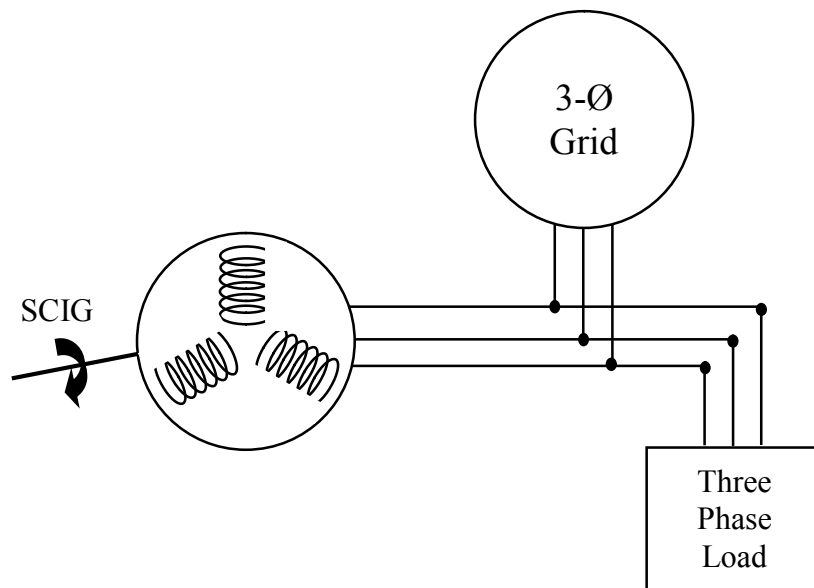


Fig. 4.1: System Configuration of SCIG

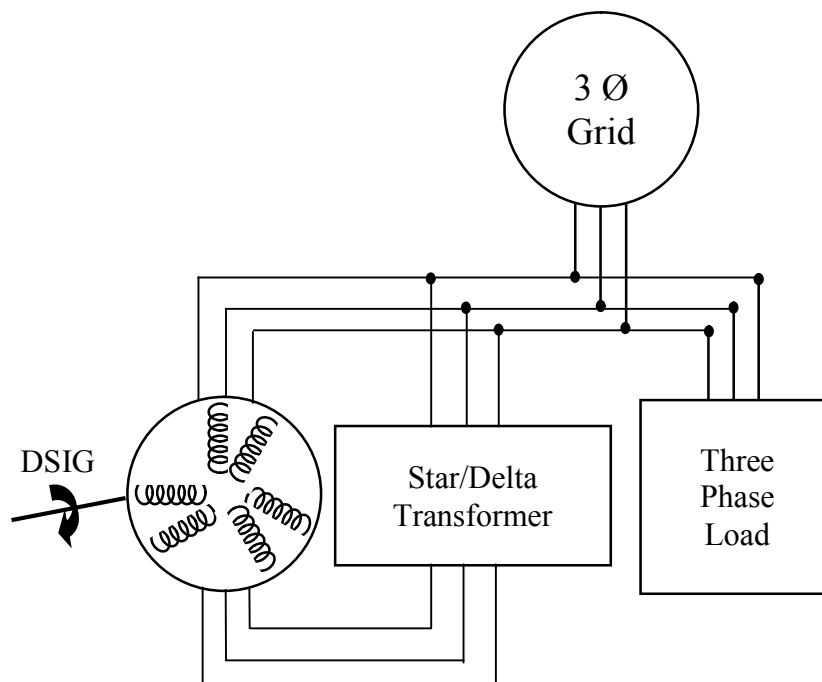


Fig. 4.2: System Configuration of ADSIG

The Systems considered for analysis and comparison of inrush current of SCIG and DSIG are shown in Fig. 4.1 and Fig 4.2 respectively. The power and voltage ratings of

SCIG and both DSIG's (SDSIG and ADSIG) are kept the same for evaluating the performance on the same scale. Respective generators are connected to a weak three-phase distribution grid, for analyzing the transient performance and behaviour of generators for inrush currents, fault conditions and low-voltage conditions.

4.3 Mathematical Analysis of Inrush Current of DSIG

This section investigates the inrush current demand at the time of insertion of SCIG and ADSIG to the power grid. A detailed transient analysis of ADSIG is done to make an assessment of inrush current, transient damping capabilities, and its ability for sustaining its operation at one phase open condition and for low voltage grid conditions on all phases by self-supporting the flux in the air gap. The equation obtained for currents of ADSIG is compared for that of SCIG.

4.3.1 Mathematical Analysis of Current of ADSIG

The per-phase equivalent circuit of ADSIG is already developed and discussed in Chapter 3 Section 3.3. In the per-phase equivalent circuit of ADSIG, two stator circuits are linked to common rotor circuit coupled through time and space displaced flux linkage. For ease of analysis, balanced and equal winding resistances and leakage inductances are considered. Besides these, the induced voltage in rotor circuit is transformed to the current source and at the instant of clutching of IG with the turbine shaft, the dynamics of the rotor are considered negligible as shown in Fig. 4.3(a).

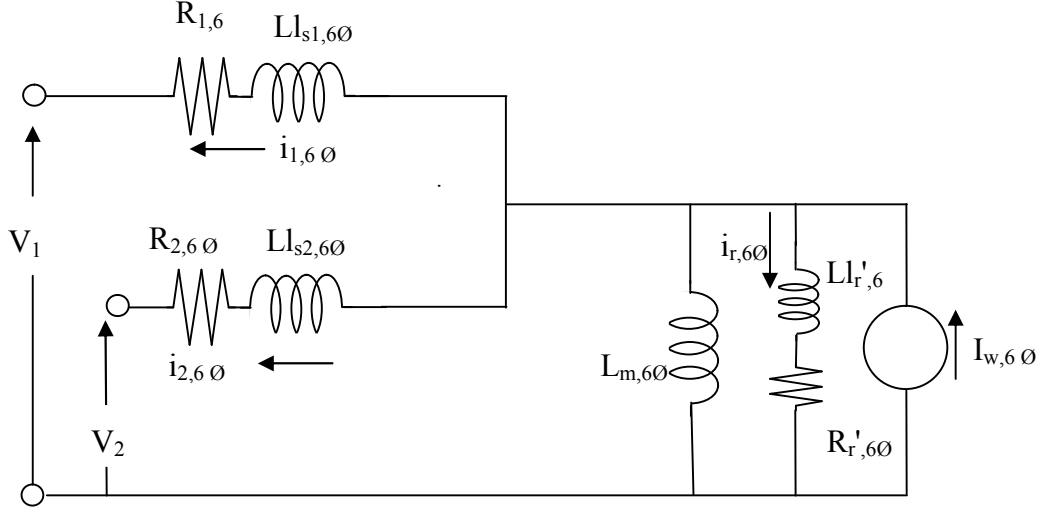


Fig. 4.3 (a): Modified per phase Equivalent Circuit of ADSIG as a Current Source

Further to make the equivalent circuit more lucid the coupling element of rotor side leakage reactance is transferred to the stator side. As a result, the net leakage reactance of stator, magnetizing reactance and equivalent rotor resistance shall witness a change in values. Accordingly, the equivalent circuit gets transferred to form presented in Fig. 4.3(b) with the modified generator parameters shown in equations (4.1a) to (4.1g).

Where

$$L_{lr}^* = \frac{2 L_{m,6\emptyset} L'_{lr,6\emptyset}}{L_{m,6\emptyset} + L'_{lr,6\emptyset}} \quad (4.1 a)$$

$$L_{lr}^{**} = -0.5 L_{lr}^* \quad (4.1 b)$$

$$r^* = -L'_{lr,6\emptyset} (L'_{lr,6\emptyset} + 2L_{m,6\emptyset} L'_{lr,6\emptyset}) \quad (4.1 c)$$

$$L_{x,6\emptyset} = L_{m,6\emptyset} + L_{lr}^{**} = \frac{L_{m,6\emptyset}^2}{L_{m,6\emptyset} + L'_{lr,6\emptyset}} \quad (4.1 d)$$

$$R_{z,6\emptyset} = R'_{r,6\emptyset} + r^* = R'_{r,6\emptyset} \left(\frac{L_{m,6\emptyset}}{L_{m,6\emptyset} + L'_{lr,6\emptyset}} \right)^2 \quad (4.1 e)$$

$$R_{1,6\emptyset} = R_{s1,6\emptyset}; L_{1,6\emptyset} = L_{ls1,6\emptyset} \quad (4.1 f)$$

$$L_{y1,6\emptyset} = L_{ls1,6\emptyset} + L_{lr}^* = L_{1,6\emptyset} + \frac{2L'_{lr,6\emptyset}L_{m,6\emptyset}}{L_{m,6\emptyset} + L'_{lr,6\emptyset}} \quad (4.1 g)$$

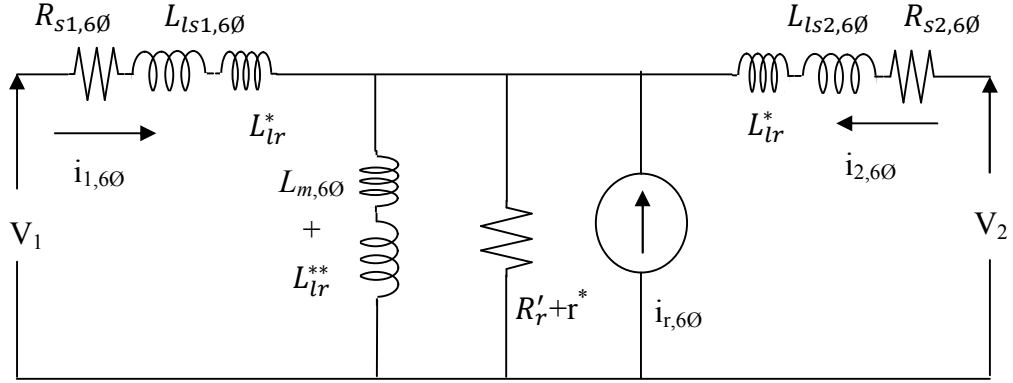


Fig. 4.3(b): Equivalent per phase circuit of ADSIG with rotor inductance referred to stator side

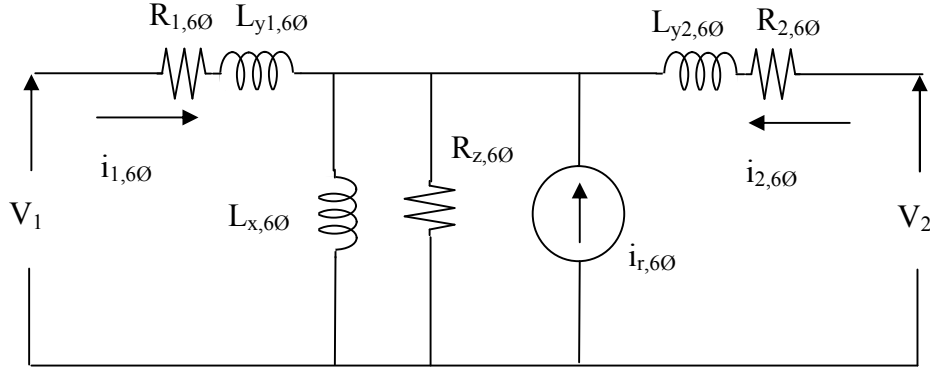


Fig. 4.3(c): Reduced equivalent circuit of ADSIG

Applying superposition theorem on circuit depicted in Fig. 4.3(b) considering the real power flowing from the current source towards each terminal and reactive power drawn from each terminal pairs of ADSIG to the reactance branch ($L_{x,6\emptyset}$). Writing voltage equations using mesh analysis at one winding side and keeping other winding side terminals open circuited (since the real power is not delivered and reactive power not drawn from the same), in equations (4.2) and equations (4.3).

$$i_{r,6\emptyset}R_{z,6\emptyset} + L_{x,6\emptyset}\frac{d}{dt}(i_{r,6\emptyset} + i_{1,6\emptyset}) = 0 \quad (4.2)$$

$$i_{1,6\emptyset}R_{1,6\emptyset} + L_{y1,6\emptyset}\frac{d}{dt}i_{1,6\emptyset} + L_{x,6\emptyset}\frac{d}{dt}(i_{1,6\emptyset} + i_{r,6\emptyset}) = v_1 \quad (4.3)$$

Taking the Laplace transform of equation (4.2) and equation (4.3), equation (4.4) and equation (4.5) are obtained.

$$I_{r,6\emptyset}(s)R_{z,6\emptyset} + sL_{x,6\emptyset}(I_{r,6\emptyset}(s) + I_{1,6\emptyset}(s)) = 0 \quad (4.4)$$

$$\begin{aligned} I_{1,6\emptyset}(s)R_{1,6\emptyset} + sL_{y1,6\emptyset}I_{1,6\emptyset}(s) + sL_{x,6\emptyset}(I_{1,6\emptyset}(s) + I_{r,6\emptyset}(s)) \\ = \frac{V_m(s \sin(\emptyset + \alpha^\circ) + \omega \cos(\emptyset + \alpha^\circ))}{s^2 + \omega^2} \end{aligned} \quad (4.5)$$

The forcing function is considered as $V_m \sin(\omega t + 15^\circ)$ (for leading side) and $V_m \sin(\omega t - 15^\circ)$ (for lagging side), \emptyset is the phase displacement of stator current with respect to its respective terminal voltage and $\alpha = 15^\circ$ is the additional phase displacement caused due to common rotor current formed by both the stator currents displaced with respect to each other by 30° . For one side α is added to \emptyset and for the other side it is subtracted. Simplifying equation (4.4) and equation (4.5) and solving for $I_{1,6\emptyset}(s)$:

$$\begin{aligned} I_{1,6\emptyset}(s) \\ = \frac{V_m(R_{z,6\emptyset} + sL_{x,6\emptyset})(s \sin(\emptyset + \alpha^\circ) + \omega \cos(\emptyset + \alpha^\circ))}{(s^2 + \omega^2) \cdot \left[s^2(L_{x,6\emptyset}L_{y1,6\emptyset}) + s(R_{1,6\emptyset}L_{x,6\emptyset} + R_{z,6\emptyset}L_{x,6\emptyset} + R_{z,6\emptyset}L_{y1,6\emptyset}) \right] + R_{1,6\emptyset}R_{z,6\emptyset}} \end{aligned} \quad (4.6)$$

Similarly writing mesh equations for the other side:

$$\begin{aligned} I_{2,6\emptyset}(s)R_{2,6\emptyset} + sL_{y2,6\emptyset}I_{2,6\emptyset}(s) + sL_{x,6\emptyset}(I_{2,6\emptyset}(s) + I_{r,6\emptyset}(s)) \\ = \frac{V_m(s \sin(\emptyset - \alpha^\circ) + \omega \cos(\emptyset - \alpha^\circ))}{s^2 + \omega^2} \end{aligned} \quad (4.7)$$

Simplifying it and solving for $I_{2,6\emptyset}(s)$ it can be written as equation (4.8).

$$I_{2,6\emptyset}(s) = \frac{V_m(R_{z,6\emptyset} + s L_{x,6\emptyset})(s \sin(\emptyset - \alpha^\circ) + \omega \cos(\emptyset - \alpha^\circ))}{(s^2 + \omega^2) \left[s^2(L_{x,6\emptyset}L_{y2,6\emptyset}) + s(R_{2,6\emptyset}L_{x,6\emptyset} + R_{z,6\emptyset}L_{x,6\emptyset} + R_{z,6\emptyset}L_{y2,6\emptyset}) + R_{2,6\emptyset}R_{z,6\emptyset} \right]} \quad (4.8)$$

The rotor current can be written as:

$$I_{r,6\emptyset}(s) = \frac{-s L_{x,6\emptyset} I_{1,6\emptyset}(s)}{R_{z,6\emptyset} + s L_{x,6\emptyset}} = \frac{-s L_{x,6\emptyset} I_{2,6\emptyset}(s)}{R_{z,6\emptyset} + s L_{x,6\emptyset}} \quad (4.9)$$

The net current drawn from the mains is calculated by adding both stator currents equation (4.6) and equation (4.8). Since $L_{y1,6\emptyset} = L_{y2,6\emptyset} = L_{y,6\emptyset}$ and $R_{1,6\emptyset} = R_{2,6\emptyset} = R_{s,6\emptyset}$; the expression of net current is given as:

$$I(s)_{6\emptyset} = \frac{1.93 V_m(R_{z,6\emptyset} + s L_{x,6\emptyset})(s \sin(\emptyset) + \omega \cos(\emptyset))}{(s^2 + \omega^2) \left[s^2(L_{x,6\emptyset}L_{y,6\emptyset}) + s(R_{s,6\emptyset}L_{x,6\emptyset} + R_{z,6\emptyset}L_{x,6\emptyset} + R_{z,6\emptyset}L_{y,6\emptyset}) + R_{s,6\emptyset}R_{z,6\emptyset} \right]} \quad (4.10)$$

The denominator of equation (4.10) depicts two distinct sets of the solution, one for natural (steady state) response of the system and the other depicts the forced (transient) response. The characteristic equation which depicts the forced response as per equation is given by equation (4.11), which is further generalized in quadratic equation form for ADSIG in equation (4.12).

$$s^2(L_{x,6\emptyset}L_{y,6\emptyset}) + s(R_{s,6\emptyset}L_{x,6\emptyset} + R_{z,6\emptyset}L_{x,6\emptyset} + R_{z,6\emptyset}L_{y,6\emptyset}) + R_{s,6\emptyset}R_{z,6\emptyset} = 0 \quad (4.11)$$

The above equation can be compared with the basic quadratic equation:

$$a_{6\emptyset}s^2 + b_{6\emptyset}s + c_{6\emptyset} = 0 \quad (4.12)$$

Where,

- $a_{6\emptyset} = L_{x,6\emptyset}L_{y,6\emptyset}$
- $b_{6\emptyset} = R_{s,6\emptyset}L_{x,6\emptyset} + R_{z,6\emptyset}L_{x,6\emptyset} + R_{z,6\emptyset}L_{y,6\emptyset}$
- $c_{6\emptyset} = R_{s,6\emptyset}R_{z,6\emptyset}$

The Roots $m_{1,2}$ which make the damping coefficient of the transient operation expressed in equation (4.13).

$$m_{1,2\ 6\emptyset} = \frac{-b_{6\emptyset} \pm \sqrt{b_{6\emptyset}^2 - 4a_{6\emptyset}c_{6\emptyset}}}{2a_{6\emptyset}} \quad (4.13)$$

Since

- $L_{lr,6\emptyset}L_{ls1,6\emptyset} = L_{lr,6\emptyset}L_{ls1,6\emptyset} \cong 0;$
- $L_{m,6\emptyset} \gg L_{lr,6\emptyset}$ and
- $L_{1,6\emptyset} = L_{2,6\emptyset} = L_{s,6\emptyset}$

The parameters $L_{y,6\emptyset}$ and $L_{x,6\emptyset}$ may be reduced as:

- $L_{y,6\emptyset} \cong L_{s,6\emptyset} + L_{lr,6\emptyset}$
- $L_{x,6\emptyset} \cong L_{m,6\emptyset}$

Accordingly:

- $a_{6\emptyset} = L_{x,6\emptyset}L_{y,6\emptyset};$
- $b_{6\emptyset} = R_{z,6\emptyset}(3L_{x,6\emptyset} + L_{y,6\emptyset});$
- $c_{6\emptyset} = R_{s,6\emptyset}R_{z,6\emptyset}$

Doing the partial fraction and taking inverse Laplace Transform of equation (4.10) the per phase current drawn from the mains by the ADSIG is expressed in equation (4.14).

Where, the former part having the exponential terms denotes the forced response, whereas, the later part denotes the natural response of the current drawn by the

ADSIG.

$$I_{1a,6\emptyset}(t) = [(X_{1,6\emptyset}e^{m_{1,6\emptyset}t} + X_{2,6\emptyset}e^{m_{2,6\emptyset}t})] \\ + 1.93 [(X_{3,6\emptyset} + X_{4,6\emptyset}) \cos(\omega t) + j(X_{3,6\emptyset} - X_{4,6\emptyset}) \sin(\omega t)] \quad (4.14)$$

The coefficients $X_{1,6\emptyset}, X_{2,6\emptyset}, X_{3,6\emptyset}$ and $X_{4,6\emptyset}$ are expressed in equations (4.15) to equation (4.18).

$$X_{1,6\emptyset} = \frac{1.93 V_m (R_{z,6\emptyset} + m_{1,6\emptyset} L_{x,6\emptyset}) (m_{1,6\emptyset} \sin(\emptyset) + \omega \cos(\emptyset))}{a_{,6\emptyset} (m_{1,6\emptyset}^2 + \omega^2) (m_{1,6\emptyset} - m_{2,6\emptyset})} \quad (4.15)$$

$$X_{2,6\emptyset} = \frac{1.93 V_m (R_{z,6\emptyset} + m_{2,6\emptyset} L_{x,6\emptyset}) (m_{2,6\emptyset} \sin(\emptyset) + \omega \cos(\emptyset))}{a_{,6\emptyset} (m_{2,6\emptyset}^2 + \omega^2) (m_{2,6\emptyset} - m_{1,6\emptyset})} \quad (4.16)$$

$$X_{3,6\emptyset} = \frac{1.93 V_m (R_{z,6\emptyset} - j\omega L_{x,6\emptyset}) (\sin(\emptyset) + j\cos(\emptyset))}{2(-a_{,6\emptyset}\omega^2 - jb_{,6\emptyset}\omega + c_{,6\emptyset})} \quad (4.17)$$

$$X_{4,6\emptyset} = \frac{1.93 V_m (R_{z,6\emptyset} + j\omega L_{x,6\emptyset}) (\sin(\emptyset) - j\cos(\emptyset))}{2(-a_{,6\emptyset}\omega^2 + jb_{,6\emptyset}\omega + c_{,6\emptyset})} \quad (4.18)$$

4.3.2 Mathematical Analysis of Current of SCIG

The analysis for inrush current of SCIG is similar to that of DSIG, but for a three-phasesystem, $\alpha = 0^\circ$ represented in equation (4.6), equation (4.7) and accordingly the resultant current for SCIG shall reduce to equation (4.19).

$$I(s)_{3\emptyset} = \frac{V_m (R_{z,3\emptyset} + s L_{x,3\emptyset}) (s \sin(\emptyset) + \omega \cos(\emptyset))}{(s^2 + \omega^2) \left[s^2 (L_{x,3\emptyset} L_{y,3\emptyset}) + s (R_{s,3\emptyset} L_{x,3\emptyset} + R_{z,3\emptyset} L_{x,3\emptyset} + R_{z,3\emptyset} L_{y,3\emptyset}) + R_{s,3\emptyset} R_{z,3\emptyset} \right]} \quad (4.19)$$

The equivalence of parameters for same capacity SCIG may be formalized in terms of ADSIG parameters as:

$$L_{x,3\emptyset} = L_{x,6\emptyset}; \quad (4.20)$$

$$R_{z,3\emptyset} = R_{z,6\emptyset}; \quad (4.21)$$

$$R_{1,3\emptyset} = 0.5 R_{16\emptyset}; \quad (4.22)$$

$$L_{y,3\emptyset} = 0.5 L_{y,6\emptyset} \quad (4.23)$$

The generalized quadratic equation and its roots for SCIG can be expressed as in equations (4.24) and equation (4.25).

$$a_{3\emptyset}s^2 + b_{3\emptyset}s + c_{3\emptyset} = 0 \quad (4.24)$$

$$m_{1,2,3\emptyset} = \frac{-b_{3\emptyset} \pm \sqrt{b_{3\emptyset}^2 - 4a_{3\emptyset}c_{3\emptyset}}}{2a_{3\emptyset}} \quad (4.25)$$

Where,

$$\left. \begin{aligned} a_{3\emptyset} &= L_{x,3\emptyset}L_{y,3\emptyset} \\ b_{3\emptyset} &= R_{z,3\emptyset}(2L_{x,3\emptyset} + L_{y,3\emptyset}) \\ c_{3\emptyset} &= R_{s,3\emptyset}R_{z,3\emptyset} \end{aligned} \right\} \quad (4.26)$$

The coefficients $X_{1,3\emptyset}$, $X_{2,3\emptyset}$, $X_{3,3\emptyset}$ and $X_{4,3\emptyset}$ are expressed in equations (4.27) to (4.30).

$$X_{1,3\emptyset} = \frac{V_m(R_{z,3\emptyset} + m_{1,3\emptyset}L_{x,3\emptyset})(m_{1,3\emptyset}\sin(\emptyset) + \omega\cos(\emptyset))}{a_{,3\emptyset}(m_{1,3\emptyset}^2 + \omega^2)(m_{1,3\emptyset} - m_{2,3\emptyset})} \quad (4.27)$$

$$X_{2,3\emptyset} = \frac{V_m(R_{z,3\emptyset} + m_{2,3\emptyset}L_{x,3\emptyset})(m_{2,3\emptyset}\sin(\emptyset) + \omega\cos(\emptyset))}{a_{,3\emptyset}(m_{2,3\emptyset}^2 + \omega^2)(m_{2,3\emptyset} - m_{1,3\emptyset})} \quad (4.28)$$

$$X_{3,3\emptyset} = \frac{V_m(R_{z,3\emptyset} - j\omega L_{x,3\emptyset})(\sin(\emptyset) + j\cos(\emptyset))}{2(-a_{,3\emptyset}\omega^2 - jb_{,3\emptyset}\omega + c_{,3\emptyset})} \quad (4.29)$$

$$X_{4,3\emptyset} = \frac{V_m(R_{z,3\emptyset} + j\omega L_{x,3\emptyset})(\sin(\emptyset) - j\cos(\emptyset))}{2(-a_{,3\emptyset}\omega^2 + jb_{,3\emptyset}\omega + c_{,3\emptyset})} \quad (4.30)$$

4.3.3 Comparison of Forced Response of SCIG and DSIG

For conclusive comparison of forced response for both the generators the damping coefficients are calculated.

The parameters for SCIG are taken from a typical three phase 5 HP machine model in MATLAB Simulink and are as follow:

- $R_1 = 0.6 \Omega$,
- $L_s = 0.35 \text{ mH}$,
- $R_r = 0.63 \Omega$,
- $L_r = 5.4 \text{ mH}$ and
- $L_m = 35.4 \text{ mH}$

And the parameters of ADSIG are taken from the Chapter 3 Section 3.5.3 (Table 3.3) as:

- $R_1 = 1.2 \Omega$,
- $L_s = 0.7 \text{ mH}$,
- $R_r = 0.63 \Omega$,
- $L_r = 5.4 \text{ mH}$ and
- $L_m = 35.4 \text{ mH}$.

Using these machine parameters and equations (4.1 a) to equation (4.1 g) and equations (4.19) to (4.23) the quadratic equation coefficients for both generators (SCIG and ADSIG) are calculated. The values of a, b and c respectively are given as:

$$\left. \begin{aligned} a_{(3)} &= 0.177 \times 10^{-3} \\ b_{(3)} &= 36.67 \times 10^{-3} \\ c_{(3)} &= 327.6 \times 10^{-3} \end{aligned} \right\} \text{for SCIG} \quad (4.31)$$

$$\left. \begin{aligned} a_{(6)} &= 0.354 \times 10^{-3} \\ b_{(6)} &= 39.8 \times 10^{-3} \\ c_{(6)} &= 655.2 \times 10^{-3} \end{aligned} \right\} \text{for ADSIG} \quad (4.32)$$

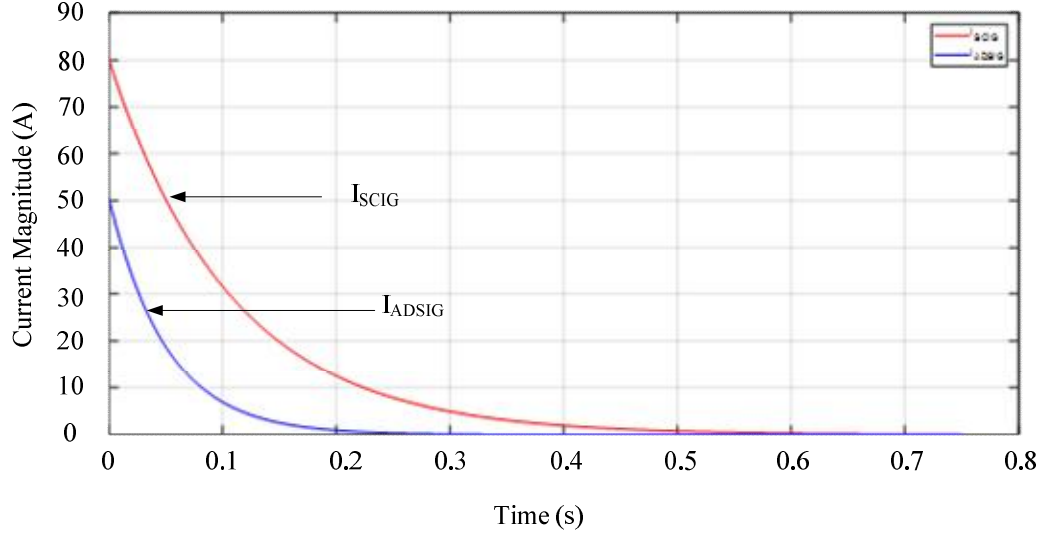


Fig. 4.4: Forced Current Response of SCIG and ADSIG

The damping coefficients $m_{1,2}$ for both ADSIG and SCIG are calculated using equations (4.13) and equation (4.25) respectively. The values of $m_{1,2}$ for ADSIG are (-92.7 and -20) whereas that for SCIG are (-198 and -9.35). The obtained value of $m_{1,2}$ are used for calculation of X_1 , X_2 , X_3 , X_4 by putting values in equation (4.15) to equation (4.18) for ADSIG and equation (4.27) to equation (4.30) for SCIG. Further the forced current $I_{a6\Phi}$ and $I_{a3\Phi}$ can be calculated from equation (4.24) and equation (4.26) respectively. The damping of initial current is observed by plotting the forced current response for both the generators using the values of damping coefficients and X_1 , X_2 for both the generators and is shown in Fig. 4.4. It may be observed that the transient response of ADSIG damps out fast as compared to a SCIG. The combined effect of damping coefficients m_1 , m_2 and the coefficients X_1 , X_2 , for respective generator helps in depicting level of inrush currents, aid to low amplitude of inrush current and its faster damping (reaching steady state current faster) for ADSIG as

compared to SCIG.

4.3.4 Comparison of Natural Response of SCIG and DSIG

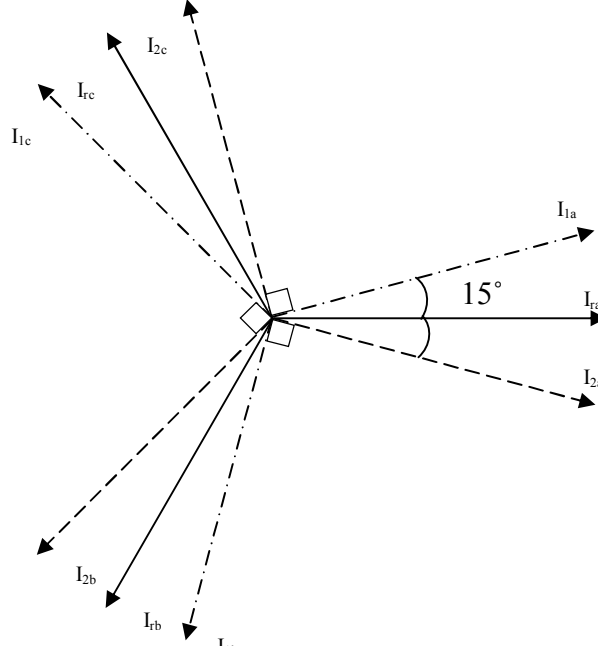


Fig. 4.5: Phasor representation of stator and rotor currents of ADSIG

Analysing the equations for natural response of current of ADSIG reveals that self-support of air gap flux through smaller changes in both the stator currents of the ADSIG. The proposition can be better understood through the phasor diagram representation of the two sets of stator currents, shown in Fig. 4.5. It may be observed that I_{2c} leads in quadrature with I_{1a} , similarly I_{2a} leads in quadrature with I_{1b} and I_{2b} leads in quadrature with I_{1c} for a sequence of 'abc'. Thus the increase in real component of the currents of second set of windings supplements reactive power support of first set of stator circuit. This becomes very important upon occurrence of low voltage condition on the grid, where the magnetic circuit is devoid of requisite reactive power from the grid. Similarly the first set partially fulfils the requirement of reactive power of second set of the windings under low voltage conditions for

strengthening of air gap flux.

Thus the configuration provides self-support of flux under low voltage condition on the grid, thereby maintaining higher energy conversion efficiency of the system for larger range of low voltage conditions on the grid, reliving it from undue stress in such condition. This analogy is cemented by dealing with steady state response of the stator current of ADSIG and its comparison with the SCIG. The imaginary part (reactive part) of the current is governed by the difference of parameters, X_3 and X_4 for both the generators. For comparing the reactive part of the current demand mathematical ratio of difference of X_3 and X_4 for both SCIG and ADSIG respectively is taken.

$$\left| \frac{X_{3(3\emptyset)} - X_{4(3\emptyset)}}{X_{3(6\emptyset)} - X_{4(6\emptyset)}} \right| = \left| \frac{0.5 (2\omega^2 L_x \sin \emptyset - R_z \omega \cos \emptyset)}{(3\omega^2 L_x \sin \emptyset - R_z \omega \cos \emptyset)} \right| \quad (4.33)$$

Using the considered machine parameters the calculated ratio becomes:

$$\left| \frac{X_{3(3\emptyset)} - X_{4(3\emptyset)}}{X_{3(6\emptyset)} - X_{4(6\emptyset)}} \right| \cong 1.1658 \quad (4.34)$$

It may be observed that the reactive current demand of SCIG is 17% (16.58%) more than the reactive current demand of ADSIG. This means that for maintaining same air gap flux or delivering same output power SCIG will require 17% more reactive current. This confirms the philosophy of ADSIG for the lower dependence of reactive current drawn from the mains, to maintain the air gap flux, keeping the conversion efficiency higher in comparison with SCIG.

4.4 MATLAB Simulation and Hardware Comparison

A validation of the mathematical analysis is carried out through simulation in MATLAB SIMULINK environment and experimentation on the developed hardware prototype of ADSIG. The inrush currents of ADSIG and SCIG are compared besides

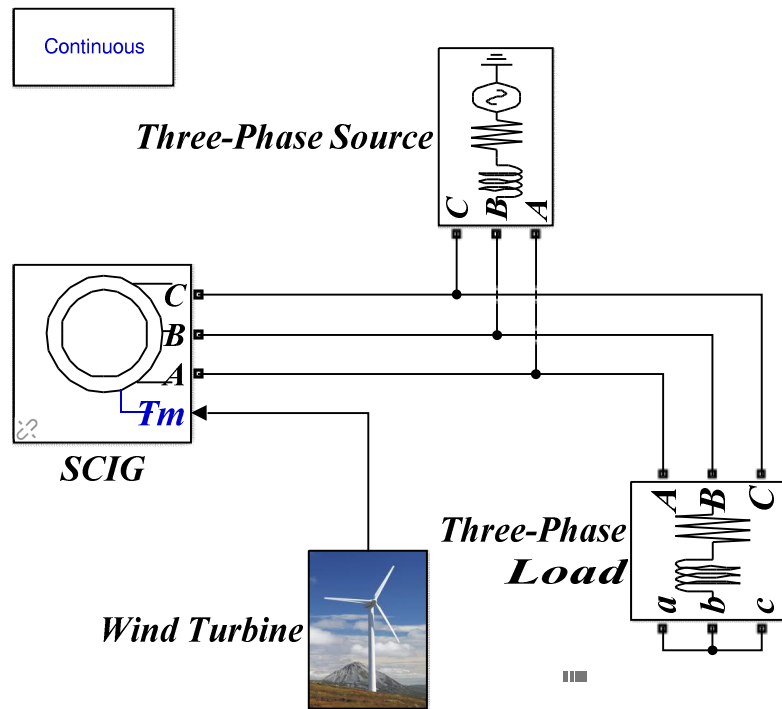


Fig. 4.6: SIMULATION Model of SCIG

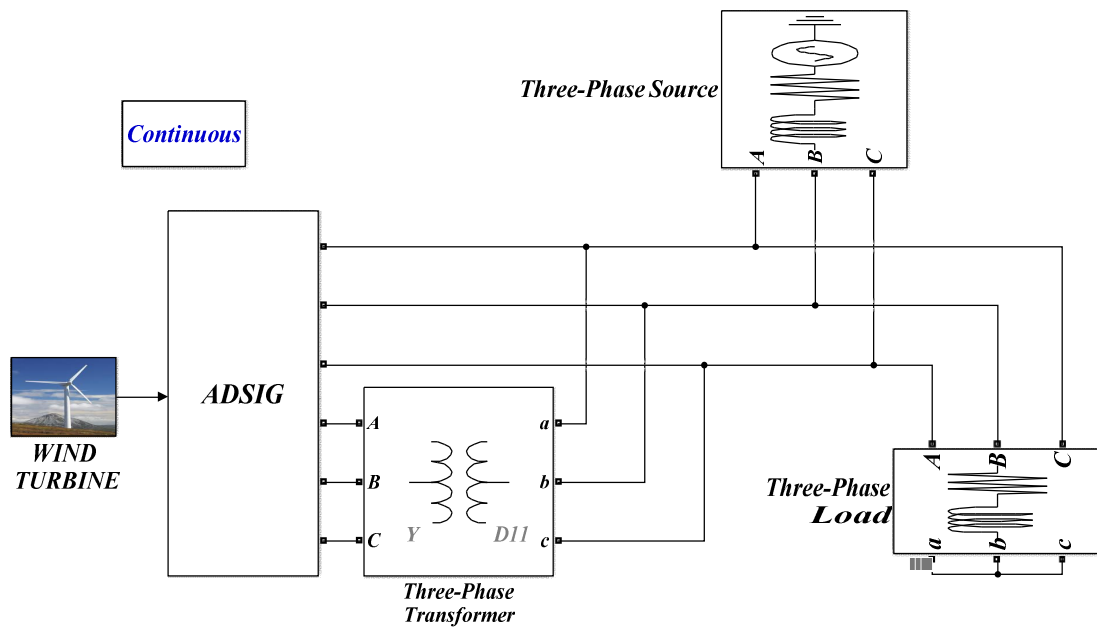


Fig. 4.7: SIMULATION Model of ADSIG

comparison made for their abilities to operate under conditions of one phase open and low voltage on all phases to establish the suitability of ADSIG in wind farm

applications. The MATLAB SIMULINK models of both SCIG and ADSIG are shown in Fig. 4.6 and Fig. 4.7 respectively.

The load connected to both generators is balanced three phase linear, passive load. Here the reactive power demand of SCIG and ADSIG is supplied by their respective grids individually. Both the generators are incapable of generation until they have sufficient reactive power which is required to magnetize the air gap. In SCIG same three-phase terminals are responsible for absorbing reactive power from the grid and transferring active power to load /grid, whereas in case of ADSIG active and reactive power flow is done via two sets of three-phase windings. Thus the power generated by ADSIG is divided into both the winding sets depending upon loading conditions and grid interconnection, thereby limiting the magnitude of the current flowing in an individual set of winding.

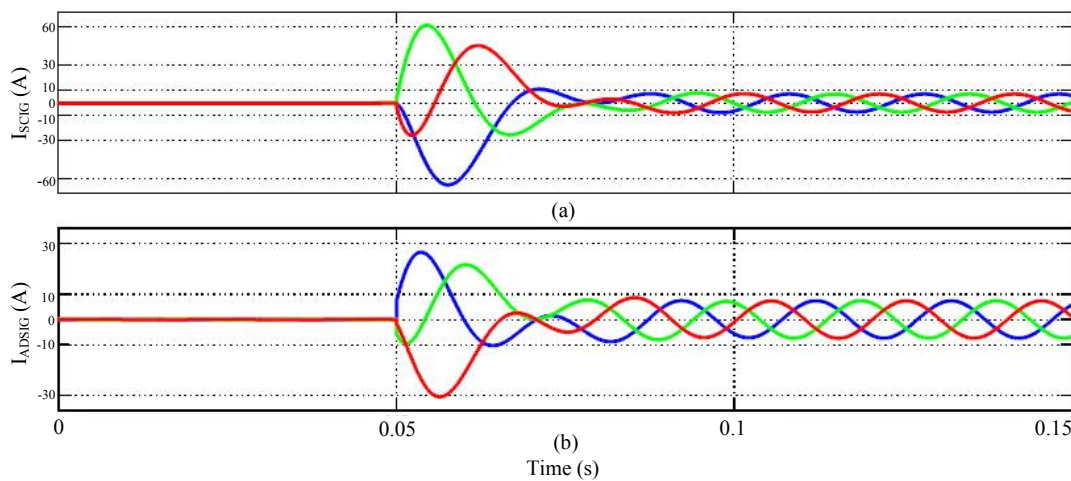


Fig. 4.8: Inrush Current of SCIG and ADSIG

A comparison of the performance is drawn between direct grid connected SCIG and ADSIG on the basis of the quantum of inrush current and settling time during starting and low voltage condition to understand their impact on other turbines for allowing coexistence. Further, the capability of the generators are accessed for an internal fault, viz. opening of one phase of both generators at the point of common coupling (PCC)

and its impact on the load side. The performance is intentionally evaluated under weak grid connection to have a clear view for inrush current during insertion of generator and fault ride through condition and the same is presented from Fig. 4.8 to Fig. 4.17 both through simulation and hardware results. During their testing both the induction, generators are kept at a fixed speed higher than the synchronous speed.

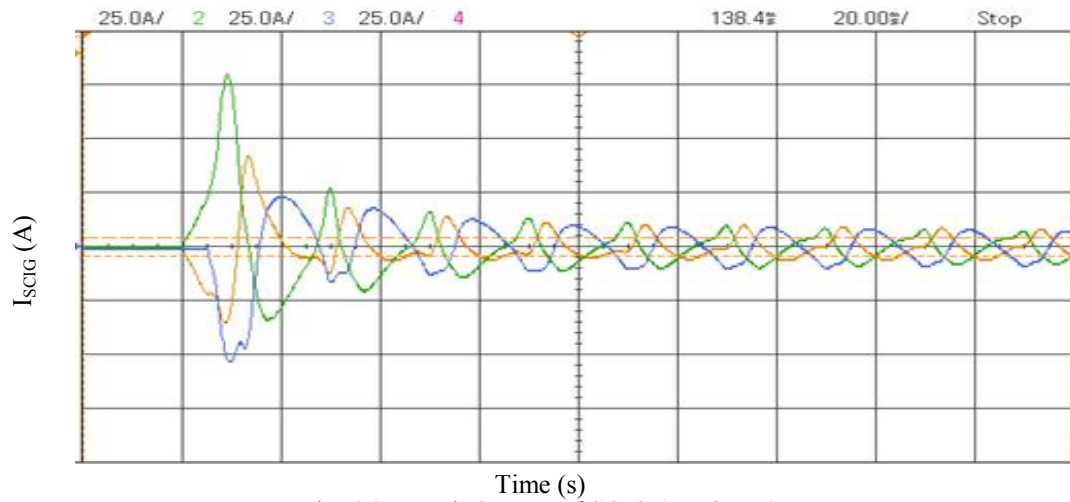


Fig. 4.9: Inrush Current of SCIG (Hardware)
X-axis: 1 div.= 20ms; Y-axis: 1 div. = 25A

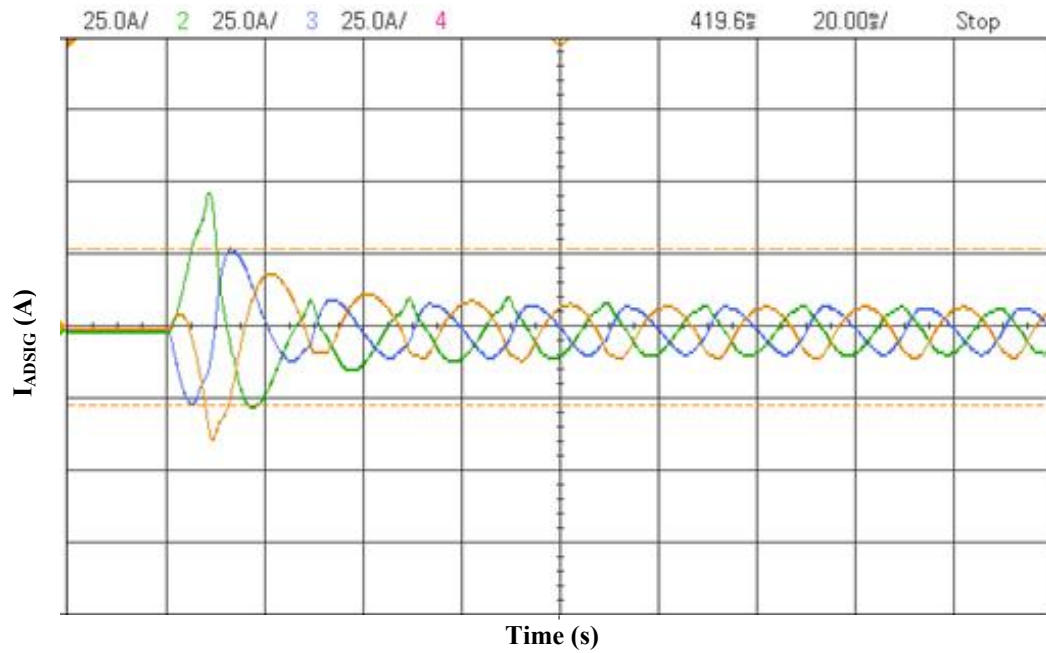


Fig. 4.10: Inrush current of ADSIG (Hardware)
X-axis: 1 div. =20ms, Y-axis: 1 div.= 25 A

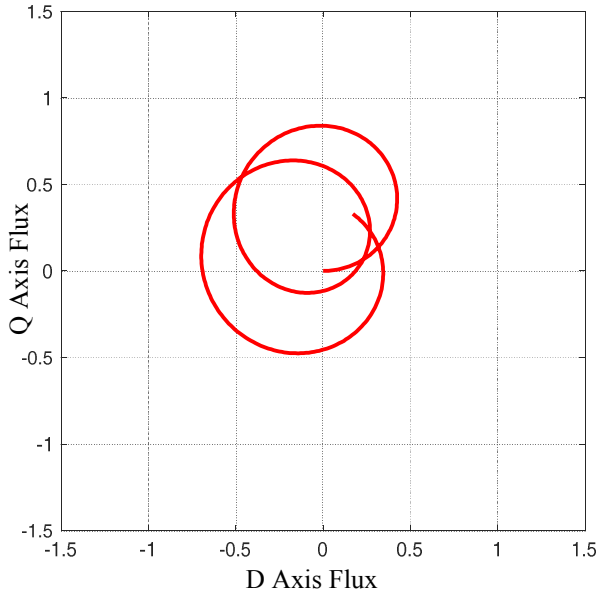


Fig. 4.11(a): D-Q Axis Flux for SCIG (0-3 cycle)

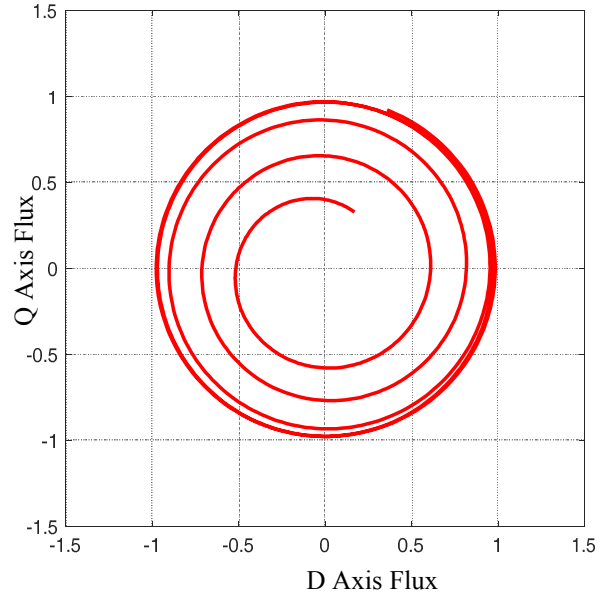


Fig. 4.11(b): D-Q Axis Flux for SCIG (3-7.5 cycle)

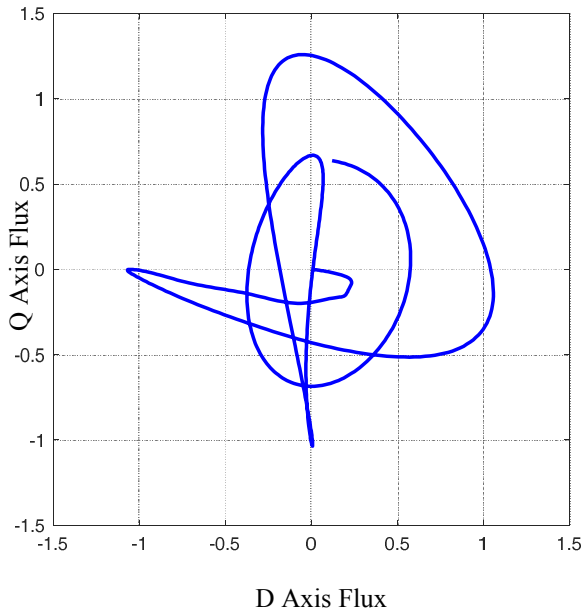


Fig. 4.12 (a): D-Q Axis Flux for ADSIG (0-3 cycle)

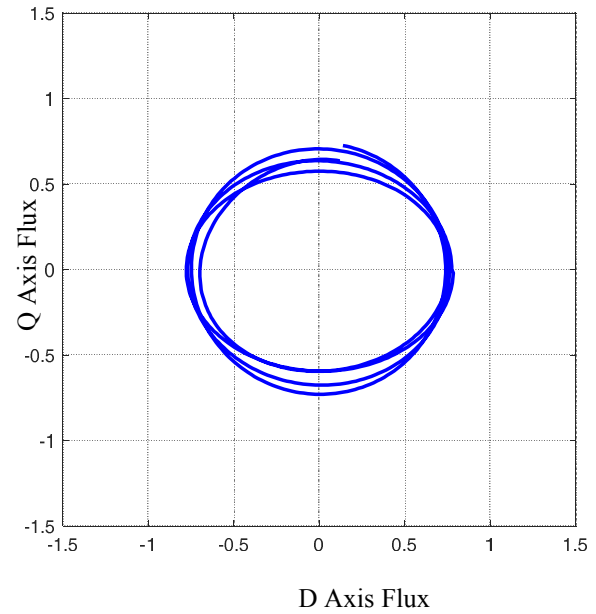


Fig. 4.12 (b): D-Q Axis Flux for ADSIG (3-7.5 cycle)

The performance of IGs is studied during the starting period when net inrush currents are drawn from the connected grid is observed and the same is presented in Fig. 4.8(a-b). Both SCIG and ADSIG are switched in at $t = 0.1$ s and are allowed to draw the excitation current from the grid, it may be observed that SCIG draws peak to peak inrush current of approximately 8 times the peak to peak steady-state current, whereas the DSIG draws net inrush currents from the grid of 2 times the peak to peak generator

current of each winding set which is presented respectively in Fig. 4.8(a) and Fig. 4.8(b).

During such inception period to the grid, the sub-synchronous resonance phenomenon is also observed which is also evident in the current waveforms of generators. It may be observed that the phenomenon is more prevalent in case of SCIG than in ADSIG due to lack of damping in the former one, which is provided by the excitation of flux in either winding in later case.. This performance is also validated for both generators through hardware results. Fig.4.9 and Fig.4.10 respectively show the experimental results observed for currents at the time of insertion of SCIG and ADSIG into the grid. The obtained results match closely with the simulation result and validate the theoretical analysis done for the same.

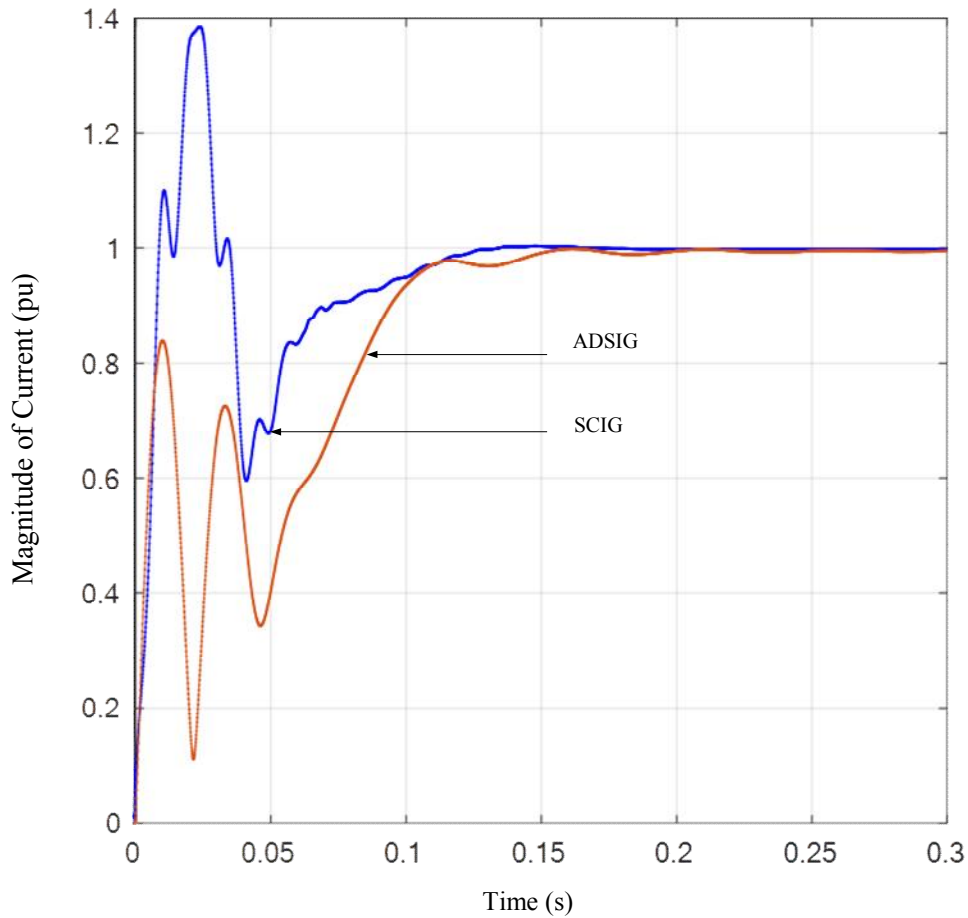


Fig. 4.13: d-q Flux for SCIG and ADSIG (resultant of Leading and Lagging Stator Winding)

To further evaluate the transient condition, during inrush currents, the d, q flux plots of both the generators are plotted when both the generators are grid-connected, are switched on at $t = 0$ s and driven at a fixed speed by the prime mover. Three flux plots are plotted for both the generators; the first plot is from instant of switching on the generator to first 3 (three) cycles (Fig.4.11 (a) for SCIG and Fig.4.12 (a) for ADSIG); second plot is plotted for data from 3 (three) cycles to 7.5 (seven and a half) cycles (Fig.4.11(b) for SCIG and Fig. 4.12(b) for ADSIG); thirdly and lastly the effective flux of both generators is plotted w.r.t. time from these instant of switching on (0 s) to first 7.5 cycles (0.15s) (Fig. 4.13).

From these flux plots, it is observed that:

- ADSIG maintains the required flux in lesser time as compared to the SCIG.
- During first three cycles only ADSIG tries to maintain the air gap flux reaches 85% of steady state whereas at the same instant SCIG is able to maintain only 57% of the steady state air gap flux.
- Thereafter also the transient response of ADSIG is faster as compared to SCIG. ADSIG enters the 10% envelope in 0.07s whereas SCIG takes 0.095s for reaching the 10% envelope of steady state air gap flux.
- In ADSIG the asymmetrical winding structure facilitates the auto compensation of reactive power demand requisite for magnetising the air gap flux. The 30° shifted windings result in two sets of three-phase current which are relatively at quadrature to each other. Thus the real component of current for one set of winding provides for the reactive power requirement of the other winding set. This is also shown in the flux figure of direct and quadrature axis for ADSIG.

- The settling time for inrush current of ADSIG is also too low as compared to that of SCIG due to auto-compensation of fluxes. The requirement of reactive current is supported by three-phase currents in a SCIG and thus there is more burden on three windings, but in ADSIG the reactive current demand is distributed in six phase currents, thereby reducing the effective reactive power demand per phase and in total due to auto-compensation.

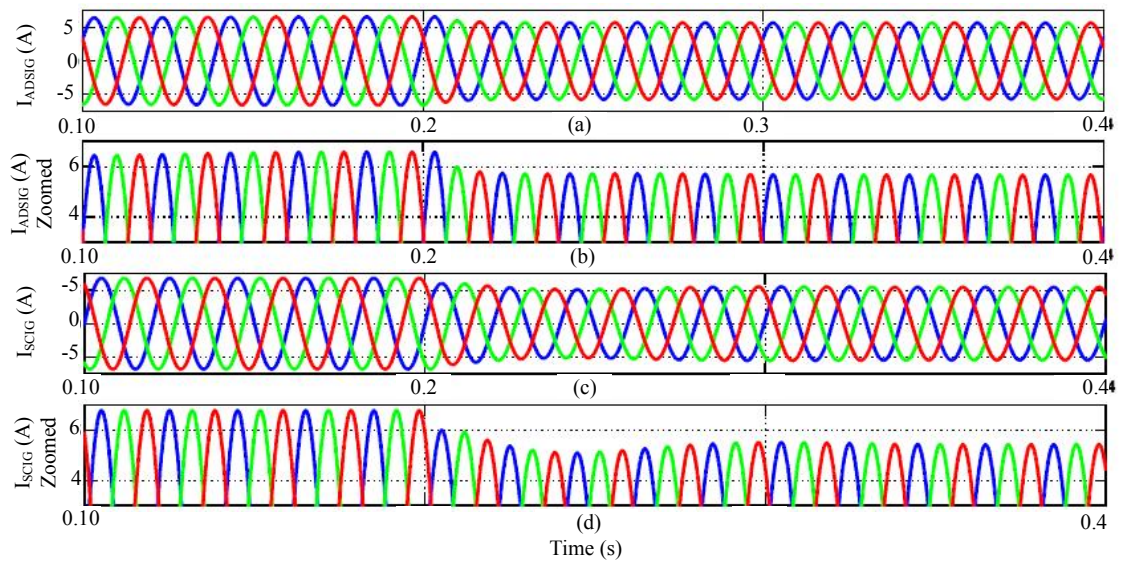


Fig. 4.14 Transient Current Response of generators due to low voltage condition

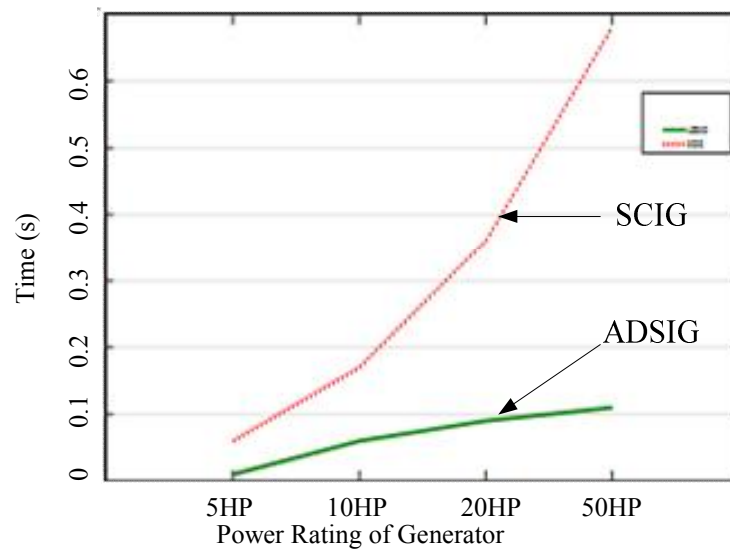


Fig. 4.15: Settling time of SCIG and ADSIG currents during Low Voltage Condition

The performances of the generators are also evaluated during low voltage conditions on the grid. Simulation results for observations on load currents are shown in Fig. 4.14(a) for SCIG and in Fig. 4.14(c) for ADSIG directly coupled with the grid. For clearer understandings zoomed waveforms for the duration of disturbance are shown in Fig. 4.14(b) and Fig. 4.14(d) for SCIG and ADSIG respectively. From Fig. 4.14(b) and Fig. 4.14(d) it is clearly observed that the response time of ADSIG is much faster as compared to that of SCIG. The load current for ADSIG fed system settles almost instantly without any oscillations, Fig. 4.14(d), whereas load currents for SCIG fed system as seen in Fig. 4.14(b) takes comparatively larger time owing to some oscillations to settle to a steady state value due to variable demand of reactive power and the fluctuation in the supply of real power.

The current response of ADSIG conforms to the response of a near critically damped system, as per the analysis of ADSIG for handling transient conditions. Such phenomenon should be more prominent in higher rated SCIG machines, due to the lesser resistance of their winding and higher moment of inertia, leading to large disturbances during start-up or black start, if not arrested may cause a cascading effect in wind farm. Fig. 4.15 shows the trends of settling time of both generators at the condition of low voltage for higher ratings. This can be seen that as the rating of generator increases the response of ADSIG is much better as compared to SCIG.

Fig. 4.16 and Fig. 4.17 presents the phasor diagram, of SCIG and ADSIG respectively, showing the voltage at PCC and node currents (Grid current, Generator current and the load current) of a phase for further understanding of real and reactive power transaction from grid and generators feeding the loads during normal condition, low voltage condition and fault condition where one phase of generator is opened

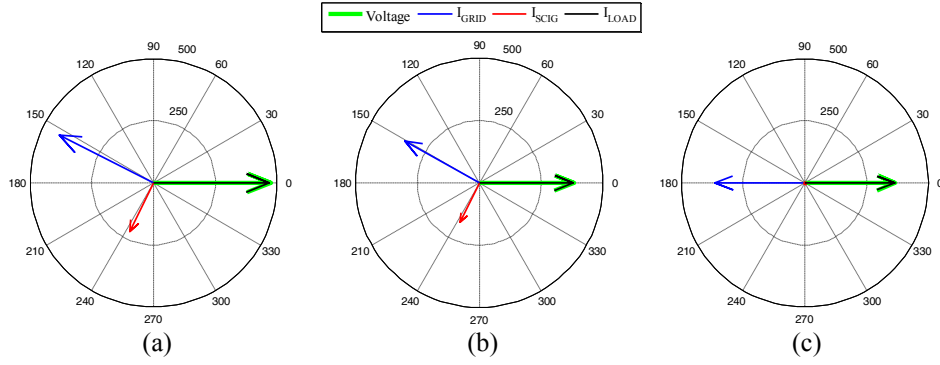


Fig. 4.16: Phasor of Voltage and Currents for (a) Normal (b) Low Voltage (c) Single Phasing Conditions when Grid and Load are connected to SCIG

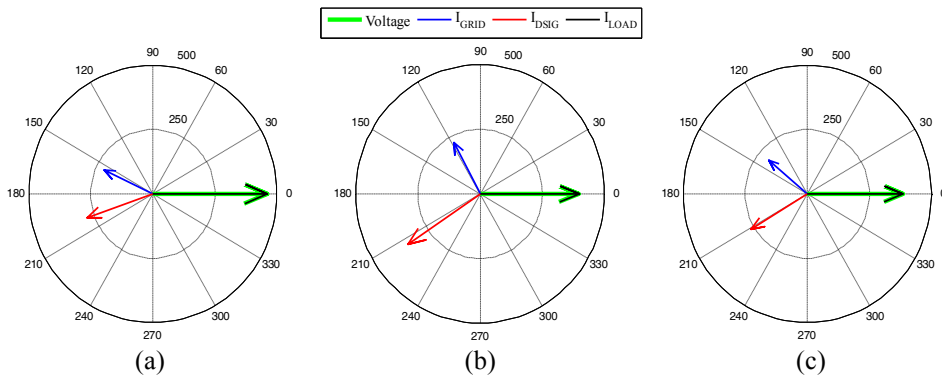


Fig. 4.17: Phasor of Voltage and Currents for (a) Normal (b) Low Voltage (c) Single Phasing Conditions when Grid and Load are connected to ADSIG

intentionally. Fig. 4.16(a) and Fig. 4.17(a) represent the normal case of operation of SCIG and ADSIG respectively for power transfer from generators and grid to their respective loads. The considered generators are lesser than the capacity of loads where the active power demand of load is fed from both grid and respective generator. Whereas, the reactive power demand of each generator is catered by the connected grid. Since the connected load is considered totally resistive to have a clear understanding of power transfer the phasor of the load current is considered superimposed on the voltage phasor.

Under low voltage condition on the grid, it may be observed from the phasor diagram for ADSIG in Fig. 4.17(b) that the grid is relieved from the excess burden and the active power contribution from the grid is decreased whereas, the ADSIG has

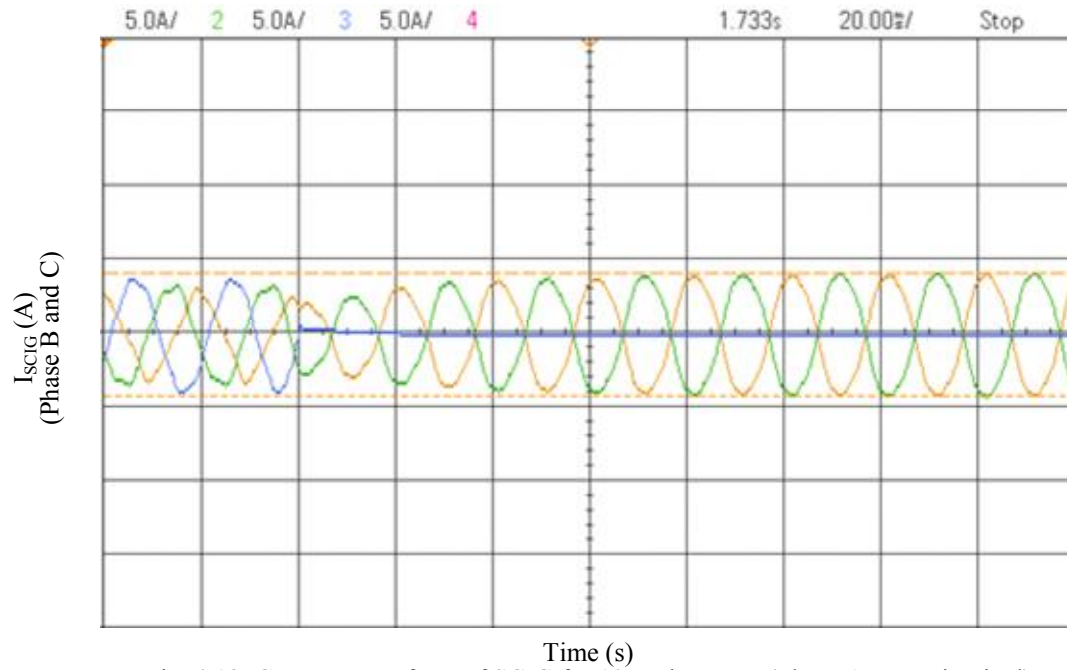


Fig. 4.18: Current Waveform of SCIG for 10 cycles FRT; (Phase A open circuited)
X-axis: 1 div. = 20ms; Y-axis: 1 div. = 5A

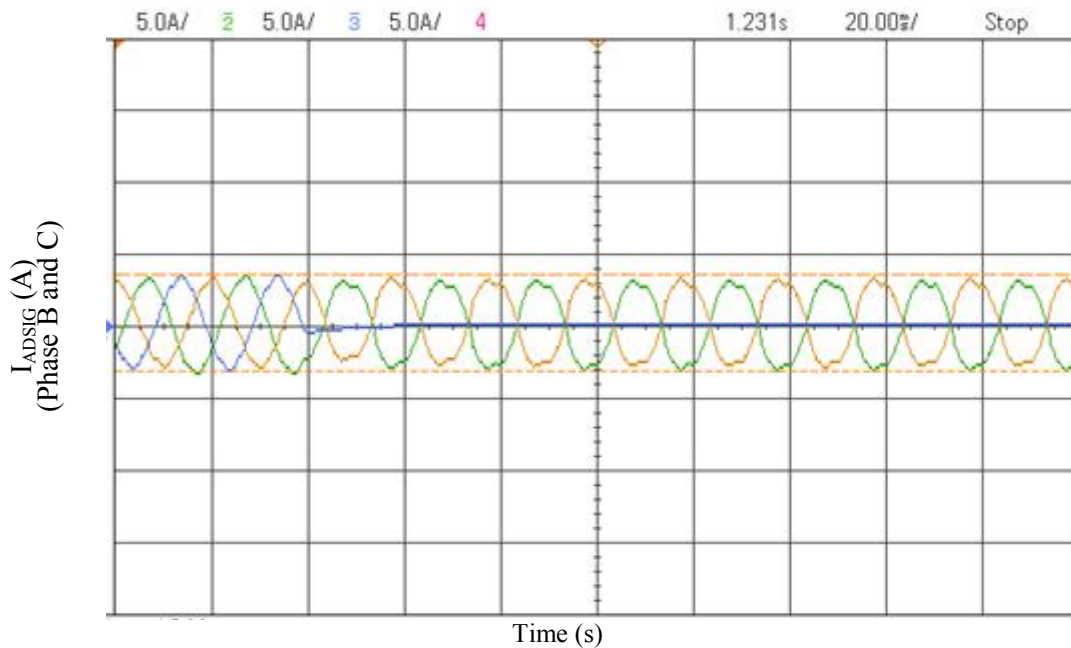


Fig. 4.19: Current Waveform of ADSIG for 10 cycles FRT; (Phase A open circuited)
X-axis: 1 div. = 20ms; Y-axis: 1 div. = 5A

increased its share in the supply of real power to the load. For increased active power delivery to the load, the ADSIG only demanded slightly increased reactive power

which it draws from the grid. On the other hand, from the phasor diagram of SCIG in Fig. 4.16(b) it is evident that SCIG decreased its generating capacity by lowering its power conversion efficiency due to fall in flux during low voltage condition. It may thus be confirmed that ADSIG enacts as a soft compensated power source for its ability to increase its current as and when there is a decrease of voltage (approx. 20%). The reliability of both the generators is also accessed in the event of opening of one phase of the generators. This refers to the opening of one phase out of the six phases. Such fault prompts the increase in currents of the healthy phases to increase to maintain the air gap flux. The phasor results are presented in Fig. 4.16(c) for SCIG and in Fig. 4.17(c) for ADSIG. It may be clearly observed in Fig. 4.16 (c) that the SCIG experiences single phasing.

While comparing the hardware results in Fig. 4.18 and Fig. 4.19 it may be observed that the percentage increase in currents of healthy phases in ADSIG remained much lesser as compared to SCIG where only two windings are sharing the extra burden of the opened phase whereas, the same is shared in five healthy phases. It may further be observed that such a fault condition drives the load with substantial unbalanced conducts which also escape as negative sequence currents into the grid causing voltage quality problems which may further harm other connected loads. The percentage current unbalances in load current while it is in fed from ADSIG remains as low as 7% in comparison to that of SCIG which gets deteriorated with 14% unbalance, which is almost double. In wind farms operating with larger rated SCIG's the unbalanced currents will be more pronounced resulting in more and more deterioration of both the grid and the load, and may also result in tripping of negative sequence relays.

4.5 Transient analysis of Air-Gap Flux

For the operation of the induction generator, there is requirement of reactive current for magnetizing the air-gap flux. The flux is required to be uniformly distributed for effective utilization of air-gap. During transient conditions, due to the variation of terminal voltage and reactive power drawn, the distribution of air-gap becomes non-uniform. For analyzing the air-gap flux of DSIG, both the configurations ADSIG and SDSIG are tested under normal conditions with different types of loading and under faulty conditions. Since the modeling equations of DSIG do not explicitly differentiate between the operation at transient conditions, a phasor analysis of both generators is carried out. The effect of loading at both leading and lagging winding of generators is observed on the resultant direct and quadrature axis flux.

Fig.4.20(a-l) shows the phasor diagram showing leading and lagging winding currents of ADSIG and SDSIG in terms of the direct axis and quadrature axis. To study the effect of leading and lagging winding current on one another the projection of one current is taken on the other current and the resultant leading and lagging current phasor are drawn. For simplification and ease of understanding the resultant phasor for both DSIGs are calculated taking leading winding as a reference. The projections of a current phasor are represented by dotted lines with the same colour as that of the current phasor. Superscript ‘*’ and ‘**’ are used to represent the direct axis and quadrature axis projections of lagging winding on leading winding axis and superscript ‘#’ and ‘##’ is used to represent the direct axis and quadrature axis projections of leading winding on lagging winding axis. Thick solid hashed lines represent the net leading and lagging winding current after incorporating the projections of their respective direct and quadrature current components. The phasor

diagram for ADSIG is represented in Fig. 4.20 (a-f).

For projection of lagging winding side on the leading winding side is given by equation (4.35) to equation (4.37).

$$I_{1q,AS} = 0 + j2.3 \quad (4.35)$$

$$I_{1d,AS} = -1.37 + j0 \quad (4.36)$$

$$I_{1NET,AS} = -1.37 + j2.37 \quad (4.37)$$

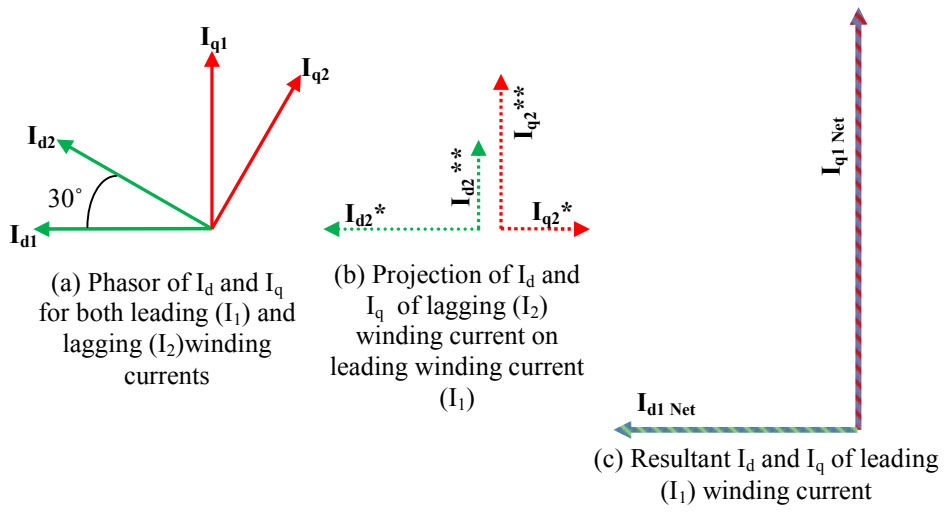


Fig. 4.20 (a), (b) and (c) Asymmetrical DSIG: Projection of Lagging to Leading Winding

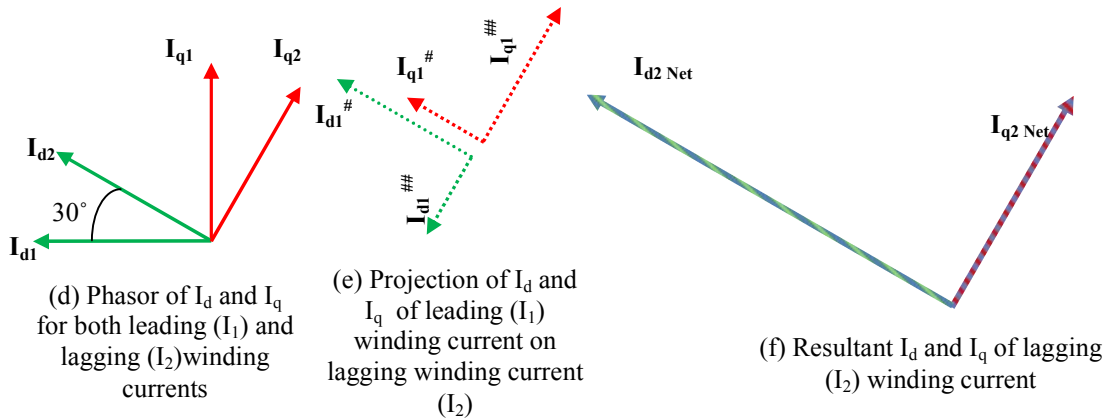


Fig. 4.20 (d), (e) and (f) Asymmetrical DSIG: Projection of Leading to Lagging Winding

Fig. 4.20(a) for represents the direct and quadrature components for current phasor of

leading and lagging winding set of ADSIG. Fig.4.20 (b) represents the projection of the lagging winding currents upon the leading winding currents of the ADSIG. Fig. 4.20(c) represents the resultant current on the leading winding current of the ADSIG incorporating the projections from the lagging side.

The projection of leading winding side on the lagging winding side is given by equation (4.38) to equation (4.40)

$$I_{2q,AS} = 0.69 + j1.19 \quad (4.38)$$

$$I_{2d,AS} = -2.05 + j1.18 \quad (4.39)$$

$$I_{2NET,AS} = -1.36 + j2.37 \quad (4.40)$$

Similarly Fig. 4.20 (d) shows the direct and quadrature axis component for current phasor of lagging winding set, Fig. 4.20 (e) represent the projections of leading winding currents on the lagging winding currents and Fig. 4.20 (f) represents the resultant lagging winding currents after incorporating the projections respectively for ADSIG.

Likewise the projection of lagging winding side on the leading winding side is given by equation (4.41) to equation (4.43).

$$I_{1q,S} = 0 + j2.37 \quad (4.41)$$

$$I_{1d,S} = -0.63 + j0 \quad (4.42)$$

$$I_{1NET,S} = -0.63 + j2.37 \quad (4.43)$$

The projection of leading winding side on the lagging winding side is given by equation (4.44) to equation (4.46).

$$I_{2q,S} = 0.55 + j0.31 \quad (4.44)$$

$$I_{2d,S} = -1.33 + j2.31 \quad (4.45)$$

$$I_{2NET,S} = -0.78 + j2.62 \quad (4.46)$$

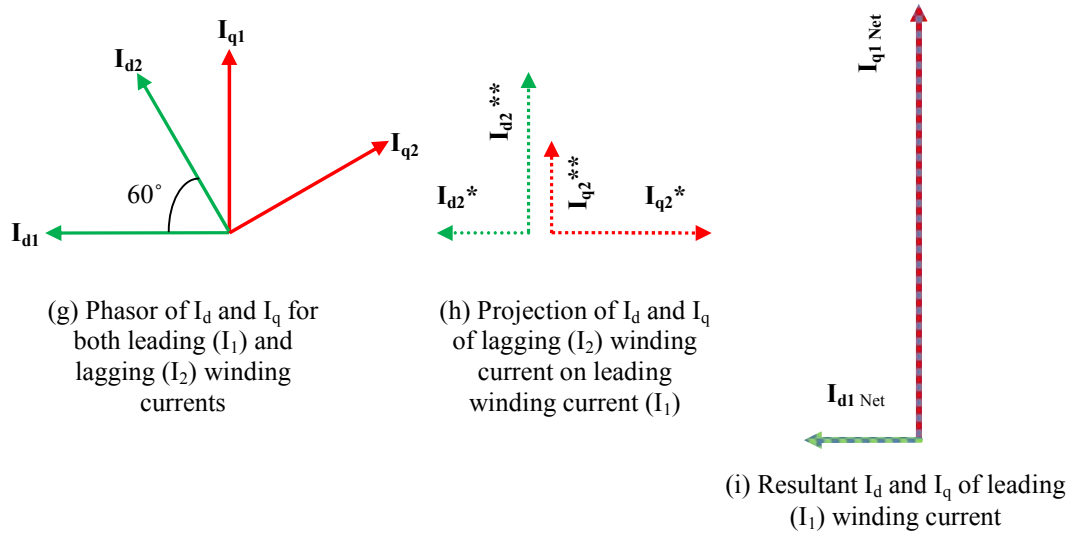


Fig. 4.20 (g), (h) and (i) Symmetrical DSIG: Projection of Lagging to Leading Winding

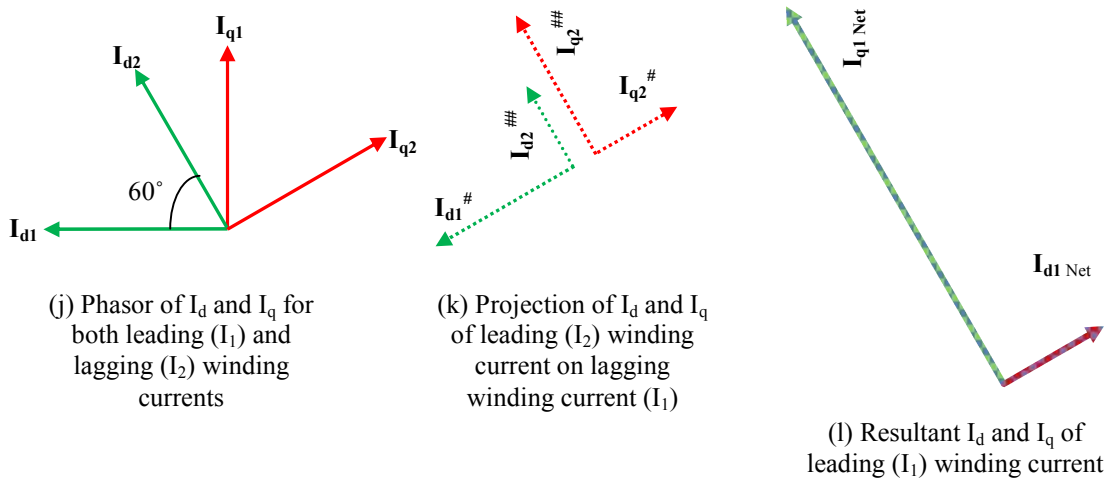


Fig. 4.20 (j), (k) and (l) Symmetrical DSIG: Projection of Leading to Lagging Winding

Fig.4.20(g-i) represent the current phasor for SDSIG for direct and quadrature components both (leading and lagging) winding current; projection of lagging winding side current on leading winding side and resultant current respectively. Similarly Fig. 4.20(j-l) shows the current phasor while referring to lagging side. Comparing equations (4.37) and (4.43), when the projection of lagging winding current

component is added with a current component of leading winding, it is observed that even for more real power generation the ADSIG demands nearly the same reactive power as demanded by the SDSIG. The same is evident from a comparison of Fig. 4.20(c) and Fig. 4.20(i) and collaborated by comparing equation (4.38) with equation (4.44).

The analysis results are again confirmed via simulation. The simulation diagram is same as used in Fig. 4.7 and the simulation model of SDSIG is similar to Fig. 4.7 except the difference in their phase angles for connection to leading side. In the Leading winding side of DSIG is connected to the grid with a respective phase shift of 30° for asymmetrical and 60° for symmetrical winding type DSIG. Similarly lagging winding side of DSIG is connected to the grid without any phase shift. Two distinct equal value three-phase capacitor banks are connected to both the winding sets (leading and lagging) of both DSIG's to partially support the excitation and to filter out any harmonics arriving from load towards generators. Different type of passive loadings (resistive and resistive-inductive loads) is considered connected to both sides with details given in Table 4.1.

Table 4.1: Rating of Different Loads

Type of Load	Value of Load
Resistive	$R = 180 \, \Omega$
Resistive-Inductive	$Z = 180 \, \Omega$ (0.8 pf)

The performance of weak grid coupled DSIGs with symmetrical and asymmetrical stator windings are evaluated comparatively on the basis of voltage regulation and

operation under low voltage which in turn is based on the establishment of air gap flux. Since the saturation of flux poses an impediment in the operation of IG a careful study of flux in the air gap is requisite. The simulated results under MATLAB environment are evaluated for different operating conditions. The connected load is perturbed intentionally to observe and compare the performance of the said two types of DSIGs in respect of direct and quadrature axis flux and the terminal voltage on the point of common coupling. The utilization of the core and transient characteristic is also been compared by analyzing the direct and quadrature axis flux under steady state and transient conditions during the occurrence of one phase open fault. Perturbing

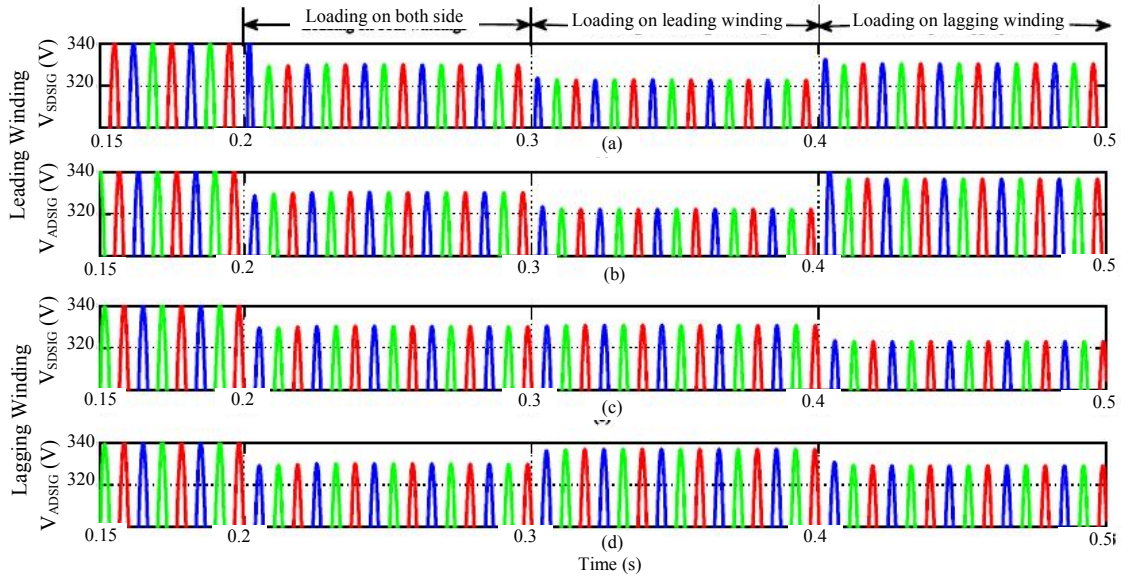


Fig. 4.21: Terminal Voltages of Symmetrical and Asymmetrical DSIG

loads are applied at the terminals of both the winding sets of DSIG and their relative effect on their voltage profile and flux are observed and evaluated. To study the effect of cross-coupling the IGs are loaded in three steps. Initially, from $t = 0$ to $t = 0.2$ s both the DSIGs are at no-load it may be observed from Fig. 4.21 that equal terminal voltages of 340 V are present. At $t = 0.2$ s when both the winding sets of the DSIG's are equally loaded with 1.75 kW UPF load on each winding set it resulted in the

voltage fall from 340 V to 330 V for both symmetrical and asymmetrical DSIG's.

Further at $t = 0.3$ s when the loading on leading winding side of both the IG's is increased by 750W each, whereas on lagging side load is kept as it is, a fall in voltage on the leading winding side of the IGs is observed, which varied from 330V to 322V. But as the cross-coupling effect which is more prominent for the ADSIG the voltage at the lagging winding side increases to 335V, whereas, in the SDSIG where the effect is not prominent the terminal voltage remains almost same at 330V. Again at $t = 0.4$ s, a load is applied at the lagging winding of both SDSIG as well as ADSIG the additional load applied is the preceding perturbation on leading side withdrawn. The terminal voltage of the lagging winding side is decreased from 331V to 322V for SDSIG and from 335V to 328V for ADSIG. The effect of cross-coupling in ADSIG is once again clearly visible with the rise of terminal voltage on the leading winding side i.e. from 322V to 335V. On the other hand, the terminal voltage of the leading winding for SDSIG shows a small effect of cross-coupling with a rise of terminal voltage (from 322V to 330V).

A detailed comparison between SDSIG and ADSIG is also carried out by analysis of the flux distribution. It may be observed in Fig. 4.22, that the utilization of core is very well justified in ADSIG where both direct and quadrature axis flux are nearly equal giving a circular shape of d-q flux graph. Also, in Fig. 4.22 it is evident that the d axis and q axis flux are highly skewed in SDSIG and the fluxes are not equal, giving it an elliptical shape on the d-q axis indicating its vulnerability to saturation of the core. Prior to loading the quadrature axis flux values of SDSIG ranges from -1 to 1 p.u. and -0.75 to 0.75 p.u. for ADSIG and, the direct axis flux value ranges from -0.25 to 0.25 p.u. and 0.75 to 0.75 p.u. for SDSIG and ADSIG respectively. It may be observed

from Fig. 4.22 that after resistive loading on lagging winding side the d-q plot of flux gets slightly compressed vertically and slightly bulges horizontally for both SDSIG and ADSIG in the same proportion. The similar effect is observed for both the IGs for the loading changes on the winding side.

The comparison of fault ride through capability of both DSIG's is done by is intentionally keeping one phase open for ten (10) cycles and d-q axis fluxes are plotted in Fig. 4.23 before fault, during fault and during the recovery period. Fig. 4.23 shows the plot for direct and quadrature axis flux during the pre-fault period for both SDSIG

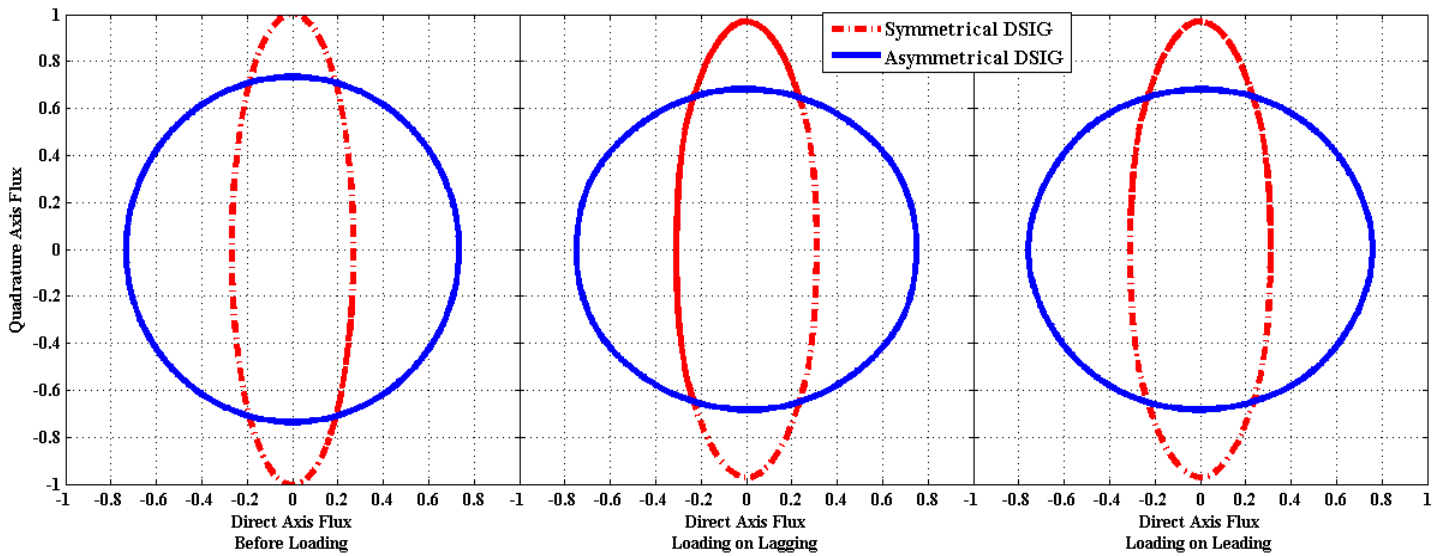


Fig. 4.22: Effect of Loading on Air Gap Flux

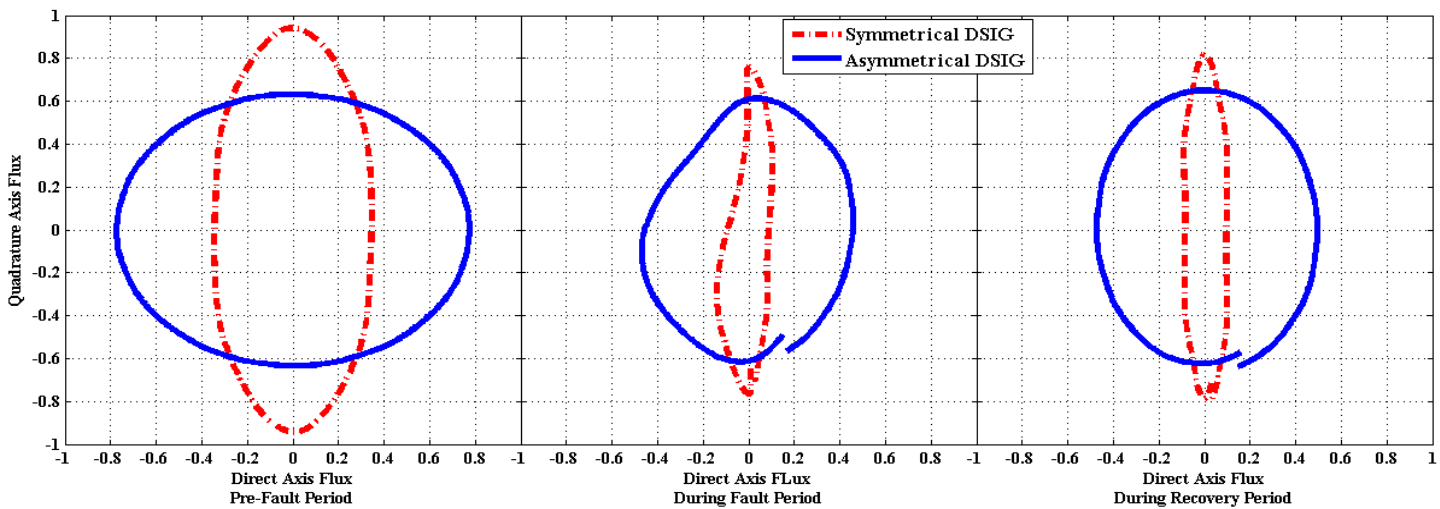


Fig. 4.23: Effect of LG Fault (10Cycles) on Air Gap Flux

(red dotted line) and ADSIG (blue solid line). It is also observed from Fig. 4.23 that ADSIG shows better stability during fault which helps during the recovery period after the fault is removed as compared to SDSIG. During pre-fault conditions the direct and quadrature axis flux values for SDSIG are observed as (-0.35 to 0.35) and (-0.95 to 0.95) respectively, whereas, for ADSIG it varies between (-0.8 to 0.8) and (-0.6 to 0.6) respectively. Quadrature flux of SDSIG shows more drastic changes when compared with ADSIG, whereas, the direct axis flux show relatively lesser decrementing tendency as for the quadrature axis.

Table 4.2: Comparative Table of different generators under Different Loading and Fault Conditions

Property	Voltage (Cross- Coupling)	Current THD	Fault Ride Through	d-q Flux Graph
Type of Generator				
SDSIG	Less pronounced	Higher	Poor	Asymmetrical
ADSIG	More pronounced	Lower	Good	Symmetrical
SCIG	Not Present	Higher	Poor	Symmetrical

The SDSIG witness a decrease from 0.35 to 0.15 p.u. (55% drop) and ADSIG witnesses the decrease from 0.8 to 0.45 p.u. (43% drop) in the direct axis flux, whereas, quadrature axis see a decrease from 0.9 to 0.75 p.u. (15% drop) for SDSIG and almost no change in quadrature axis flux for ADSIG. As the quadrature axis flux shows lesser deviation from a normal position in ADSIG, the recovery is fast, and the same is evident from the growth of flux in quadrature axis than in the case of SDSIG. During recovery period also the tendency of ADSIG to get back to normal position as fast as the growth in quadrature axis flux is more rapid than in the case of SDSIG. The

SDSIG shows a slower response as compared to ADSIG during recovery.

The results of the comprehensive analysis are presented in Table 4.2, which depicts the relative merits of ADSIG over the conventional SCIG and SDSIG for different operating conditions including LVRT and fault conditions and substantiate the suitability of ADSIG for wind farms.

4.6 Conclusion

In this chapter a detailed comparison of the ADSIG performance is done with similar rating SCIG and SDSIG. Firstly mathematical analysis of ADSIG current (during transient and steady state condition) is done with the help of its reduced equivalent circuit developed in the last chapter. The coefficients X_1 , X_2 , X_3 and X_4 for ADSIG and for a similar rating SCIG are calculated and the comparison of inrush and steady state currents for both the generators is done. The comparison of ADSIG and SCIG is also verified through MATLAB SIMULINK environment and further the comparison is extended and is conformed through the results of hardware prototype. Both simulation and hardware results show the superiority of ADSIG over SCIG during starting as well as steady state condition. The performance of both the generators for one phase open condition is also carried out in SIMULINK and hardware. The performance of ADSIG is better as compared to SCIG for such faulty conditions at the grid.

The transient air gap analysis of ADSIG is also done and the same is compared with the response of a similar rating SDSIG in simulation. A comprehensive phasor analysis is performed for both the generators and it is observed that the reactive power

requirement of ADSIG is less as compared to that of SDSIG for delivering a same active power to a load with all the other factors remaining same. Simulation is further carried out to study the effect of loading on the air-gap flux and the effect of a single line to ground fault on the air-gap flux. The results of both the tests show that ADSIG shows a better performance behavior as compared to its counterpart SDSIG.

Chapter 5

Three-Port Energy Integration and Soft Coupling of Two Distribution Feeders Using DSIG

5.1 General

Dual stator induction generator (DSIG) has recently emerged as a three-port power harvesting utility delivery device where, both the stator windings are operating at power frequency and are coupled with squirrel cage rotor, thus forming the magnetic circuit with an equal number of poles. This enables direct power coupling through both stator windings independently and via rotor circuit, thus, enhancing transient characteristics and efficiency. The main limitation of DSIG rests with narrow speed range operation, which often is supplemented through multi-gear systems. These demerits are offset by its increased power density, cheaper and rugged rotor structure, standard stator stampings/frames and conventional winding strategies. The reliability of power generation is also increased in DSIG as two three-phase ports deliver the power to the connected sets of three phase loads or feeders on either terminal.

DSIG having two sets of three phase terminals for soft interconnects with the feeders or loads with electrical isolation, together with the integration of wind energy harvesting made from connectivity at the shaft. The DSIG acts as a normal transformer while not in the generation and when the wind speed is adequate for a generation the power is injected from the shaft to either terminals based on the demanded power, thereby reducing the effective loading on either or both feeders connected on different

sides of the DSIG. An assembly/cluster of such small rating DSIGs connected in parallel by soft coupling and interconnection of feeders and may avert the need for up-scaling the electrical infrastructure to a great extent besides providing additional benefits of generation support from wind energy.

This chapter presents a soft inter-connect between two weak feeders using DSIG with asymmetrical stator windings for injection of power from wind energy and also contribute routing of power through its two winding sets to feeders. A detailed circuit analysis for demonstrating both generator and transformer action with electrical isolation to soft couple two feeders and analysis and performance has been done for application of DSIG as soft interconnect to two different feeders for routing of power and load management. A detailed phasor analysis is presented to affirm the claims. The performance is evaluated based on experimental results on a small scale prototype and single unit of DSIG for interconnection for voltage regulation, LVRT/FRT capability and inter-winding power transfer capability. The reactive power demand of DSIG is supported on both sides through the capacitor banks and difference demand through feeders connected to each winding sets respectively. Three phase passive loads are connected on both the sets of three-phase windings of DSIG to study the effect of load dynamics. Further study is conducted for power injection by DSIG during the disturbances on feeders.

5.2 System Configuration and Salient features of Three Port

Network

The system considered for studying the suitability of ADSIG acting as a soft coupler in a three port network is shown in Fig. 5.1. ADSIG is connected directly to two

different sets of three-phase AC mains supplies (feeders) with appropriate relative phase shifts provided through transformer connections; star-star transformer on the leading winding side of the ADSIG and star-delta transformer on the lagging winding side of the ADSIG. Respective feeder on both the side are assumed to have voltage source and loads associated with the feeder. Both the winding side of the ADSIG may be supported by the capacitor banks such that the difference in the reactive power required is fed by the grid on the respective winding set.

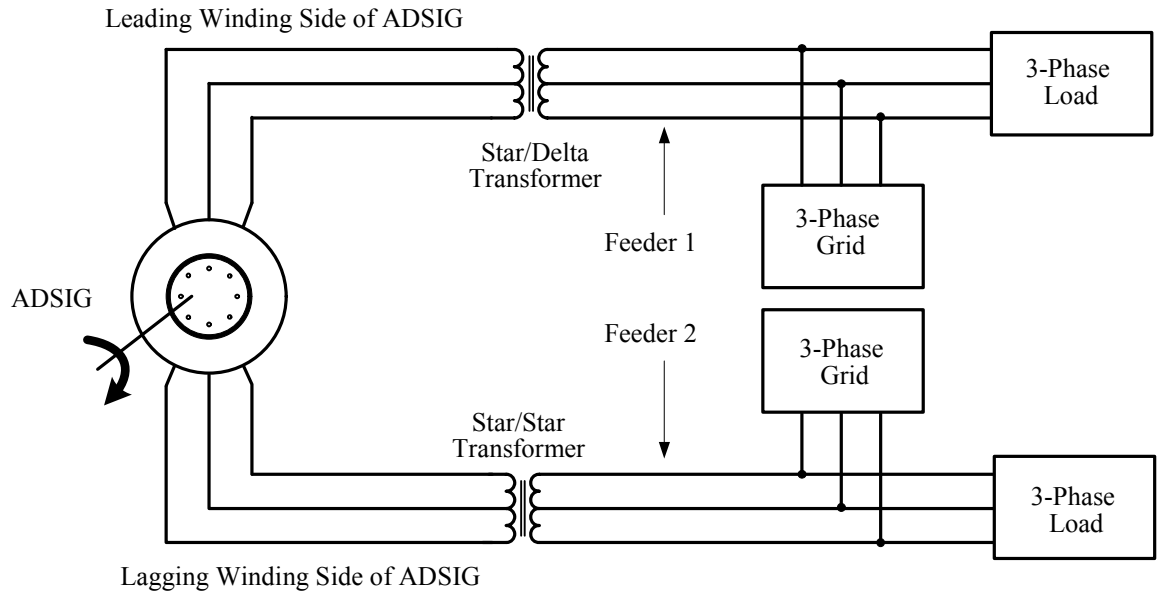


Fig. 5.1: System Configuration for ADSIG acting as Soft Coupler Between two Feeders

5.3 Mathematical Analysis of ADSIG for Power Routing

Capability of ADSIG Incorporating Loading on Feeders

The power routing capability of ADSIG enacting as a soft coupler for AC feeders can be more explicitly demonstrated by incorporating the loading on the feeders. The routing from one feeder to the other can be in more lucid way by connecting more

loads on the other feeder while being observed on the current feeder as depicted in Fig. 5.2(a). Z_1 and Z_2 are the modified stator impedance of leading and lagging winding side respectively incorporating connected to feeders at leading and lagging winding set of ADSIG. Similarly the loads connected to these feeders are represented respectively as Z_{L1} and Z_{L2} . Depending on the effective loading done at either feeder the power flow of ADSIG varies or the power is routed to auto compensate the demand. ADSIG routes its generated power to the feeder which is more loaded and thus helps in maintaining stability of the power system. To further elucidate the action of power routing the analysis is carried out for two conditions; as generator where power is evacuated to both /one feeder depending on the situation and other as transformer where generation action is not present.

CASE A: GENERATOR ACTION

Under the generator action the current generated by ADSIG is probed for distribution to the two feeders based on the loading conditions. The inference may be taken from Fig. 5.2(a).

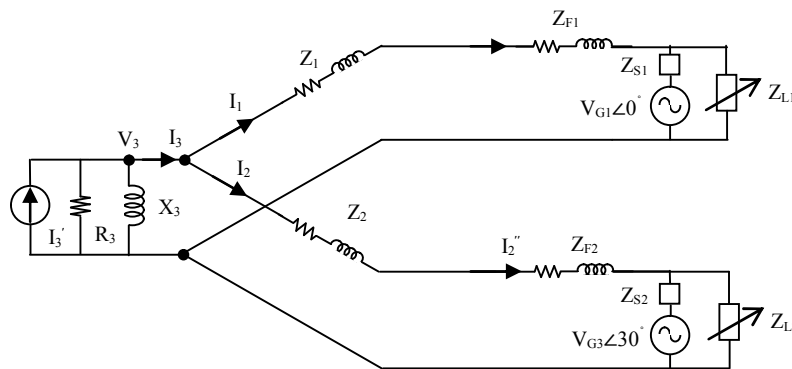


Fig. 5.2 (a) Equivalent Circuit of Proposed System with ADSIG as Soft Coupler

The expressions for currents of ADSIG flowing in the leading and lagging winding set are represented as:

$$I_1 = I_3 \left[\frac{Z_2 + Z_{F21} + Z'_{S2}}{(Z_1 + Z_{F1}) + (Z_2 + Z_{F2}) + Z'_{S1} + Z'_{S2}} \right]$$

$$I_2 = I_3 \left[\frac{Z_1 + Z_{F1} + Z'_{S1}}{(Z_1 + Z_{F1}) + (Z_2 + Z_{F2}) + Z'_{S1} + Z'_{S2}} \right]$$

Where,

$$Z'_{S1} = \frac{Z_{S1}Z_{L1}}{(Z_{S1}+Z_{L1})} ; \text{ and } Z'_{S2} = \frac{Z_{S2}Z_{L2}}{(Z_{S2}+Z_{L2})}$$

Taking $Z_1 + Z_{F1} = A$; $Z_2 + Z_{F2} = B$

$$I_1 = I_3 \left[\frac{B + Z'_{S2}}{A + B + Z'_{S1} + Z'_{S2}} \right]$$

and

$$I_2 = I_3 \left[\frac{A + Z'_{S1}}{A + B + Z'_{S1} + Z'_{S2}} \right]$$

For similar feeder capabilities we may assume $A = B = X$:

$$I_1 = I_3 \left[\frac{X + Z'_{S2}}{2X + Z'_{S1} + Z'_{S2}} \right] \quad (5.1)$$

$$I_2 = I_3 \left[\frac{X + Z'_{S1}}{2X + Z'_{S1} + Z'_{S2}} \right] \quad (5.2)$$

Analysing bound on two conditions of loading

$$(1) Z'_{S1} = Z'_{S2} = C; \text{ and } (2) Z'_{S1} = 0.5Z'_{S2} = D:$$

Condition (1): $Z'_{S1} = Z'_{S2} = C$

$$I_1 = I_3 \left[\frac{X + C}{2X + 2C} \right] \text{ and } I_2 = I_3 \left[\frac{X + C}{2X + 2C} \right];$$

$$\text{i.e. } I_1 = I_2 = 0.5I_3 \quad (5.3)$$

Condition (2): $Z'_{S1} = 0.5Z'_{S2} = D$

$$I_1 = I_3 \left[\frac{X + 2D}{2X + 3D} \right] \text{ and } I_2 = I_3 \left[\frac{X + D}{2X + 3D} \right];$$

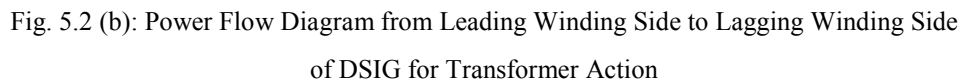
$$\text{i.e. } I_1 > I_2 \quad (5.4)$$

From the above analysis (equation (5.3) and equation (5.4)) it is clear that the power routing between the feeders is a function of their respective impedances and loadings applied on each feeder. When both the feeders are equally loaded then there is equal power sharing between them but when the loading on any one of the feeder changes the power division does not remain same any more and more power is routed to the feeder which is more loaded.

CASE B: TRANSFORMER ACTION

For clear cut understanding of the transformer action, it is taken that part load on the other side is fed by the former, where it is acting as a current source respectively to the PCC voltage, which in turn is maintained by the later side feeder. For transformer action it is assumed that the wind speed is very low (less than the cut-in speed) and the ADSIG is unable to generate the power.

Firstly the power flow from leading winding side to lagging winding side via transformer action is analyzed. As the load on the lagging winding side is increased, the voltage V_{G2} [shown in Fig. 5.3 (a) and Fig. 5.3 (b)] decreases and to regulate this decreased voltage, some power is accessed from the leading winding side of DSIG connected to the former feeder, through transformer action. The routed power depends upon the voltage gradient so formed between the voltages on the leading winding side to the voltage on the lagging winding side. Since the voltage at PCC is regulated by later side feeder the contribution of former side feeder should be taken as current source and is defined in terms of the current drawn from the leading winding side to the lagging winding side.


$$I_2 = \frac{V_{B1}}{Z_{L21}} \quad (5.5)$$

This current (lagging winding side current) is independent of the DSIG stator impedance on the lagging winding side (Z_2) and feeder impedance (Z_{F21} , Partial feeder impedance only up to load Z_{L21}). The partial feeder impedance may be neglected as it is very small value and as it is not affecting the value of I_2 . This demonstrates the feeder independence of the routed current (hence power) from the leading winding side to the lagging winding side. To understand the transformer action in detail the equivalent impedances ($Z_{2eq} = Z_2 + Z_{L21}$) are referred on the leading winding side, these referred values are phase shifted by 30° . In the shifted referred impedance the resultant impedance seems to be more inductive and less resistive, as understood from phasor diagram shown in Fig. 5.2 (c) which is duly supported by equation (5.6) and equation (5.7).

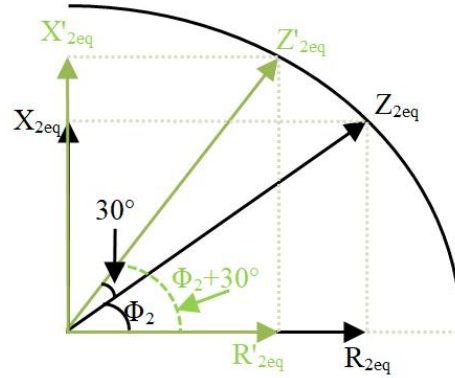


Fig. 5.2(c): Phasor diagram for lagging Side Impedance for leading it by 30°

From the Phasor Diagram, two impedance triangles are formed; the cosine and sine of both the angle can be written to find out their referred and shifted values.

$$\cos \phi_2 = \frac{R_{2eq}}{Z_{2eq}} \quad \text{and} \quad \sin \phi_2 = \frac{X_{2eq}}{Z_{2eq}}$$

$$\cos(\phi_2 + 30) = \frac{R'_{2eq}}{Z'_{2eq}} \quad \text{and} \quad \sin(\phi_2 + 30) = \frac{X'_{2eq}}{Z'_{2eq}}$$

But as the magnitude of both the impedance remain the same,

$$\therefore \cos(\phi_2 + 30^\circ) = \frac{R'_{2eq}}{Z_{2eq}} \quad \text{and} \quad \sin(\phi_2 + 30^\circ) = \frac{X'_{2eq}}{Z_{2eq}}$$

$$\text{or } \cos \phi_2 \cos 30^\circ - \sin \phi_2 \sin 30^\circ = \frac{R'_{2eq}}{Z_{2eq}} \quad \text{and}$$

$$\cos \phi_2 \sin 30^\circ + \sin \phi_2 \cos 30^\circ = \frac{X'_{2eq}}{Z_{2eq}}$$

$$\text{or } \left(\frac{R_{2eq}}{Z_{2eq}} \right) \left(\frac{\sqrt{3}}{2} \right) - \left(\frac{X_{2eq}}{Z_{2eq}} \right) \left(\frac{1}{2} \right) = \frac{R'_{2eq}}{Z_{2eq}} \quad \text{and}$$

$$\left(\frac{R_{2eq}}{Z_{2eq}} \right) \left(\frac{1}{2} \right) + \left(\frac{X_{2eq}}{Z_{2eq}} \right) \left(\frac{\sqrt{3}}{2} \right) = \frac{X'_{2eq}}{Z_{2eq}}$$

$$\text{or } R'_{2eq} = \frac{\sqrt{3}(R_{2eq}) - X_{2eq}}{2} \quad \text{and}$$

$$X'_{2eq} = \frac{\sqrt{3}X_{2eq} + R_{2eq}}{2}$$

$$\text{Where, } R_{2eq} = R_2 + R_{L21} \quad \text{and} \quad X_{2eq} = \omega(L_2 + L_{L21})$$

Considering 'k' as the coupling coefficient between the two windings (leading and lagging) of the DSIG the equivalent referred impedance is modified as:

$$R'_{2eq} = k^2 \left(\frac{\sqrt{3}(R_2 + R_{L21}) - \omega(L_2 + L_{L21})}{2} \right) \quad \text{and} \quad (5.6)$$

$$X'_{2eq} = k^2 \left(\frac{\sqrt{3}\omega(L_2 + L_{L21}) + (R_2 + R_{L21})}{2} \right) \quad (5.7)$$

While the DSIG is not generating any real power some current from the leading winding side is also taken by the rotor to meet its losses and for core magnetization.

The current is given by:

$$I_3 = \frac{V_3}{Z_{3eq}} \quad (5.8)$$

Where,

$$Z_{3eq} = R_{3eq} + jX_{3eq} = \left(\frac{R_3 X_3^2}{R_3^2 + X_3^2} \right) + j \left(\frac{R_3^2 X_3}{R_3^2 + X_3^2} \right)$$

This also needs to be incorporated in the transformer action of the DSIG to depict the shunt losses. For this impedance of the rotor side is also required to be referred on the leading winding side, and get shifted by 15° . This can be calculated using phasor diagram in Fig. 5.2(d). The cosine and sine of both the angles (ϕ_3 and ϕ'_3) can be written to find out their referred and shifted values.

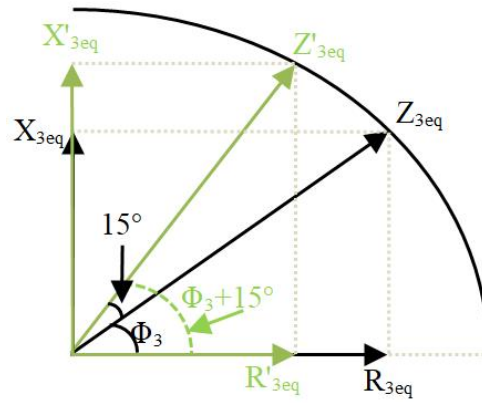


Fig. 5.2 (d): Phasor Diagram for rotor Impedance for leading it by 15°

$$\cos \phi_3 = \frac{R_{3eq}}{Z_{3eq}} \quad \text{and} \quad \sin \phi_3 = \frac{X_{3eq}}{Z_{3eq}}$$

$$\cos(\phi_3 + 15^\circ) = \frac{R'_{3eq}}{Z'_{3eq}} \quad \text{and} \quad \sin(\phi_3 + 15^\circ) = \frac{X'_{3eq}}{Z'_{3eq}}$$

But the magnitude of both the impedance remain the same (only the phasor has been shifted),

$$\therefore \cos(\phi_3 + 15^\circ) = \frac{R'_{3eq}}{Z_{3eq}} \quad \text{and}$$

$$\sin(\phi_3 + 15^\circ) = \frac{X'_{3eq}}{Z_{3eq}}$$

$$\text{or } \cos \phi_3 \cos 15^\circ - \sin \phi_3 \sin 15^\circ = \frac{R'_{3eq}}{Z_{3eq}} \quad \text{and}$$

$$\cos \phi_3 \sin 15^\circ + \sin \phi_3 \cos 15^\circ = \frac{X'_{3eq}}{Z_{3eq}}$$

$$\text{or } \left(\frac{R_{3eq}}{Z_{3eq}} \right) \left(\frac{\sqrt{3} + 1}{2\sqrt{2}} \right) - \left(\frac{X_{3eq}}{Z_{3eq}} \right) \left(\frac{\sqrt{3} - 1}{2\sqrt{2}} \right) = \frac{R'_{3eq}}{Z_{3eq}} \quad \text{and}$$

$$\left(\frac{R_{3eq}}{Z_{3eq}} \right) \left(\frac{\sqrt{3} - 1}{2\sqrt{2}} \right) + \left(\frac{X_{3eq}}{Z_{3eq}} \right) \left(\frac{\sqrt{3} + 1}{2\sqrt{2}} \right) = \frac{X'_{3eq}}{Z_{3eq}}$$

$$\text{or } R'_{3eq} = \frac{(\sqrt{3} + 1)(R_{3eq}) - (\sqrt{3} - 1)X_{3eq}}{2\sqrt{2}} \quad \text{and} \quad (5.9)$$

$$X'_{3eq} = \frac{(\sqrt{3} - 1)(R_{3eq}) + (\sqrt{3} + 1)X_{3eq}}{2\sqrt{2}} \quad (5.10)$$

The referred impedances in Z'_{2eq} and Z'_{3eq} can be used to draw the overall equivalent circuit seen by the leading winding side grid across the terminal A_1A_2 (in Fig. 5.2(a)) is represented in Fig. 5.2(e). The current entering into the leading winding set of ADSIG is divided into referred lagging winding current ($I'_2 = k \cdot I_2$) and referred rotor current (I'_3) and is given as:

$$I_1 = I'_3 + I'_2 \quad (5.11)$$

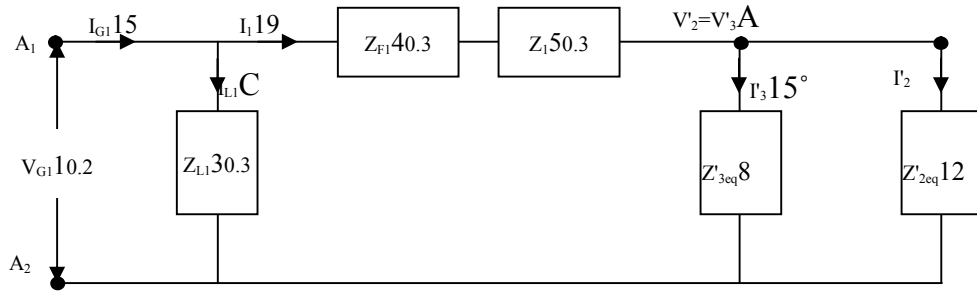


Fig. 5.2(e): Equivalent circuit seen by leading winding side grid for routing power to lagging winding side

Thus the current entering on the leading winding side of DSIG is sum of current required by the lagging winding side and the current needed to meet the losses of the rotor. The current from the grid is further the sum of current supplied to load and the

current entering into the grid and is given by:

$$I_{G1} = I_{L1} + I_1 \quad (5.12)$$

The referred load on the lagging winding side grid which is catered by the leading winding side grid can also be estimated from the equivalent circuit drawn on the leading winding side. From the equivalent circuit as it is observed that referred rotor impedance and referred lagging winding impedance are connected in parallel. Therefore,

$$V'_3 = V'_2 \quad (5.13)$$

$$I'_3 \cdot Z'_{3eq} = I'_2 \cdot Z'_{2eq}$$

In the above equation all the other parameters except Z'_{2eq} are known and thus the value of Z'_{2eq} can be calculated from the expression:

$$Z'_{2eq} = \frac{I'_3 \cdot Z'_{3eq}}{I'_2} \quad (5.14)$$

Equation (5.3), equation (5.4) and equation (5.14) can be used to calculate value actual load ($Z_{L21} = R_{L21} + jX_{L21}$.) catered by the transformer action.

Similarly, the transformation action for flow of power from lagging winding side to the leading winding side can be seen. This is exactly the reverse case of the previous case, where the limited load on leading side is fulfilled by the lagging winding side (through transformation action) and remaining load from leading winding side grid itself. The difference lies in the referred impedances; here the referred impedances from the leading winding side and rotor impedances shift 30° and 15° backward respectively. This results into increased resistance and decreased value of effective impedance as compared to the actual value of resistance and inductance. This can be seen from the phasor diagram shown in Fig. 5.2(f) and Fig. 5.2(g) and are supported by equation (5.15), equation (5.16) equation (5.17) and equation (5.18).

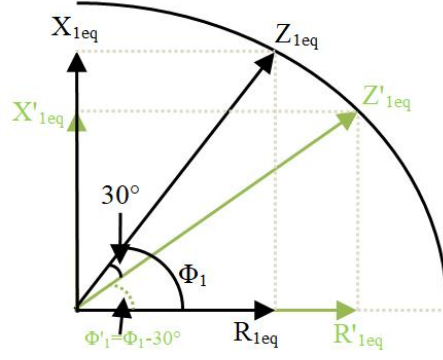


Fig. 5.2 (f): Phasor diagram for leading Side Impedance for lagging it by 30°

The phasor diagram in Fig. 5.2(f) shows the shifting of impedance from leading to lagging winding side. Cosine and sine of the angles are taken to and compared and solved for Z'_1 .

$$\cos \phi_1 = \frac{R_{3eq}}{Z_{3eq}} \quad \text{and} \quad \sin \phi_1 = \frac{X_{3eq}}{Z_{3eq}}$$

$$\cos(\phi_1 - 30^\circ) = \frac{R''_{3eq}}{Z''_{3eq}} \quad \text{and} \quad \sin(\phi_1 - 30^\circ) = \frac{X''_{3eq}}{Z''_{3eq}}$$

But as the magnitude of both the impedance remain the same,

$$\therefore \cos(\phi_1 - 30^\circ) = \frac{R''_{3eq}}{Z_{3eq}} \quad \text{and}$$

$$\sin(\phi_1 - 30^\circ) = \frac{X''_{3eq}}{Z_{3eq}}$$

$$\text{or} \quad \cos \phi_3 \cos 30^\circ + \sin \phi_3 \sin 30^\circ = \frac{R''_{3eq}}{Z_{3eq}} \quad \text{and}$$

$$\sin \phi_3 \cos 30^\circ - \cos \phi_3 \sin 30^\circ = \frac{X''_{3eq}}{Z_{3eq}}$$

$$\text{or} \quad \left(\frac{R_{3eq}}{Z_{3eq}} \right) \left(\frac{\sqrt{3}}{2} \right) + \left(\frac{X_{3eq}}{Z_{3eq}} \right) \left(\frac{1}{2} \right) = \frac{R''_{3eq}}{Z_{3eq}} \quad \text{and}$$

$$\left(\frac{X_{3eq}}{Z_{3eq}} \right) \left(\frac{\sqrt{3}}{2} \right) - \left(\frac{R_{3eq}}{Z_{3eq}} \right) \left(\frac{1}{2} \right) = \frac{X''_{3eq}}{Z_{3eq}}$$

$$R'_{1eq} = k^2 \left(\frac{\sqrt{3}(R_1 + R_{L11}) + \omega(L_1 + L_{L11})}{2} \right) \quad \text{and} \quad (5.15)$$

$$X'_{1eq} = k^2 \left(\frac{\sqrt{3}\omega(L_1 + L_{L11}) - (R_1 + R_{L11})}{2} \right) \quad (5.16)$$

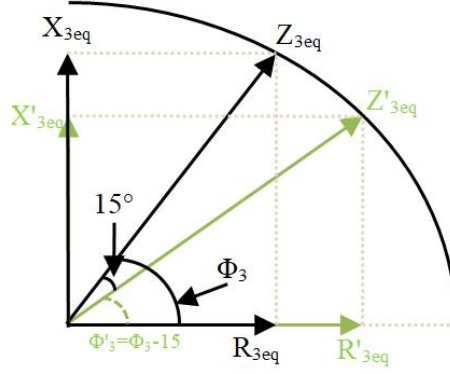


Fig. 5.2(g): Phasor Diagram for rotor Impedance for lagging it by 15°

Similarly from the phasor diagram in Fig. 5.2(g) the cosine and sine of the angle are taken and solved as follow to find out the impedance Z''_{3eq} .

$$\cos \phi_3 = \frac{R_{3eq}}{Z_{3eq}} \quad \text{and} \quad \sin \phi_3 = \frac{X_{3eq}}{Z_{3eq}}$$

$$\cos(\phi_3 - 15^\circ) = \frac{R''_{3eq}}{Z''_{3eq}} \quad \text{and} \quad \sin(\phi_3 - 15^\circ) = \frac{X''_{3eq}}{Z''_{3eq}}$$

But as the magnitude of both the impedance remain the same,

$$\therefore \cos(\phi_3 - 15^\circ) = \frac{R''_{3eq}}{Z_{3eq}} \quad \text{and}$$

$$\sin(\phi_3 - 15^\circ) = \frac{X''_{3eq}}{Z_{3eq}}$$

$$\text{or } \cos \phi_3 \cos 15^\circ + \sin \phi_3 \sin 15^\circ = \frac{R''_{3eq}}{Z_{3eq}} \quad \text{and}$$

$$\sin \phi_3 \cos 15^\circ - \cos \phi_3 \sin 15^\circ = \frac{X''_{3eq}}{Z_{3eq}}$$

$$\text{or } \left(\frac{R_{3eq}}{Z_{3eq}} \right) \left(\frac{\sqrt{3} + 1}{2\sqrt{2}} \right) + \left(\frac{X_{3eq}}{Z_{3eq}} \right) \left(\frac{\sqrt{3} - 1}{2\sqrt{2}} \right) = \frac{R''_{3eq}}{Z_{3eq}} \quad \text{and}$$

$$\left(\frac{X_{3eq}}{Z_{3eq}} \right) \left(\frac{\sqrt{3} + 1}{2\sqrt{2}} \right) - \left(\frac{R_{3eq}}{Z_{3eq}} \right) \left(\frac{\sqrt{3} - 1}{2\sqrt{2}} \right) = \frac{X''_{3eq}}{Z_{3eq}}$$

$$\text{or } R'_{3eq} = \frac{(\sqrt{3} + 1)(R_{3eq}) + (\sqrt{3} - 1)X_{3eq}}{2\sqrt{2}} \quad \text{and} \quad (5.17)$$

$$X'_{3eq} = \frac{(\sqrt{3} - 1)(R_{3eq}) - (\sqrt{3} + 1)X_{3eq}}{2\sqrt{2}} \quad (5.18)$$

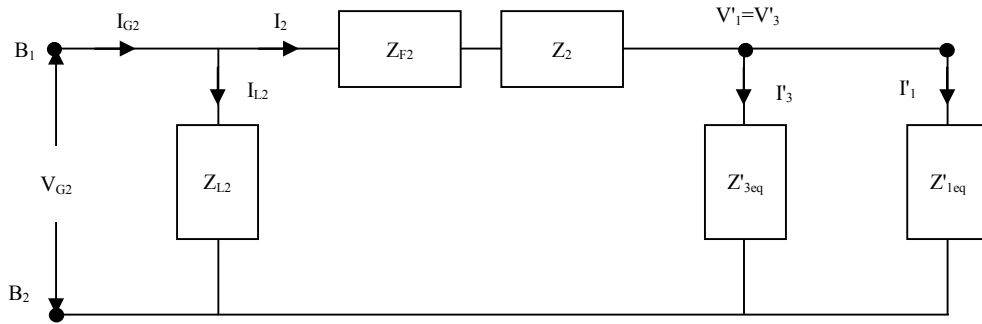


Fig. 5.2(h): Equivalent circuit seen by lagging winding side grid for routing power to leading winding side

Thus the equivalent circuit seen for the power transfer from lagging to leading winding side is shown in Fig. 5.2(h). The current flowing from leading winding set of ADSIG. The current entering into the leading winding set of ADSIG is

$$I_2 = I'_3 + I'_1 \quad (5.19)$$

Where,

- I'_1 is the current of lagging winding side referred on the leading winding side and is given as $I'_1 = k \cdot I_1$
- I'_3 is the magnetizing current required by ADSIG rotor.

Thus the current entering on the lagging winding side of DSIG is sum of current required by the leading winding side and the current needed to meet the losses of the

rotor. The current from the grid on lagging side is the sum of current supplied to load (Z_{L1}) and the current entering into the grid and is given by:

$$I_{G2} = I_{L2} + I_2 \quad (5.20)$$

The referred load on the leading winding side grid which is catered by the lagging winding side grid can also be estimated from the equivalent circuit drawn on the lagging winding side and is given by:

$$Z'_{1eq} = \frac{I'_3 \cdot Z'_{3eq}}{I'_2} \quad (5.21)$$

Equation (5.15), equation (5.16) and equation (5.21) can be used to calculate value actual load ($Z_{L2l} = R_{L2l} + jX_{L2l}$) catered by the transformer action.

The DSIG may also work in third mode where some power is generated from wind power and the deficit power on any of winding side is fulfilled by the other winding side so that the voltage on both the side remain same. And the resultant current on any winding side is the sum of both the modes. Thus ADSIG works as an auto-compensator for routing power to different feeders depending upon their respective loadings and thus substantiates the idea of using ADSIG as a soft coupler.

5.4 MATLAB simulation of DSIG as Three Port Network

Performance of ADSIG as a soft coupler in three port network is evaluated through MATLAB simulation and Hardware prototype. The simulation model is developed with the SimPowerSystems toolbox of the MATLAB SIMULINK environment. The simulation diagram for the same is shown in Fig. 5.3. The simulation model consists of ADSIG connected to two different feeders via star-delta transformer (415V/415V, 5kVA, 50 Hz) on the leading winding side of ADSIG and via star-star transformer

(415V/415V, 5kVA, 50 Hz) on the lagging winding side. The feeder is realised with three phase voltage source and a three phase load connected to it in parallel to it, depicting load connected to feeder. The loads considered are three phase linear balanced loads (unity power factor) implemented with three phase series RLC branch.

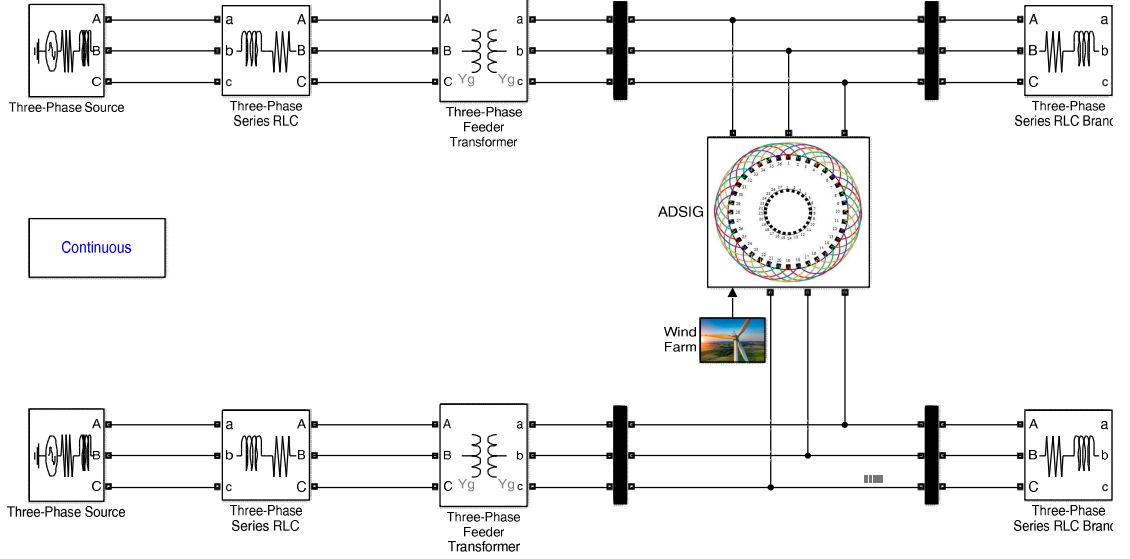


Fig. 5.3: Matlab Simulink Model of Three Port Network

5.5 Hardware Implementation of DSIG for Routing Power in Three Port Network

The experimental setup for the proposed configuration is made on the developed prototype in the lab. Photograph of the developed prototype and hardware test bed of the proposed system is shown in Fig. 5.4. Since in the laboratory the supply is fed only through one feeder, two weak feeders are created by using two transformers in star/star and star/delta connections. For case under study primary and secondary of the star-delta transformer are respectively connected to grid side and ADSIG, (star side is connected to the leading winding set of ADSIG and the delta side is connected to the lagging winding set of ADSIG). While the primary and secondary of Star three phase

configuration transformer are respectively connected to grid side and ADSIG lagging side. The performance of the proposed system is analyzed and the results show effective coupling between the feeders with power injection and effective power distribution by ADSIG under perturbing load conditions.



Fig. 5.4: Photograph of the developed prototype and hardware test bed of the proposed system

5.6 Results and Discussion

The performance of weak grid coupled ADSIG enacting as soft interconnect and renewable energy system (RES) is evaluated on the basis of power routing between feeders, automatic load management, transient response, voltage recovery and demonstration of low voltage with a ride through capability. Terminal voltage and current at the point of common coupling are recorded for performance evaluation with intentional load perturbations to observe the capability of the proposed system to enact as soft interconnect between feeders for power routing feature. The utilization of core

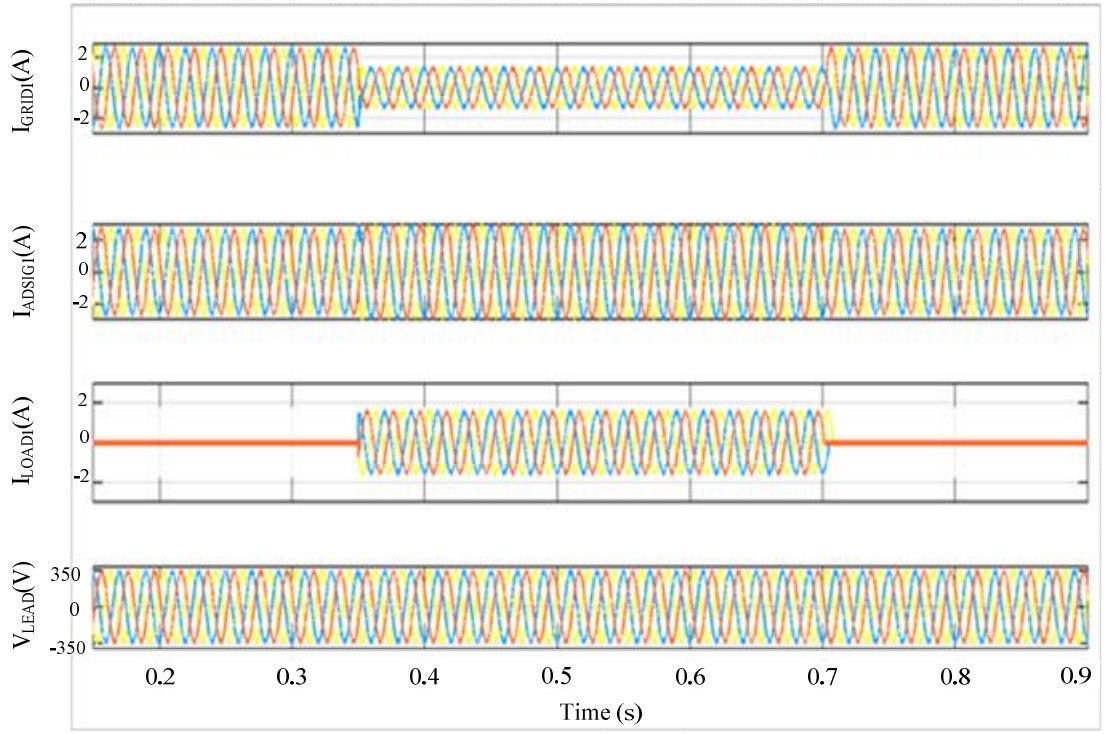


Fig. 5.5: Performance with load perturbation at leading winding of DSIG

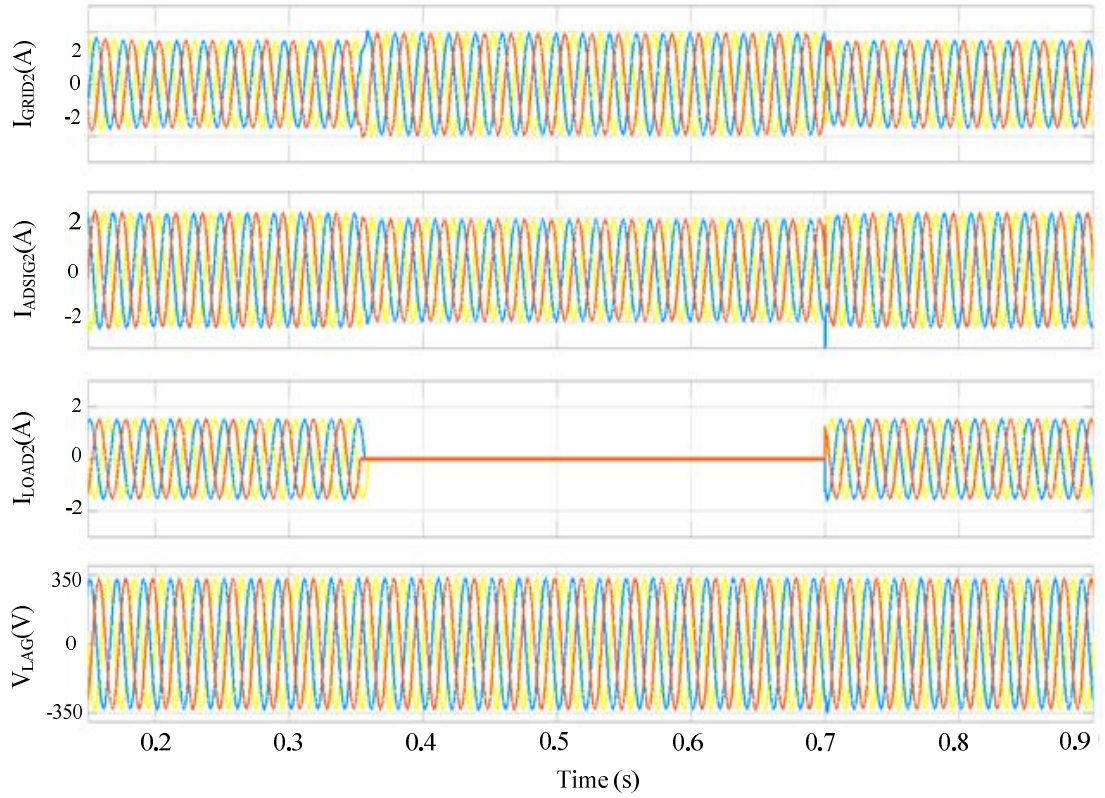


Fig. 5.6: Performance with load perturbation at lagging winding of DSIG

and transient characteristics are also evaluated experimentally through observations in

steady-state and transient operating conditions.

Fluctuating loads are applied at both winding terminals of ADSIG which are considered connected to two feeders supplied by two separate distribution transformers (DTs). The balancing act due to the cross-coupling effect equalizes the active and reactive power support from one winding side of ADSIG on one feeder to the other winding side of ADSIG connected to the other feeder. The evaluation of such a balancing act is also demonstrated ahead in the remaining section. The performance evaluation is carried out in three stages, where the first stage deals with establishment of the ADSIG as soft coupling element between the feeders and demonstrating its power routing capability, whereas, in second stage ride through capability under low voltage and in the third stage the capability of fast voltage recovery after the fault or transients is demonstrated.

The performance of ADSIG as soft interconnect between two feeders is evaluated through simulation and experimental results with load perturbations on either end one by one to gauge the capability of power routing of the proposed scheme. Fig. 5.5 and Fig. 5.6 are the simulation results for load swapping on both sides of ADSIG whereas Fig. 5.7 and Fig. 5.8 show the experimental results of load swapping. A three phase load of 800W is switched/ swapped from leading winding set terminal to lagging winding set and back. From Fig 5.5 and Fig. 5.6 it is observed that from starting a load (800W) is applied at lagging winding of ADSIG whereas leading winding set is unloaded. Lagging winding set of ADSIG caters to the active demand of local load and the excess power is transferred to the connected feeder. At leading winding set of ADSIG, all the generated active power is transferred to its respective feeder. At 352ms load (800W) is swapped to leading winding set of ADSIG as in Fig. 5.5 and Fig. 5.6.

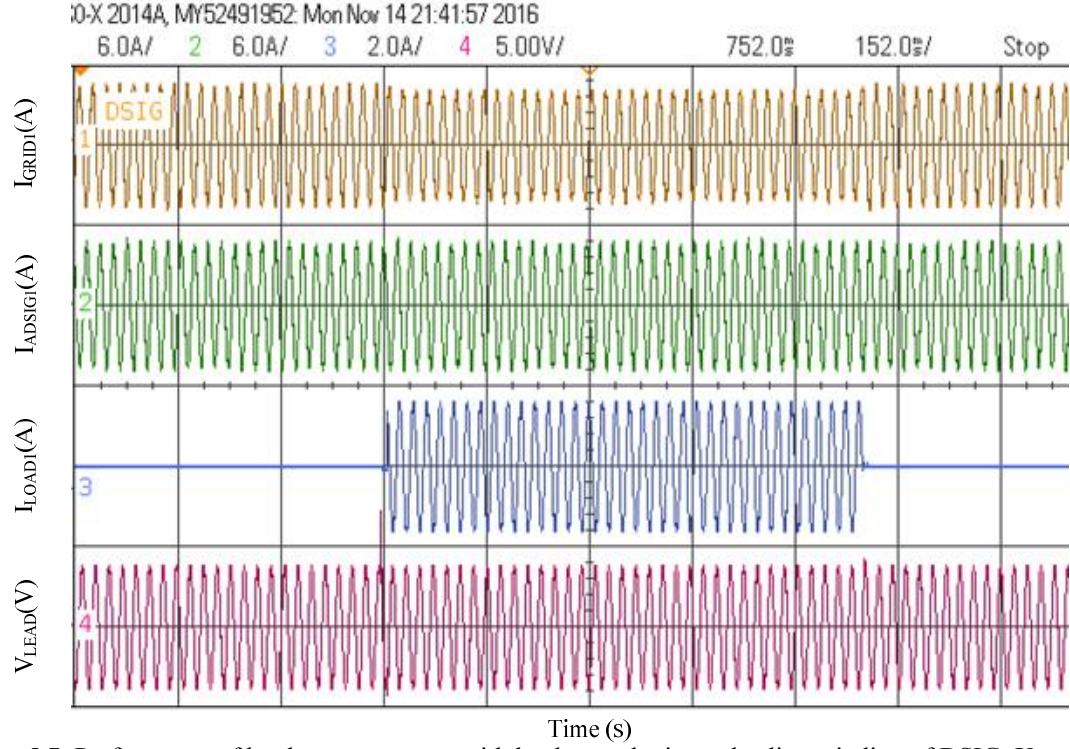


Fig. 5.7: Performance of hardware prototype with load perturbation at leading winding of DSIG. X-axis: 152ms/div; Y axis: Current: I_{Grid} : 6A/div, I_{ADSI1} : 6A/div and I_{Load} : 2A/div; V_{Lead} : 450V/div

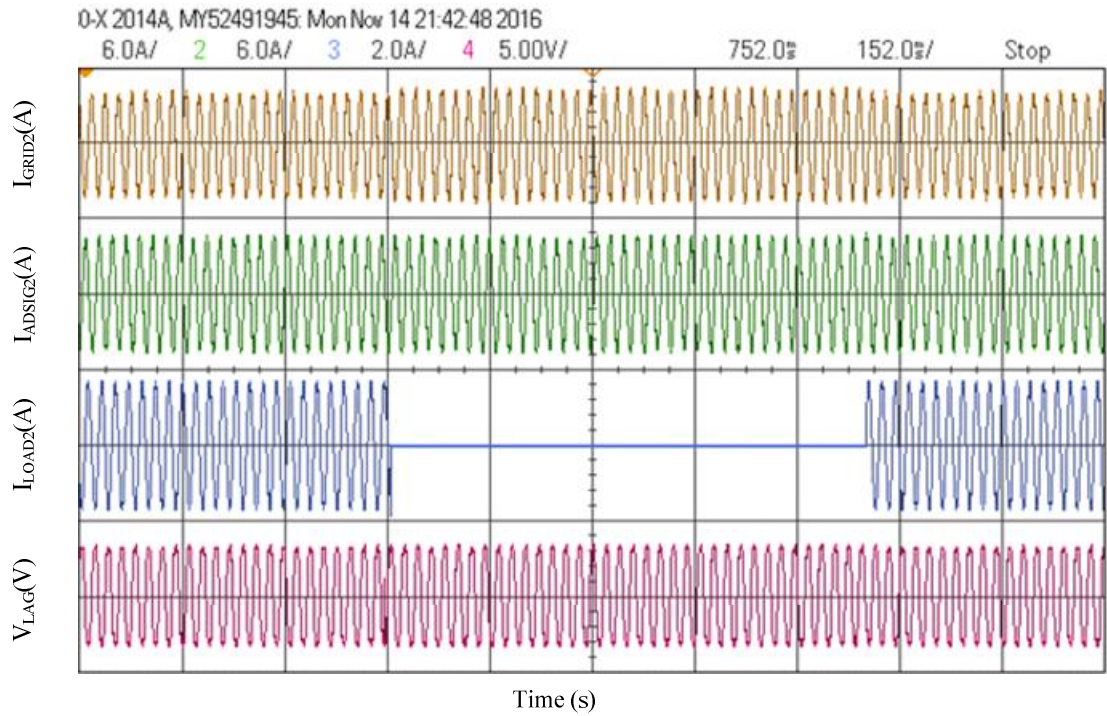


Fig. 5.8: Performance of hardware prototype with load perturbation at lagging winding of DSIG. X-axis: 152ms/div; Y axis: Current: I_{Grid} : 6A/div, I_{ADSI2} : 6A/div and I_{Load} : 2A/div; V_{Lag} : 450V/div

It is observed that as soon as lagging side load (I_{L2}) is removed the contribution of

lagging side ADSIG current (I_{D2}) to its respective feeder increases resulting in approximately 8% increase of feeder current (I_{G2}) also the PCC voltage increases by 0.8% resulting in a further increase of 0.5% ADSIG current (I_{D2}). Whereas as soon as the load is applied at leading winding set of ADSIG it is observed that the leading winding feeder current (I_{G1}) reduces by 8% as now leading winding ADSIG current (I_{D1}) is also feeding to its local load (I_{L1}). The PCC voltage of leading winding set of ADSIG (V_1) also falls by 0.5% resulting in a further decrease of ADSIG current (I_{D1}) by 0.5%. At 700ms when the load (800W) is again switched back to lagging winding set, the initial conditions are maintained. Similar test of load swapping is performed on the hardware test bed of ADSIG and the results are shown in Fig. 5.7 and Fig. 5.8 for load perturbation on leading and lagging winding set respectively. Initially load is connected to the lagging winding set and at 455 ms load is swapped to leading winding set. Likewise at 1.170 s load is again swapped back to lagging winding set. The experimental results are similar to the simulation results and support for the power routing capability of ADSIG's enacting as a soft coupler for two AC feeders.

The reliability of ADSIG as a soft coupler between two feeders is evaluated under low voltage and single phasing conditions also to access for the low voltage ride through (LVRT) and fault ride through (FRT) capabilities both on the leading and the lagging winding sets of ADSIG experimentally. To depict in more lucid way phasor plots are also plotted beside analysis of waveforms. Fig. 5.9(a-c) and 5.11(a-c) show the experimental results (waveform and phasor respectively) with the voltage perturbations on leading winding set and Fig. 5.10(a-c) and 5.12(a-c) show the experimental results (waveform and phasor respectively) for voltage perturbations on the lagging side. For clarity in the depiction of results, three synchronized

oscilloscopes are used, which show currents of feeder, ADSIG and load on either side.

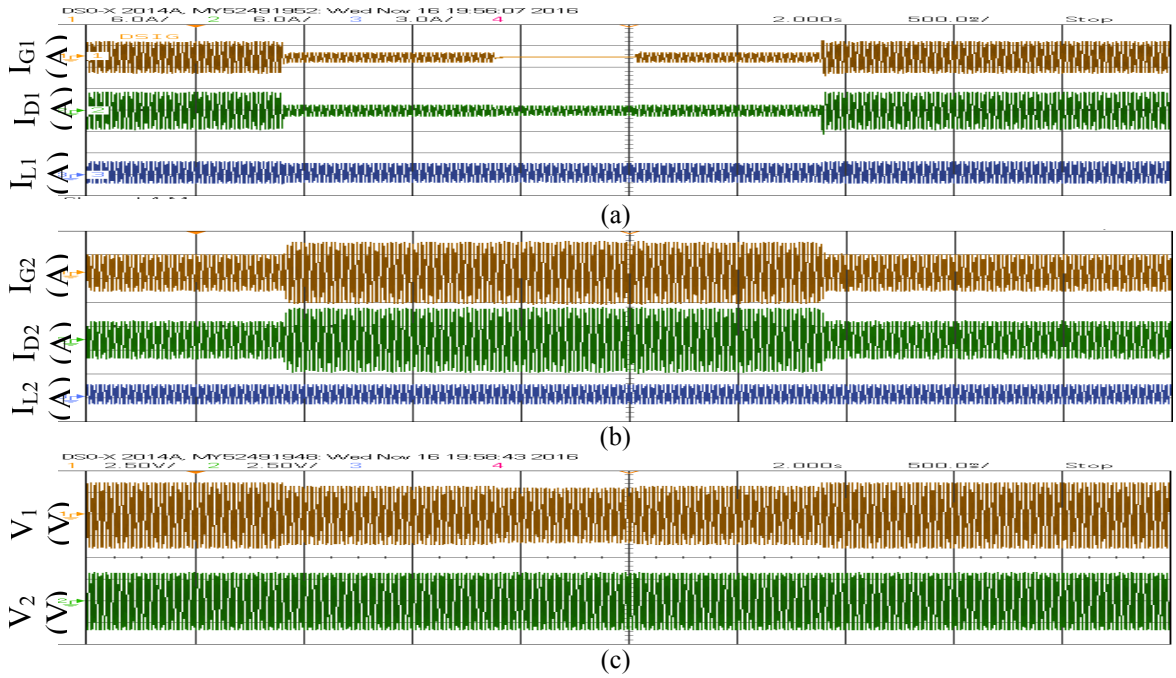


Fig. 5.9: Performance under low voltage and fault condition at leading side of DSIG (3 synchronized oscilloscopes) 6A/div, 6A/div, 2A/div; 6A/div, 6A/div, 2A/div; 250V/div, 250V/div

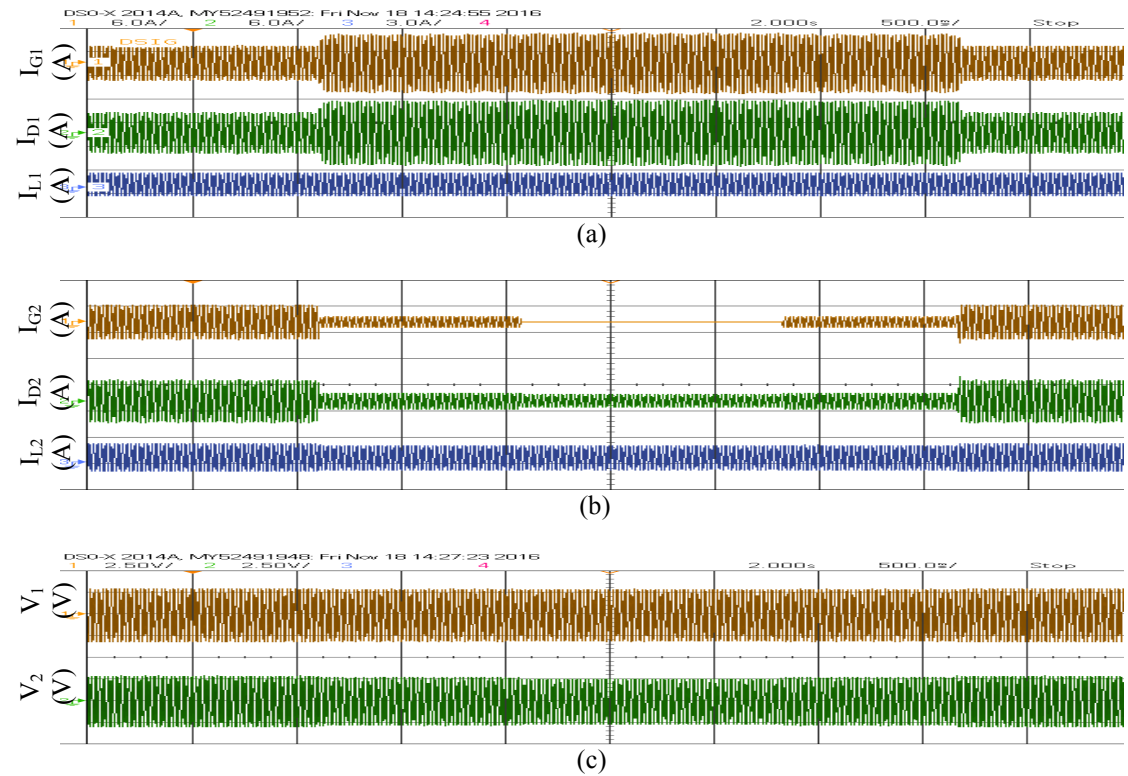


Fig. 5.10: Performance under low voltage and fault condition at lagging side of DSIG (3 synchronized oscilloscopes) 6A/div, 6A/div, 2A/div; 6A/div, 6A/div, 2A/div; 250V/div, 250V/div

In Fig. 5.9 from $t = 0$ to $t = 0.91$ s the system is operating under normal conditions when both the end of ADSIG supply power to respective connected local loads and remaining to their respective feeders. These results are further supported by the phasor

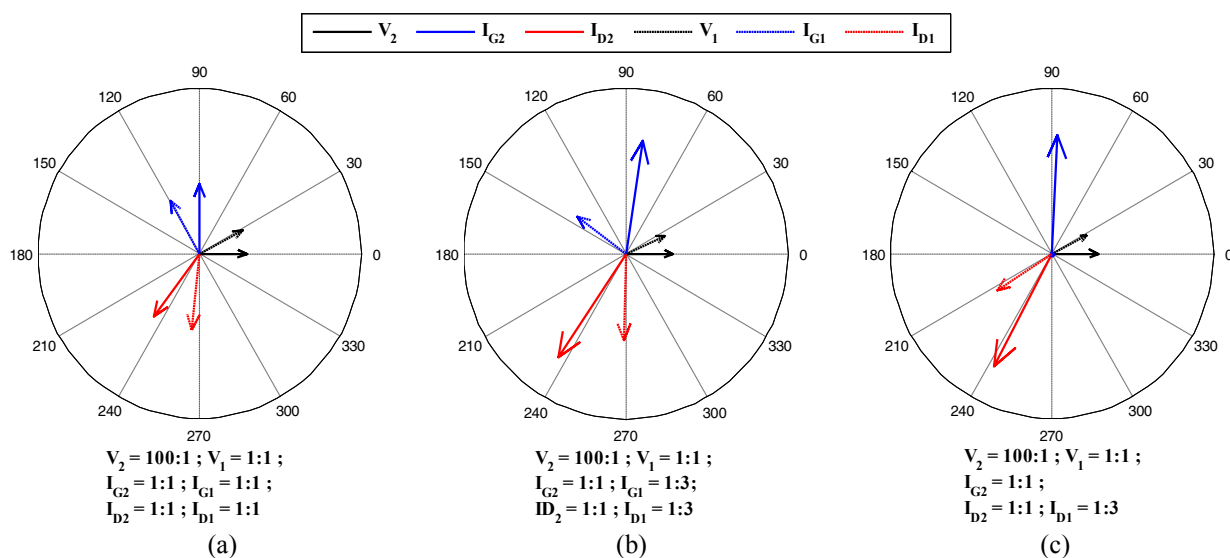


Fig. 5.11: Phasors depicting (a) Normal (b) Under Low voltage at leading winding and (c) Single phasing condition at leading winding of DSIG. Depiction of both leading and lagging side currents for power routing enacting soft coupling. Circle represents radius of 10 units.

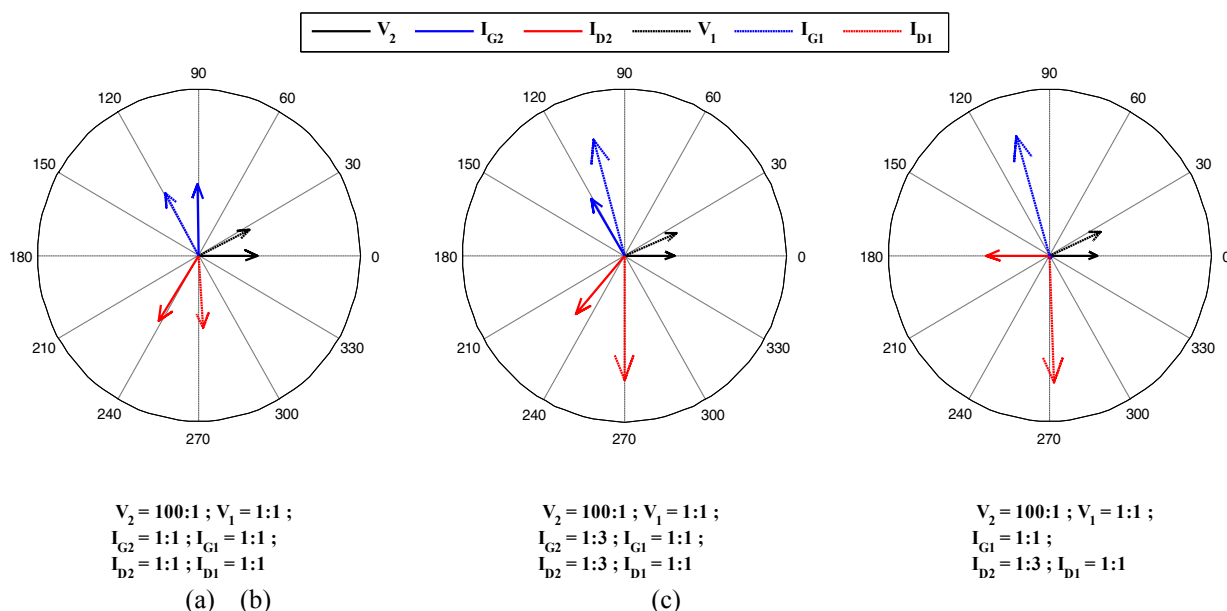


Fig.5.12: Phasors depicting (a) Normal (b) Under Low voltage at lagging winding and (c) Single phasing condition at lagging winding of DSIG. Depiction of both leading and lagging side currents for power routing enacting soft coupling. Circle represents radius of 10 units.

diagrams in Fig. 5.11(a) to (c), which also depict the transaction of real and reactive power between ADSIG, load and feeder, in terms of their respective phase voltage and phase current. In Fig. 5.9(a) which depicts the normal condition of the ADSIG show phasor of I_{G1} and I_{G2} in quadrature to their respective phase voltages showing that both feeders are supplying only reactive power to respective sides of ADSIG windings. Further I_{D1} and I_{D2} , which are nearly at 120° with respect to V_1 and V_2 respectively, represent reactive power consumption with real power delivery to load on their respective sides.

To investigate further for LVRT capabilities first the low voltage condition is caused to imitate increased load or voltage sag condition on the feeder, connected to the leading winding set of ADSIG. As shown in Fig. 5.9 from $t = 0.91$ s to $t = 1.88$ s and phasor diagram in Fig. 5.11(b), the ADSIG current (I_{D1}) and feeder current (I_{G1}) decrease drastically from 4.7 A to 1.54 A and 4.28 A to 1.32 A respectively, moreover I_{G1} changes phase significantly due to the reduction of PCC voltage (V_1).

It may be observed in Fig. 5.11(b) that both I_{D1} and I_{D2} are still displaced nearly by 120° with respect to their phase voltages, V_1 and V_2 respectively, with the decreased magnitude of I_{D1} and increased magnitude of I_{D2} . Due to low voltage on the feeder 1 ADSIG decreases its reactive power intake, thereby decreasing the supply of real power to leading winding set of ADSIG. The remaining generated real power and deficit reactive power demand of ADSIG is handled by the lagging winding set of ADSIG. Whereas, for the same terminal voltage on lagging winding (V_2), the magnitude of the feeder current I_{G2} increases to supply the extra reactive power to compensate for the deficiency in the flux of the magnetic circuit of the ADSIG. Moreover, ADSIG diverts the remaining real power to the feeder 2, the same is

marked by a reduction in the angle between the I_{G2} and V_2 less than 90° .

Further, the system is investigated for the faulty condition, where one phase of leading winding set of ADSIG is intentionally made open to emulate the effect of a single phasing fault as shown in Fig. 5.9 from $t = 1.88$ s to $t = 2.54$ s and phasor diagram Fig. 5.11(c). The ADSIG current (I_{D1}), of the faulty phase, feeds its local load and the terminal voltage of ADSIG settles at a further lesser value due to the decrement of net reactive power supply from the leading winding set. On the other hand, the ADSIG current (I_{D2}) is now handling both the increased active power transfer from ADSIG to load and feeder and the increased reactive current demand of the ADSIG from the lagging feeder. This is shown as the increased magnitude of both I_{D2} and I_{G2} in Fig. 5.11(c). Similarly, the considered system is also investigated for the perturbations on the lagging side for all the three stages. The lagging side perturbations are shown in Fig. 5.10(a-c) and the phasor diagrams in Fig. 5.12(a-c). The waveform and phasor diagram shows a similar response as seen for the leading winding side perturbations. Similarly, for soft coupling of different feeders asymmetrical ADSIG can be directly coupled/connected through a star-delta transformer of unity turns ratio, together with real power injection by the third port making it as a better alternative.

5.7 Conclusion

Improved performance of six phase asymmetrical DSIG prototype developed has been successfully demonstrated for up-to rated condition of loading. A mathematical analysis based on the impedance model of the system is done and the results show that power routing to any winding in DSIG is dependent on the respective loading at the other winding. The simulation and experimental results confirm that DSIG is

capable of injecting the generated power into the different feeders based on their loading conditions without any complicated control and additional hardware. It has also been established that the proposed system effectively provides ride through capabilities for low voltage and faults, thereby proving its immunity to transients. The three port network architecture of the DSIG has been demonstrated to couple the feeders effectively, providing modular approach for augmentation of similar units in parallel for even more effective soft coupling and load balancing on feeders, besides integration of more turbines into the system. The results also demonstrated that inrush transients have been tremendously subsided to prevent bottleneck for multiple coupling of such units in a cost effective and rugged way. The proposed configuration thus paves the way for incorporation of DSIG in future distribution systems with multiple coupling of feeder together with effective integration of wind energy system.

Chapter 6

ADSIG as Hybrid Micro Grid with ESS

6.1 Introduction

To fulfill the increasing power demand of consumers the penetration of renewable sources is increasing day by day and installation of more (renewable energy based) micro-grids have become inevitable. Extensive research in the field of power electronics and machines has opened the flood gates for different power generation techniques using renewable energy systems (RES). The emergence of solar and wind-based power plants few to cite. The intermittent nature of wind poses a problem for reliable power generation and meeting the demand of micro grids. Energy storage systems (ESS) are reported as a remedial solution for meeting the challenges proved by intermittency. Induction generator based wind farms usually employ the ESS to cater such challenges. When ESS involving a three-phase VSC is tied with each conventional three phase induction generators then a large capacity power filter circuits are required to smooth out the voltage and current distortions besides taking care of starting coupling and other transient operations. These adds to the cost, complexity and space requirement of the micro grids.

This chapter discusses the ADSIG with ESS operating on one of its winding sets, while the other to the grid is used for generation from wind energy source and for supplying a fixed committed real power to the grid to enact a synchronous generator. The flux coupling maintained in air gap reduces the requirement of filter circuits,

isolation transformer, requirements and interactions between two winding sets. When the power generated by ADSIG is more than the committed power then the surplus power is stored in the storage system and when the power generated becomes less than the committed power then this stored energy is fed to the grid to curb intermittency. Such topology for power generation by wind energy is particularly suitable for onshore wind farms where there are more fluctuations in wind. Moreover, as the two stator windings are displaced by 30° with respect to each other the active power injected at one stator winding set is seen as combination of both active and reactive power to the other stator winding set, thereby reduces the net reactive power requirements of ADSIG by mere active power control reducing burden on the grid and elevating the power transfer capability of the system.

6.2 System Configuration and Salient features of ADSIG with ESS for grid coupling

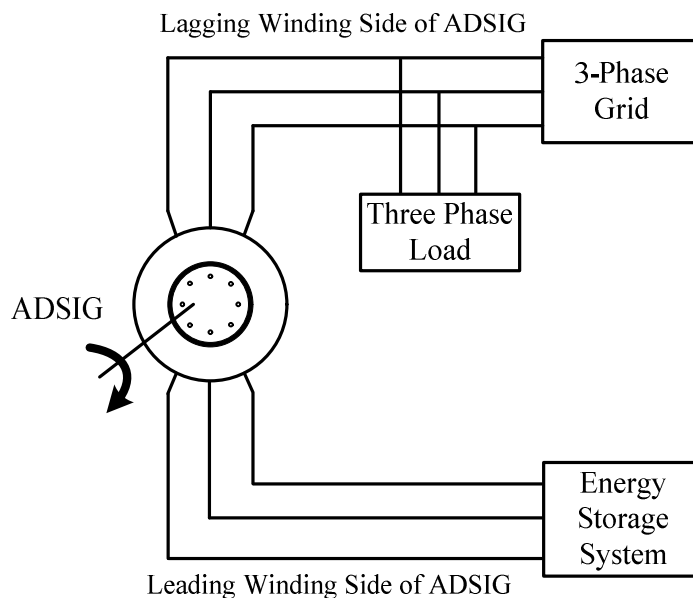


Fig. 6.1: Block diagram for system configuration of ADSIG with ESS for grid-coupling

The proposed scheme of ADSIG in tandem with ESS delivering committed active

power to three phase grid is shown in Fig. 6.1. A 5 HP, 6 Pole ADSIG is connected to three phase AC grid on one of the three phase winding set and an energy storage system connected to the other three phase winding set of the ADSIG. The reactive power requirement of ADSIG is met mostly by grid and partly by the energy storage system connected at the other end to enable coupling for wider way to operation. Further the cross magnetization phenomenon (explained in the subsequent section) shall substantiate the reactive power requirements upon locally at off-grid end. There is no capacitor bank connected for the reactive power support however, it may relieve the grid from supplying reactive power. The local loads are considered connected to grid side in parallel. However, on the off-grid side ESS forms the main load while ADSIG is generating. The ESS system comprises of current controlled VSC unit with storage unit on the DC side.

6.3 Analysis of Power Flow to Grid from ADSIG coupled with ESS

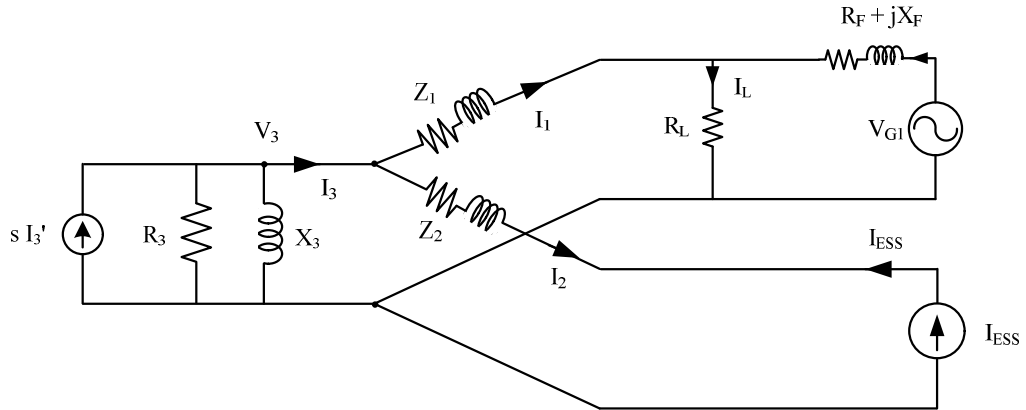


Fig. 6.2(a): Equivalent circuit of grid connected hybrid microgrid with ADSIG and ESS

The equivalent circuit of the proposed system is shown in Fig. 6.2(a). In the equivalent circuit the ADSIG fed by wind turbine is modelled as a current source when it is generating power and as a simple transformer when there is no generation of power in ADSIG. ' R_3 ' represents the transformed equivalent rotor resistance and ' X_3 ' represents

the transformed magnetizing inductance of ADSIG. ' Z_1 ' and ' Z_2 ' represent the magnitude of per-phase stator winding resistances of both stator windings with ' ϕ_1 ' and ' ϕ_2 ' as their respective phase angles. ' $Z_{F1} \angle \phi_{F1}$ ' represents the feeder impedance of the connected feeder. ESS is considered as a current source (for delivering real power, depending upon the requirement) with both grid (major contributor) and ESS (minor contributor) providing reactive power to ADSIG.

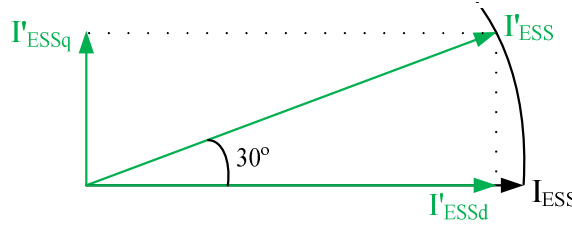


Fig. 6.2(b): Phasor Diagram for I_{ESS} as seen on the leading winding side (grid side) of ADSIG

The current from the ESS (connected to the lagging winding set of ADISG) when transferred to the grid side (leading side winding set of ADSIG) witness a phase shift of 30° anticlockwise with (as shown in Fig. 6.2(b)). The real power from ESS is divided into both real and reactive component when shifted by 30° but the magnitude of shifted current is same as the I_{ESS} and can be expressed as:

$$|I'_{ESS}| = |I_{ESS}|$$

But also from the phasor diagram $I'_{ESSd} = |I'_{ESS}| \cos 30^\circ$ and $I'_{ESSq} = |I'_{ESS}| \sin 30^\circ$

$$\text{or } I'_{ESSd} = \frac{\sqrt{3}}{2} |I'_{ESS}| \quad \text{and} \quad (1)$$

$$I'_{ESSq} = \frac{1}{2} |I'_{ESS}| \quad (2)$$

Similarly, the current drawn (for magnetization of ADSIG and to meet its internal losses) or provided (during generation) by the ADSIG when seen from the leading winding side witness a shift of (leaded) by 15° clockwise, this can be expressed with the help of the phasor diagram (Fig. 6.2(c)) and is derived as below. From the phasor

diagram, two triangles are formed; the cosine and sine of both the angle can be written to find out their referred and shifted values.

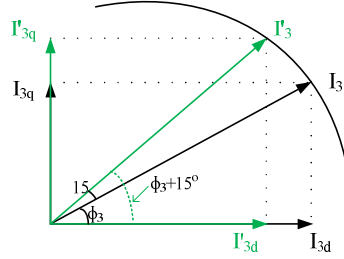


Fig. 6.2(c): Phasor Diagram for ADSIG current for leading it by 15°

$$\cos \phi_3 = \frac{I_{3d}}{I_3} \quad \text{and} \quad \sin \phi_3 = \frac{I_{3q}}{I_3}$$

$$\cos(\phi_3 + 15^\circ) = \frac{I'_{3d}}{I'_3} \quad \text{and} \quad \sin(\phi_3 + 15^\circ) = \frac{I'_{3q}}{I'_3}$$

But as the magnitude of both the currents I'_3 and I_3 remain the same,

$$\therefore \cos(\phi_3 + 15^\circ) = \frac{I'_{3d}}{I_3} \quad \text{and} \quad \sin(\phi_3 + 15^\circ) = \frac{I'_{3q}}{I_3}$$

$$\text{or } \cos \phi_3 \cos 15^\circ - \sin \phi_3 \sin 15^\circ = \frac{I'_{3d}}{I_3} \quad \text{and}$$

$$\cos \phi_3 \sin 15^\circ + \sin \phi_3 \cos 15^\circ = \frac{I'_{3q}}{I_3}$$

$$\text{or } \left(\frac{I_{3d}}{I_3}\right)\left(\frac{\sqrt{3}+1}{2\sqrt{2}}\right) - \left(\frac{I_{3q}}{I_3}\right)\left(\frac{\sqrt{3}-1}{2\sqrt{2}}\right) = \frac{I'_{3d}}{I_3} \quad \text{and}$$

$$\left(\frac{I_{3d}}{I_3}\right)\left(\frac{\sqrt{3}-1}{2\sqrt{2}}\right) + \left(\frac{I_{3q}}{I_3}\right)\left(\frac{\sqrt{3}+1}{2\sqrt{2}}\right) = \frac{I'_{3q}}{I_3}$$

$$\text{or } I'_{3d} = \frac{(\sqrt{3}+1)I_{3d} - (\sqrt{3}-1)I_{3q}}{2\sqrt{2}} \quad \text{and}$$

$$I'_{3q} = \frac{(\sqrt{3}+1)I_{3q} + (\sqrt{3}-1)I_{3d}}{2\sqrt{2}}$$

Considering 'k' as the coupling coefficient between the two windings (leading and

lagging) of the DSIG the equivalent referred currents are modified as:

$$I'_{3d} = k^2 \left(\frac{(\sqrt{3} + 1)I_{3d} - (\sqrt{3} - 1)I_{3q}}{2\sqrt{2}} \right) \quad \text{and} \quad (3)$$

$$I'_{3q} = k^2 \left(\frac{(\sqrt{3} + 1)I_{3q} + (\sqrt{3} - 1)I_{3d}}{2\sqrt{2}} \right) \quad (4)$$

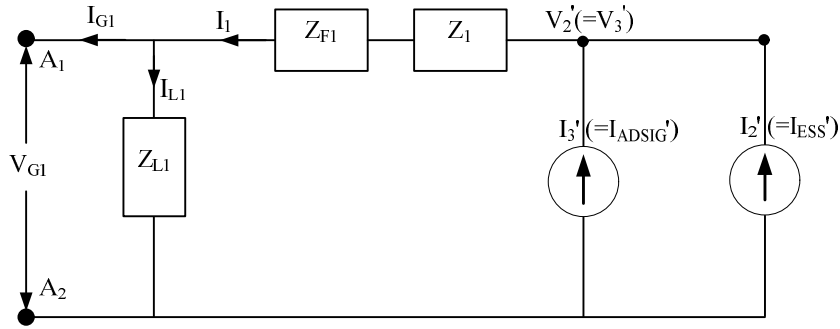


Fig. 6.2(d): Equivalent circuit seen on the leading winding side grid

From the above phasors and equation a modified equivalent circuit as seen from the leading winding side is shown in Fig. 6.2(d) where I_3' ($=I_{\text{ADSIG}}'$) and I_2' ($=I_{\text{ESS}}'$) are the currents transacted by the ADSIG (phase shifted by 15°) and current of ESS (phase shifted by 30°). The current I_1 (I_{Grid}) respected to the grid thus can be given by:

$$I_1 (= I_{\text{Grid}}) = I_3' + I_2' (= I_{\text{ESS}}') \quad (5)$$

Where,

$$I_1 = I_{G1} + I_{L1}$$

And accordingly,

$$I_{\text{Grid}d} - jI_{\text{Grid}q} = (I'_{3d} + j \cdot I'_{3q}) + (I'_{\text{ESS}d} + j \cdot I'_{\text{ESS}q}) \quad (6)$$

Here, the $I_{\text{Grid}d}$ always flow is considered flowing from ADSIG coupled with ESS to grid side and $I_{\text{Grid}q}$ is considered always flowing from grid side to ADSIG for

contribution to reactive power requirements of ADSIG. The magnitude of I_{Grid_q} is affected by the magnetization requirement of ADSIG as well as the power pushed by the ESS (from the lagging winding side) marking the cross magnetization effect. As there is no capacitor connected, as such but the reactive power demand from the grid may increase/decrease in accordance with real power supplied/absorbed from/by the ESS which is also evident, as shown compensating for the reactive power due to phase shifting effect ($I'_{ESS q}$).

Further the Power delivered to grid from ADSIG coupled ESS via leading winding set of ADSIG is analysed for four different modes of operation which depends on different wind speeds resulting in different levels active power generations and reactive power transaction by ADSIG.

Mode 1:

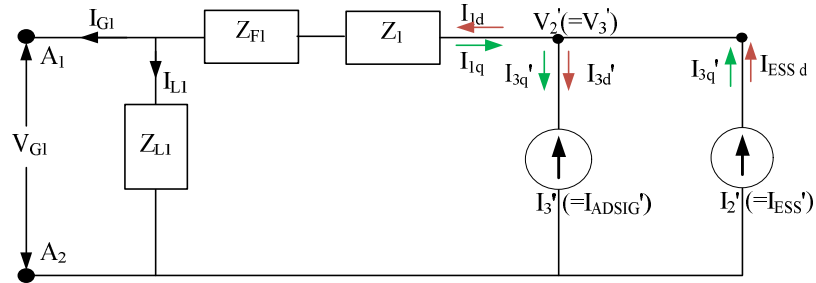


Fig. 6.2(e): Equivalent circuit seen on the leading winding side grid as in Mode 1

Wind speed below synchronous speed, results in no active power generation. Moreover, it adds to the burden of power losses in running the ADSIG duly declutched from the turbine. In this mode ADSIG acts only as an isolation transformer formed by the winding sets and the stored power of ESS fed from lagging winding set of ADSIG to grid. To transfer the committed active power to the grid, the ESS has to supply the committed power in addition to the active power losses occurring in the

ADSIG. Under this mode due to larger real power supply from the ESS side, the current supplied to grid shall also witness operation at leading p.f. due to cross magnetizing effect. The equivalent circuit for this mode of operation is shown in Fig. 6.2(e). The current to the grid is given as:

$$I_{Grid_d} - jI_{Grid_q} = (-I'_{3d} + j.I'_{3q}) + (I'_{ESS_d} - j.I'_{ESS_q}) \quad (5)$$

The negative sign of $(-I'_{3d})$ show that the ADSIG is taking active current as it not generating any real power in this mode of operation. Similarly the negative sign of $(-j.I'_{ESS_q})$ show that the ADSIG is also supplying reactive power when shifted by 30° on the leading winding side of the ADSIG.

Mode 2:

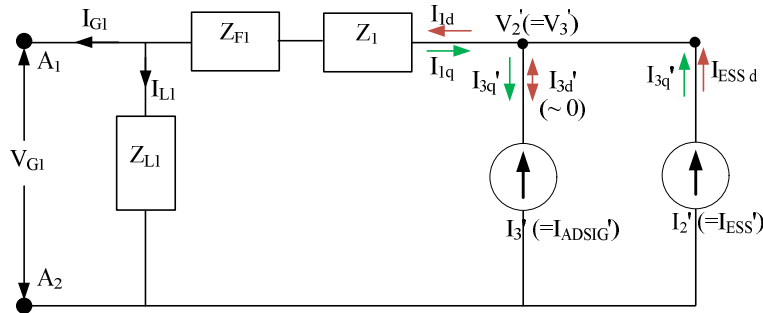


Fig. 6.2(f): Equivalent circuit seen on the leading winding side grid as in Mode 2

When wind speed is just above synchronous speed so that ADSIG is in generating mode but the active power generated is only sufficient for catering its own active power losses happening in the machine. Thus ESS is responsible for transferring only the committed active power to grid via the two isolated stator windings of ADSIG. The equivalent circuit for this mode of operation is shown in Fig. 6.2(f). The current to the grid is given as:

$$I_{Grid_d} - jI_{Grid_q} = (\pm I'_{3d} + j.I'_{3q}) + (I'_{ESS_d} - j.I'_{ESS_q}) \quad (7)$$

The active current requirement of ADSIG is reduced in this mode of operation and it lies very close to zero. Here \pm symbol for ADSIG current pertaining to real power ($\pm I'_{3d}$) represent that it may supply or take a very small value of current. Similarly, the negative sign of ($-j \cdot I'_{ESSq}$) show that the ADSIG is still supplying reactive power when shifted by 30° on the leading winding side of the ADSIG but its value is reduced as compared to previous case.

Mode 3:

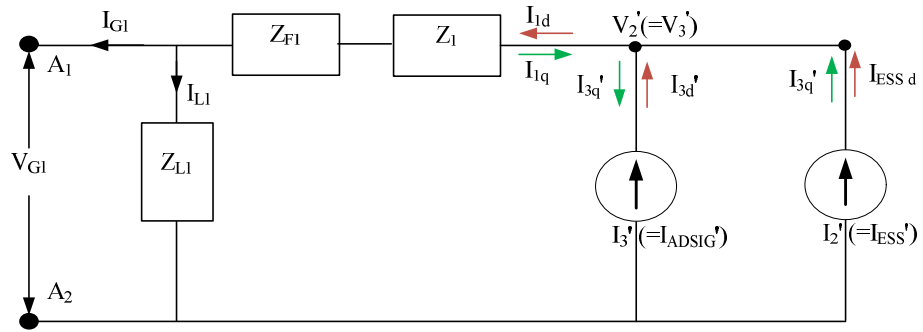


Fig. 6.2(g): Equivalent circuit seen on the leading winding side grid as in Mode 3

When wind speed is more than synchronous speed and that the active power generated by ADSIG is more than its active power losses. Thus remaining active power of ADSIG (after catering its own losses) is transferred to the grid. ESS supplies the remaining power to the grid to fulfil the active power commitment. The equivalent circuit for this mode of operation is shown in Fig. 6.2(g). Since, the real power coming from ESS reduces but is sufficient enough to meet the requirements of ADSIG; the current to the grid is given as:

$$I_{Grid_d} - jI_{Grid_q} = (I'_{3d} + j \cdot I'_{3q}) + (I'_{ESSd} - j \cdot I'_{ESSq}) \quad (7)$$

Mode 4:

When wind speed is more than the third mode resulting in generation of active power exceeding the committed power to grid. The excess power after catering to the power

commitment and internal losses of ADSIG is also routed to ESS for storage. The equivalent circuit for this mode of operation is shown in Fig. 6.2(h). The current to the grid is given as:

$$I_{Grid_d} - jI_{Grid_q} = (I'_{3d} + j \cdot I'_{3q}) + (-I'_{ESS_d} \pm j \cdot I'_{ESS_q}) \quad (8)$$

The negative sign of ESS active current ($-I'_{ESS_d}$) show that the ESS is taking the excess power generated by the ADSIG.

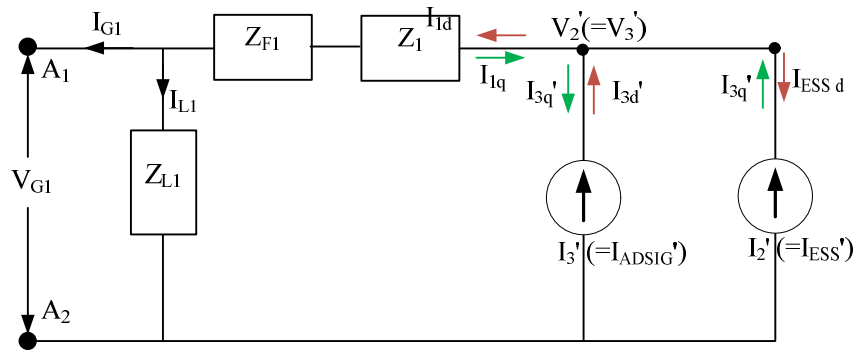


Fig. 6.2(h): Equivalent circuit seen on the leading winding side grid as in Mode 4

6.4 Control of ESS

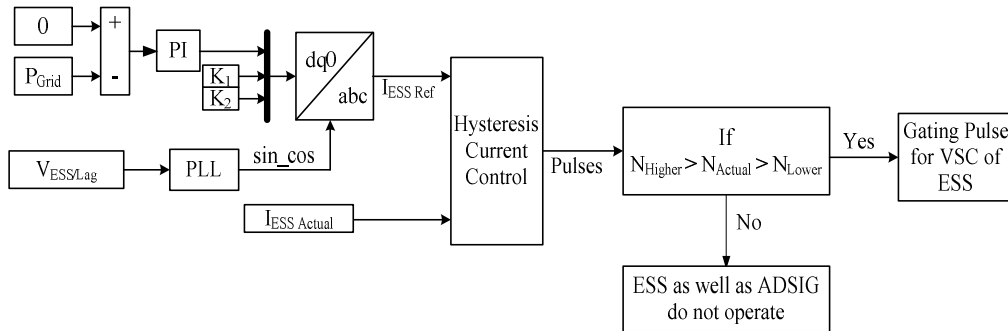


Fig. 6.3: Block Diagram of ESS

The battery energy storage system is modelled as a current controlled VSC, which uses an IGBT bridge having battery source connected on the DC bus. It injects a current into the lagging winding side set of the ADSIG in such a way that the current from the ESS always meets the committed power requirements at the grid side of the ADSIG. The reference value of current for devising the gating pulse of VSC of ESS is

obtained by using synchronous reference frame theory as shown in Fig. 6.3. Here the actual grid power is compared with reference committed power and the error so produced is passed through the proportional-integral (PI) controller to derive the reference value, which forms the d-axis component of current of ESS. The control may also be used to generate the reactive power if needed but to keep the control simpler, only d-axis component is controlled by the controller. And the q-axis component is set to zero (or may be to a certain value to give a fixed amount of reactive power through ESS). The dq0 components are then developed using reverse Park transform to generate abc reference frame with the help of synchronizing signal, synchronous with the voltage at the lagging side of the ADSIG. This $I_{\text{ESS ref}}$ is then passed through Hysteresis current controller to produce the gating pulse for the VSC. The power which is to be transacted between ADSIG and ESS depends upon these switching pulses provided to the VSC. This system works only in a particular range of wind speed depending on the capacity of ESS and characteristics of the induction machine. Every time gating pulses given to ESS are compared with the range of wind speed and if the speed lies within the range of operation ($N_{\text{Higher}} > N_{\text{Actual}} > N_{\text{Lower}}$) then the operation continues and for any other value of wind speed the generating units (ADSIG in tandem with ESS) are declutched from the main grid and generation from ADSIG is stopped.

6.5 Performance Evaluation of ADSIG in tandem with ESS for Power Flow Control

The prototype of ADSIG generator coupled with ESS is tested experimentally amidst different wind speeds, emulated by a VFD coupled at the shaft to study the performance of the considered system. The performance is gauged by recording

voltage and current waveforms for all the modes of operations, along with this power analyzer screenshots (showing active and reactive power flow) on both the winding side of the ADSIG and analysing the obtained results. Harmonics in current waveforms on both the winding side of the ADSIG are also recorded to establish its capability to avert the harmonic proliferations.

Mode 1:

In this mode since the wind speed is considered lesser than the synchronous speed and ADSIG is unable to generate any active power. ESS takes up the responsibility of catering the ADSIG losses and fulfilling the active power commitment to the grid. Fig. 6.4(a) and 6.4(d) shows the screenshots of power analyzer recorded on the ESS side of ADSIG and grid side of ADSIG respectively. It may be observed that the committed power of 1000 W is nearly achieved by the transformer action of the ADSIG even when the wind speed is below cut-in speed. The ESS supplied 1560 W of active power, where the excess power of 550W is consumed by the ADSIG and to cater the part reactive power requirement of ADSIG (due to cross magnetization effect). Fig 6.4(b) and 6.4(e) shows the three phase current waveforms and voltage waveform of one phase of ADSIG on the ESS side of ADSIG and Grid side of ADSIG respectively. Only a support of 480VAR is drawn from ESS to magnetize the ADSIG to the required level, while the major portion is met from cross-coupling effect. It may be observed that the current waveform on ESS side of ADSIG has a larger component of harmonics and the same is restricted to enter grid side due to isolation of ADSIG windings and flux coupling only at fundamental frequency. Further the current harmonics spectrum on ESS side and grid side winding of ADSIG is shown in Fig. 6.4(c) and 6.4(f), where the ESS side current is shown to have THD of 20.5% and only

	A	B	C	Total
W	540	500	520	1560
VA	570	530	560	1660
var	150	150	180	480
PF	0.94	0.94	0.93	0.94

25/05/18 10:22:46 440V 50Hz 3Ø WYE FN50160

Fig. 6.4(a): Active and Reactive Power of ESS (off-grid) side of ADSIG –Mode 1

	A	B	C	Total
W	- 360	- 310	- 340	-1010
VA	730	710	800	2240
var	640	630	720	1990
PF	-0.49	-0.44	-0.43	-0.45

25/05/18 10:25:07 440V 50Hz 3Ø WYE FN50160

Fig. 6.4(d): Active and Reactive Power of Grid side of ADSIG-Mode 1

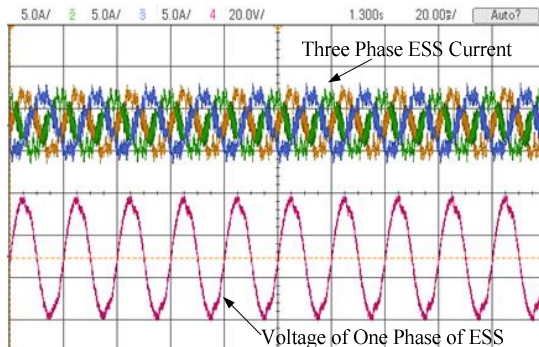


Fig. 6.4(b): Phasor of three phase current and voltage of one phase of ESS (off-grid) side of ADSIG-Mode 1. X axis: 20ms/div; Y axis: Current 5A/div; Voltage 250v/div

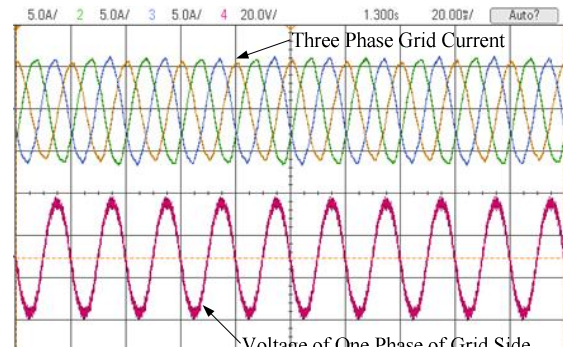


Fig. 6.4(e): Phasor of three phase current and voltage of one phase of Grid side of ADSIG-Mode 1 X axis: 20ms/div; Y axis: Current 5A/div; Voltage 250v/div

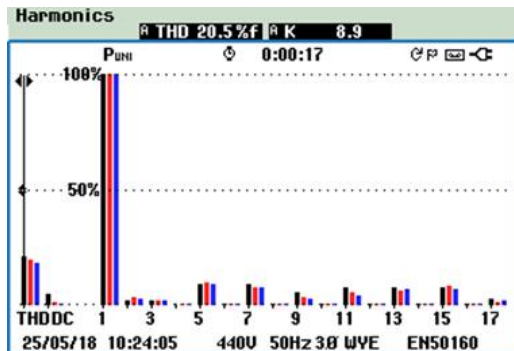


Fig. 6.4(c): Current THD at ESS (off-grid) side of ADSIG-Mode 1

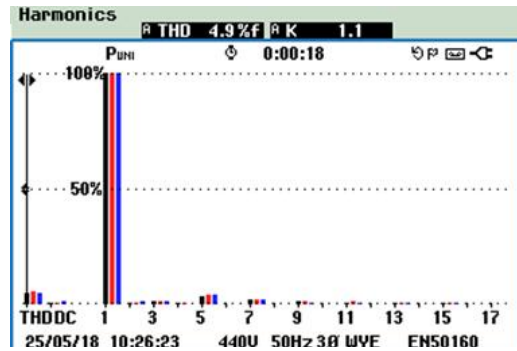


Fig. 6.4(f): Current THD at Grid side of ADSIG-Mode 1

4.9% THD is reflected on the grid side of ADSIG.

Mode 2:

In this mode the wind speed lies near synchronous speed to (slightly above) and is sufficient to keep the ADSIG in generating mode to cater to ohmic losses. If the operation is conducted without ESS in such conditions the power reversal from grid

	A	B	C	Total
W	380	350	360	1090
VA	420	390	400	1210
var	160	140	170	480
PF	0.90	0.91	0.88	0.90

25/05/18 11:08:05 440V 50Hz 3Ø WYE ENS0160

Fig. 6.5(a): Active and Reactive Power of ESS (off-grid) side of ADSIG-Mode 2

	A	B	C	Total
W	- 360	- 320	- 350	-1030
VA	720	700	780	2210
var	620	620	700	1940
PF	-0.50	-0.45	-0.45	-0.47

25/05/18 11:10:54 440V 50Hz 3Ø WYE ENS0160

Fig. 6.5(d): Active and Reactive Power of Grid side of ADSIG-Mode 2

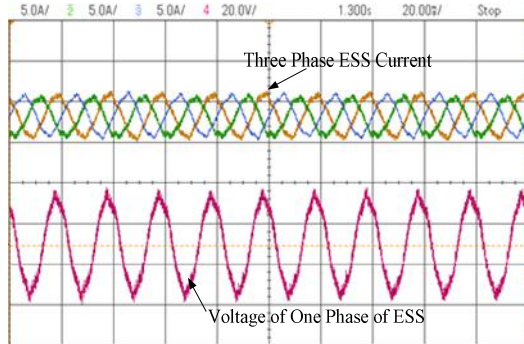


Fig. 6.5(b): Phasor of three phase current and voltage of one phase of ESS (off-grid) side of ADSIG-Mode 2. X axis: 20ms/div; Y axis: Current 5A/div; Voltage 250V/div

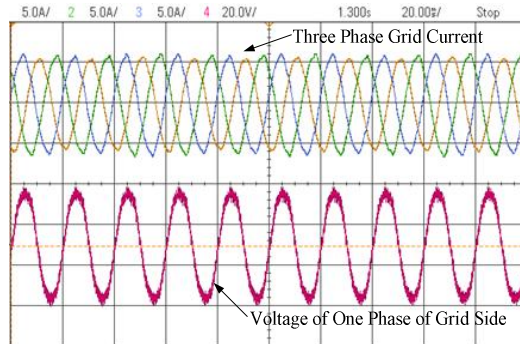


Fig. 6.5(e): Phasor of three phase current and voltage of one phase of Grid side of ADSIG-Mode 2. X axis: 20ms/div; Y axis: Current 5A/div; Voltage 250V/div



Fig. 6.5(c): Current THD at ESS (off-grid) side of ADSIG-Mode 2

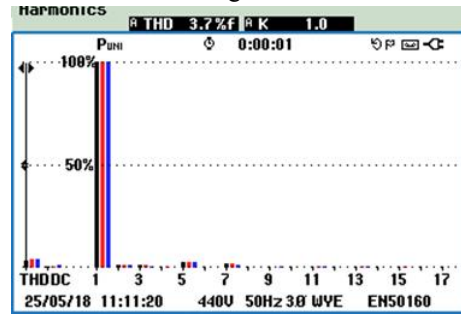


Fig. 6.5(f): Current THD at Grid side of

takes place and to avoid this ADSIG has to be detached. But in this case due to presence of ESS on the lagging winding side of ADSIG it able to meet the committed power and avert such situations. It may be observed from Fig. 6.5(a) and Fig. 6.5(d) that 1090W supplied by ESS is transferred to grid side without any pilferage to ADSIG. The reactive power required from the grid is also didn't changed much when compared for mode 1 (Fig. 6.4(b)) and mode 2 (Fig. 6.5(b)), this is a result of cross magnetization phenomenon observed in case of ADSIGs. The harmonic content of ESS current is lesser than the previous mode and there is subsequently lesser harmonic

content in the grid side current of ADSIG as seen from Fig 6.5(c), and Fig 6.5(f).

Mode 3:

	A	B	C	Total
W	170	150	150	470
VA	240	210	230	690
var	160	150	170	480
PF	0.70	0.69	0.65	0.68

25/05/18 11:14:11 440V 50Hz 3Ø WYE EN50160

Fig. 6.6(a): Active and Reactive Power of ESS (off-grid) side of ADSIG-Mode 3

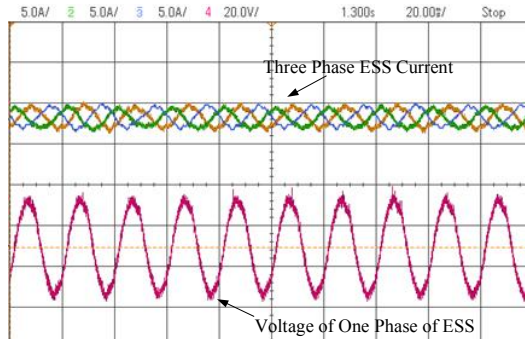


Fig. 6.6(b): Phasor of three phase current and voltage of one phase of ESS (off-grid) side of ADSIG-Mode 3. X axis: 20ms/div; Y axis: Current 5A/div; Voltage 250V/div



Fig. 6.6(c): Current THD at ESS (off-grid) side of ADSIG-Mode 3

	A	B	C	Total
W	- 360	- 310	- 350	-1030
VA	740	730	820	2290
var	640	660	740	2040
PF	-0.49	-0.42	-0.43	-0.45

25/05/18 11:16:54 440V 50Hz 3Ø WYE EN50160

Fig. 6.6(d): Active and Reactive Power of Grid side of ADSIG-Mode 3

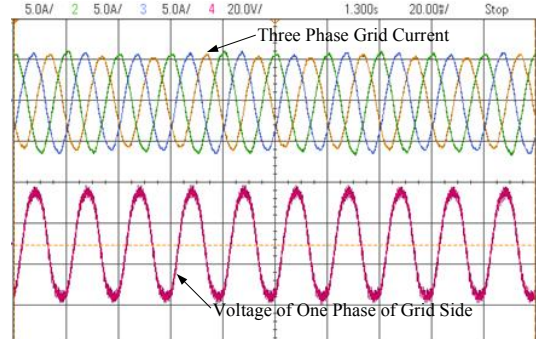


Fig. 6.6(e): Phasor of three phase current and voltage of one phase of Grid side of ADSIG-Mode 3. X axis: 20ms/div; Y axis: Current 5A/div; Voltage 250V/div

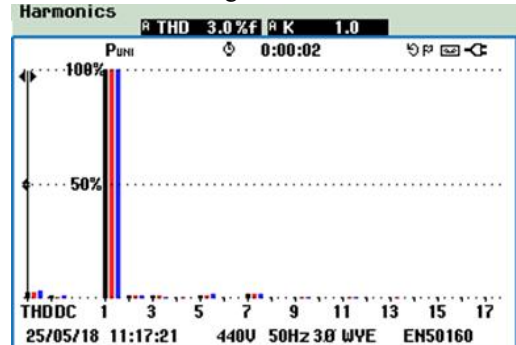


Fig. 6.6(f): Current THD at Grid side of ADSIG-Mode 3

Third mod is evaluated for a wind speed moderately higher than the cut-in speed. At such wind speeds the generated power by ADSIG is lesser than the committed power but greater than its ohmic loss component. If the ADSIG is present without the support of ESS then this difference of active power (generated minus ohmic loss) would have transferred to the grid and with the variation of wind speed the active power transfer

would also have varied, in cubic relation with the wind speed. But with ADSIG coupled with ESS the deficit active power, is fulfilled by the ESS so that always fixed committed power is transferred to the grid as seen from Fig. 6.6(d) with the share of ESS decreased considerably to 470 W (Fig. 6.6(a)). From the Fig. 6.6(b) and Fig. 6.6(e) it is seen that the harmonics content of currents are further considerably reduced both in ESS current and current on the grid side of ADSIG.

Mode 4:

PUNI 0:02:35				
	A	B	C	Total
W	- 200	- 130	- 150	- 480
	A	B	C	Total
VA	260	230	190	690
	A	B	C	Total
var	160	180	110	450
	A	B	C	Total
PF	-0.77	-0.56	-0.78	-0.70
25/05/18 11:18:50 440V 50Hz 3Ø WVE ENS0160				

Fig. 6.7(a): Active and Reactive Power of ESS (off-grid) side of ADSIG-Mode 4

PUNI 0:03:09				
	A	B	C	Total
W	- 350	- 280	- 370	- 990
	A	B	C	Total
VA	800	830	930	2560
	A	B	C	Total
var	720	780	850	2350
	A	B	C	Total
PF	-0.43	-0.33	-0.40	-0.39
25/05/18 11:21:32 440V 50Hz 3Ø WVE ENS0160				

Fig. 6.7(d): Active and Reactive Power of Grid side of ADSIG-Mode 4

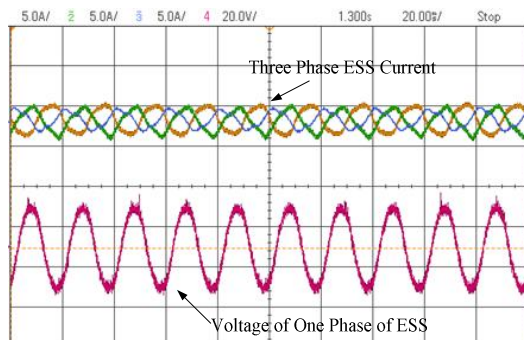


Fig. 6.7(b): Phasor of three phase current and voltage of one phase of ESS (off-grid) side of ADSIG-Mode 4. X axis: 20ms/div; Y axis: Current 5A/div; Voltage 250V/div

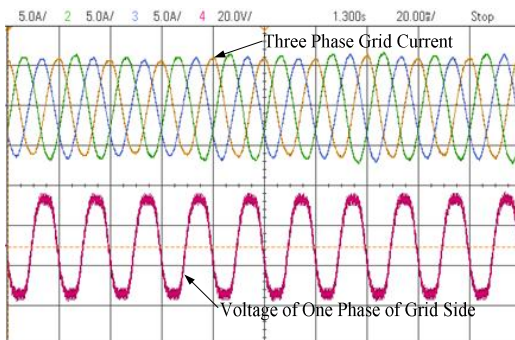


Fig. 6.7(e): Phasor of three phase current and voltage of one phase of Grid side of ADSIG-Mode 4. X axis: 20ms/div; Y axis: Current 5A/div; Voltage 250V/div



Fig. 6.7(c): Current THD at ESS (off-grid) side of ADSIG-Mode 4

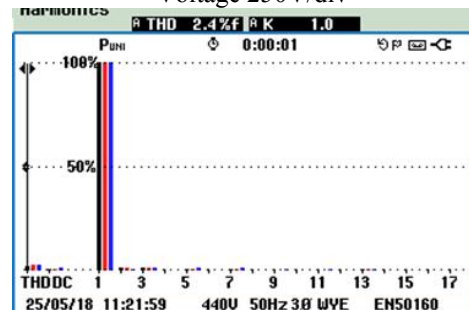


Fig. 6.7(f): Current THD at Grid side of ADSIG-Mode 4

In fourth mode when the wind speed is significantly higher than synchronous speed and the ADSIG generates more power than the committed value, after catering to its ohmic losses and transferring the committed power to the grid the remaining amount of power is supplied to the ESS. It may be observed from Fig. 6.7(a) the excess power generated (480W) from wind is fed to the ESS, while committed power of 990W is supported to the grid (Fig. 6.7(a)). Fig. 6.7(b) shows the voltage and current waveforms of ESS and Fig. 6.7(e) shows the voltage and current waveforms of the grid side. Fig. 6.7(c) and Fig. 6.7(f) show the current harmonics of ESS and the grid respectively. In absence of any storage system the DSIG would transfer such large amount of power to the grid, which may cause disturbances (voltage and frequency) in grid and may even result in reverse power flow in the transmission lines. Such anomalies may cause tripping of protection devices and unwanted shutdown of the system.

6.6 Conclusion

The analysis of ADSIG based coupled with ESS has been done for transaction of power under sufficient wind conditions to feed committed power to grid. The same has been also validated through the experimental results obtained on the hardware prototype developed in the laboratory. The analysis and testing both are done in four different mode of operation amidst a wide range of wind speed. The results demonstrate that the current proposal is successful in overcoming intermittent nature of wind. The advantage of cross magnetization effect of the ADSIG is established through both analysis and experimental study for use of ADSIG coupled with ESS for application to seamless operation wind farm. The action of ADSIG as a harmonic isolator between two winding sets is also successfully demonstrated through results.

Chapter 7

Performance Analysis of Grid Coupled ADSIG for Rural Electrification

7.1 General

The growth of new, economic and reliable power generation techniques have yielded sustainable growth in the generation of electricity but still, scarcity of power looms largely. This deficit of electrical power is more severely pronounced in rural areas. Meeting the increasing energy demand in rural areas is one of the major problems faced by utility engineers as their locations are usually far from the power transformers dealing with buck power and transferring power at distribution level voltage over longer distances are having their own problems. Moreover, the rural loads are very intermittent in nature so the efficiency of such distribution transformers, feeding power to the rural loads, is very poor which adds to the drawbacks of rural electrification. Therefore delivering power to such areas is economical only if the generating units are closer to the load ends and the generation is eco-friendly. Power generation from wind is a better solution for coastal rural locations as the wind speed is usually good and, sufficient for a generation.

This chapter introduces a concept for cheaper power generation technique utilising the Asymmetrical Dual Stator Induction Generators (ADSIG) for coupling rural feeder with a distribution network for providing electricity to rural areas along with harvesting available wind energy. As per discussions on ADSIG enacting as a GENFORMER (Generator-Transformer unit) in earlier chapter, the ADSIG act as a generator by delivering power to both stator windings skewed towards the side which

witness larger loading, and in case of insufficient wind speed, the ADSIG is declutched and pays the way for isolation transformer mode for seamless power feeding to the loads on rural distribution feeder. Multiple smaller rated ADSIG may be utilised for catering the power demand rural loads and thereby reducing the effective loading/demand from the utility grid.

7.2 System Considered for Utilization of ADSIG for Rural Electrification

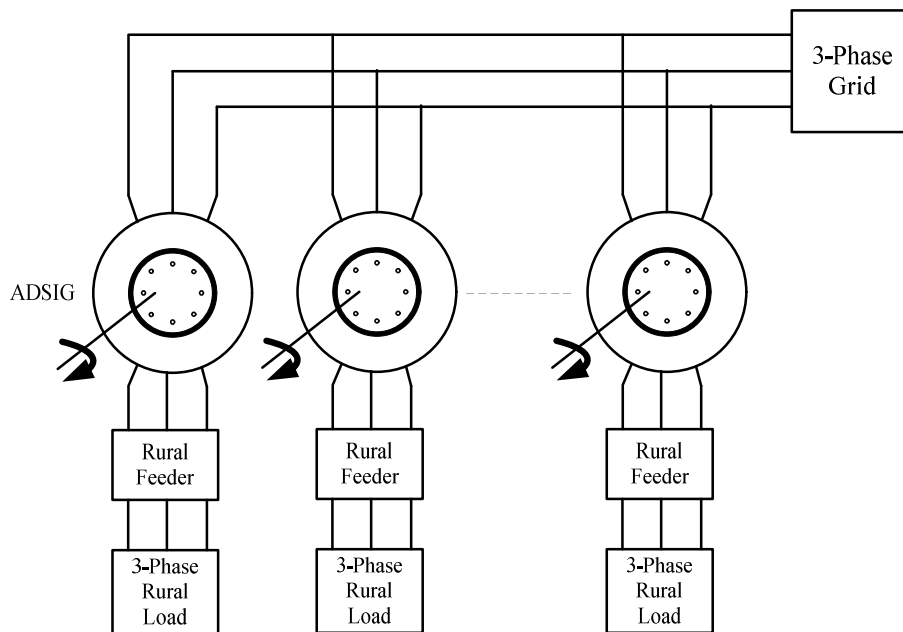


Fig. 7.1: Configuration 1- ADSIG connected to Substation and feeding Rural loads via rural distribution feeder

For studying the application of wind generation using ADSIG, it may be considered connected in two different configurations (Fig. 7.1 and Fig. 7.2). In the first configuration as shown in Fig. 7.1, the ADSIG is near to the substation and at a certain distance from the loads. The distance between the load and ADSIG is shown with the feeder drop. Substation and the loads are connected on the different winding sets of ADSIGs.

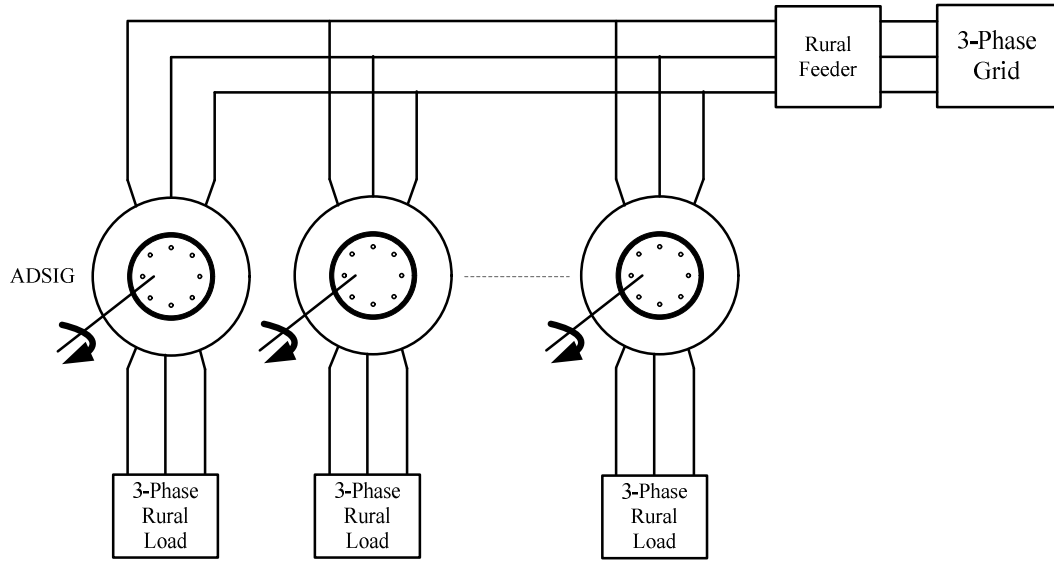


Fig. 7.2: Configuration 2- ADSIG connected to grid and feeding Local/Home Loads

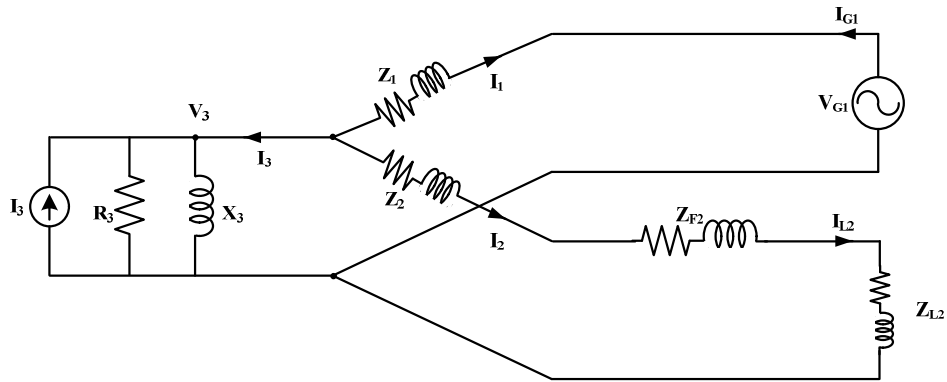


Fig. 7.3: Equivalent circuit of ADSIG connected to Substation and feeding Rural loads via rural distribution feeder

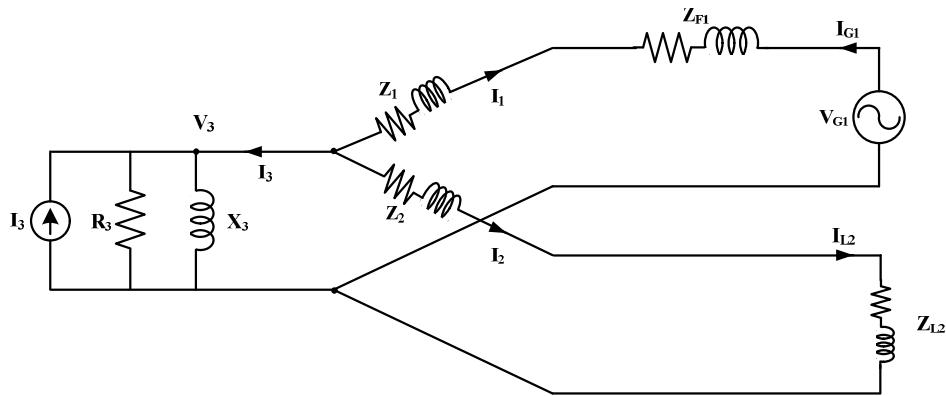


Fig. 7.4: Equivalent circuit of ADSIG connected to grid and feeding Local/Home Loads

The equivalent circuits for the networks under consideration with three-phase grid delivering power to rural loads via ADSIG is drawn for analysing the capabilities of the system and power flow as shown in Fig. 7.3. As discussed in the previous chapters, the ADSIG fed by wind is modelled as a current source when it is generating power and as a simple transformer when there is no generation of power. As shown in Fig. 7.3, V_{G1} represents the grid/substation voltage and Z_{L2} represents the load connected to the feeder via feeder impedance Z_{F2} . The equivalent circuit of the second configuration is shown in Fig. 7.4 where the ADSIGs are in the vicinity of the local loads and at a certain distance from the grid/substation.

The grid voltage is represented by V_{G1} which connected to the ADSIGs via feeder with impedance Z_{F2} and in turn ADSIG is feeding the load Z_{L2} , representing the local/home loads. In both the configuration the reactive power demand of ADSIG is supported by a feeder or local capacitor bank (if any) connected at the feeder side of the ADSIG winding. Only three phase rural passive loads are assumed to be connected to the off-grid side windings of ADSIG to study the power flow and load dynamics.

7.3 Mathematical Analysis of Power Flow from/across ADSIG

The power flow studies for both the configurations are similar except the difference of respective feeder impedance introduced at different places. Thus a combined set of the equations are discussed here. The power flow depends upon the transformer action or the generation action of the ADSIG.

Mode 1: Generation Mode

Now as the wind speed increases and the ADSIG start pitching in generating mode, it starts delivering power to the load and the excess power if any, is transferred to the

grid/substation side loads. The expressions for currents of ADSIG flowing in the leading and lagging winding set depending upon the configuration and are represented as:

- For the first configuration as per equivalent circuit is shown in Fig. 7.3, when the ADSIG is near to substation and connected to local loads on the other winding set of the ADSIG, the current in ADSIG are represented as:

$$I_1(\text{Grid Side}) = I_3 \left[\frac{Z_2 + Z_{L2} + Z_{F2}}{(Z_1 + Z_{L1}) + (Z_2 + Z_{F2} + Z_{L2})} \right] \quad (7.1)$$

$$I_2(\text{Off - grid Side}) = I_3 \left[\frac{Z_1 + Z_{L1}}{(Z_1 + Z_{L1}) + (Z_2 + Z_{F2} + Z_{L2})} \right] \quad (7.2)$$

- For the second configuration when the ADSIG is near to local loads.

$$I_1(\text{Grid Side}) = I_3 \left[\frac{Z_2 + Z_{L2}}{(Z_1 + Z_{L1} + Z_{F1}) + (Z_2 + Z_{L2})} \right] \quad (7.3)$$

$$I_2(\text{Off - grid Side}) = I_3 \left[\frac{Z_1 + Z_{L1} + Z_{F1}}{(Z_1 + Z_{L1} + Z_{F1}) + (Z_2 + Z_{L2})} \right] \quad (7.4)$$

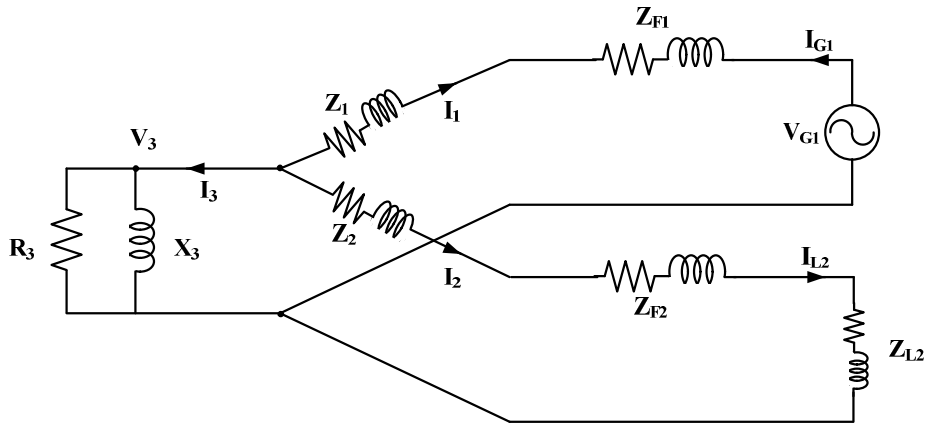


Fig. 7.5: Generalized Equivalent Circuit (for both configuration) for Transformer Action

Mode 2: Transformer Action

For the transformer action, the circuits are reduced as shown in Fig. 7.5, the current source pertaining ADSIG is open circuited representing transformer action mode.

Further, a transformer based equivalent circuit is drawn and are shown in Fig. 7.6. Net power from the grid/substation depends upon the current drawn as the voltage of the grid is approximately constant. The current drawn from the grid is given by:

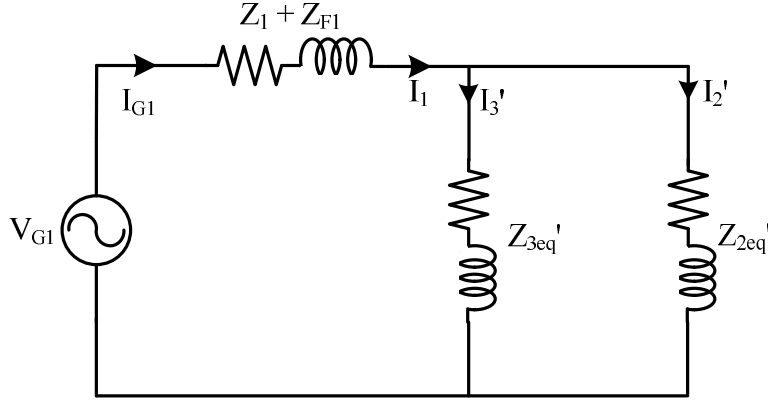


Fig. 7.6(a): Transformer Action Reduced Equivalent Circuit (Both configuration) as seen on the Grid/substation side of ADSIG

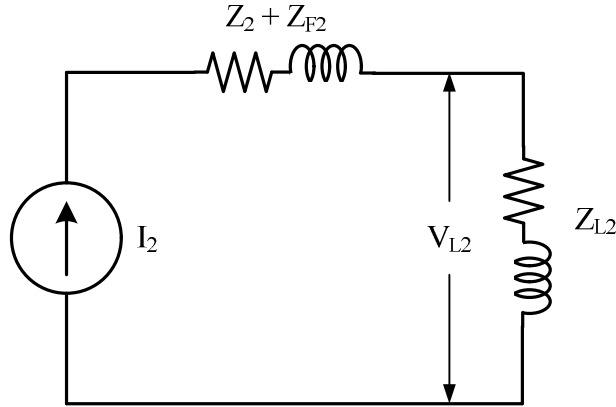


Fig. 7.6(b): Transformer Action Reduced Equivalent Circuit (Both configuration) as seen on the load/rural feeder side of ADSIG

$$I_{G1} = I_1 \quad (7.5)$$

Where, I_1 is the current entering from the grid side ADSIG winding and is given as:

$$I_1 = \frac{V_{G1}}{Z_{eq}} \quad (7.6)$$

Where,

$$Z_{eq} = Z_{1eq} + (Z'_{2eq} \parallel Z'_{3eq})$$

$$Z_{eq} = Z_{1eq} + \frac{Z'_{2eq} \cdot Z'_{3eq}}{Z'_{2eq} + Z'_{3eq}} \quad (7.7)$$

Where, Z_{1eq} , Z'_{2eq} and Z'_{3eq} depends upon winding side on which grid is connected and the configuration selected and are as follow (depicted from the generalized form discussed in Chapter 5):

- For the first configuration when the ADSIG is near to substation and connected on the **Leading Winding** set of the ADSIG.

$$Z_{1eq} = Z_1 \quad (7.8)$$

$$Z_{2eq} = R_{2eq} + j \cdot X_{2eq} = (R_2 + R_{F2} + R_{L2}) + j(X_2 + X_{F2} + X_{L2}) \quad (7.9)$$

$$Z'_{2eq} = k^2 \left[\left(\frac{\sqrt{3}(R_2 + R_{F2} + R_{L2}) - (X_2 + X_{F2} + X_{L2})}{2} \right) + j \left(\frac{\sqrt{3}(X_2 + X_{F2} + X_{L2}) + (R_2 + R_{F2} + R_{L2})}{2} \right) \right] \quad (7.10)$$

$$Z_{3eq} = R_{3eq} + jX_{3eq} = \left(\frac{R_3 X_3^2}{R_3^2 + X_3^2} \right) + j \left(\frac{R_3^2 X_3}{R_3^2 + X_3^2} \right) \quad (7.11)$$

$$Z'_{3eq} = \left(\frac{(\sqrt{3} + 1)(R_{3eq}) - (\sqrt{3} - 1)X_{3eq}}{2\sqrt{2}} \right) + j \left(\frac{(\sqrt{3} - 1)(R_{3eq}) + (\sqrt{3} + 1)X_{3eq}}{2\sqrt{2}} \right) \quad (7.12)$$

- For the first configuration when the ADSIG is near to substation and connected on the **Lagging Winding** set of the ADSIG.

$$Z_{1eq} = Z_1 \quad (7.13)$$

$$Z_{2eq} = R_{2eq} + j \cdot X_{2eq} = (R_2 + R_{F2} + R_{L2}) + j(X_2 + X_{F2} + X_{L2}) \quad (7.14)$$

$$Z'_{2eq} = k^2 \left[\left(\frac{\sqrt{3}(R_2 + R_{F2} + R_{L2}) + (X_2 + X_{F2} + X_{L2})}{2} \right) + j \left(\frac{\sqrt{3}(X_2 + X_{F2} + X_{L2}) - (R_2 + R_{F2} + R_{L2})}{2} \right) \right] \quad (7.15)$$

$$Z_{3eq} = R_{3eq} + jX_{3eq} = \left(\frac{R_3 X_3^2}{R_3^2 + X_3^2} \right) + j \left(\frac{R_3^2 X_3}{R_3^2 + X_3^2} \right) \quad (7.16)$$

$$Z'_{3eq} = \left(\frac{(\sqrt{3} + 1)(R_{3eq}) + (\sqrt{3} - 1)X_{3eq}}{2\sqrt{2}} \right) + j \left(\frac{(\sqrt{3} - 1)(R_{3eq}) - (\sqrt{3} + 1)X_{3eq}}{2\sqrt{2}} \right) \quad (7.17)$$

- For the second configuration when the ADSIG is near to local loads and connected on the **Leading Winding** set of the ADSIG.

$$Z_{1eq} = Z_1 + Z_{F1} \quad (7.18)$$

$$Z_{2eq} = R_{2eq} + j.X_{2eq} = (R_2 + R_{L2}) + j(X_2 + X_{L2}) \quad (7.19)$$

$$Z'_{2eq} = k^2 \left[\left(\frac{\sqrt{3}(R_2 + R_{L2}) - (X_2 + X_{L2})}{2} \right) + j \left(\frac{\sqrt{3}(X_2 + X_{L2}) + (R_2 + R_{L2})}{2} \right) \right] \quad (7.20)$$

$$Z_{3eq} = R_{3eq} + jX_{3eq} = \left(\frac{R_3 X_3^2}{R_3^2 + X_3^2} \right) + j \left(\frac{R_3^2 X_3}{R_3^2 + X_3^2} \right) \quad (7.21)$$

$$Z'_{3eq} = \left(\frac{(\sqrt{3} + 1)(R_{3eq}) - (\sqrt{3} - 1)X_{3eq}}{2\sqrt{2}} \right) + j \left(\frac{(\sqrt{3} - 1)(R_{3eq}) + (\sqrt{3} + 1)X_{3eq}}{2\sqrt{2}} \right) \quad (7.22)$$

- For the second configuration when the ADSIG is near to local loads and

connected on the **Lagging Winding** set of the ADSIG

$$Z_{1eq} = Z_1 + Z_{F1} \quad (7.23)$$

$$Z_{2eq} = R_{2eq} + j.X_{2eq} = (R_2 + R_{L2}) + j(X_2 + X_{L2}) \quad (7.24)$$

$$Z'_{2eq} = k^2 \left[\left(\frac{\sqrt{3}(R_2 + R_{L2}) + (X_2 + X_{L2})}{2} \right) + j \left(\frac{\sqrt{3}(X_2 + X_{L2}) - (R_2 + R_{L2})}{2} \right) \right] \quad (7.25)$$

$$Z_{3eq} = R_{3eq} + jX_{3eq} = \left(\frac{R_3 X_3^2}{R_3^2 + X_3^2} \right) + j \left(\frac{R_3^2 X_3}{R_3^2 + X_3^2} \right) \quad (7.26)$$

$$Z'_{3eq} = \left(\frac{(\sqrt{3} + 1)(R_{3eq}) + (\sqrt{3} - 1)X_{3eq}}{2\sqrt{2}} \right) + j \left(\frac{(\sqrt{3} - 1)(R_{3eq}) - (\sqrt{3} + 1)X_{3eq}}{2\sqrt{2}} \right) \quad (7.27)$$

The current entering into the grid/substation side winding divides into I'_2 and I'_3 as per current division rule and is given by:

$$I'_2 = \frac{I_1 Z'_{3eq}}{Z'_{2eq} + Z'_{3eq}} \quad \text{and} \quad (7.28)$$

$$V'_2 = I'_2 \cdot Z'_{2eq} = V_1 - I_1 Z_{eq} \quad (7.29)$$

By shifting this voltage by 30° (leading or lagging depending upon which winding set grid/substation is connected) the voltage on the ADSIG winding connected to the load side can be calculated and which can be further used to estimate the voltage on the load terminals and are given as (depending upon the configurations):

- For the first configuration when the ADSIG is near to substation.

$$V_{L2} = V_2 - I_2(Z_2 + Z_{F2}) = I_2 Z_{L2} \quad (7.30)$$

- For the second configuration when the ADSIG is near to local loads.

$$V_{L2} = V_2 - I_2(Z_2) = I_2 Z_{L2} \quad (7.31)$$

From the above equations, it is observed that both configurations the voltage on the off-grid side is lesser than the value of the voltage at the grid side. As the load increases the drop in voltages further increase and the terminal voltage at the load end further decreases.

7.4 Performance Evaluation based on MATLAB simulation and Hardware implementation of ADSIG for Rural Electrification

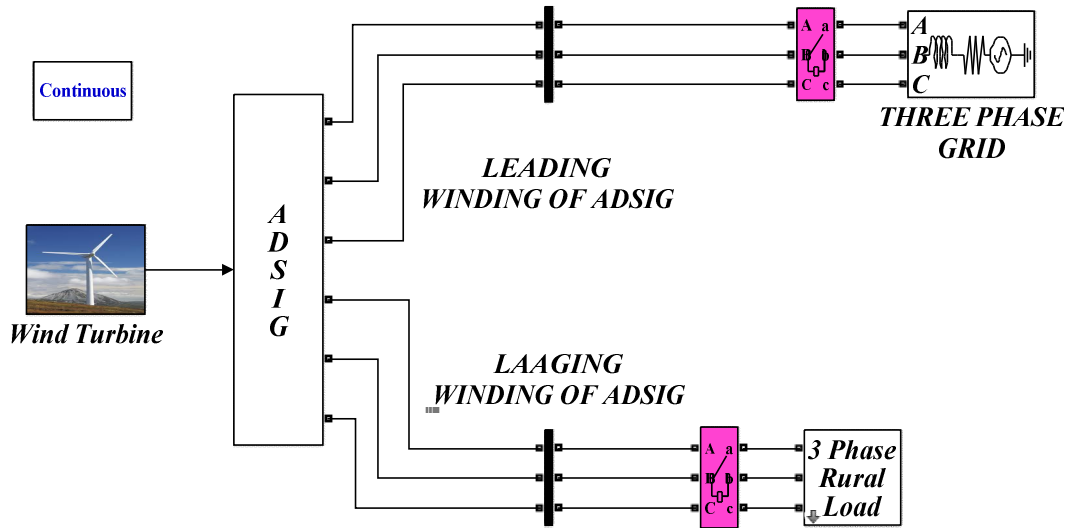


Fig. 7.7: Matlab Simulink Model for Rural Electrification

Performance of ADSIG as Gen-Former for Rural Electrification is studied using MATLAB Simulation followed by performing experiments done on the developed prototype. The MATLAB SIMULINK model is shown in Fig. 7.7. The model is tested for different wind speeds and for different loading levels. The same has been validated with a similar test on the hardware prototype. In the simulation as well as the hardware

implementation the grid is connected on the leading winding side of the ADSIG and the rural load is connected on the lagging winding side of the ADSIG. Fig. 7.8 (voltage and current waveform of both side of ADSIG) and Fig 7.9 (real and reactive power on both winding side of ADSIG) show the performance of ADSIG (simulation results) for different wind speeds conditions.

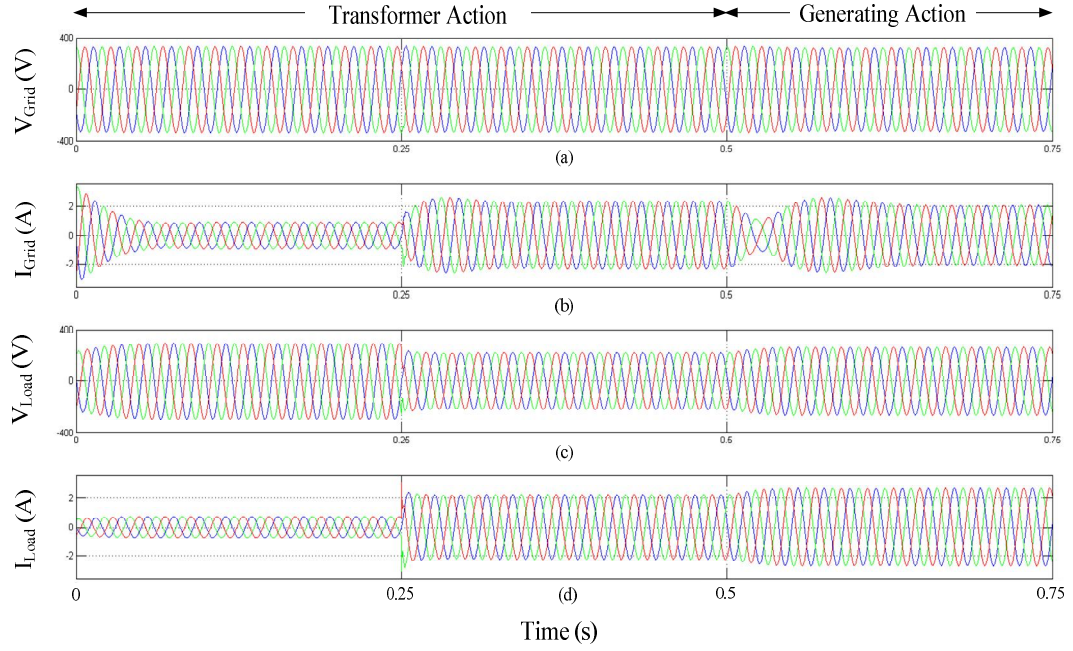


Fig. 7.8: Voltage and Current waveform of Leading (Grid Side) and Lagging (Load Side) Winding Side of ADSIG during Change in Wind Speed

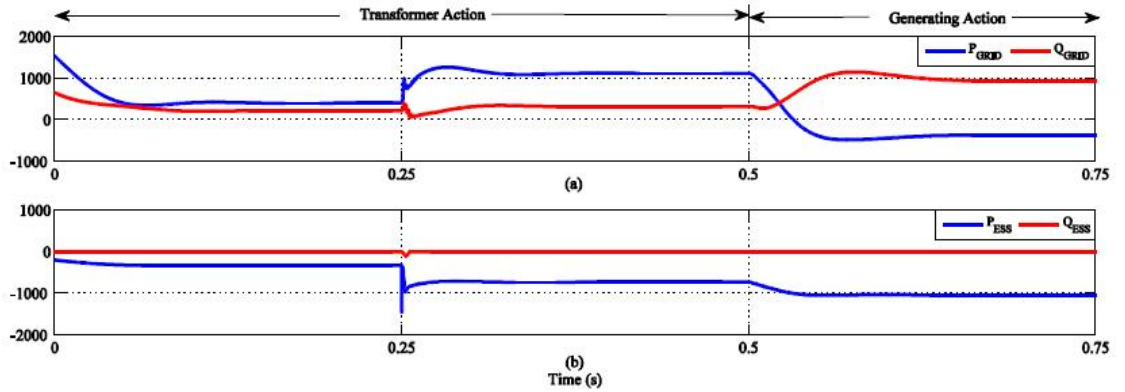


Fig. 7.9: Real and Reactive power drawn/supplied of Leading (Grid Side) and Lagging (Load Side) Winding Side of ADSIG during change in Wind Speed

Firstly from $t = 0$ to $t = 0.5$ s the when wind speed is not sufficient to drive the ADSIG in generating mode and the machine is operating in the motoring mode and due to

declutching from the turbine, thus acting as a transformer. Initially a very small load is applied from $t = 0$ to $t = 0.25$ s and therefore the grid is shown feeding (400 W) the losses of ADSIG as motor along with feeding the small load connected (325 W) on the lagging winding side of ADSIG, besides meeting requirement of magnetisation drawn in form reactive power (220 VAr). Load on the lagging winding side of the ADSIG always operate in upf as the load connected is a resistive load. From $t = 0.25$ s when load with $R = 100 \Omega$ is applied which increase the real power demand drawn from the grid rises to 1120 W as seen from Fig. 7.9 (a). And the reactive power level varies (320 VAr) but not changed much. Then at $t = 0.5$ s the wind speed increases to a level where the ADSIG act as a generator such that it starts feeding both the grid (375 W) as well it local loads (1174 W) or to the rural load feeder. During this period the reactive power demand by ADSIG increases from 320 VAr to 943 VAr, as during transformer action it requires reactive power only to meet its losses while in generating mode the magnetization requirement increase. As the ADSIG operates in generating mode the voltage level on the lagging winding side also improves (Fig. 7.8 (c)).

The hardware results for developed prototype when evaluated for wind speed change; when wind speed less than the cut-in speed and ADSIG operating as a transformer and for wind speed greater than cut-in speed such that the ADSIG operating as generator show the similar trend. Fig. 7.10 to Fig 7.13 shows the voltage and current waveforms of leading (grid side) and lagging (rural load side) winding side of ADSIG, screenshots of three-phase power analyser depicting real and reactive power exchange on both the winding side of the ADSIG and the phasor diagram recorded from the three-phase power analyser during the transformer action of ADSIG. For the first case from the hardware results shown in Fig. 7.10 (b) and Fig. 7.12 (b) it is observed that

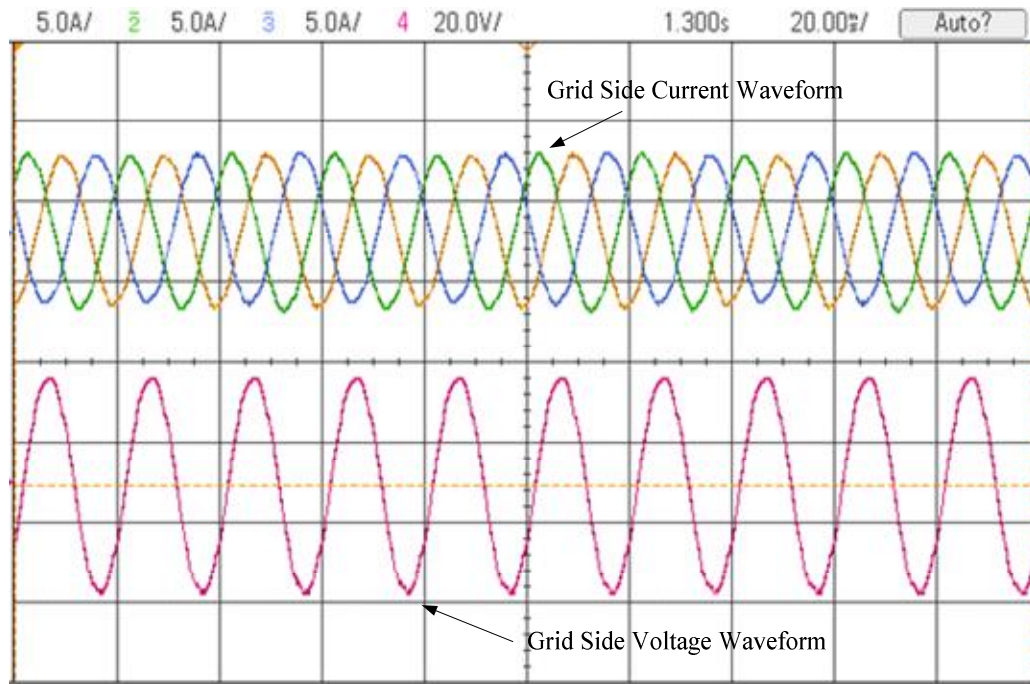


Fig. 7.10(a): Current (3- Φ) and Voltage (I- Φ) waveforms of Grid side ADSIG for Rural Electrification without Prime-mover and ADSIG operating in motoring mode and acting as Isolation Transformer.
Scale: Y axis: Current Waveform 5A/div; Voltage Waveform 250 V/div; X axis: Time 20ms/div

P _{Unit}	A	B	C	Total
W	360	380	380	1110
VA	740	760	730	2230
var	650	660	620	1930
PF	0.48	0.50	0.52	0.50

24/05/18 17:14:20 440V 50Hz 3 Φ WYE EN50160

Fig. 7.10(b): Active and Reactive Power of Grid side ADSIG for Rural Electrification without Prime-mover and ADSIG operating in motoring mode and acting as Isolation Transformer.

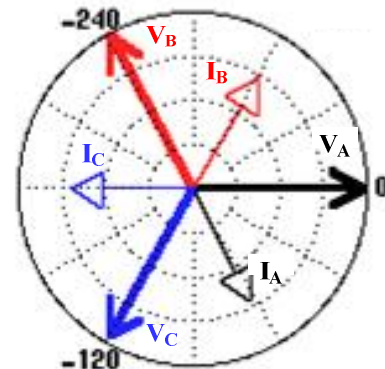


Fig. 7.10(c): Phasor Diagram of 3- Φ Current of Grid side ADSIG for Rural Electrification without Prime-mover and ADSIG operating in motoring mode and acting as Isolation Transformer.

the ADSIG is taking 1110 W real power from the grid during the transformer action of ADSIG and start giving 350 W power during the generating action of the ADSIG. It is also observed that the reactive power demand also increased from 190 VAR to 2560 VAR due to the higher magnetization requirement during generating action. This may be decreased by installing some local capacitor for the ADSIG. The negative value of

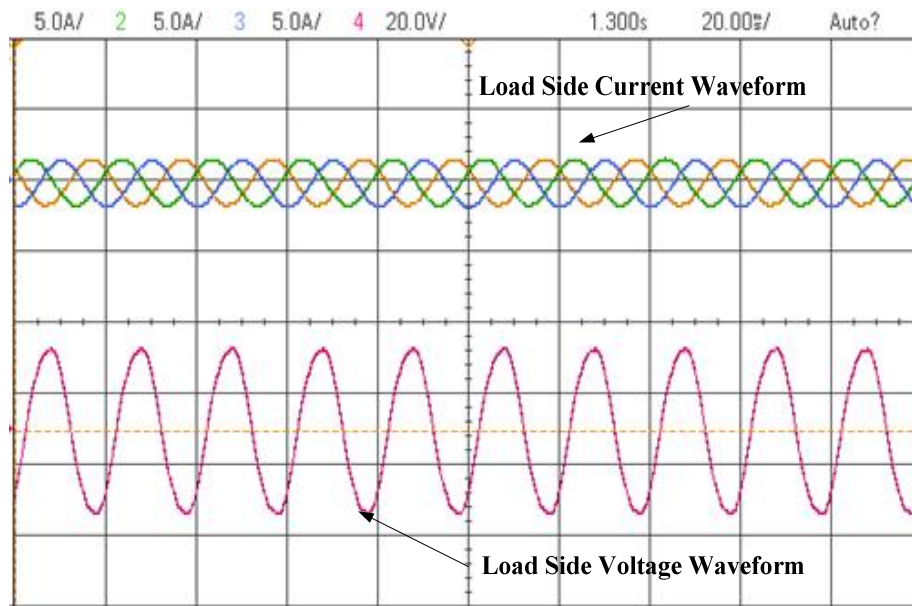


Fig. 7.11(a): Current (3- Φ) and Voltage (1- Φ) waveforms of Load (off-grid) side ADSIG for Rural Electrification without Prime mover and ADSIG operating in motoring mode and acting as Isolation Transformer

Scale: Y axis: Current Waveform 5A/div; Voltage Waveform 250 V/div; X axis: Time 20ms/div

Puni	A	B	C	Total
W	- 220	- 230	- 230	- 680
UR	220	230	230	680
var	10	10	10	20
PF	-1.00	-1.00	-1.00	-1.00
24/05/18 17:16:35	440V	50Hz	3Ø WYE	EN50160

Fig. 7.11(b): Active and Reactive Power of Load (off-grid) side ADSIG for Rural Electrification without Prime-mover and ADSIG operating in Motoring mode and acting as Isolation Transformer

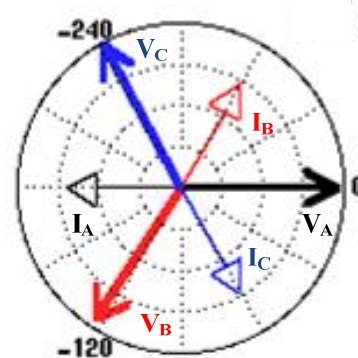


Fig. 7.11(c): Phasor Diagram of 3- Φ Current of Load (off-grid) side ADSIG for Rural Electrification without Prime-mover and ADSIG operating in motoring mode and acting as Isolation Transformer

power factor shown is due to the fact that the three-phase power analyser used in the laboratory simply takes the ratio of real and reactive power, and the reactive power became negative as soon as the ADSIG start supplying power to the grid in the generating mode. These results are supported by the phasor diagram recorder in the three-phase power analyser shown in Fig. 7.10 (c) and Fig. 7.12 (c). The phase difference between phase voltage and current is increased to a value greater than 90° due to the reversal of real component of the grid current which start flowing from

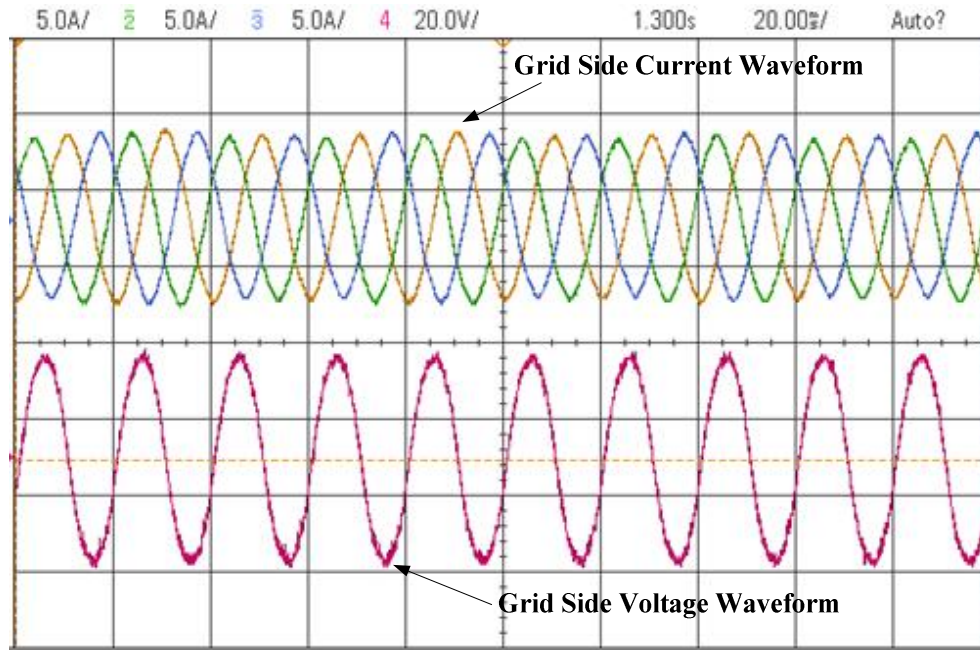


Fig. 7.12(a): Current (Three Phase) and Voltage (Single Phase) waveforms of Grid side ADSIG for Rural Electrification with Prime-mover and ADSIG acting as Generator
Scale: Y axis: Current Waveform 5A/div; Voltage Waveform 250 V/div; X axis: Time 20ms/div

P _{avg}	A	B	C	Total
W	-130	-110	-110	-350
VA	A	B	C	Total
	880	870	840	2590
var	A	B	C	Total
	870	860	830	2560
PF	A	B	C	Total
	-0.15	-0.12	-0.13	-0.13
24/05/18 17:28:26 440V 50Hz 3Ø WYE EN50160				

Fig. 7.12(b): Active and Reactive Power of Grid side ADSIG for Rural Electrification with Prime-mover and ADSIG acting as Generator

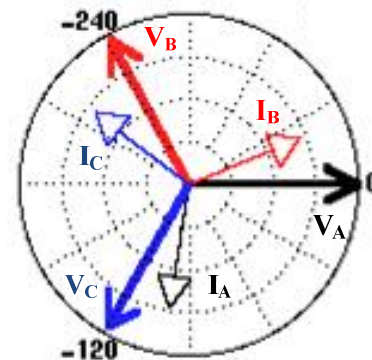


Fig. 7.12(c): Phasor Diagram of 3-Ø Current of Grid side ADSIG for Rural Electrification with Prime-mover and ADSIG acting as Generator

ADSIG to the grid while the reactive component of current still flows from the grid to ADSIG.

Further, the performance of ADSIG for different loading condition is evaluated from simulation and experimentation on hardware prototype. In both, the cases three different loading conditions are studied and ADSIG is operated in generating mode with a constant speed throughout for different loads are applied to it. In the simulation

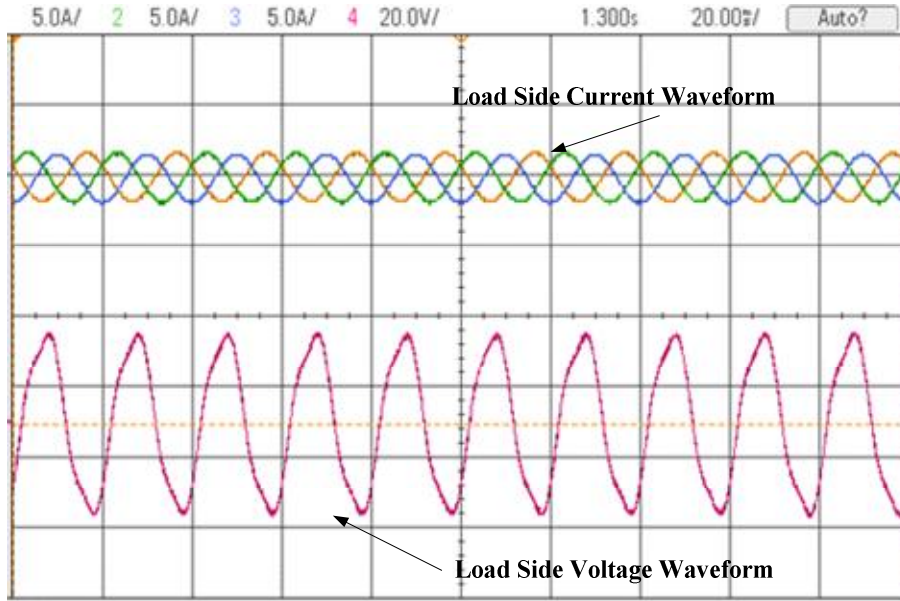


Fig. 7.13(a): Current (Three Phase) and Voltage (Single Phase) waveforms of Load (off-grid) side ADSIG for Rural Electrification with Prime mover and ADSIG acting as Generator
Scale: Y axis: Current Waveform 5A/div; Voltage Waveform 250 V/div; X axis: Time 20ms/div

P _{Unit}	A	B	C	Total
W	- 240	- 250	- 260	- 760
VA	240	250	260	760
var	10	10	10	30
PF	-1.00	-1.00	-1.00	-1.00
24/05/18 17:30:41	440V	50Hz	3Ø WYE	EN50160

Fig. 7.13(b): Active and Reactive Power of Load (off-grid) side ADSIG for Rural Electrification with Prime-mover and ADSIG acting as Generator

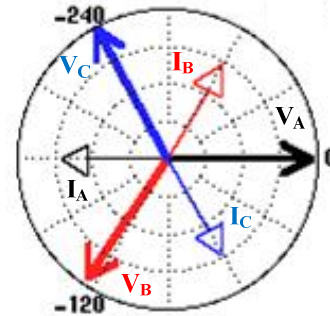


Fig. 7.13(c): Phasor Diagram of 3-Ø Current of Load (off-grid) side ADSIG for Rural Electrification with Prime-mover and ADSIG acting as Generator

results voltage and current waveform of both winding side of ADSIG are shown in Fig. 7.14 and real and reactive power of both winding side of ADSIG are shown in Fig. 7.15. From $t = 0$ to $t = 0.25$ s a resistive loading of $R=125 \Omega$ is applied on the lagging winding side of the ADSIG, the real power generated by ADSIG is routed to grid 200 W (Fig 7.14 (a)) and rest 9800 W (Fig 7.14 (b)) is transferred to the load on off-grid winding set of ADSIG. Similarly, at $t = 0.25$ s the load is

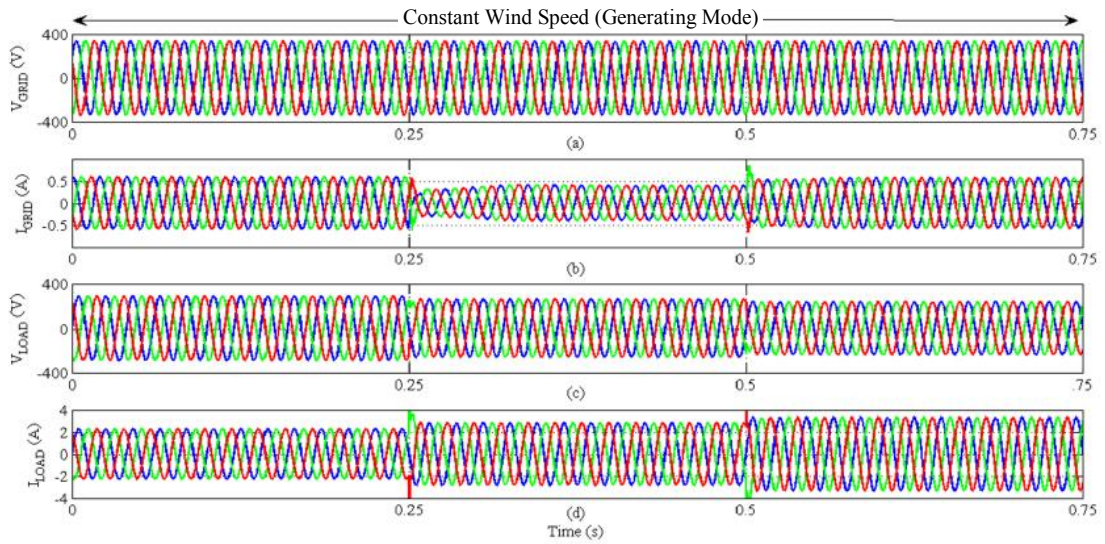


Fig. 7.14: Voltage and Current waveform of Leading (Grid Side) and Lagging (Load Side) Winding Side of ADSIG during change in Load Levels

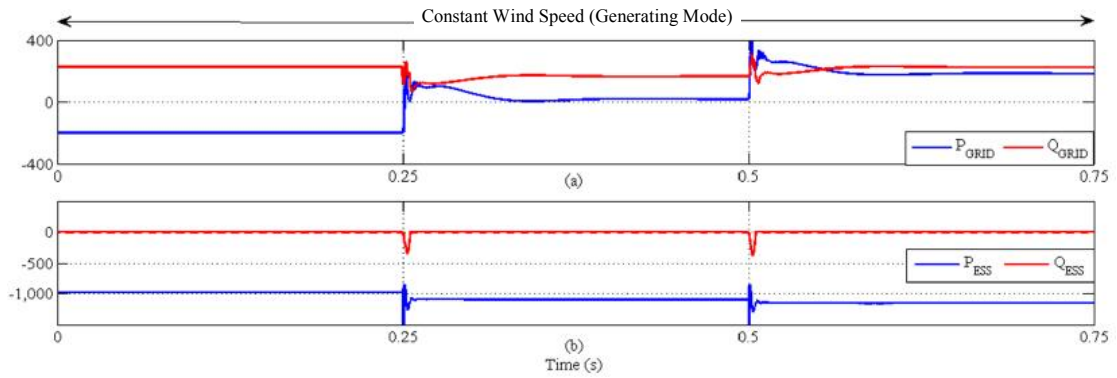


Fig. 7.15: Real and Reactive power drawn/supplied of Leading (Grid Side) and Lagging (Load Side) Winding Side of ADSIG during change in Load Levels

increased such that $R = 90 \, \Omega$. Now the power demanded by ADSIG is almost similar to the power generated by ADSIG. Therefore, the nearly total power of 1100 W is transferred to the off-grid/load-side of ADSIG. And the grid side provides the reactive power with negligible (15 W) real power demand by ADSIG at constant wind speed do not increase much but is decreased by a small amount. This is due to the cross magnetisation effect absorbed between two winding set of ADSIG. Further at $t = 0.5 \, \text{s}$ the load demand is increased such that $R = 70 \, \Omega$, now the power demanded by the load is more than the power generated by ADSIG, so here the power supplied to load is a combination of transformer action and generator action of ADSIG i.e. power

transferred to load is a combination of power from grid and power the generated by ADSIG. Here 185 W is contributed by the grid to meet the load requirement of load on the off-grid side of ADSIG. The reactive power demand, in this case, is increased to 230 VAR caused due to the decreased voltage on the off-grid side of ADSIG but the difference is less due to the cross magnetization effect.

PUNI 0:00:03				
	A	B	C	Total
W	- 10	20	10	20
	A	B	C	Total
VA	850	850	810	2510
	A	B	C	Total
var	850	840	810	2510
	A	B	C	Total
PF	-0.01	0.02	0.02	0.01
24/05/18 17:31:51 440V 50Hz 3Ø WYE EN50160				

Fig. 7.16 (a): Active and Reactive Power of Grid side ADSIG for Rural Electrification with ADSIG acting as Generator (with 1.5 A Load Current)

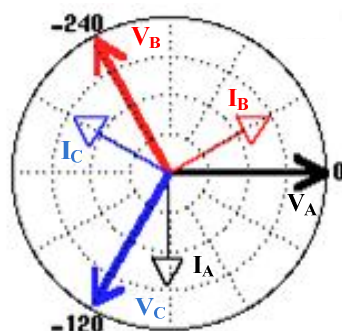


Fig. 7.16 (b): Phasor of Three Phase Current of Grid side ADSIG for Rural Electrification with ADSIG acting as Generator (with 1.5 A Load Current)

PUNI 0:00:05				
	A	B	C	Total
W	- 340	- 350	- 360	-1050
	A	B	C	Total
VA	340	350	360	1050
	A	B	C	Total
var	10	20	10	30
	A	B	C	Total
PF	-1.00	-1.00	-1.00	-1.00
24/05/18 17:34:03 440V 50Hz 3Ø WYE EN50160				

Fig. 7.17 (a): Active and Reactive Power of Load (off-grid) side ADSIG for Rural Electrification with ADSIG acting as Generator (with 1.5 A Load Current)

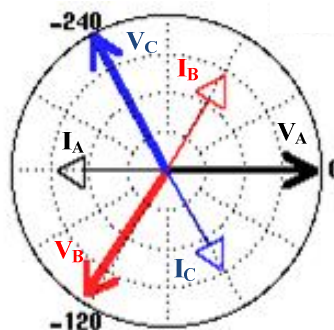


Fig. 7.17 (b): Phasor of Three Phase Current of Load (off-grid) side ADSIG for Rural Electrification with ADSIG acting as Generator (with 1.5 A Load Current)

Similar tests are performed on the hardware prototype of the ADSIG. Different resistive loads drawing a current of 1A, and 2 A are connected on the off-grid winding side of ADSIG. Here also the speed of wind is kept constant and loads are varied such that the current drawn by the loads is 1A, 1.5 A and 2 A. When resistive load draws 1A current, ADSIG generation is more than the rural load demand, 350W and excess

P _{UNI}	A	B	C	Total
W	100	120	120	330
VA	860	860	830	2550
var	850	850	820	2530
PF	0.11	0.13	0.14	0.13

24/05/18 17:32:37 440V 50Hz 3Ø WYE EN50160

Fig. 7.18 (a): Active and Reactive Power of Grid side ADSIG for Rural Electrification with ADSIG acting as Generator (with 2 A Load Current)

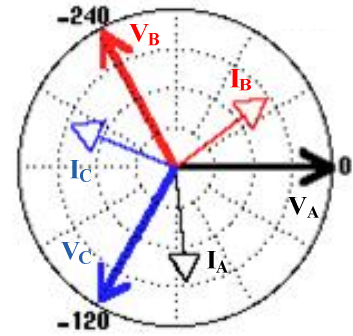


Fig. 7.18 (b): Phasor of Three Phase Current of Grid side ADSIG for Rural Electrification with ADSIG acting as Generator (with 2 A Load Current)

P _{UNI}	A	B	C	Total
W	- 420	- 430	- 450	-1310
VA	420	440	450	1310
var	10	20	10	40
PF	-1.00	-1.00	-1.00	-1.00

24/05/18 17:34:50 440V 50Hz 3Ø WYE EN50160

Fig. 7.19 (a): Active and Reactive Power of Load (off-grid) side ADSIG for Rural Electrification with ADSIG acting as Generator (with 2 A Load Current)

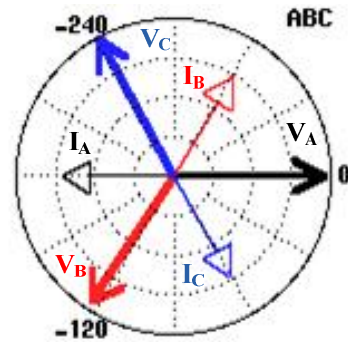


Fig. 7.19 (b): Phasor of Three Phase Current of Load (off-grid) side ADSIG for Rural Electrification with ADSIG acting as Generator (with 2 A Load Current)

power of 760 W is delivered to the grid as observed from in Fig. 7.12 (b) and Fig. 7.13 (b). Further, the load is increased such that the load current is 1.5 A and the now as the load is increased; total power generated by ADSIG is transformed load and only reactive power exchange of 2510 VAR is done from the grid, which is supported by the phasor diagram shown in Fig. 7.16 (b). The reactive power required by the ADSIG is decreased due to cross magnetization effect discussed earlier, between the two winding set of ADSIG. Further, the load is increased and the load current is equal to 2 A. now the grid support the load of 1310 W (Fig. 7.18 (a)) by supplying 330 W of real

power (Fig. 7.19 (a)). The net reactive power demand of ADSIG is still 2530 VAr only even though the real power demand on ADSIG has doubled. The increase in real load demand usually leads to increased reactive power demand in induction generators. But for ADSIG the net reactive power demand decreases or remains almost the same with increasing load. This clearly supports the ideology of the cross-coupling effect in ADSIG and it can be said that the total reactive power demand of ADSIG can be effectively controlled by applying loadings on the other terminals of ADSIG. Here in the developed prototype, the reactive power demand of ADSIG is still high due to the fact that the machine is hand wound and has a large air-gap, as the machine was re-wound. By proper selection of ADSIG machine and adopting good winding practices, the demand of reactive power of ADSIG can be remarkably reduced. This makes ADSIG as a suitable choice for power routing and an induction generator with controlled reactive power demand.

7.5 Conclusion

In this chapter, ADSIG is used as a Gen-Former for delivering electrical power to rural loads. The analysis of the configuration is done and the power routing and the dependency of the voltage profile on the loading are also established. The system is analysed for two different conditions, condition one when the wind speed is low and generation of power is not possible and ADSIG acts as a transformer. In the second condition, the wind speed is sufficient for power generation and ADSIG routes the tapped wind power to rural load and grid (if the generated power is more than the connected load). Intentional load changes on the off-grid side of ADSIG level that an increase in the loading on the off-grid side of ADSIG reduces the reactive power demand from the grid considerably. This phenomenon clearly explains the self-

balancing act of ADSIG for reactive power demand. In this chapter cross magnetization effect on both the winding set of ADSIG is also explained and demonstrated. Thus a cost-effective method to cater the rural load demands using ADSIG is successfully tested using analysis, simulation and hardware results. The configuration also reduces the overall loading on the grid due to tapped wind energy.

Chapter 8

Conclusion and Future Scope

8.1 Main Conclusions

ADSIG has been investigated in this thesis with mathematical analysis, through simulation under MATLAB / Simulink environment with help of SimPowerSystems toolbox and through experimentation on hardware prototype developed in the laboratory. The obtained result clearly demonstrated the suitability of ADSIG for power generation from the wind under various conditions and applications. Main conclusion of the work/thesis is as follow:

- The mathematical model of the ADSIG and its equivalent circuit is developed using voltage and flux equations in d-q axis. To make the equivalent circuit more lucid, the coupling element of rotor side leakage reactance and resistance are decoupled and the rotor leakage inductance is transferred to magnetizing branch and towards both stator side circuit. The decoupled real and imaginary components of rotor circuitry allow easy analysis and reveal lucid power flow study.
- A detailed comparison of the ADSIG performance is drawn with similar rating SCIG and SDSIG. Firstly mathematical analysis of ADSIG current (during transient and steady state condition) is done with the help of its reduced equivalent circuit developed. Then similar rating SCIG and ADSIG are compared for inrush and steady state currents. The analytical/mathematical results obtained are verified through MATLAB SIMULINK environment and is conformed through the results of hardware prototype. Both simulation and

hardware results show the superiority of ADSIG over SCIG during starting as well as steady state condition.

- The comparison of SCIG and ADSIG is made for one phase open circuited condition through both simulation and hardware testing. The performance of ADSIG is found out to be better as compared to SCIG for such conditions when operating with the grid.
- The transient air gap analysis of ADSIG is also done and the same is compared with the response of a similar rating SDSIG in simulation. A comprehensive phasor analysis is performed for both the generators and it is observed that the reactive power requirement of ADSIG is lesser as compared to that of SDSIG for delivering the same active power to a load under similar operating conditions. Simulation is further carried out to study the effect of loading on the air-gap flux and the effect of a single line to ground fault on the air-gap flux. The results of both the tests show that ADSIG shows better performance as compared to SDSIG.
- The performance of ADSIG developed has been successfully demonstrated for up-to the rated condition of loading. A mathematical analysis based on the impedance model of the system is done and the results show that power routing to any winding in ADSIG is dependent on the respective loading at the other winding. The simulation and experimental results confirm that ADSIG is capable of injecting the generated power into the different feeders based on their loading conditions without any complicated control and additional hardware. It has also been established that the proposed system effectively provides ride through capabilities for low voltage, thereby proving its immunity to transients.

- The three port network architecture of the ADSIG has been demonstrated to couple with the feeders effectively, providing modular approach for augmentation of similar units in parallel for even more effective soft coupling and load balancing on feeders, besides integration of more turbines into the system. The results also demonstrated that inrush transients have been tremendously subsided to prevent bottleneck for coupling multiple of such units in a cost effective and rugged way. The proposed configuration thus paves the way for incorporation of ADSIG in future distribution systems with multiple coupling of feeder together with effective integration of wind energy system.
- Application of ADSIG utilizing energy storage for transferring fixed committed active power to the grid in a wide range of wind speed (below synchronous speeds to above synchronous speeds) is analysed and tested both in simulation and through hardware. This proves to be a cost effective method with least requirement of power electronic and magnetic circuits for transferring the requisite committed active power to the grid. The electrically isolated windings of stator act as natural filter to suppress the current harmonics emanated by ESS converter to infiltrate into the grid. The simulation and hardware results confirm the superiority of using ADSIG to work in cohesion and cooperation in wind farms located at places having large variations in wind speed.
- Application of ADSIG as a Gen-Former for delivering electrical power to rural loads is also done. The analysis of the configuration is done and the power routing and the dependency of voltage profile on the loading is also established. The system is analysed for two different conditions (in generating

mode and motoring mode as transformer). It is clearly established that an increase in the loading on off-grid side of ADSIG reduces the reactive power demand from the grid considerably. This phenomenon clearly explains the self-balancing act of ADSIG for reactive power demand.

8.2 Future Scopes of Work

The analysis and application of ADSIG for WECS presented in the thesis offer a lot of scope for future improvement in the strategies, implementation in the present power system. Some of the suggested future scope of work is listed below:

- ADSIG has been used a soft coupler in the thesis for routing and coupling power between two AC grids depending on the loading on each side. However, this topology can be further be extended for routing power from one AC feeder to interlinking DC microgrids for coupling to another AC feeder with incorporation of BESS and supercapacitor.
- ADSIG in tandem with BESS and supercapacitor can also be used for remote off-grid electrification.
- Power electronic converters can also be used for maintaining the UPF etc. at the load end using different control schemes. The study of the effect of both shunt (STATCOM) and series (DVR) on reactive power control. Distributed reactive power compensation, by minimal injection from one/both sides utilising the merits of cross-coupling feature of the windings.
- ADSIG is also be used in conjunction with the energy storage system (deportable system) and PV/ wind (not deportable) hybrid system utilizing its both sides for reducing the effect of intermittency.

References

- [1] A. Miller, E. Muljadi and D. S. Zinger, "A variable speed wind turbine power control," in *IEEE Transactions on Energy Conversion*, vol. 12, no. 2, pp. 181-186, June 1997.
- [2] A. S. Neris, N. A. Vovos and G. B. Giannakopoulos, "A variable speed wind energy conversion scheme for connection to weak AC systems," in *IEEE Transactions on Energy Conversion*, vol. 14, no. 1, pp. 122-127, March 1999.
- [3] F. Blaabjerg, R. Teodorescu, M. Liserre and A. V. Timbus, "Overview of Control and Grid Synchronization for Distributed Power Generation Systems," in *IEEE Transactions on Industrial Electronics*, vol. 53, no. 5, pp. 1398-1409, Oct. 2006.
- [4] M. Chinchilla, S. Arnaltes and J. C. Burgos, "Control of permanent-magnet generators applied to variable-speed wind-energy systems connected to the grid," in *IEEE Transactions on Energy Conversion*, vol. 21, no. 1, pp. 130-135, March 2006.
- [5] S. Muller, M. Deicke and R. W. De Doncker, "Doubly fed induction generator systems for wind turbines," in *IEEE Industry Applications Magazine*, vol. 8, no. 3, pp. 26-33, May-June 2002.
- [6] R. Pena, J. C. Clare and G. M. Asher, "Doubly fed induction generator using back-to-back PWM converters and its application to variable-speed wind-energy generation," in *IEE Proceedings - Electric Power Applications*, vol. 143, no. 3, pp. 231-241, May 1996.
- [7] S. Muller, M. Deicke and R. W. De Doncker, "Adjustable speed generators for wind turbines based on doubly-fed induction machines and 4-quadrant IGBT converters linked to the rotor," *Conference Record of the 2000 IEEE Industry Applications Conference. Thirty-Fifth IAS Annual Meeting and World Conference on Industrial Applications of Electrical Energy (Cat. No.00CH37129)*, Rome, Italy, 2000, pp. 2249-2254 vol.4.
- [8] J. M. Carrasco *et al.*, "Power-Electronic Systems for the Grid Integration of Renewable Energy Sources: A Survey," in *IEEE Transactions on Industrial Electronics*, vol. 53, no. 4, pp. 1002-1016, June 2006.

- [9] Carrasco, J. M., et al. "Power electronic systems for the grid integration of wind turbines." *IEEE Industrial Electronics, IECON 2006-32nd Annual Conference on*. IEEE, 2006.
- [10] J. M. Carrasco *et al.*, "Power-Electronic Systems for the Grid Integration of Renewable Energy Sources: A Survey," in *IEEE Transactions on Industrial Electronics*, vol. 53, no. 4, pp. 1002-1016, June 2006.
- [11] F. Blaabjerg, M. Liserre and K. Ma, "Power Electronics Converters for Wind Turbine Systems," in *IEEE Transactions on Industry Applications*, vol. 48, no. 2, pp. 708-719, March-April 2012.
- [12] Teodorescu, Remus, Marco Liserre, and Pedro Rodriguez. *Grid converters for photovoltaic and wind power systems*. Vol. 29. John Wiley & Sons, 2011.
- [13] W. Carlin, P & S. Laxson, A & Muljadi, Eduard, "The History and State of the Art of Variable-Speed Wind Turbine Technology," in *Wind Energy*, vol. 6, pp. 129 - 159, April 2003.
- [14] F. Blaabjerg, F. Iov, Z. Chen and K. Ma, "Power electronics and controls for wind turbine systems," *2010 IEEE International Energy Conference*, Manama, 2010, pp. 333-344.
- [15] F. Blaabjerg, F. Iov, T. Kerekes and R. Teodorescu, "Trends in power electronics and control of renewable energy systems," *Proceedings of 14th International Power Electronics and Motion Control Conference EPE-PEMC 2010*, Ohrid, 2010, pp. K-1-K-19.
- [16] F. Blaabjerg, M. Liserre and K. Ma, "Power Electronics Converters for Wind Turbine Systems," in *IEEE Transactions on Industry Applications*, vol. 48, no. 2, pp. 708-719, March-April 2012.
- [17] F. Blaabjerg and K. Ma, "Future on Power Electronics for Wind Turbine Systems," in *IEEE Journal of Emerging and Selected Topics in Power Electronics*, vol. 1, no. 3, pp. 139-152, Sept. 2013.
- [18] Blaabjerg, Frede, and Ke Ma. "Wind energy systems." in *Proceedings of IEEE*, vol 105, no. 11, Nov. 2017.
- [19] Ma, Ke, Yongheng Yang, and Frede Blaabjerg. "Introduction to Renewable Energy Systems." in *Advanced and Intelligent Control in Power Electronics and Drives*, Springer, vol 531, pp. 3-40, 2014.

- [20] Slootweg, J. G., et al. "General model for representing variable speed wind turbines in power system dynamics simulations." *IEEE Transactions on power systems* 18.1 (2003): 144-151.
- [21] J. A. Baroudi, V. Dinavahi and A. M. Knight, "A review of power converter topologies for wind generators." *IEEE International Conference on Electric Machines and Drives*, pp. 458-465, 2005.
- [22] SanjibakumarBisoyi, R.K.Jarial, R.A.Gupta. "A review of the state of the art of generators and power electronics converter topologies for wind energy conversion system." *International Journal of Emerging Technology and Advanced Engineering*, vol. 3, no. 3, pp. 283-291, Feb. 2013.
- [23] C. E. A. Silva, R. T. Bascope and D. S. Oliveira, "Three-phase power factor correction rectifier applied to wind energy conversion systems," *2008 Twenty-Third Annual IEEE Applied Power Electronics Conference and Exposition*, Austin, TX, 2008, pp. 768-773.
- [24] M. Chinchilla, S. Arnaltes and J. C. Burgos, "Control of permanent-magnet generators applied to variable-speed wind-energy systems connected to the grid," in *IEEE Transactions on Energy Conversion*, vol. 21, no. 1, pp. 130-135, March 2006.
- [25] J. M. Carrasco *et al.*, "Power-Electronic Systems for the Grid Integration of Renewable Energy Sources: A Survey," in *IEEE Transactions on Industrial Electronics*, vol. 53, no. 4, pp. 1002-1016, June 2006.
- [26] F. Blaabjerg, Zhe Chen and S. B. Kjaer, "Power electronics as efficient interface in dispersed power generation systems," in *IEEE Transactions on Power Electronics*, vol. 19, no. 5, pp. 1184-1194, Sept. 2004.
- [27] A. Timbus, M. Liserre, R. Teodorescu and F. Blaabjerg, "Synchronization methods for three phase distributed power generation systems - An overview and evaluation," *2005 IEEE 36th Power Electronics Specialists Conference*, Recife, 2005, pp. 2474-2481.
- [28] Z. Chen, J. M. Guerrero and F. Blaabjerg, "A Review of the State of the Art of Power Electronics for Wind Turbines," in *IEEE Transactions on Power Electronics*, vol. 24, no. 8, pp. 1859-1875, Aug. 2009.
- [29] H. Polinder, F. F. A. van der Pijl, G. -. de Vilder and P. J. Tavner, "Comparison of direct-drive and geared generator concepts for wind turbines,"

- in *IEEE Transactions on Energy Conversion*, vol. 21, no. 3, pp. 725-733, Sept. 2006.
- [30] M. Tsili and S. Papathanassiou, "A review of grid code technical requirements for wind farms," in *IET Renewable Power Generation*, vol. 3, no. 3, pp. 308-332, Sept. 2009.
 - [31] J. Ekanayake and N. Jenkins, "Comparison of the response of doubly fed and fixed-speed induction generator wind turbines to changes in network frequency," in *IEEE Transactions on Energy Conversion*, vol. 19, no. 4, pp. 800-802, Dec. 2004.
 - [32] G. Lalor, A. Mullane and M. O'Malley, "Frequency control and wind turbine technologies," in *IEEE Transactions on Power Systems*, vol. 20, no. 4, pp. 1905-1913, Nov. 2005.
 - [33] G. Ramtharan, J. B. Ekanayake and N. Jenkins, "Frequency support from doubly fed induction generator wind turbines," in *IET Renewable Power Generation*, vol. 1, no. 1, pp. 3-9, March 2007.
 - [34] M. Kayikci and J. V. Milanovic, "Dynamic Contribution of DFIG-Based Wind Plants to System Frequency Disturbances," in *IEEE Transactions on Power Systems*, vol. 24, no. 2, pp. 859-867, May 2009.
 - [35] J. F. Conroy and R. Watson, "Frequency Response Capability of Full Converter Wind Turbine Generators in Comparison to Conventional Generation," in *IEEE Transactions on Power Systems*, vol. 23, no. 2, pp. 649-656, May 2008.
 - [36] R. Doherty, A. Mullane, G. Nolan, D. J. Burke, A. Bryson and M. O'Malley, "An Assessment of the Impact of Wind Generation on System Frequency Control," in *IEEE Transactions on Power Systems*, vol. 25, no. 1, pp. 452-460, Feb. 2010.
 - [37] F. Blaabjerg, Zhe Chen and S. B. Kjaer, "Power electronics as efficient interface in dispersed power generation systems," in *IEEE Transactions on Power Electronics*, vol. 19, no. 5, pp. 1184-1194, Sept. 2004.
 - [38] F. Blaabjerg, F. Iov, R. Teodorescu and Z. Chen, "Power Electronics in Renewable Energy Systems," *2006 12th International Power Electronics and Motion Control Conference*, Portoroz, 2006, pp. 1-17.

- [39] Z. Chen and E. Spooner, "Grid Power Quality with Variable-Speed Wind Turbines," in *IEEE Power Engineering Review*, vol. 21, no. 6, pp. 70-70, June 2001.
- [40] Z. Chen and E. Spooner, "Grid interface options for variable-speed, permanent-magnet generators," in *IEE Proceedings - Electric Power Applications*, vol. 145, no. 4, pp. 273-283, July 1998.
- [41] Blaabjerg, Frede, and Zhe Chen. "Power electronics as an enabling technology for renewable energy integration." *Journal of Power Electronics*, vol. 3, no. 2, pp. 81-89, 2003.
- [42] T. Thiringer and J. Linders, "Control by variable rotor speed of a fixed-pitch wind turbine operating in a wide speed range," in *IEEE Transactions on Energy Conversion*, vol. 8, no. 3, pp. 520-526, Sept. 1993.
- [43] Yoshida, Shigeo. "Horizontal axis wind turbine and method for controlling horizontal axis wind turbine." U.S. Patent No. 7,244,100, 17 Jul. 2007.
- [44] Jayalakshmi, V. "Variable Speed Cage Machine Wind Generation Unit." *Middle-East Journal of Scientific Research*, vol. 20, no. 11, pp. 1670-1676, 2014.
- [45] Hassan, A. A., et al. "Robust control of a wind driven induction generator connected to the utility grid." *Journal of the Engineering Sciences*, vol. 34, no.1, pp. 107-121, 2006.
- [46] Z. Chen, Y. Hu and F. Blaabjerg, "Stability improvement of induction generator-based wind turbine systems," in *IET Renewable Power Generation*, vol. 1, no. 1, pp. 81-93, March 2007.
- [47] Y. Hu and Z. Chen, "Effects of Capacitor Bank on Fault Ride Through Capability of Induction Generator Based Wind Turbines," *2010 Asia-Pacific Power and Energy Engineering Conference*, Chengdu, 2010, pp. 1-4.
- [48] Sun, Tao, Zhe Chen, and FredeBlaabjerg. "Transient stability of DFIG wind turbines at an external short-circuit fault." *Wind energy*, vol.8, no. 3, pp. 345-360, 2005.
- [49] J. Ren, Y. Hu, Y. Ji and C. Liu, "Low voltage ride-through control for fixed speed wind generators under grid unbalanced fault," *2012 Twenty-Seventh Annual IEEE Applied Power Electronics Conference and Exposition (APEC)*, Orlando, FL, 2012, pp. 686-689.

- [50] E. A. Klingshirn, "High Phase Order Induction Motors - Part II-Experimental Results," in *IEEE Transactions on Power Apparatus and Systems*, vol. PAS-102, no. 1, pp. 54-59, Jan. 1983.
- [51] Roberts, P. C., "Study of brushless doubly-fed (induction) machines: contributions in machine analysis, design and control," *University of Cambridge, Cambridge, England* (Doctoral thesis), 2005.
- [52] K. Gopakumar, V. T. Ranganthan and S. R. Bhat, "Split-phase induction motor operation from PWM voltage source inverter," in *IEEE Transactions on Industry Applications*, vol. 29, no. 5, pp. 927-932, Sept.-Oct. 1993.
- [53] H. Li and Z. Chen, "Overview of different wind generator systems and their comparisons," in *IET Renewable Power Generation*, vol. 2, no. 2, pp. 123-138, June 2008.
- [54] B. Feifei, H. Wenxin, H. Yuwen, C. Xiaobo, S. Kai and W. Qianshuang, "A novel 6/3-phase dual stator-winding induction generator system applied in wind power generation," *2009 International Conference on Power Electronics and Drive Systems (PEDS)*, Taipei, 2009, pp. 1360-1365.
- [55] Samira Chekkal, NarimenAouzellagLahaçani, DjamelAouzellag, KaciGhedamsi, "Fuzzy logic control strategy of wind generator based on the dual-stator induction generator," *International Journal of Electrical Power & Energy Systems*, vol. 59, pp. 166-175, 2014.
- [56] F. Bu, Y. Hu, W. Huang and S. Zhuang, "Parameter Design and Static Performance of Dual Stator-Winding Induction Generator Variable Frequency AC Generating System With Inductive and Capacitive Loads," in *IEEE Transactions on Industrial Electronics*, vol. 61, no. 8, pp. 3902-3914, Aug. 2014.
- [57] G. K. Singh, K. B. Yadav and R. P. Saini, "A self-excited six-phase induction generator for stand-alone renewable energy generation," *2007 International Aegean Conference on Electrical Machines and Power Electronics*, Bodrum, 2007, pp. 690-695.
- [58] Z. Chen, "Issues of Connecting Wind Farms into Power Systems," *2005 IEEE/PES Transmission & Distribution Conference & Exposition: Asia and Pacific*, Dalian, 2005, pp. 1-6.

- [59] Z. Chen, J. M. Guerrero and F. Blaabjerg, "A Review of the State of the Art of Power Electronics for Wind Turbines," in *IEEE Transactions on Power Electronics*, vol. 24, no. 8, pp. 1859-1875, Aug. 2009.
- [60] E. J. Coster, A. Ishchenko, J. M. A. Myrzik and W. L. Kling, "Modeling, Simulating and Validating Wind Turbine Behavior During Grid Disturbances," *2007 IEEE Power Engineering Society General Meeting*, Tampa, FL, 2007, pp. 1-6.
- [61] T. Thiringer, "Grid-friendly connecting of constant-speed wind turbines using external resistors," in *IEEE Transactions on Energy Conversion*, vol. 17, no. 4, pp. 537-542, Dec. 2002.
- [62] Iov, F, Hansen, AD, Blaabjerg, F & Teodorescu, R, "Modelling of soft-starters for wind turbine applications." in *Proc. 40th International Intelligent Motion Conference*, 2003.
- [63] R. Ahshan and M.T. Iqbal and George K.I Mann, "Power resistors based soft-starter for a small grid connected Induction Generator based wind turbine", in *Proc. of 17th IEEE NECEC Newfoundland Electrical and Computer Engineering Conference*, Nov. 2006.
- [64] G. Quinonez-Varela and A. Cruden, "Modelling and validation of a squirrel cage induction generator wind turbine during connection to the local grid," in *IET Generation, Transmission & Distribution*, vol. 2, no. 2, pp. 301-309, March 2008.
- [65] A. Luna, P. Rodriguez, R. Teodorescu and F. Blaabjerg, "Low voltage ride through strategies for SCIG wind turbines in distributed power generation systems," *2008 IEEE Power Electronics Specialists Conference*, Rhodes, 2008, pp. 2333-2339.
- [66] M. Elnashar, M. Kazerani, R. El Shatshat and M. M. A. Salama, "Comparative evaluation of reactive power compensation methods for a stand-alone wind energy conversion system," *2008 IEEE Power Electronics Specialists Conference*, Rhodes, 2008, pp. 4539-4544.
- [67] B. Singh, S. S. Murthy and S. Gupta, "An improved electronic load controller for self-excited induction generator in micro-Hydel applications," *IECON'03. 29th Annual Conference of the IEEE Industrial Electronics Society (IEEE Cat. No.03CH37468)*, Roanoke, VA, USA, 2003, pp. 2741-2746 Vol.3.

- [68] M. Vlasák, "Reduction of exciting current of induction machine during connection to electrical grid," *2014 ELEKTRO*, Rajecké Teplice, 2014, pp. 395-399.
- [69] Z. Chen, J. M. Guerrero and F. Blaabjerg, "A Review of the State of the Art of Power Electronics for Wind Turbines," in *IEEE Transactions on Power Electronics*, vol. 24, no. 8, pp. 1859-1875, Aug. 2009.
- [70] Z. Chen, "Issues of Connecting Wind Farms into Power Systems," *2005 IEEE/PES Transmission & Distribution Conference & Exposition: Asia and Pacific*, Dalian, 2005, pp. 1-6.
- [71] F. Blaabjerg, M. Liserre and K. Ma, "Power Electronics Converters for Wind Turbine Systems," in *IEEE Transactions on Industry Applications*, vol. 48, no. 2, pp. 708-719, March-April 2012.
- [72] Chen, Zhe. "A Review of Power Electronics for Wind Power." *DianliDianziJishu*, vol. 45, no.8, pp. 11-23, 2011.
- [73] Zhu, Ke, Xiao Hui Lu, and Bo Zhang. "A New Method to Reduce the Interconnection Transients of Induction Generators." *Applied Mechanics and Materials*, Vols. 130-134, pp. 524-528, 2012.
- [74] A. P. Grilo, A. Sharghi and W. Freitas, "An Analytical Approach to Determine the Optimal Resistance for the Three-Series-Resistor Method for Induction Generator Connection," in *IEEE Transactions on Energy Conversion*, vol. 23, no. 4, pp. 1111-1113, Dec. 2008.
- [75] C. L. Souza, L. M. Neto, G. C. Guimaraes and A. J. Moraes, "Power system transient stability analysis including synchronous and induction generators," *2001 IEEE Porto Power Tech Proceedings (Cat. No.01EX502)*, Porto, Portugal, 2001, pp. 6 pp. vol.2-.
- [76] T. F. Chan, "Performance analysis of a three-phase induction generator connected to a single-phase power system," in *IEEE Transactions on Energy Conversion*, vol. 13, no. 3, pp. 205-213, Sept. 1998.
- [77] J. M. Smith, "Three-Phase Induction Generator for Single-Phase Line," in *IEEE Transactions on Energy Conversion*, vol. EC-2, no. 3, pp. 382-387, Sept. 1987.

- [78] M. O. Durham and R. Ramakumar, "Power System Balancers for an Induction Generator," in *IEEE Transactions on Industry Applications*, vol. IA-23, no. 6, pp. 1067-1072, Nov. 1987.
- [79] H. Zhong, B. Wang, C. Wu and J. Wang, "Performance analysis of three-phase self-excited induction generator under single-phase load," *2016 19th International Conference on Electrical Machines and Systems (ICEMS)*, Chiba, 2016, pp. 1-5.
- [80] S. K. Sharma, B. Singh, A. Chandra and K. Al-Haddad, "Single-Phase Power Generation Employing VFC for Stand-Alone Three-Phase Doubly Wound Asynchronous Generator," in *IEEE Transactions on Industry Applications*, vol. 51, no. 6, pp. 4785-4796, Nov.-Dec. 2015.
- [81] E. A. Klingshirn, "High Phase Order Induction Motors - Part I-Description and Theoretical Considerations," in *IEEE Transactions on Power Apparatus and Systems*, vol. PAS-102, no. 1, pp. 47-53, Jan. 1983.
- [82] R. H. Nelson and P. C. Krause, "Induction Machine Analysis for Arbitrary Displacement Between Multiple Winding Sets," in *IEEE Transactions on Power Apparatus and Systems*, vol. PAS-93, no. 3, pp. 841-848, May 1974.
- [83] S. Williamson and S. Smith, "Pulsating torque and losses in multiphase induction machines," *Conference Record of the 2001 IEEE Industry Applications Conference. 36th IAS Annual Meeting (Cat. No.01CH37248)*, Chicago, IL, USA, 2001, pp. 1155-1162 vol.2.
- [84] Lipo, T. A. "A dq model for six phase induction machines." *proc. Int. conf. Electrical machines*. vol. 2. 1980.
- [85] E. A. Klingshirn, "Harmonic Filters for Six-Phase and Other Multiphase Motors on Voltage Source Inverters," in *IEEE Transactions on Industry Applications*, vol. IA-21, no. 3, pp. 588-594, May 1985.
- [86] H. A. Toliyat, T. A. Lipo and J. C. White, "Analysis of a concentrated winding induction machine for adjustable speed drive applications. I. Motor analysis," in *IEEE Transactions on Energy Conversion*, vol. 6, no. 4, pp. 679-683, Dec. 1991.
- [87] H. A. Toliyat, T. A. Lipo and J. C. White, "Analysis of a concentrated winding induction machine for adjustable speed drive applications. II. Motor design

- and performance," in *IEEE Transactions on Energy Conversion*, vol. 6, no. 4, pp. 684-692, Dec. 1991.
- [88] Singh, G. K. "Multi-phase induction machine drive research—A survey." *Electric Power Systems Research, Elsevier*, vol. 61 no. 2, pp. 139-147, Mar. 2002.
 - [89] Klingshirn, Eugene A. "Analytical and experimental study of high phase order induction motors," 1989.
 - [90] J. G. Slootweg, S. W. H. de Haan, H. Polinder and W. L. Kling, "General model for representing variable speed wind turbines in power system dynamics simulations," in *IEEE Transactions on Power Systems*, vol. 18, no. 1, pp. 144-151, Feb. 2003.
 - [91] J. G. Slootweg, H. Polinder and W. L. Kling, "Representing wind turbine electrical generating systems in fundamental frequency simulations," in *IEEE Transactions on Energy Conversion*, vol. 18, no. 4, pp. 516-524, Dec. 2003.
 - [92] M. V. A. Nunes, U. H. Bezerra and H. H. Zurn, "Transient stability margin of variable versus fixed speed wind systems in electrical grids," *2003 IEEE Bologna Power Tech Conference Proceedings*, Bologna, Italy, 2003, pp. 7 pp. Vol.3-.
 - [93] T. Petru and T. Thiringer, "Modeling of wind turbines for power system studies," in *IEEE Transactions on Power Systems*, vol. 17, no. 4, pp. 1132-1139, Nov. 2002.
 - [94] D. Harrington and J. E. McElligott, "New Developments in Armature Winding Arrangements for Large Turbine Generators [includes discussion]," in *Transactions of the American Institute of Electrical Engineers. Part III: Power Apparatus and Systems*, vol. 73, no. 1, pp. 582-587, Jan. 1954.
 - [95] Rockhill, Andrew Allen. "On the modeling and control of high phase order synchronous machines," *The University of Wisconsin-Madison*, 2012.
 - [96] P. Vas, J. E. Brown and A. Shirley, "The Application of N-Phase Generalized Rotating Field Theory to Induction Machines with Arbitrary Stator Winding Connection," in *IEEE Power Engineering Review*, vol. PER-4, no. 6, pp. 39-40, June 1984.

- [97] E. F. Fuchs and L. T. Rosenberg, "Analysis of an Alternator with Two Displaced Stator Windings," in *IEEE Transactions on Power Apparatus and Systems*, vol. PAS-93, no. 6, pp. 1776-1786, Nov. 1974.
- [98] Alger, Philip L., E. H. Freiburghouse, and D. D. Chase. "Double windings for turbine alternators." *Transactions of the American Institute of Electrical Engineers*, vol. 49, no. 1, pp. 226-244, 1930.
- [99] E. E. Ward and H. Härer, "Preliminary investigation of an inverter-fed 5-phase induction motor," in *Proceedings of the Institution of Electrical Engineers*, vol. 116, no. 6, pp. 980-984, June 1969.
- [100] E. A. Klingshirn, "High Phase Order Induction Motors - Part I. Description and Theoretical Considerations," in *IEEE Power Engineering Review*, vol. PER-3, no. 1, pp. 27-27, Jan. 1983.
- [101] Jones, M. "A literature survey of state-of-the-art in multiphase ac drives." *Conf. Rec. Universities Power Engineering Conf. UPEC*, 2002.
- [102] R. H. Nelson and P. C. Krause, "Induction Machine Analysis for Arbitrary Displacement Between Multiple Winding Sets," in *IEEE Transactions on Power Apparatus and Systems*, vol. PAS-93, no. 3, pp. 841-848, May 1974.
- [103] A. R. Munoz and T. A. Lipo, "Dual stator winding induction machine drive," in *IEEE Transactions on Industry Applications*, vol. 36, no. 5, pp. 1369-1379, Sept.-Oct. 2000.
- [104] P. C. Krause and J. R. Hake, "Method of Multiple Reference Frames Applied to the Analysis of a Rectifier - Inverter Induction Motor Drive," in *IEEE Transactions on Power Apparatus and Systems*, vol. PAS-88, no. 11, pp. 1635-1641, Nov. 1969.
- [105] Dong Wang, Weiming Ma, Fei Xiao, Botao Zhang, Dezhi Liu and An Hu, "A novel stand-alone dual stator-winding induction generator with static excitation regulation," in *IEEE Transactions on Energy Conversion*, vol. 20, no. 4, pp. 826-835, Dec. 2005.
- [106] F. Bu, W. Huang, Y. Hu, J. Shi and K. Shi, "A Stand-Alone Dual Stator-Winding Induction Generator Variable Frequency AC Power System," in *IEEE Transactions on Power Electronics*, vol. 27, no. 1, pp. 10-13, Jan. 2012.

- [107] F. Bu, Y. Hu, W. Huang, S. Zhuang and K. Shi, "Wide-Speed-Range-Operation Dual Stator-Winding Induction Generator DC Generating System for Wind Power Applications," in *IEEE Transactions on Power Electronics*, vol. 30, no. 2, pp. 561-573, Feb. 2015.
- [108] Z. Wu, O. Ojo and J. Sastry, "High-Performance Control of a Dual Stator Winding DC Power Induction Generator," in *IEEE Transactions on Industry Applications*, vol. 43, no. 2, pp. 582-592, March-april 2007.
- [109] Singh, G. K. "Modeling and experimental analysis of a self-excited six-phase induction generator for stand-alone renewable energy generation." *Renewable energy*, vol. 33, no. 7, pp. 1605-1621, 2008.
- [110] L. Parsa, "On advantages of multi-phase machines," *31st Annual Conference of IEEE Industrial Electronics Society, 2005. IECON 2005.*, Raleigh, NC, 2005, pp. 6 pp.-.
- [111] S. Williamson and S. Smith, "Pulsating torque and losses in multiphase induction machines," *Conference Record of the 2001 IEEE Industry Applications Conference. 36th IAS Annual Meeting (Cat. No.01CH37248)*, Chicago, IL, USA, 2001, pp. 1155-1162 vol.2.
- [112] E. Levi, R. Bojoi, F. Profumo, H. A. Toliyat and S. Williamson, "Multiphase induction motor drives - a technology status review," in *IET Electric Power Applications*, vol. 1, no. 4, pp. 489-516, July 2007.
- [113] O. Ojo and I. E. Davidson, "A dual stator winding induction generator with a four switch inverter-battery scheme for control," *2000 IEEE 31st Annual Power Electronics Specialists Conference. Conference Proceedings (Cat. No.00CH37018)*, Galway, Ireland, 2000, pp. 230-234 vol.1.
- [114] Zhiqiao Wu, O. Ojo and J. Sastry, "Control of a dual stator winding induction machine as a source of dc power," *Fourtieth IAS Annual Meeting. Conference Record of the 2005 Industry Applications Conference, 2005.*, Kowloon, Hong Kong, 2005, pp. 1089-1096 Vol. 2.
- [115] Bu, Feifei, et al. "Control strategy and dynamic performance of dual stator-winding induction generator variable frequency AC generating system with inductive and capacitive loads." *IEEE Trans. Power Electron*, vol. 29, no. 4, pp. 1681-1692, 2014.

- [116] Li Yong, Hu Yuwen, Huang Wenxin, Zhang Yong, HaoZhenyang and Liu Lingshun, "Decoupling control of the dual stator-winding induction generator using SVM," *2008 IEEE Power Electronics Specialists Conference*, Rhodes, 2008, pp. 3366-3370.
- [117] Li Yong, Hu Yuwen, Huang Wenxin, Zhang Yong, HaoZhenyang and TengFulin, "Dual stator-winding induction generator based automotive power generation system using direct power control," *2008 IEEE Vehicle Power and Propulsion Conference*, Harbin, 2008, pp. 1-5.
- [118] Z. Wu and O. Ojo, "High performance control of a dual winding induction generator with series connected boost rectifiers," *2006 37th IEEE Power Electronics Specialists Conference*, Jeju, 2006, pp. 1-7.
- [119] D. Wang, W. Ma and Y. Guo, "Optimal design of a self-excited capacitor in a dual-stator winding induction generator," in *IET Electric Power Applications*, vol. 3, no. 4, pp. 334-342, July 2009.
- [120] O. Ojo and I. E. Davidson, "PWM-VSI inverter-assisted stand-alone dual stator winding induction generator," in *IEEE Transactions on Industry Applications*, vol. 36, no. 6, pp. 1604-1611, Nov.-Dec. 2000.
- [121] Y. Li, Y. Hu, W. Huang, L. Liu and Y. Zhang, "The Capacity Optimization for the Static Excitation Controller of the Dual-Stator-Winding Induction Generator Operating in a Wide Speed Range," in *IEEE Transactions on Industrial Electronics*, vol. 56, no. 2, pp. 530-541, Feb. 2009.
- [122] Weiming Ma, Dong Wang, Botao Zhang, Dezhi Liu, An Hu and Lijun Fu, "A high speed induction generator based on power integration techniques," *Fourtieth IAS Annual Meeting. Conference Record of the 2005 Industry Applications Conference, 2005.*, Kowloon, Hong Kong, 2005, pp. 2272-2279 Vol. 4.
- [123] L. Xiping, L. Heyun, Y. Chengfeng, F. Shuhua and G. Jian, "A Novel Dual-Stator Hybrid Excited Synchronous Wind Generator," *2007 7th International Conference on Power Electronics and Drive Systems*, Bangkok, 2007, pp. 22-26.
- [124] L. Xu and Y. Tang, "A novel wind-power generating system using field orientation controlled doubly-excited brushless reluctance

- machine," *Conference Record of the 1992 IEEE Industry Applications Society Annual Meeting*, Houston, TX, USA, 1992, pp. 408-413 vol.1.
- [125] Amimeur, Hocine, et al. "Modeling and analysis of dual-stator windings self-excited induction generator." *Journal of Electrical Engineering (JEE)*, vol. 8, no.3, pp. 18-24, 2008.
- [126] L. N. Tutelea, S. I. Deaconu, N. Budisan and I. Boldea, "Double stator winding induction generator for wind and hydro applications: 2D-FEM analysis and optimal design," *2013 15th European Conference on Power Electronics and Applications (EPE)*, Lille, 2013, pp. 1-10.
- [127] B. Feifei, H. Wenxin, H. Yuwen, C. Xiaobo, S. Kai and W. Qianshuang, "A novel 6/3-phase dual stator-winding induction generator system applied in wind power generation," *2009 International Conference on Power Electronics and Drive Systems (PEDS)*, Taipei, 2009, pp. 1360-1365.
- [128] L. N. Tutelea, S. I. Deaconu, I. Boldea and N. Budişan, "Design, control and 2D-FEM validation for an Double Stator Winding Induction Generator," *IECON 2013 - 39th Annual Conference of the IEEE Industrial Electronics Society*, Vienna, 2013, pp. 2732-2737.
- [129] G.K. Singh, "Modeling and experimental analysis of a self-excited six-phase induction generator for stand-alone renewable energy generation," *Renewable Energy*, Volume 33, Issue 7, 2008, Pages 1605-1621.
- [130] G. K. Singh, K. Nam and S. K. Lim, "A Simple Indirect Field-Oriented Control Scheme for Multiphase Induction Machine," *IEEE TRANSACTIONS ON INDUSTRIAL ELECTRONICS*, VOL. 52, NO. 4, AUGUST 2005.
- [131] Mircea Eremia and Mohammad Shahidehpour, "Handbook of Electrical Power System Dynamics: Modeling, Stability, and Control," Wiley Publication.

List of Publications

- Ramesh Singh, Vishal Verma and Ritika Gour, “ADSIG as Gen-Former providing Three Port Network for Soft Coupling of Distribution Feeders in Addition to Wind Energy Harvesting”, in International Journal of Electrical Power and Energy Systems (IJPES – ELSEVIER) – **SCIE Indexed Journal**.
- Ramesh Singh, Vishal Verrma, “Performance Analysis and Comparison of Symmetrical and Asymmetrical Dual Stator Induction Generator for Wind Energy Conversion Systems”, in Engineering, Technology & Applied Science Research (ETASR), **ESCI Indexed Journal**.
- Ramesh Singh, Vishal Verrma, “Dual Stator Induction Generator for Rural Electrification”, in International Journal of Applied Engineering Research (IJAER), **SCOPUS Indexed Journal**.

BIODATA

Name	Ramesh Singh
Date of Birth	05.07.1978
Place of Birth	Varanasi, UP, India
Nationality	Indian
Fathers Name	Late Dr. D.R. Singh
Mothers Name	Late Smt. Kamala Singh

Educational Qualifications

B.Tech. Electrical	REC Hamirpur, 1995 - 1999
M.Tech. Power Systems	NIT Jamshedpur, 2004 – 2006

Experience

Presently working as an Assistant Professor in KIET Group of Institutions, Ghaziabad. Teaching experience of more than twelve years in different Engineering Colleges in VBSPU Jaunpur UP, AKTU Lucknow UP and IPU Delhi.

Area of Interest

Multi-Phase Machines, Renewable Sources of Energy.